ADVANCEMENTS IN BIOMASS RECALCITRANCE: THE USE OF LIGNIN FOR THE PRODUCTION OF FUELS AND CHEMICALS

frontiers Research Topics

About Frontiers

Frontiers is more than just an open-access publisher of scholarly articles: it is a pioneering approach to the world of academia, radically improving the way scholarly research is managed. The grand vision of Frontiers is a world where all people have an equal opportunity to seek, share and generate knowledge. Frontiers provides immediate and permanent online open access to all its publications, but this alone is not enough to realize our grand goals.

Frontiers Journal Series

The Frontiers Journal Series is a multi-tier and interdisciplinary set of open-access, online journals, promising a paradigm shift from the current review, selection and dissemination processes in academic publishing. All Frontiers journals are driven by researchers for researchers; therefore, they constitute a service to the scholarly community. At the same time, the Frontiers Journal Series operates on a revolutionary invention, the tiered publishing system, initially addressing specific communities of scholars, and gradually climbing up to broader public understanding, thus serving the interests of the lay society, too.

Dedication to Quality

Each Frontiers article is a landmark of the highest quality, thanks to genuinely collaborative interactions between authors and review editors, who include some of the world's best academicians. Research must be certified by peers before entering a stream of knowledge that may eventually reach the public - and shape society; therefore, Frontiers only applies the most rigorous and unbiased reviews.
Frontiers revolutionizes research publishing by freely delivering the most outstanding research, evaluated with no bias from both the academic and social point of view. By applying the most advanced information technologies, Frontiers is catapulting scholarly publishing into a new generation.

What are Frontiers Research Topics?

Frontiers Research Topics are very popular trademarks of the Frontiers Journals Series: they are collections of at least ten articles, all centered on a particular subject. With their unique mix of varied contributions from Original Research to Review Articles, Frontiers Research Topics unify the most influential researchers, the latest key findings and historical advances in a hot research area! Find out more on how to host your own Frontiers Research Topic or contribute to one as an author by contacting the Frontiers Editorial Office: researchtopics@frontiersin.org

ADVANCEMENTS IN BIOMASS RECALCITRANCE: THE USE OF LIGNIN FOR THE PRODUCTION OF FUELS AND CHEMICALS

Topic Editors:
Arthur J. Ragauskas, Oak Ridge National Laboratory, United States
Chang Geun Yoo, SUNY College of Environmental Science and Forestry, United States

"Lignin Valorization" by Arthur J. Ragauskas and Chang Geun Yoo.

Lignocellulosic biomass has great potentials as an alternative feedstock for fuels and chemicals. For effective utilization of biomass, biomass recalcitrance, which is inherent resistance of plant cell walls to biological deconstruction, needs to be reduced. Among many factors in biomass, lignin is significantly related to biomass recalcitrance. Lignin, a complex aromatic polymer, is the largest non-carbohydrate component (15-40% dry weight) in most terrestrial plants. In nature, it provides a structural integrity, facilitates water and nutrient transport, and protects plants from microbial attack. From a different angle, lignin significantly contributes to biomass recalcitrance, so it is necessary to reduce and/or modify the lignin for effective conversion of biomass.

Genetic modifications of the lignin biosynthetic pathway and lignin-targeting pretreatments have been developed to minimize the lignin-induced biomass recalcitrance. High carbon content of lignin also renders it an attractive feedstock for many applications. About 100,000 to 200,000 tons of lignin can be generated per year as a byproduct from cellulosic ethanol production, so valorization of these lignins could be one of keys for achieving economic biorefinery. However, investigations of lignin conversion have not been accomplished as the utilization of carbohydrates in biomass. Depolymerization of lignin is still challenging because of its broad distribution of bond strengths, recondensation of low-molecular species, and poor product selectivity. Diverse biological and thermochemical depolymerization methods have been investigated to overcome these barriers.

In this Research Topic, recent advancements in biomass recalcitrance by effective utilization of lignin are introduced.

Citation: Ragauskas, A. J., Yoo, C. G., eds. (2019). Advancements in Biomass Recalcitrance: The Use of Lignin for the Production of Fuels and Chemicals. Lausanne: Frontiers Media. doi: 10.3389/978-2-88945-706-9

Table of Contents

Editorial: Advancements in Biomass Recalcitrance: The Use of Lignin for the Production of Fuels and Chemicals

Arthur J. Ragauskas[1,2,3]* and Chang Geun Yoo[4]

[1] Center for Bioenergy Innovation, Biosciences Division, Oak Ridge National Laboratory, Oak Ridge, TN, United States,
[2] UT-ORNL Joint Institute for Biological Science, Oak Ridge National Laboratory, Oak Ridge, TN, United States, [3] Department of Chemical and Biomolecular Engineering, Forestry, Wildlife, and Fisheries, Center for Renewable Carbon, University of Tennessee, Knoxville, TN, United States, [4] Department of Paper and Bioprocess Engineering, State University of New York College of Environmental Science and Forestry, Syracuse, NY, United States

Editorial on the Research Topic

Advancements in Biomass Recalcitrance: The Use of Lignin for the Production of Fuels and Chemicals

The valorization of lignin has become a dominant translational research theme in biorefining in the last few years (Ragauskas et al., 2014). Historically, lignin has been sourced from kraft and sulfite pulping operations, and each of these sources provides some natural limitations to their usage. Commercially, this type of lignin has been used as a dispersant, dust suppression agent, surfactant, binder, and emulsifiers; however, most of these applications are low-value, and the markets are saturated (Gargulak and Lebo, 2000). The general limitation of these lignins is due to the presence of sulfur, extensive cross-linking, difficult process ability, purity, and low-molecular-weight profiles in the case of kraft lignin.

The next phase in lignin application is to use the intrinsic structural features of lignin to develop value-added products. Several studies have shown that lignin may be well suited for *bio-based* plastics and composite applications, in particular, for lignin resources isolated from biomass using an organosolv extraction protocol. Depending on the exact lignin extraction procedure used, the structure of lignin may be kept mostly intact. Several promising lignin applications include the use of oxypropylated lignin for polyurethane foams (Li and Ragauskas, 2012), inclusion into polystyrene (Henry et al., 2012), as a potential green antioxidant (Pouteau et al., 2003), or flame-retardant additive (Matsushita et al., 2017). Furthermore, lignin is also being actively developed as an adhesive for non-formaldehyde wood resins for flooring (Aracri et al., 2014), packaging, and composite wood board production (Li et al., 2018) which leverage the intrinsic reactivity between lignin and oxidoreductase enzymes, such as laccase, which catalyzes further lignin polymerization. The use of lignin has been leveraged with epoxy resins to yield printed circuit boards (Luukko et al., 2013), and for molding (Nam and Son, 2015). As reported by Stewart, the starting plant resource and lignin extraction process have a substantial impact on the resulting physical properties and the purification cost of lignin (Stewart, 2008). Finally, there is a growing interest in using lignin in the polyolefin markets (i.e., polyethylene and polypropylene) as the aromatic unit of lignin provides photo-stabilization, strength enhancement, and elongation effects (Lv et al., 2011). In addition to

FIGURE 1 | Three phenyl propane precursors of lignin and illustration for SW lignin. (DOE, 2006).
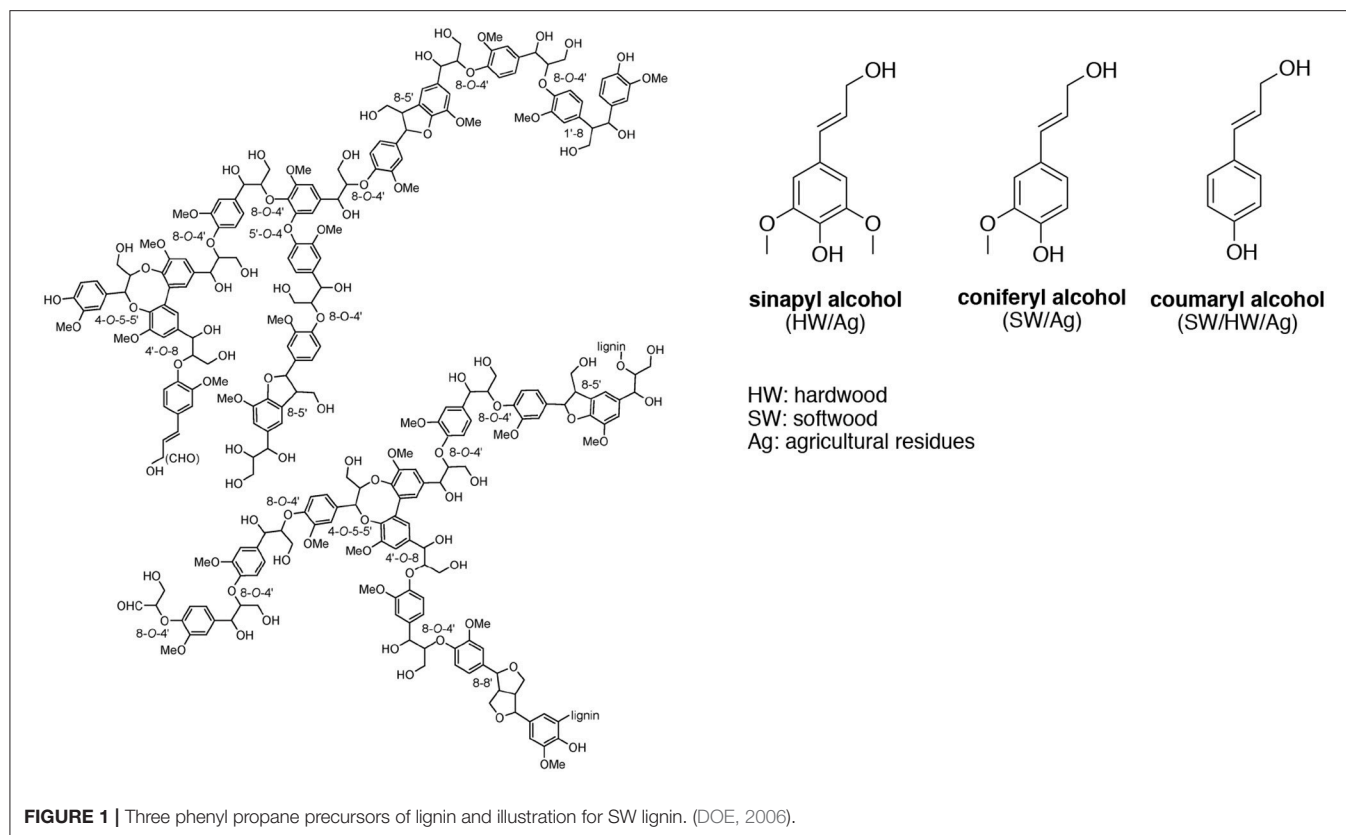
these efforts, the conversion of lignin to chemicals and fungible fuels for ground and aviation transportation is being aggressively developed using thermal and/or catalytic processes (Ben and Ragauskas, 2011; Bi et al., 2015). As an alternative to these chemical technologies, the power of biology is also being investigated to convert lignin to fatty acids and esters using *Rhodococcus* (Le et al., 2017), and *Pseudomonas putida* for PHAs (Liu et al., 2017), to name just a few promising pathways.

In each of these applications, the structure and purity of lignin play a critical role in determining its chemical and physical properties. Lignin is one of the most complex natural polymers in regards to its chemical structure and composition. It is synthesized by enzymatic dehydrogenative polymerization of 4-hydroxyphenyl propanoid units (**Figure 1**). Major types of interunit linkages and the reported abundance in softwood (SW) and hardwood (HW) lignins are presented in **Table 1**. Also, the molecular weights of various lignins isolated from native and pretreated biomass are presented in **Table 2**. There are several techniques that can be used to determine the molecular weight of lignin, but one of the most commonly used methods is lignin acetylation followed by gel permeation chromatography (GPC) analysis conducted via external standards or using multi-angle laser light scattering (MALLS) (Tolbert et al., 2014).

The breadth of lignin molecular weight and its structural features have become significantly more complex as genetic engineering of the monolignol pathways have demonstrated the ability to significantly alter the S (syringyl): G (guaiacyl):

H (*p*-hydroxyl) ratio in plants. In these days, the structure of lignin is widely determined using advanced 1D and 2D NMR techniques (Yoo et al., 2016b) supplemented with selected lignin functionalization techniques followed by heteronuclear single quantum coherence (HSQC) NMR techniques (Pu et al., 2011). These techniques have been refined so that all the key functional groups of lignin can now be established quantitatively or semi-quantitatively. Also, they made it possible to detect the acetylation of lignin in nature and the incorporation of *p*-hydroxybenzoate, ferulate, *p*-coumaric acid, and other structures in lignin (Yoo et al., 2016a, 2017b). The presence of lignin-carbohydrate complexes (LCCs) in native and process lignin remains difficult to establish fully and yet is believed to cause challenges in the processing of lignin. This special issue highlights recent advances in lignin characterization, conversion, and valorization.

AUTHOR CONTRIBUTIONS

All authors listed have made a substantial, direct and intellectual contribution to the work, and approved it for publication.

ACKNOWLEDGMENTS

TABLE 1 | Reported abundance of major linkages in softwood and hardwood lignins (Chakar and Ragauskas, 2004; Zakzeski et al., 2010).
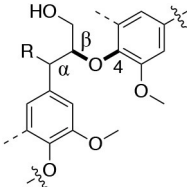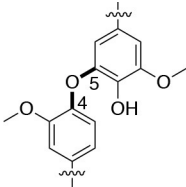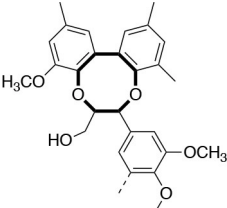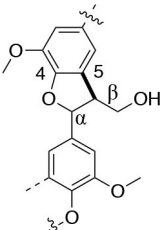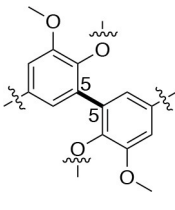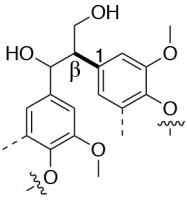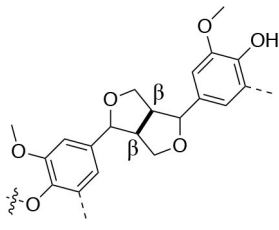
Linkage	β-*O*-4 (%)	4-*O*-5 (%)	Dibenzodioxocin (%)	
C-O linkage Abundance Per 100 C$_9$-units				
Softwood	45–50	4–8	5–7	
Hardwood	60–62	7–9	0–2	

Linkage	β-5 (%)	5-5 (%)	β-1 (%)	β-β (%)
C-C linkage Abundance Per 100 C$_9$-units				
Softwood	9–12	18–25	7–10	2–4
Hardwood	3–11	3–9	1–7	3–12

TABLE 2 | Weight-average molecular weight (M$_W$), number-average molecular weight (M$_n$), and polydispersity index (PDI) of various lignins.

Origin	M$_W$	M$_n$	PDI
Switchgrass	5,000	2,940	1.7
Buddleja davidii	16,800	7,260	2.3
Populus	13,260	5,047	2.6
Sugarcane Bagasse	3,176	1,673	1.9
Kraft softwood lignin	6,300	955	6.6
Ammonia lignin (Corn stover)	3,975	1,827	2.2
Ethanol organosolv lignin (Miscanthus)	13,800	8,300	1.6

David and Ragauskas (2010); Zeng et al. (2014); Sen et al. (2015); Bezerra and Ragauskas (2016); and Yoo et al. (2016a, 2017a).

REFERENCES

Aracri, E., Blanco, C. D., and Tzanov, T. (2014). An enzymatic approach to develop a lignin-based adhesive for wool floor coverings. *Green Chem.* 16, 2597–2603. doi: 10.1039/c4gc00063c

Ben, H., and Ragauskas, A. J. (2011). Pyrolysis of kraft lignin with additives. *Energy Fuels* 25, 4662–4668. doi: 10.1021/ef2007613

Bezerra, T. L., and Ragauskas, A. J. (2016). A review of sugarcane bagasse for second-generation bioethanol and biopower production. *Biofuels Bioprod. Biorefin.* 10, 634–647. doi: 10.1002/bbb.1662

Bi, P., Wang, J., Zhang, Y., Jiang, P., Wu, X., Liu, J., et al. (2015). From lignin to cycloparaffins and aromatics: directional synthesis of jet and diesel fuel range biofuels using biomass. *Bioresour. Technol.* 183, 10–17. doi: 10.1016/j.biortech.2015.02.023

Chakar, F. S., and Ragauskas, A. J. (2004). Review of current and future softwood kraft lignin process chemistry. *Ind. Crops Prod.* 20, 131–141. doi: 10.1016/j.indcrop.2004.04.016

David, K., and Ragauskas, A. J. (2010). Switchgrass as an energy crop for biofuel production: a review of its ligno-cellulosic chemical properties. *Energy Environ. Sci.* 3, 1182–1190. doi: 10.1039/b926617h

DOE, U.S. (2006). "Breaking the biological barriers to cellulosic ethanol: a joint research Agenda," in *DOE/SC/EE-0095* (U.S. Department of Energy Office of Science and Office of Energy Efficiency and Renewable Energy), 94.

Gargulak, J. D., and Lebo, S. E. (2000). "Commercial use of lignin-based materials," in *ACS Symposium Series,* Washington, DC.

Henry, N., Harper, D., and Dadmun, M. (2012). Optimizing noncovalent interactions between lignin and synthetic polymers to develop effective compatibilizers. *Macromol. Chem. Phys.* 213, 1196–1205. doi: 10.1002/macp.201100633

Le, R. K., Das, P., Mahan, K. M., Anderson, S. A., Wells, T., Yuan, J. S., et al. (2017). Utilization of simultaneous saccharification and fermentation residues as feedstock for lipid accumulation in *Rhodococcus opacus*. *AMB Express* 7:185. doi: 10.1186/s13568-017-0484-0

Li, R. J., Gutierrez, J., Chung, Y.-L., Frank, C. W., Billington, S. L., and Sattely, E. S. (2018). A lignin-epoxy resin derived from biomass as an alternative to formaldehyde-based wood adhesives. *Green Chem.* 20, 1459–1466. doi: 10.1039/C7GC03026F

Li, Y., and Ragauskas, A. J. (2012). Ethanol organosolv lignin-based rigid polyurethane foam reinforced with cellulose nanowhiskers. *RSC Adv.* 2, 3347–3351. doi: 10.1039/c2ra00646d

Liu, Z.-H., Olson, M. L., Shinde, S., Wang, X., Hao, N., Yoo, C. G., et al. (2017). Synergistic maximization of the carbohydrate output and lignin processability by combinatorial pretreatment. *Green Chem.* 19, 4939–4955. doi: 10.1039/C7GC02057K

Luukko, K., Kahari, H., and Fors, S. (2013). *A Biodegradable Circuit Board,* WO2013144420. World Intellectual Property Organization.

Lv, X. Y., Gao, Z. H., Zhang, Y. H., and Di, M. W. (2011). Mechanical study and microscopic characterization of lignin/PE composites. *Adv. Mater. Res. Trans. Tech. Publ.* 335–336, 191–194. doi: 10.4028/www.scientific.net/AMR.335-336.191

Matsushita, Y., Hirano, D., Aoki, D., Yagami, S., Takagi, Y., and Fukushima, K. (2017). A biobased flame-retardant resin based on lignin. *Adv. Sustain. Syst.* 1:1700073. doi: 10.1002/adsu.201700073

Nam, K. G., and Son, J. I. (2015). *Wood Plastic Composites and Manufacturing Method Thereof*, WO2013151287. World Intellectual Property Organization.

Pouteau, C., Dole, P., Cathala, B., Averous, L., and Boquillon, N. (2003). Antioxidant properties of lignin in polypropylene. *Polym. Degrad. Stab.* 81, 9–18. doi: 10.1016/S0141-3910(03)00057-0

Pu, Y., Cao, S., and Ragauskas, A. J. (2011). Application of quantitative 31P NMR in biomass lignin and biofuel precursors characterization. *Energy Environ. Sci.* 4, 3154–3166. doi: 10.1039/c1ee01201k

Ragauskas, A. J., Beckham, G. T., Biddy, M. J., Chandra, R., Chen, F., Davis, M. F., et al. (2014). Lignin valorization: improving lignin processing in the biorefinery. *Science* 344:1246843. doi: 10.1126/science.1246843

Sen, S., Patil, S., and Argyropoulos, D. S. (2015). Methylation of softwood kraft lignin with dimethyl carbonate. *Green Chem.* 17, 1077–1087. doi: 10.1039/C4GC01759E

Stewart, D. (2008). Lignin as a base material for materials applications: chemistry, application and economics. *Ind. Crops Prod.* 27, 202–207. doi: 10.1016/j.indcrop.2007.07.008

Tolbert, A., Akinosho, H., Khunsupat, R., Naskar, A. K., and Ragauskas, A. J. (2014). Characterization and analysis of the molecular weight of lignin for biorefining studies. *Biofuels Bioprod. Biorefin.* 8, 836–856. doi: 10.1002/bbb.1500

Yoo, C. G., Kim, H., Lu, F., Azarpira, A., Pan, X., Oh, K. K., et al. (2016a). Understanding the physicochemical characteristics and the improved enzymatic saccharification of corn stover pretreated with aqueous and gaseous ammonia. *Bioenergy Res.* 9, 67–76. doi: 10.1007/s12155-015-9662-6

Yoo, C. G., Li, M., Meng, X., Pu, Y., and Ragauskas, A. J. (2017a). Effects of organosolv and ammonia pretreatments on lignin properties and its inhibition for enzymatic hydrolysis. *Green Chem.* 19, 2006–2016. doi: 10.1039/c6gc03627ai

Yoo, C. G., Pu, Y., Li, M., and Ragauskas, A. J. (2016b). Elucidating Structural Characteristics of biomass using solution-state 2D NMR with a mixture of deuterated dimethylsulfoxide and hexamethylphosphoramide. *ChemSusChem* 9, 1090–1095. doi: 10.1002/cssc.201600135

Yoo, C. G., Yang, Y., Pu, Y., Meng, X., Muchero, W., Yee, K. L., et al. (2017b). Insights of biomass recalcitrance in natural Populus trichocarpa variants for biomass conversion. *Green Chem.* 19, 5467–5478. doi: 10.1039/C7GC 02219K

Zakzeski, J., Bruijnincx, P. C., Jongerius, A. L., and Weckhuysen, B. M. (2010). The catalytic valorization of lignin for the production of renewable chemicals. *Chem. Rev.* 110, 3552–3599. doi: 10.1021/cr900354u

Zeng, J., Tong, Z., Wang, L., Zhu, J., and Ingram, L. (2014). Isolation and structural characterization of sugarcane bagasse lignin after dilute phosphoric acid plus steam explosion pretreatment and its effect on cellulose hydrolysis. *Bioresour. Technol.* 154, 274–281. doi: 10.1016/j.biortech.2013.12.072

Conflict of Interest Statement: The authors declare that the research was conducted in the absence of any commercial or financial relationships that could be construed as a potential conflict of interest.

frontiers
in Energy Research

Recent Efforts to Prevent Undesirable Reactions From Fractionation to Depolymerization of Lignin: Toward Maximizing the Value From Lignin

Kwang Ho Kim* and Chang Soo Kim

Clean Energy Research Center, Korea Institute of Science and Technology, Seoul, South Korea

Lignin is a major component of lignocellulosic biomass along with cellulose and hemicellulose, currently underutilized with the bulk of technical lignin being combusted for heat generation in plant. From the technoeconomic perspective, the success of a future biorefinery is highly dependent on lignin valorization. However, structural complexity, heterogeneity of lignin, and several undesirable reactions associated with the nature of lignin and process conditions obstruct the effective utilization of lignin. Lignin condensation has been a long-lasting problem from conventional to recent biorefineries, which makes the recovered lignin more difficult to decompose. Also, the undesirable condensation and repolymerization during the depolymerization of lignin is more problematic as this significantly limits its ability to be depolymerized to low molecular weight products at high yields. To solve this problem, which ultimately enables maximizing lignin utilization, there have been many efforts in various aspects. In this review, we focus on the undesirable reactions occurring during the fractionation and depolymerization process of lignin and introduce recent efforts to suppress or minimize those unwanted reactions. The aim of all these efforts is to maximize lignin conversion to low molecular weight products.

Keywords: lignocellulosic biomass, fractionation, condensation, repolymerization, lignin modification, capping agent

INTRODUCTION

Renewable biofuels and chemicals produced from lignocellulosic biomass have great potential to reduce our overdependence on fossil fuels and eventually mitigate climate change. However, there are still many technical barriers in developing economically feasible processes for converting biomass to fuels and chemicals (Himmel, 2009). Inherent recalcitrance of lignocellulosic biomass mainly associated with the presence of lignin is a major obstacle in developing a sustainable biorefinery. Lignin is the second most abundant natural polymer next to cellulose, accounting for 15–30 wt% of lignocellulosic biomass (Zakzeski et al., 2010). In addition to the existing pulp and paper industries, a significant amount of residual lignin is expected to be produced from the emerging lignocellulosic biorefineries. The availability of such biorefinery lignins further encourages the development of lignin valorization

technologies, particularly for the production of high value-added chemicals (Zakzeski et al., 2012). Despite high-value opportunities, the technical lignin is simply burned to produce process heat in plants or sold as a natural ingredient of animal feed due to its natural heterogeneity and recalcitrance. From the industrial perspective, lignin valorization is essential for developing sustainable and advanced biorefineries in the future. In this respect, there have been substantial endeavors in developing an efficient and effective conversion process to produce value-added products from lignin because the development of such a conversion process is an important starting point for lignin valorization strategies (Ragauskas et al., 2014; Rahimi et al., 2014). However, due to the condensed and degraded nature of conventional technical lignins, it is challenging to develop effective depolymerization processes. Considering the fact that the yield of lignin-derived monomer is proportional to the frequency of inter-unit ether bonds (α-O-4 or β-O-4), preserving these cleavable linkages in lignin during the fractionation of biomass components is very important.

In addition to the effort to separate lignin as much as possible, researchers have put an enormous effort to develop an effective downstream depolymerization process for lignin valorization. Most conversion technologies developed recently use heat and metal catalysts to effectively break down lignin into low molecular weight aromatics. There are two important considerations for developing any processes, which are (1) maximizing the activity and stability of the catalyst under the reaction conditions and (2) controlling the condensation and repolymerization reactions of lignin that can form complex recondensed products (Xu et al., 2014). Taking the structural recalcitrance of lignin into account, an in-depth understanding of reaction mechanisms occurring during lignin depolymerization is important in maximizing value-added products. It is important to point out that the yields of target lignin products, liquid oil and low molecular weight phenolic products, are limited by the self-condensation and oligomerization reactions of the primary products (Roberts et al., 2011). Therefore, suppressing or preventing undesired reactions has been an important goal in lignin valorization.

Figure 1 shows the scheme of lignin depolymerization and repolymerization. There are competing reactions in the lignin depolymerization process. These reactions include recondensation to large molecular weight products or char between the primary products and stabilization to low molecular weight phenolic monomers. Although the competition is highly dependent on the reaction environment, the catalysts, and the quality of lignin, the undesirable reactions are very difficult to avoid. Thus, researchers have been exerting more efforts to minimize these unwanted secondary reactions in many aspects to maximize the value of lignin. This mini-review introduces the secondary reactions occurring during lignin extraction and the depolymerization process. Recent efforts to reduce or prevent undesirable reactions are also covered, providing insights toward further improvement of lignin valorization.

LIGNIN CONDENSATION IN THE PRETREATMENT PROCESS AND NEW FRACTIONATION APPROACH

The lignin condensation reaction has been a key problem at all stages of the process from the fractionation of biomass components to the depolymerization. The conventional fractionation process, namely biomass pretreatment, focuses on its effectiveness to remove lignin from biomass structure, generally employing acid or base catalysts. The resulting residual solid, mainly lignin, significantly undergoes irreversible repolymerization depending on the pretreatment conditions, which limits its ability to be depolymerized to low molecular weight products at high yields. Under acidic and neutral conditions, new intermolecular bonds (i.e., C–C bond) between lignin fragments form by the carbocation (Pielhop et al., 2015). Also, aryl-ether cleavage in Cα position in the presence of free Ar-OH group can lead to the formation of quinone methides, which further participate in cross-linking reactions (Grabber, 2005). In alkaline media, the reactive intermediates are mainly quinone methides. An addition reaction between phenolate ions and quinone methides results in the formation of C–C bonds, forming a lignin molecule with a larger size (Chakar and Ragauskas, 2004). In spite of their abundancy, the condensed lignin is very challenging to work with, even under harsh conditions with an effective catalyst and solvent system.

With the development of a recent biorefinery that integrates the conversion of carbohydrates and lignin, finding a suitable isolation process of lignin is becoming a primary research topic. As the proportion of β-O-4 linkages in lignin structure is the central factor for the yield and the nature of the monomeric products (Bouxin et al., 2015), a new lignin extraction method should be able to preserve the most frequent but readily cleavable aryl-ether linkages. As part of this effort, several fractionation processes have been developed and introduced, which utilize new types of solvents and catalysts. This includes ionic liquids (Shi et al., 2014, 2016; Sun et al., 2016; Xu et al., 2016; Dutta et al., 2017), deep eutectic solvents (Kim K. H. et al., 2018; Xu et al., 2018), γ-valerolactone (GVL; Luterbacher et al., 2014, 2015; Shuai et al., 2016b) and 2,5-furandicarboxylic acid (Weidener et al., 2018). Basically, the new solvent system demonstrated its applicability under mild processing conditions without strong acid or base catalysts, which minimizes carbocation- and quinone methides-induced condensation and repolymerization reactions. This could preserve the original structure of lignin with high aryl-ether linkages.

UNDESIRABLE REACTIONS DURING LIGNIN DEPOLYMERIZATION PROCESS

In the liquefaction process of lignin, a substantial amount of solid residue is produced after reactions, which restricts the liquid oil yield. It is believed that formation of undesired solid products from intermediate products occurs significantly during the lignin depolymerization reactions (Bai et al., 2014). There have been many proposed reaction networks to explain these

FIGURE 1 | Lignin depolymerization and repolymerization scheme.
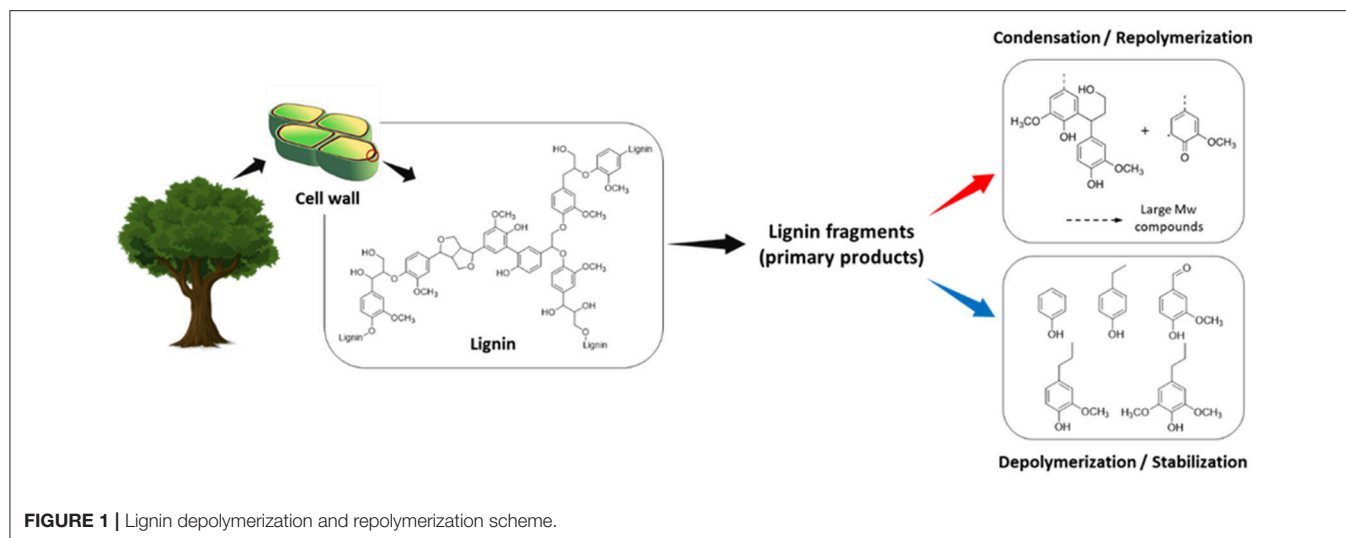
secondary condensation and repolymerization reactions. At high temperatures, the cleavage of abundant ether linkages (e.g., β-O-4 and α-O-4) in lignin can form highly reactive and unstable free radicals, with half-lives of $<10^{-3}$ s (Fossey et al., 1995). These radical species, in the early stage of the conversion process, can further react through rearrangement, abstraction and irreversible radical-radical coupling reactions to form large molecular weight products (Kim et al., 2017b).

As primary products, allyl- and vinyl-substituted intermediates (e.g., 4-vinylphenol, 2-methoxy-4-vinylphenol, isoeugenol, etc.) are produced from thermal lignin decomposition (Patwardhan et al., 2011; Ye et al., 2012). Because of their highly reactive nature toward polymerization and condensation reactions, rapid stabilization of reactive intermediates is required to prevent undesirable reactions, otherwise they readily repolymerize to form oligomers or even larger undesirable products (Hosoya et al., 2008; Bai et al., 2014; Kotake et al., 2014). Additionally, phenolic products with unsaturated carbonyl groups frequently found in lignin derivatives are prone to repolymerization (Shu et al., 2016).

Formaldehyde directly obtained from the cleavage of Cγ position at lignin side chains is also found to participate in repolymerization reactions between lignin decomposition products and char formation (Saisu et al., 2003; Huang et al., 2015). Considering the high reactivity of formaldehyde toward polymerization (e.g., phenol-formaldehyde resin), a cross-linking reaction between formaldehyde and phenolic fragments derived from lignin can readily occur resulting in the formation of large molecular weight products or char.

In addition to the lignin derived products or lignin fragments discussed above, some major functional groups in lignin are also key players in secondary reactions occurring in lignin decomposition. From the structural point of view, the Ar-OH group (free phenolic hydroxyl group) in lignin has gained much attention for its contribution to the secondary reactions due to its strong reactivity. The Ar-OH group is believed to be highly reactive toward electrophilic substitution reactions, and

it can form reactive quinone methide intermediates depending on the reaction conditions (Kim et al., 2017a). All these species are responsible for secondary repolymerization. Furthermore, methoxyl groups have also been demonstrated to influence on char formation during lignin pyrolysis (Hosoya et al., 2009).

There are multiple condensation and repolymerization pathways that form larger molecules or char, which include (1) radical coupling, (2) vinyl condensation, (3) reactive fragments (e.g., formaldehyde) involving polymerization, and (4) reactive functional group (e.g., Ar-OH) induced repolymerization reactions. Apparently, the solid products or char produced in lignin depolymerization results from the combination of above reaction pathways (Nakamura et al., 2007).

STRUCTURAL MODIFICATION OF LIGNIN

Although the exact structure of lignin still remains unclear, improvements in modern analytical techniques have elucidated some important structural features of lignin. These features include functional groups and inter-unit linkages from their formation and reaction networks involved in lignin depolymerization. Abundant functional groups typically found in the lignocellulosic biomass include methoxyl ($-OCH_3$), phenolic hydroxyl (Ar-OH), aliphatic hydroxyl, and carbonyl groups, depending on biomass species and extraction method (Chakar and Ragauskas, 2004). Among the different functional groups, the Ar-OH group has been of great interest to researchers since it is one of the most reactive functional groups in the lignin macromolecule (Kim et al., 2017a). Under both acidic and basic conditions, the primary products derived from lignin readily undergo facile addition and condensation reactions, forming high molecular weight products (Roberts et al., 2011). A recent study revealed that chemoselective masking of an Ar-OH group with a methyl group (Ar-OCH_3) can dramatically reduce quinone methide-induced secondary condensation reactions up to 50% (Kim et al., 2017a). *In-situ* detection of free radical

species, likely quinone methide radicals, using an electron paramagnetic resonance spectroscopy, elucidated that radical-induced reactions are involved in lignin depolymerization. If the Ar-OH is blocked by other groups, lignin cannot form quinone methide intermediates, which reduces repolymerization reactions. Even under pyrolysis conditions, selective methylation of Ar-OH enhances the production of aromatic hydrocarbon and inhibits secondary undesirable reactions (Kim J. Y et al., 2018). Ethanol is also found to be an effective reagent in suppressing char formation. In the lignin depolymerization with supercritical ethanol, ethanol not only acts as a hydrogen-donor solvent to stabilize the primary products, but it also forms O-alkylation of Ar-OH groups suppressing repolymerization reactions (Huang et al., 2014).

Another approach to enhance the yield of low molecular weight aromatic compounds is to oxidize lignin prior to the depolymerization reaction. A previous computational study indicated that the bond dissociation energy of the C_β-O bond in β-O-4 linkages in lignin structure is substantially decreased (∼14 kcal/mol) upon the oxidation of the Cα and Cγ (Kim et al., 2011). Thus, it has been hypothesized that the selective oxidation of lignin side chains could increase the cleavage of the most frequent β-O-4 linkages. Rahimi and coworkers focused on selective oxidation of the secondary benzylic alcohol to ketone at the Cα position using 4-acetamido-TEMPO, and the subsequent mild depolymerization with aqueous formic acid resulted in more than 60 wt% yield of phenolic monomers (Rahimi et al., 2013, 2014). Selective lignin oxidation enables the benzylic carbonyl group to polarize the C–H bond and lower the barrier for the rate-limiting elimination reaction during lignin depolymerization, producing more monoaromatic products. Another tests with model compounds demonstrated lignin degradation strategy by combining selective benzylic oxidation followed by catalytic C–O bond cleavage using zinc (Lancefield et al., 2015), NiMo sulfide (Zhang et al., 2017) or photocatalyst [Ir(ppy)$_2$(dtbbpy)]PF$_6$ (Nguyen et al., 2014).

More recently, a novel lignin extraction method that can prevent interunit C–C coupling while preserving aryl-ether (C–O) has been developed using formaldehyde (Shuai et al., 2016a). This effort aimed to strategically block the reactive benzylic positions with a protecting agent during lignin extraction. The addition of formaldehyde prevents lignin condensation reactions by forming 1,3-dioxane structures with –OH groups at the Cα and Cγ positions. The subsequent hydrogenolysis of structurally modified lignin results in near theoretical yields of monomers. Besides formaldehyde as a protecting agent, acetaldehyde and propionaldehyde were found to stabilize primary and secondary –OH groups at the lignin side chain (Lan et al., 2018). Hydrogenolysis of protected lignin significantly increased selectivity of final products (80% of 4-n-propanolsyringol).

It is also believed that the source of lignin (biomass origin) can affect the repolymerization reaction. For example, guaiacyl lignin (G unit) typically found in softwood lignin would be more susceptible to repolymerization and condensation reaction because it contains a greater proportion of unsubstituted C5 aromatic carbons. On the other hand, syringyl lignin (S unit), a main lignin unit in hardwood and herbaceous biomass contains relatively few condensed substructure, it would not undergo unwanted reactions significantly compared with G unit-rich lignins (Wariishi et al., 1991). New strategies including a selective substitution of open C5 aromatic carbons during the isolation of lignin can be considered before lignin depolymerization reactions.

The recent findings discussed above suggest that a slight structural modification of lignin can dramatically increase the valued products known as building block chemicals from lignin (**Figure 2**). Also this approach can be directed toward altering the biosynthesis process of lignin in the biomass cell wall to produce substrates that are more amenable to chemical depolymerization (Kim et al., 2017a).

FIGURE 2 | Chemoselective structural modification of lignin for maximizing the value.
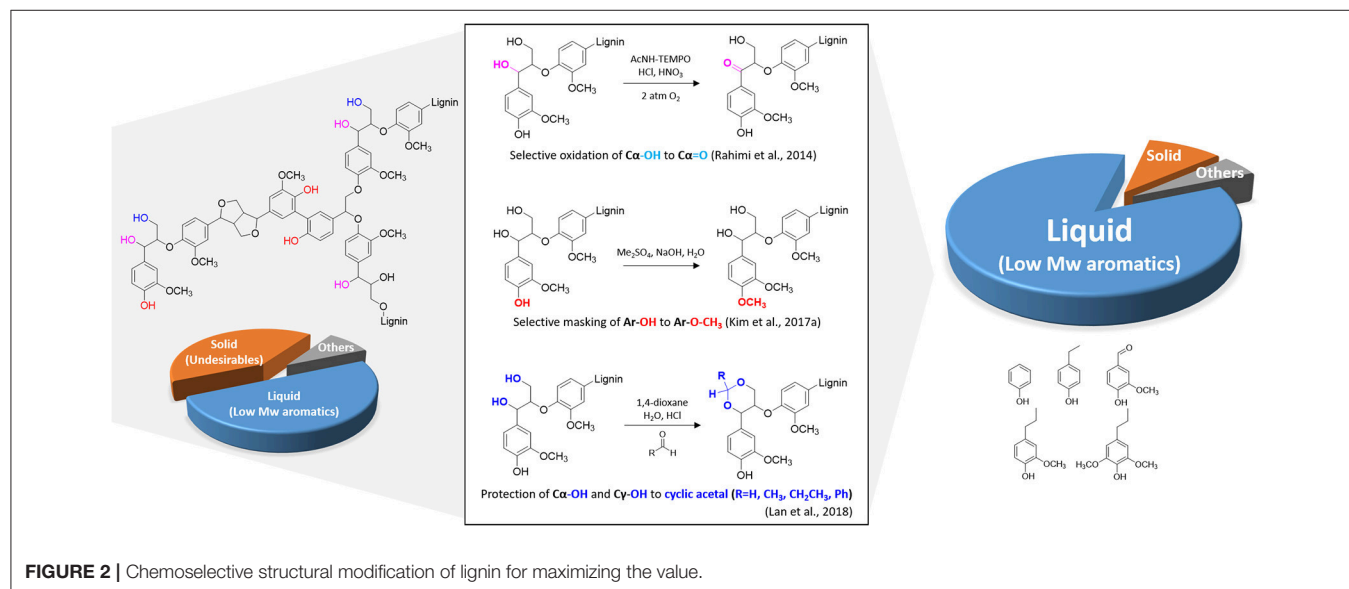
INTRODUCING CAPPING AGENTS

Researchers strategically introduced capping agents to stabilize the intermediates or reactive sites of lignin fragments. Boric acid has been used to protect the Ar-OH groups in the base-catalyzed lignin depolymerization (Roberts et al., 2011; Toledano et al., 2014a). Boric acid blocks addition and condensation reactions between the primary products by capping the Ar-OH groups with formation of boric esters (Roberts et al., 2011). The combination of base-catalyzed lignin breakdown and the boric acid as a protecting agent increases product yields (oil) to over 85 wt%. Based on the high reactivity of boric acid toward nucleophiles (Rietjens and Steenbergen, 2005), the addition of boric acid to lignin, a polymeric phenol, results in a strongly coordinated boric acid-lignin complex. This strong coordination can suppress the undesired reactions initiated from the reactive Ar-OH groups, although in-depth study is necessary to elucidate the detailed mechanisms.

Phenol has also been widely tested as a capping agent to stabilize phenolic moiety and formaldehyde. (Okuda et al., 2004; Yuan et al., 2010; Mahmood et al., 2013; Toledano et al., 2014a). Under the base-catalyzed lignin depolymerization reaction, the addition of phenol was able to reduce char and residual lignin, forming the production of a wide variety of phenolic compounds (Toledano et al., 2014a). Hydrolytic degradation of lignin under water-ethanol mixture in the presence of phenol as a capping agent reduced the char yield up to 70% (Yuan et al., 2010). However, it seems that the reaction conditions (i.e., reaction temperature, time and phenol to lignin ratio) need to be carefully controlled to maximize the conversion of lignin to low molecular weight products. Due to the highly reactive nature of phenol, it could lead to repolymerization reactions between the reactive sites of the combined phenol and the side chains of the lignin fragments, typically at higher temperature and longer reaction time.

A rapid quenching reactive radical species and unstable intermediates formed during depolymerization is another strategy to minimize the side reactions and produce low molecular weight phenols (Toledano et al., 2014b; Brittain et al., 2018). A hydrogenolytic approach of lignin with the assistance of an external hydrogen source and reducing catalysts is widely examined with an effort to quench the reactive intermediates and suppress the undesirable reactions. In principle, this approach employs hydrogens from molecular hydrogen or hydrogen donor solvents (e.g., ethanol, isopropyl alcohol, tetralin etc.) in the presence of metal catalysts (Ru, Pt, Pd, Ni, etc.). This strategy has been studied extensively and thoroughly reviewed elsewhere (Deuss and Barta, 2016; Sun et al., 2018).

SUMMARY AND PERSPECTIVES

Although there have been substantial efforts to identify the technical barriers for better utilization of lignins, the development of economically attractive processes is still challenging due to the complex nature of lignin. From the conventional pulp and paper industries to recent biorefineries, most of these processes significantly modify or damage lignin structure, which have restricted the yield of liquid oil and low molecular weight phenolic compounds to high level. Also, several undesirable reactions between the primary products to form large molecular weight oligomers or char during the lignin conversion process seem to be unavoidable. As discussed above, there are many contributing factors associated with inherent characteristics of lignin in this unwanted reaction network.

The history of lignin isolation and utilization traces back to the early 1900s, but researchers are still eagerly searching for effective lignin valorization methods. This highlights how lignin is definitely one of the most challenging materials to work with. To better utilize lignin, so that it brings benefits for future biorefineries, lignin valorization research has to be multidisciplinary. This multidisciplinary research may include computational modeling to calculate bond dissociation energy of linkages, plant science to engineer cell wall structures that are more amenable to chemical depolymerization, and chemistry along with process engineering to develop feedstock-agnostic biomass fractionation and depolymerization. Remembering the complex nature of lignin, there are still many unknown factors that affect the reaction network in lignin preparation and depolymerization, leaving opportunities for the scientific community to valorize lignin.

AUTHOR CONTRIBUTIONS

KK organized and prepared all this manuscript; CK contributed for writing and reviewing the part of the manuscript.

ACKNOWLEDGMENTS

REFERENCES

Bai, X., Kim, K. H., Brown, R. C., Dalluge, E., Hutchinson, C., Lee, Y. J., et al. (2014). Formation of phenolic oligomers during fast pyrolysis of lignin. *Fuel* 128, 170–179. doi: 10.1016/j.fuel.2014.03.013

Bouxin, F. P., McVeigh, A., Tran, F., Westwood, N. J., Jarvis, M. C., and Jackson, S. D. (2015). Catalytic depolymerisation of isolated lignins to fine chemicals using a Pt/alumina catalyst: part 1-impact of the lignin structure. *Green Chem.* 17, 1235–1242. doi: 10.1039/C4GC01678E

Brittain, A. D., Chrisandina, N. J., Cooper, R. E., Buchanan, M., Cort, J. R., Olarte, M. V., et al. (2018). Quenching of reactive intermediates during mechanochemical depolymerization of lignin. *Catal. Today* 302, 180–189. doi: 10.1016/j.cattod.2017.04.066

Chakar, F. S., and Ragauskas, A. J. (2004). Review of current and future softwood kraft lignin process chemistry. *Ind. Crops Prod.* 20, 131–141. doi: 10.1016/j.indcrop.2004.04.016

Deuss, P. J., and Barta, K. (2016). From models to lignin: transition metal catalysis for selective bond cleavage reactions. *Coord. Chem. Rev.* 306, 510–532. doi: 10.1016/j.ccr.2015.02.004

Dutta, T., Isern, N. G., Sun, J., Wang, E., Hull, S., Cort, J. R., et al. (2017). Survey of lignin-structure changes and depolymerization during ionic liquid pretreatment. *ACS Sust. Chem. Eng.* 5, 10116–10127. doi: 10.1021/acssuschemeng.7b02123

Fossey, J., Lefort, D., and Sorba, J. (1995). *Free Radicals in Organic Chemistry*. Paris: Wiley.

Grabber, J. H. (2005). How do lignin composition, structure, and cross-linking affect degradability? A review of cell wall model studies. *Crop Sci.* 45, 820–831. doi: 10.2135/cropsci2004.0191

Himmel, M. E. (2009). *Biomass Recalcitrance: Deconstructing the Plant Cell Wall for Bioenergy*. Oxford, UK: Wiley-Blackwell.

Hosoya, T., Kawamoto, H., and Saka, S. (2008). Secondary reactions of lignin-derived primary tar components. *J. Anal. Appl. Pyrolysis* 83, 78–87. doi: 10.1016/j.jaap.2008.06.003

Hosoya, T., Kawamoto, H., and Saka, S. (2009). Role of methoxyl group in char formation from lignin-related compounds. *J. Anal. Appl. Pyrolysis* 84, 79–83. doi: 10.1016/j.jaap.2008.10.024

Huang, X., Korányi, T. I., Boot, M. D., and Hensen, E. J. (2014). Catalytic depolymerization of lignin in supercritical ethanol. *ChemSusChem* 7, 2276–2288. doi: 10.1002/cssc.201402094

Huang, X., Korányi, T. I., Boot, M. D., and Hensen, E. J. (2015). Ethanol as capping agent and formaldehyde scavenger for efficient depolymerization of lignin to aromatics. *Green Chem.* 17, 4941–4950. doi: 10.1039/C5GC01120E

Kim, J. Y., Heo, S., and Choi, J. W. (2018). Effects of phenolic hydroxyl functionality on lignin pyrolysis over zeolite catalyst. *Fuel* 232, 81–89. doi: 10.1016/j.fuel.2018.05.133

Kim, K. H., Dutta, T., Sun, J., Simmons, B., and Singh, S. (2018). Biomass pretreatment using deep eutectic solvents from lignin derived phenols. *Green Chem.* 20, 809–815. doi: 10.1039/C7GC03029K

Kim, K. H., Dutta, T., Walter, E. D., Isern, N. G., Cort, J. R., Simmons, B. A., et al. (2017a). Chemoselective methylation of phenolic hydroxyl group prevents quinone methide formation and repolymerization during lignin depolymerization. *Acs Sust. Chem. Eng.* 5, 3913–3919. doi: 10.1021/acssuschemeng.6b03102

Kim, K. H., Singh, S., Custodis, V., and van Bokhoven, J. (2017b). "Role of free radicals in fast pyrolysis," in *Fast Pyrolysis of Biomass* (London, UK), 117–137.

Kim, S., Chmely, S. C., Nimos, M. R., Bomble, Y. J., Foust, T. D., Paton, R. S., et al. (2011). Computational study of bond dissociation enthalpies for a large range of native and modified lignins. *J. Phys. Chem. Lett.* 2, 2846–2852. doi: 10.1021/jz201182w

Kotake, T., Kawamoto, H., and Saka, S. (2014). Mechanisms for the formation of monomers and oligomers during the pyrolysis of a softwood lignin. *J. Anal. Appl. Pyrolysis* 105, 309–316. doi: 10.1016/j.jaap.2013.11.018

Lan, W., Amiri, M. T., Hunston, C. M., and Luterbacher, J. S. (2018). Protection group effects during alpha, gamma-diol lignin stabilization promote high-selectivity monomer production. *Angew. Chem. Int. Edn.* 57, 1356–1360. doi: 10.1002/anie.201710838

Lancefield, C. S., Ojo, O. S., Tran, F., and Westwood, N. J. (2015). Isolation of functionalized phenolic monomers through selective oxidation and C-O bond cleavage of the beta-O-4 linkages in lignin. *Angew. Chem. Int. Edn.* 54, 258–262. doi: 10.1002/anie.201409408

Luterbacher, J. S., Azarpira, A., Motagamwala, A. H., Lu, F., Ralph, J., and Dumesic, J. A. (2015). Lignin monomer production integrated into the γ-valerolactone sugar platform. *Energy Env. Sci.* 8, 2657–2663. doi: 10.1039/C5EE01322D

Luterbacher, J. S., Rand, J. M., Alonso, D. M., Han, J., Youngquist, J. T., Maravelias, C. T., et al. (2014). Nonenzymatic sugar production from biomass using biomass-derived γ-valerolactone. *Science* 343, 277–280. doi: 10.1126/science.1246748

Mahmood, N., Yuan, Z. S., Schmidt, J., and Xu, C. B. (2013). Production of polyols via direct hydrolysis of kraft lignin: effect of process parameters. *Bioresour. Technol.* 139, 13–20. doi: 10.1016/j.biortech.2013.03.199

Nakamura, T., Kawamoto, H., and Saka, S. (2007). Condensation reactions of some lignin related compounds at relatively low pyrolysis temperature. *J. Wood Chem. Technol.* 27, 121–133. doi: 10.1080/02773810701515143

Nguyen, J. D., Matsuura, B. S., and Stephenson, C. R. J. (2014). A Photochemical strategy for lignin degradation at room temperature. *J. Am. Chem. Soc.* 136, 1218–1221. doi: 10.1021/ja4113462

Okuda, K., Umetsu, M., Takami, S., and Adschiri, T. (2004). Disassembly of lignin and chemical recovery–rapid depolymerization of lignin without char formation in water-phenol mixtures. *Fuel Process. Technol.* 85, 803–813. doi: 10.1016/j.fuproc.2003.11.027

Patwardhan, P. R., Brown, R. C., and Shanks, B. H. (2011). Understanding the fast pyrolysis of lignin. *ChemSusChem* 4, 1629–1636. doi: 10.1002/cssc.201100133

Pielhop, T., Larrazabal, G. O., Studer, M. H., Brethauer, S., Seidel, C. M., and von Rohr, P. R. (2015). Lignin repolymerisation in spruce autohydrolysis pretreatment increases cellulase deactivation. *Green Chem.* 17, 3521–3532. doi: 10.1039/C4GC02381A

Ragauskas, A. J., Beckham, G. T., Biddy, M. J., Chandra, R., Chen, F., Davis, M. F., et al. (2014). Lignin valorization: improving lignin processing in the biorefinery. *Science* 344:1246843. doi: 10.1126/science.1246843

Rahimi, A., Azarpira, A., Kim, H., Ralph, J., and Stahl, S. S. (2013). Chemoselective metal-free aerobic alcohol oxidation in lignin. *J. Am. Chem. Soc.* 135, 6415–6418. doi: 10.1021/ja401793n

Rahimi, A., Ulbrich, A., Coon, J. J., and Stahl, S. S. (2014). Formic-acid-induced depolymerization of oxidized lignin to aromatics. *Nature* 515, 249. doi: 10.1038/nature13867

Rietjens, M., and Steenbergen, P. A. (2005). Crosslinking mechanism of boric acid with diols revisited. *Eur. J. Inorg. Chem.* 2005, 1162–1174. doi: 10.1002/ejic.200400674

Roberts, V. M., Stein, V., Reiner, T., Lemonidou, A., Li, X. B., and Lercher, J. A. (2011). Towards quantitative catalytic lignin depolymerization. *Chem. Eur. J.* 17, 5939–5948. doi: 10.1002/chem.201002438

Saisu, M., Sato, T., Watanabe, M., Adschiri, T., and Arai, K. (2003). Conversion of lignin with supercritical water–phenol mixtures. *Energy Fuels* 17, 922–928. doi: 10.1021/ef0202844

Shi, J., Balamurugan, K., Parthasarathi, R., Sathitsuksanoh, N., Zhang, S., Stavila, V., et al. (2014). Understanding the role of water during ionic liquid pretreatment of lignocellulose: co-solvent or anti-solvent? *Green Chem.* 16, 3830–3840. doi: 10.1039/C4GC00373J

Shi, J., Pattathil, S., Parthasarathi, R., Anderson, N. A., Im Kim, J., Venketachalam, S., et al. (2016). Impact of engineered lignin composition on biomass recalcitrance and ionic liquid pretreatment efficiency. *Green Chem.* 18, 4884–4895. doi: 10.1039/C6GC01193D

Shu, R., Long, J., Xu, Y., Ma, L., Zhang, Q., Wang, T., et al. (2016). Investigation on the structural effect of lignin during the hydrogenolysis process. *Bioresour. Technol.* 200, 14–22. doi: 10.1016/j.biortech.2015.09.112

Shuai, L., Amiri, M. T., Questell-Santiago, Y. M., Heroguel, F., Li, Y. D., Kim, H., et al. (2016a). Formaldehyde stabilization facilitates lignin monomer production during biomass depolymerization. *Science* 354, 329–333. doi: 10.1126/science.aaf7810

Shuai, L., Questell-Santiago, Y. M., and Luterbacher, J. S. (2016b). A mild biomass pretreatment using γ-valerolactone for concentrated sugar production. *Green Chem.* 18, 937–943. doi: 10.1039/C5GC02489G

Sun, J., Konda, N. M., Shi, J., Parthasarathi, R., Dutta, T., Xu, F., et al. (2016). CO$_2$ enabled process integration for the production of cellulosic ethanol using bionic liquids. *Energy Environ. Sci.* 9, 2822–2834. doi: 10.1039/C6EE00913A

Sun, Z. H., Fridrich, B., de Santi, A., Elangovan, S., and Barta, K. (2018). Bright side of lignin depolymerization: toward new platform chemicals. *Chem. Rev.* 118, 614–678. doi: 10.1021/acs.chemrev.7b00588

Toledano, A., Serrano, L., and Labidi, J. (2014a). Improving base catalyzed lignin depolymerization by avoiding lignin repolymerization. *Fuel* 116, 617–624. doi: 10.1016/j.fuel.2013.08.071

Toledano, A., Serrano, L., Pineda, A., Romero, A. A., Luque, R., and Labidi, J. (2014b). Microwave-assisted depolymerisation of organosolv lignin via mild hydrogen-free hydrogenolysis: catalyst screening. *Appl. Catal. B Environ.* 145, 43–55. doi: 10.1016/j.apcatb.2012.10.015

Wariishi, H., Valli, K., and Gold, M. H. (1991). *In vitro* depolymerization of lignin by manganese peroxidase of Phanerochaete chrysosporium. *Biochem. Biophys. Res. Commun.* 176, 269–275. doi: 10.1016/0006-291X(91)90919-X

Weidener, D., Klose, H., Leitner, W., Schurr, U., Usadel, B., Domínguez de María, P., et al. (2018). One-step lignocellulose fractionation using 2,5-furandicarboxylic acid as biogenic and recyclable catalyst. *ChemSusChem.* 11:2051–2056. doi: 10.1002/cssc.201800653

Xu, C. P., Arancon, R. A. D., Labidi, J., and Luque, R. (2014). Lignin depolymerisation strategies: towards valuable chemicals and fuels. *Chem. Soc. Rev.* 43, 7485–7500. doi: 10.1039/C4CS00235K

Xu, F., Sun, J., Konda, N. M., Shi, J., Dutta, T., Scown, C. D., et al. (2016). Transforming biomass conversion with ionic liquids: process intensification and the development of a high-gravity, one-pot process for the production of cellulosic ethanol. *Energy Environ. Sci.* 9, 1042–1049. doi: 10.1039/C5EE02940F

Xu, F., Sun, J., Wehrs, M., Kim, K. H., Rau, S. S., Chan, A. M., et al. (2018). Biocompatible choline-based deep eutectic solvents enable one-pot production of cellulosic ethanol. *ACS Sust. Chem. Eng.* 6, 8914–8919. doi: 10.1021/acssuschemeng.8b01271

Ye, Y., Fan, J., and Chang, J. (2012). Effect of reaction conditions on hydrothermal degradation of cornstalk lignin. *J. Anal. Appl. Pyrolysis* 94, 190–195. doi: 10.1016/j.jaap.2011.12.005

Yuan, Z. S., Cheng, S. N., Leitch, M., and Xu, C. B. (2010). Hydrolytic degradation of alkaline lignin in hot-compressed water and ethanol. *Bioresour. Technol.* 101, 9308–9313. doi: 10.1016/j.biortech.2010.06.140

Zakzeski, J., Bruijnincx, P. C., Jongerius, A. L., and Weckhuysen, B. M. (2010). The catalytic valorization of lignin for the production of renewable chemicals. *Chem. Rev.* 110, 3552–3599. doi: 10.1021/cr900354u

Zakzeski, J., Jongerius, A. L., Bruijnincx, P. C., and Weckhuysen, B. M. (2012). Catalytic lignin valorization process for the production of aromatic chemicals and hydrogen. *ChemSusChem* 5, 1602–1609. doi: 10.1002/cssc.201100699

Zhang, C. F., Li, H. J., Lu, J. M., Zhang, X. C., MacArthur, K. E., Heggen, M., et al. (2017). Promoting lignin depolymerization and restraining the condensation via an oxidation-hydrogenation strategy. *ACS Catal.* 7, 3419–3429. doi: 10.1021/acscatal.7b00148

High Catalytic Efficiency of Lignin Depolymerization over Low Pd-Zeolite Y Loading at Mild Temperature

Yuling Qin[1], Hongliang Wang[1], Hao Ruan[1], Maoqi Feng[2] and Bin Yang[1]*

[1] Bioproducts, Sciences and Engineering Laboratory, Department of Biological Systems Engineering, Washington State University, Richland, WA, United States, [2] Chemistry and Chemical Engineering Division, Southwest Research Institute, San Antonio, TX, United States

This article reported a novel low-temperature process for aromatics production through lignin depolymerization catalyzed by 0.1 wt% Pd-zeolite Y catalyst prepared by a facile method. Under the same reactive condition, the as-prepared Pd-zeolite Y catalysts exhibited much higher catalytic efficiency than zeolite Y or commercial Pd/Al$_2$O$_3$–zeolite composites. The selectivity of the Pd-zeolite Y toward lignin depolymerization was also much higher than the other commercial zeolite-based catalysts. With the presence of hydrogen, aromatics were the predominant products with high yields of phenols and dimers (over 99%). The as-obtained aromatics can be promising feedstock for production of fuels or chemicals for various applications. Results revealed that the Pd-zeolite Y catalyst is a highly active catalyst for the cleavage of lignin interlinkages, especially the C–O–C bonds by hydrogenolysis.

Keywords: lignin conversion, biomass, Pd, zeolite, phenols, aromatics, high efficiency and selectivity
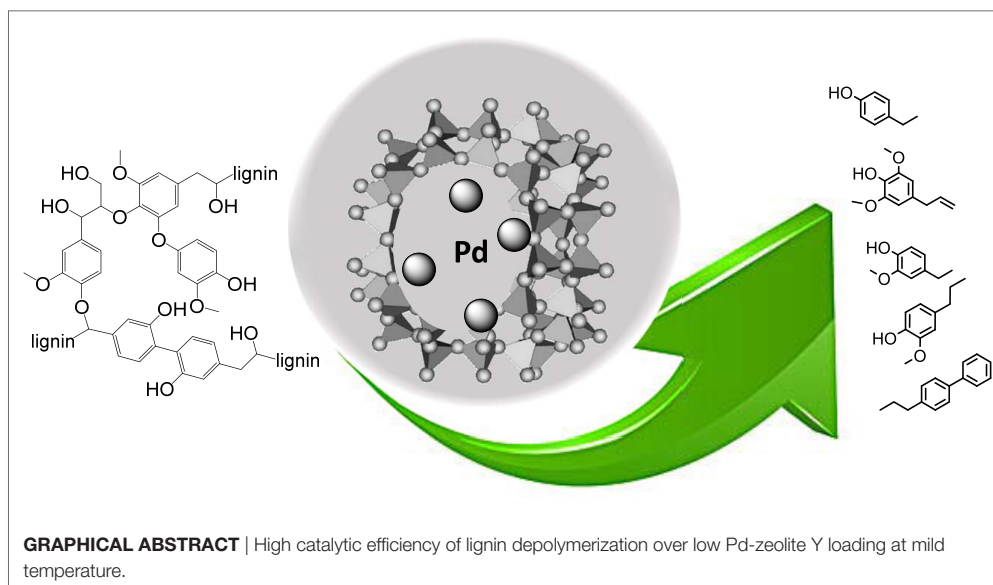
GRAPHICAL ABSTRACT | High catalytic efficiency of lignin depolymerization over low Pd-zeolite Y loading at mild temperature.

INTRODUCTION

Catalytic conversion of biomass lignin into value-added chemicals and fuels is a promising route to resolve the energy crisis (Jae et al., 2010; Ragauskas et al., 2014; Kong et al., 2015; Wang et al., 2016). Nevertheless, state-of-the-art lignin utilization technologies still face tremendous challenges, including depolymerization and upgradation, especially the catalytic depolymerization process (Alonso et al., 2010; Xu et al., 2014; Li et al., 2015; Yang et al., 2015). Among various catalysts for lignin depolymerization, zeolites are widely accepted due to their low-cost, high surface area, and outstanding acid sites catalytic performance (Taarning et al., 2011; Ben and Ragauskas, 2012; Wang et al., 2017). External Brønsted acidity in meso-/microporous zeolites was reported to effectively affect the selectivity of de-alkylation and de-etherification reactions in parallel during lignin conversion (Taarning et al., 2011; Singh and Ekhe, 2014; Deepa and Dhepe, 2015). Deepa reported that aromatic monomers were the predominant products using zeolite as solid acid catalysts for lignin depolymerization at 250°C in H_2O/CH_3OH mixture (Deepa and Dhepe, 2015).

However, challenges remain for catalytic lignin depolymerization by zeolites because the current zeolite-based catalysis requires high temperature (250°C or above), which leads to faster catalyst deactivation by coking and dealumination (Jia et al., 2011). Furthermore, the high temperature for solid acid-catalyzed lignin hydrolysis process possibly results in extensive side products from condensation reactions (Jia et al., 2011; Li et al., 2015). Therefore, the development of low-cost zeolite-based catalysts for lignin conversion at mild temperature will enhance lignin conversion to valuable products.

A group of catalysts with a combination of zeolite and noble metal nanoparticles drew increasing attention due to their excellent catalytic activity in lignin degradation. For example, lignin degradation and/or hydrodeoxygenation reaction were reportedly enhanced by a combination of Pt, Ru, and Pd nanoparticles supported on zeolites (Laskar et al., 2014; Wang et al., 2015). However, the complexity of the preparation of these catalysts hinders their further application.

Combining the outstanding catalytic performance of zeolites and metals, metal-exchanged zeolites potentially have higher activity than non-exchanged zeolites (Hui et al., 2010; Singh et al., 2015). The Pd metal in Pd-zeolites can become reactive sites for the cleavage of lignin bonds due to its high hydrogen-activation ability. Notably, Pd^{2+} ions exchanged on the zeolite frameworks appeared highly stable against metal agglomeration while maintaining high catalytic activities in hydrogen atmosphere (Choi et al., 2009). It was proposed that the catalytic reactions were carried out by the Pd(0) species, which was generated *in situ* under the tested reaction conditions. Furthermore, because of the strong metal-catalyst support interaction and pore limitation, the catalysts were reportedly stable in the zeolite pore without agglomeration (Zhang et al., 2014a).

In this study, the Pd-zeolite Y catalysts were prepared *via* both the facile and maneuverable ion-exchange methods for depolymerizing lignin at relatively low temperatures (180–200°C). We studied catalytic activity and selectivity of these catalysts on depolymerization of alkali lignin compare with zeolite alone and

commercial Pd/Al$_2$O$_3$–zeolite composite catalysts (with more Pd loading) and Pd-zeolite Y catalyst (with the synergistic effect of palladium and zeolite Y). The mechanism of Pd-zeolite catalysis of lignin conversion was explored. It was found that the high efficiency of surficial Pd atoms and the synergistic effects between Pd and zeolite Y played critical roles in lignin depolymerization and conversion.

EXPERIMENTAL

Preparation of Pd-Zeolite Y

CBV 300 purchased from Zeolyst International was heated in air at 550°C for 5 h. $Pd(NO_3)_2$ (Aldrich) was dissolved in diluted aqueous HNO_3 (0.01 M) solution. Then 1 g of zeolite (CBV300) was dispersed into 50 mL of water solution by stirring, followed by adding aqueous $Pd(NO_3)_2$ solution [containing 5 mg of $Pd(NO_3)_2$]. Stirring continued for 30 min. Then 20 mg of NH_4NO_3 was added, followed by stirring for another 2 h. The mixture was then centrifuged and thoroughly washed with distilled water. The precipitate was dried at room temperature before catalytic reaction tests. Commercial Pd/C (5 wt%) was purchased from Aldrich.

Lignin Depolymerization in a Parr Reactor

For a typical catalytic depolymerization experiment, 30 mL of deionized water was added into a 100 mL Parr reactor as solvent for the reaction, followed by adding 200 mg of lignin and 200 mg of Pd-zeolite catalysts. After sealing the vessel, H$_2$ was used to flush out the air in the reactor at least four times, and then the reactor was pressurized to 3.5 MPa at room temperature. The reactor was heated to reach the reaction temperature (180–200°C) where the reaction time was started. The reaction was conducted for 3 h. Then the vessel was plunged into cold water to cool the reaction system. Ethyl acetate was used to extract products while the 0.5 wt% of toluene (in ethyl acetate) was added as an internal standard. Then a sample was acquired from the organic phase for GC–MS analysis. For GC–MS analysis, the response factor for each product was standardized with the use of efficient carbon number (Scanion and Willis, 1985; Zhang et al., 2014b), which enabled the analysis of compounds without pure standards.

GC–MS Analysis and Structural Analysis of Catalysts

After ethyl acetate extraction, the organic phase was analyzed by GC–MS. 1 µL of sample was injected with 0.6 mL/min of He (carrier gas) into a DB-5 (30 m length × 250 µm I.D. × 0.25 µm film thickness, J&W Scientific) capillary column installed in an Agilent Technologies 7890A GC that was set at splitless mode. The GC oven was set to maintain 45°C for 2 min, then heated to 200°C at the rate of 15°C/min then held at 200°C for another 1 min. After that, the oven was heated up to 300°C at the rate of 10°C/min and held for 5 min. Eluting compounds were determined using a MS (Agilent Technologies 5975C) inter XL EI/CI MSD with a triple axis detector and matched to NIST GC–MS libraries (Wang et al., 2017).
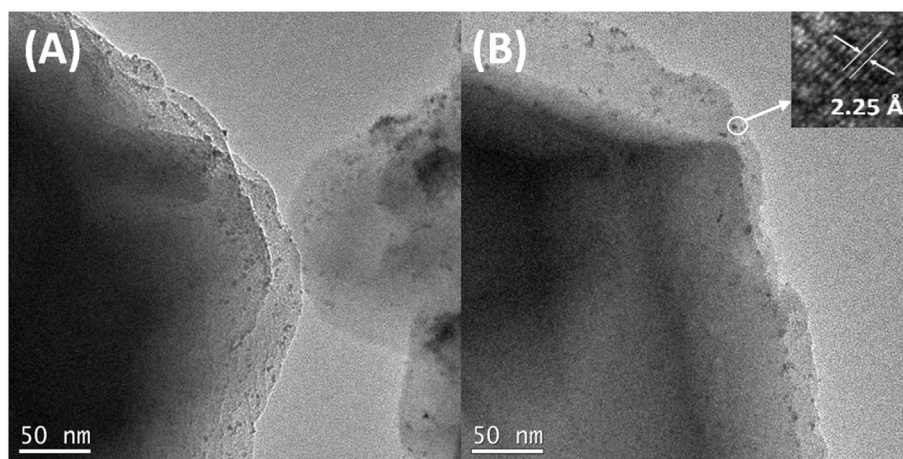
FIGURE 1 | Transmission electron microscopy images of Pd-zeolite Y before (A) and after (B) H_2 treatment under 200°C. Inset in panel (B): high-resolution transmission electron microscopy image of Pd nanoparticle on zeolite Y.

Scanning electron microscopy (SEM) analysis was performed using a field emission SEM instrument (Hitachi S-4800), operating at an accelerating voltage of 10 kV. Transmission electron microscope analysis was performed using an FEI Tecnai G2 S-Twin instrument with a field emission gun operating at 200 kV. Inductively coupled plasma atomic emission spectroscopy (ICP-AES) measurements were performed on a Thermo Jarrell Ash Atom scan Advantage instrument.

Equations

The mass yield of each product and its selectivity from lignin depolymerization were calculated as follows:

$$Yield_x(wt\%) = \frac{\dfrac{Mass\ of\ toluene}{92} \times \dfrac{area_x/ECN_x}{area\ of\ toluene/7} \times MW_x}{Mass\ of\ lignin},$$

$$Selectivity_x = \frac{Yield_x}{Yield\ of\ total\ calculated\ products} \times 100\%,$$

$$Toal\ product\ yield = \sum_{n=1}^{7} Yield_{x_n}.$$

RESULTS AND DISCUSSION

Transmission electron microscopy (TEM) image in **Figure 1A** shows that Pd-precursor dispersed very well on the surface of zeolite Y, which could enhance lignin degradation because the macromolecular lignin depolymerization reacts on the surface of the zeolite. In this study, the commercial zeolite Y, Zeolyst CBV 300, was used as a support for Pd after thermal treatment. Clearly, Pd-precursor nanoparticles with small particle size were evenly dispersed on the zeolite, while the smaller particle size led to higher atom efficiency. As seen in **Figure 1B**, after the H_2 treatment at 200°C, Pd^{2+} was successfully reduced into Pd(0) *in situ* while no obvious aggregation of Pd was found. Furthermore, the
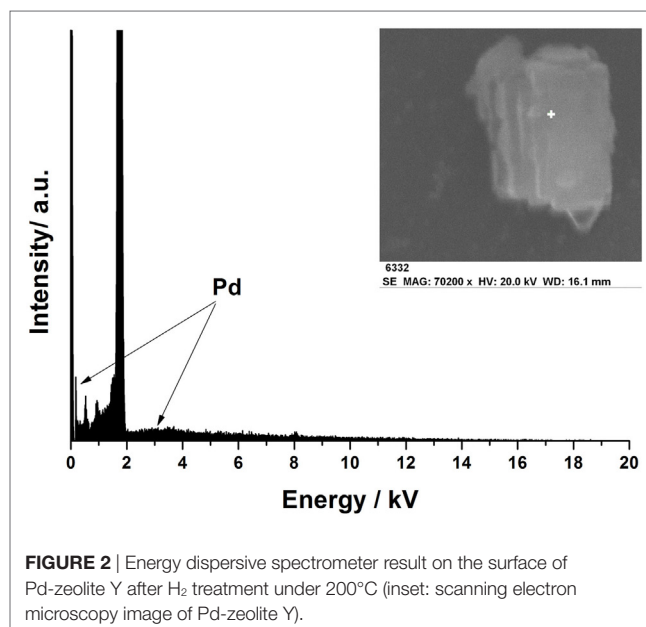
FIGURE 2 | Energy dispersive spectrometer result on the surface of Pd-zeolite Y after H_2 treatment under 200°C (inset: scanning electron microscopy image of Pd-zeolite Y).

high-resolution transmission electron microscopy image of the as-obtained Pd(0) is shown in **Figure 1B** inset. The d-spacing of the nanoparticle is ~2.25 Å, which corresponds to the (111) of *fcc* Pd, indicating the existence of Pd(0). On the other hand, the ICP-AES results showed that the loading of Pd in Pd-zeolite was 0.1 wt%. Due to the very low Pd loading in this catalyst, it is difficult to use the X-ray diffraction spectroscopy or X-ray photoelectron spectroscopy to prove the existence of Pd in Pd-zeolite. Therefore, the energy dispersive spectrometer (from the inset scanning electron microscope image) was further employed for the characterization of Pd. As shown in **Figure 2**, Pd was found from the energy dispersive spectrometer results even if its loading was low. Although the loading of Pd was quite low, it significantly improved lignin depolymerization as proved in the following lignin conversion process.
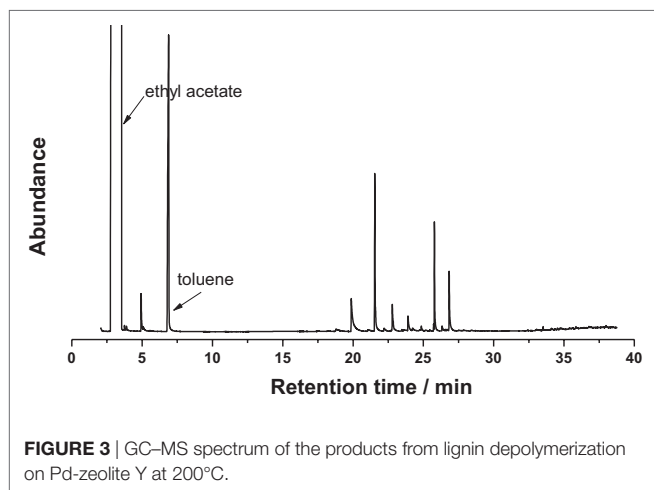
FIGURE 3 | GC–MS spectrum of the products from lignin depolymerization on Pd-zeolite Y at 200°C.
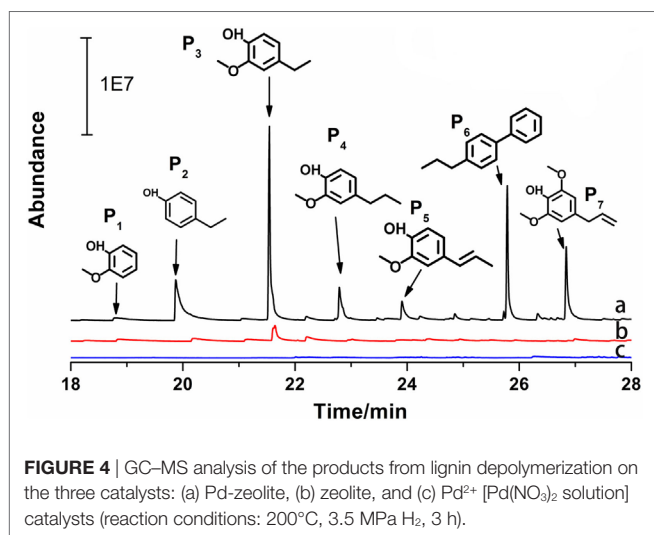
FIGURE 4 | GC–MS analysis of the products from lignin depolymerization on the three catalysts: (a) Pd-zeolite, (b) zeolite, and (c) Pd^{2+} [$Pd(NO_3)_2$ solution] catalysts (reaction conditions: 200°C, 3.5 MPa H_2, 3 h).

TABLE 1 | The major products from lignin conversion.

Number	Name	Formula	$Y_{Pd\text{-}zeolite}/Y_{zeolite}$
P_1	Phenol, 2-methoxy-		1.25
P_2	Phenol, 4-ethyl-		6.6
P_3	Phenol, 4-ethyl-2-methoxy-		4.6
P_4	Phenol, 2-methoxy-4-propyl-		2.8
P_5	Phenol, 2-methoxy-4-(1-propenyl)-,(E)-		–
P_6	4-Propyl-1,1′-diphenyl		–
P_7	Phenol, 2,6-dimethoxy-4-(2-propenyl)-		8.7

$Y_{Pd\text{-}zeolite}$: the yield of the product x (x = 1, 2, 3, …, 7) from lignin conversion over Pd-zeolite Y catalyst; $Y_{zeolite}$: the yield of the product x (x = 1, 2, 3, …, 7) from lignin conversion over zeolite Y catalyst; –: the value of $Y_{Pd\text{-}zeolite}/Y_{zeolite}$ was not calculated because the products from lignin conversion over zeolite were too low to be detected.

The GC–MS results of the products derived from catalytic lignin conversion are concentrated in 18–28 min interval (**Figure 3**). In Deepa's report (Deepa and Dhepe, 2015), lignin conversion generated wide range of products from 10 to 25 min. However, in this work, only seven products were detected by GC–MS, indicating much higher selectivity of this catalyst. Furthermore, as shown in **Figure 4**, phenols and substituted phenols, including guaiacols, phenol, and dimers, were the major products from lignin depolymerization on Pd-zeolite, indicating the high efficiency of the catalysts toward the cleavage of C_β–O–C and dehydroxylation on branched alkanes. In addition, no aromatic saturated products (i.e., cyclohexane and its derivatives) were observed, implying low catalytic activity of Pd-zeolite Y toward hydrogenation of aromatics. This results indicated that Pd-zeolite Y can be efficiently employed to selectively produce aromatics with wide applications in the production of useful chemicals from lignin.

Furthermore, Pd-zeolite Y showed much higher activity than both zeolite Y and Pd when they were applied separately, suggesting strong synergistic effects of Pd and zeolite Y on lignin depolymerization. Under the same reaction conditions, as shown in **Figure 4**, zeolite Y exhibited much lower catalytic activity than Pd-zeolite Y toward lignin degradation, while for Pd^{2+}, almost no lignin depolymerization products were detected. From **Table 1**, for the major products (P_2, P_3, and P_7), Pd-zeolite Y led to at least four times higher of product yields (P_2, P_3, and P_7) than commercial zeolite, indicating that the addition of Pd significantly improved lignin depolymerization. Specially, P_6 was only found in lignin depolymerization over Pd-zeolite but not over commercial zeolite.

Zeolites have been widely used as solid acid catalysts for lignin depolymerization. In this work, *in situ* generated Pd can be used as a new catalytic site for C–O–C bond cleavage in hydrogen atmosphere. With the addition of Pd as-prepared catalyst exhibited much higher activity than zeolite Y with sole H^+-sites for lignin depolymerization, probably due to the accessorial depolymerization caused by Pd induced hydrogenolysis reaction. However, without the acidic support of zeolite Y, Pd alone showed negligible catalytic activity on lignin depolymerization. It indicated that zeolite Y dramatically improved the hydrogenolysis activity of Pd. Similar synergetic effects of acids and noble metals on lignin depolymerization were reported in previous studies (Laskar et al., 2014; Zhang et al., 2014a; Wang et al., 2015). Except for OH and –OCH_3 bonds, no other O-content functional groups was found on the side chains of the products. It suggested that Pd-zeolite facilely removed "O" from the side chains of lignin through deoxygenation.

Based on the products in this work, potential reaction pathways to generate phenols and guaiacols are summarized in **Figure 5**. It was reported that the dehydration of Cα hydroxyl group in the side chains of lignin occurred first and formed a double carbon bond prior to β-O-4 bond cleavage (Jia et al., 2010).
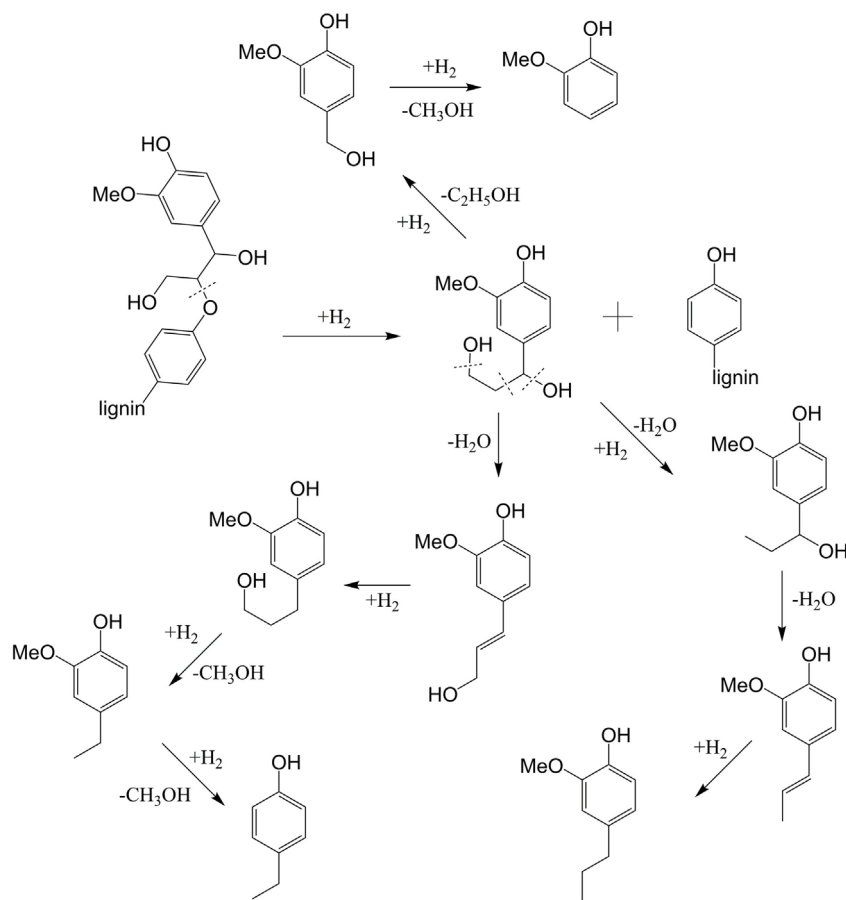
FIGURE 5 | Proposed reaction pathways for the formation of the major products from cleavage of the β-O-4 lignin.
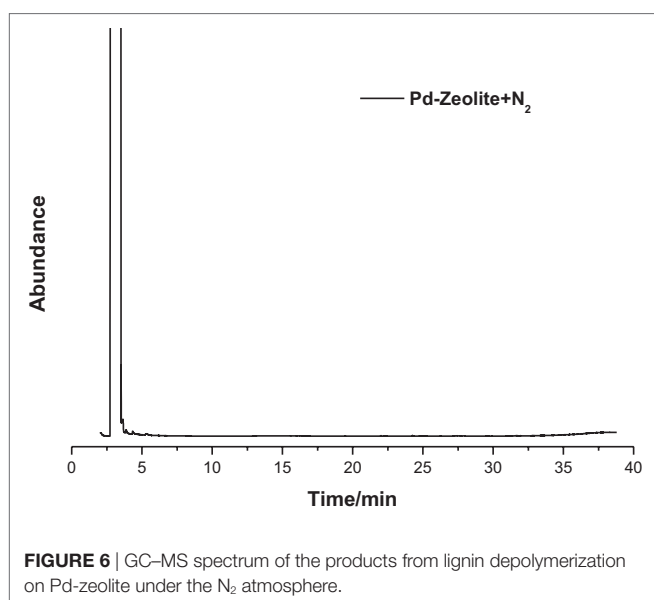
FIGURE 6 | GC–MS spectrum of the products from lignin depolymerization on Pd-zeolite under the N_2 atmosphere.

TABLE 2 | Percentage of lignin aromatic inter-unit linkages and the selectivity of the major products *via* Pd-zeolite Y catalysis.

Lignin inter-unit linkages (%)[a]				Major products selectivity (%)[b]						
β-O-4	β-5	β-β	β-1	P_1	P_2	P_3	P_4	P_5	P_6	P_7
43	44	9	4	2.9	19.9	28	10.3	5.4	17.8	15.7

[a]*Percentage data are from our previous NMR results, assuming β-O-4, β-5, β-β, and β-1 add up to 100%* (Wang et al., 2015).
[b]*Assuming products (P_1–P_7) add up to 100%.*

and Ni-based catalysts (Zakzeski and Weckhuysen, 2011; Song et al., 2012). For the next step, three routes can react in parallel. One route is to generate guaiacol (P_1, **Figure 5**) through removing the hydroxyl-containing side chains. The second route is the formation of a double bond through dehydration reaction of Cα, which can further generate P_3 (**Figure 5**) by hydrogenation. The methoxy group linked on the benzene ring can be activated by the adjacent hydroxyl group and converted into hydroxyl through demethylation and further generate phenol structure P_2 (**Figure 5**) (Peters et al., 2015). On the other hand, dehydroxylation may also happen on the Cγ position to generate P_5 and P_4 through further dehydration and hydrogenation reaction successively (Li et al., 2015). For product 6, biphenyl structure

However, in this work, the cleavage of β-O-4 bond can occur first because of the high hydrogen transferring ability of Pd, which is similar to the reaction path previously reported using Pt-based
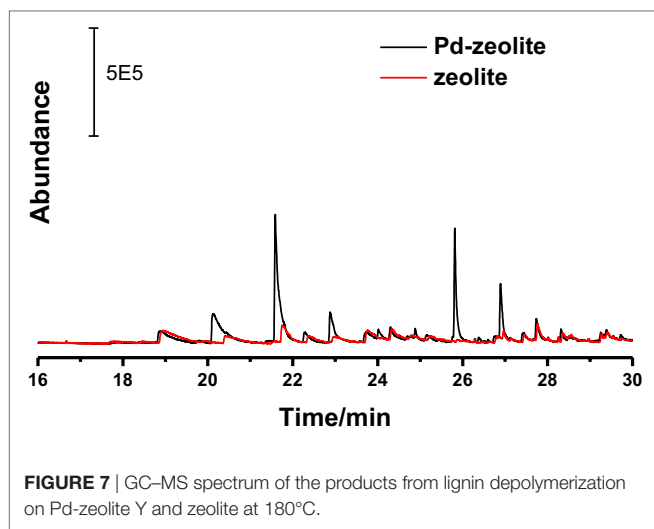
FIGURE 7 | GC–MS spectrum of the products from lignin depolymerization on Pd-zeolite Y and zeolite at 180°C.
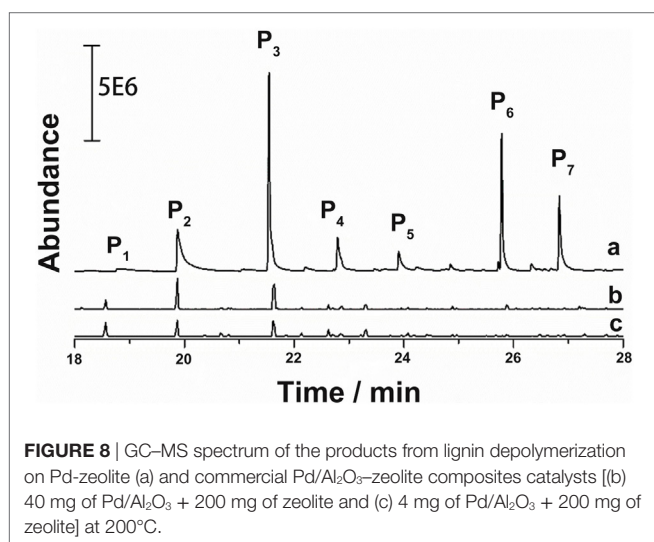
FIGURE 8 | GC–MS spectrum of the products from lignin depolymerization on Pd-zeolite (a) and commercial Pd/Al$_2$O$_3$–zeolite composites catalysts [(b) 40 mg of Pd/Al$_2$O$_3$ + 200 mg of zeolite and (c) 4 mg of Pd/Al$_2$O$_3$ + 200 mg of zeolite] at 200°C.

may be generated by coupling reaction between two aromatics (Hong et al., 2010).

Besides the catalysts as mentioned in the previous mechanism, hydrogen also plays a pivotal role in lignin depolymerization. From previous reports, lignin depolymerization in aqueous phase through hydrolysis by a solid acid catalyst is the dominant route (Taarning et al., 2011; Deepa and Dhepe, 2014). However, after Pd was loaded, results showed that hydrogenolysis was the principal route for bonds cleavage in hydrogen atmosphere at 200°C. To further verify the significant role of hydrogen in this depolymerization process, lignin conversion without hydrogen was performed. As shown in **Figure 6**, under the same temperature and catalyst conditions, almost no product was detected in the N$_2$ atmosphere. It is plausible that due to the existence of Pd, the hydrogen-activation ability was significantly increased, thus further promoted lignin conversion. While in the N$_2$ atmosphere, Pd-zeolite Y showed very low hydrolysis activity at

the relatively low temperature. On the other hand, the product selectivity was also different on Pd-zeolite from that on zeolite because of the different hydrogen reactive ability. For example, about 18% P$_6$ (**Table 2**) was obtained from Pd-zeolite while almost no obvious P$_6$ peak could be found in zeolite Y catalysis because Pd showed high activity toward coupling reactions to form biphenyls.

Furthermore, compositions of lignin inter-unit linkages obtained from NMR analysis and the major product selectivity are shown in **Table 2**. The alkali lignin used in this study was prepared and analyzed as reported in our previous work (Wang et al., 2015). Results suggested that the major products were divided into two categories: ~82% phenols and ~18% biphenyls. More than half (56.8%) of the phenols were guaiacols, indicating the high preeminent selectivity of Pd-zeolite toward lignin degradation. The catalytic performance of Pd-zeolite Y and zeolite Y alone toward lignin degradation at even lower temperature (180°C, initial H$_2$ pressure 3.5 MPa) was studied. As shown in **Figure 7**, similar products selectivity was obtained on Pd-zeolite Y as compared with the reaction under 200°C, and the products P$_1$–P$_7$ were clearly observed. Pd-zeolite Y still exhibited much better catalytic performance than zeolite at 180°C. Results indicated that lignin was depolymerized at the temperature as low as 180°C.

Lignin depolymerization on the state-of-the-art commercial Pd/Al$_2$O$_3$–zeolite composites catalysts with equal amount of Pd and zeolite was tested to compare with the catalytic performance of Pd-zeolite Y. As shown in **Figure 8**, 4 mg of Pd/Al$_2$O$_3$ (0.2 mg Pd) with 200 mg of zeolite displayed much lower catalytic activity than Pd-zeolite. Generation of P$_1$–P$_7$ products remained similar even with 10 times Pd/Al$_2$O$_3$ loading, which proves the high Pd atom efficiency of the Pd-zeolite Y catalyst developed in this study. From the abovementioned TEM images (**Figure 1**), it is observed that the particle size of the Pd is quite small, corresponding to the "atom economy" catalysis. The high catalytic activity of Pd-zeolite Y can be attributed to the high efficiency of surficial Pd atoms and the synergistic effects between Pd and zeolite Y.

CONCLUSION

Herein, we demonstrated that the Pd-zeolite Y catalysts prepared *via* the facile method were effective catalysts to depolymerize lignin to phenols and phenol derivatives at 99% yield. Due to the synergistic effects, Pd-zeolite led to much higher total yield of products than non-metalized zeolite or Pd^{2+} did when applied separately. In addition to catalysts, hydrogen was proved to have a critical role in lignin depolymerization. Although the as-prepared Pd-zeolite Y exhibited excellent catalytic performance toward the cleavage of ether bonds, its dehydroxylation and demethoxylation (on benzene) performance needs further improvement. Taking the advantage of the synergy effect of palladium and zeolite Y, the Pd-zeolite Y catalyst in this study could be more cost effective and efficient than many other previously reported catalysts for conversion of lignin to value-added chemicals and fuels.

REFERENCES

Alonso, D. M., Bond, J. Q., and Dumesic, J. A. (2010). Catalytic conversion of biomass to biofuels. *Green Chem.* 12, 1493–1513. doi:10.1039/c004654j

Ben, H., and Ragauskas, A. J. (2012). In situ NMR characterization of pyrolysis oil during accelerated aging. *RSC Adv.* 2, 12892–12898. doi:10.1039/c2ra22616b

Choi, M., Lee, D. H., Na, K., Yu, B. W., and Ryoo, R. (2009). High catalytic activity of palladium(II)-exchanged mesoporous sodalite and NaA zeolite for bulky aryl coupling reactions: reusability under aerobic conditions. *Angew. Chem. Int. Ed. Engl.* 121, 3727–3730. doi:10.1002/anie.200806334

Deepa, A. K., and Dhepe, P. L. (2014). Solid acid catalyzed depolymerization of lignin into value added aromatic monomers. *RSC Adv.* 2014, 12625–12629. doi:10.1039/c3ra47818a

Deepa, A. K., and Dhepe, P. L. (2015). Lignin depolymerization into aromatic monomers over solid acid catalysts. *ACS Catal.* 5, 365–379. doi:10.1021/cs501371q

Hong, D. Y., Miller, S. J., Agrawal, P. K., and Jones, C. W. (2010). Hydrodeoxygenation and coupling of aqueous phenolics over bifunctional zeolite-supported metal catalysts. *Chem. Commun.* 46, 1038–1040. doi:10.1039/b918209h

Hui, K. S., Kwong, C. W., and Chao, C. Y. H. (2010). Methane emission abatement by Pd-ion-exchanged zeolite 13X with ozone. *Energy Environ. Sci.* 3, 1092–1098. doi:10.1039/c002669g

Jae, J., Tompsett, G. A., Lin, Y.-C., Carlson, T. R., Shen, J., Zhang, T., et al. (2010). Depolymerization of lignocellulosic biomass into fuel precursors: maximizing carbon efficiency by combining hydrolysis with pyrolysis. *Energy Environ. Sci.* 3, 358–365. doi:10.1039/b924621p

Jia, S., Cox, B. J., Guo, X., Zhang, Z. C., and Ekerdt, J. G. (2010). Cleaving the β-O-4 bonds of lignin model compounds in an acidic ionic liquid, 1-H-3-methylimidazolium chloride: an optional strategy for the degradation of lignin. *ChemSusChem* 3, 1078–1084. doi:10.1002/cssc.201000112

Jia, S., Cox, B. J., Guo, X., Zhang, Z. C., and Ekerdt, J. G. (2011). Hydrolytic cleavage of β-O-4 ether bonds of lignin model compounds in an ionic liquid with metal chlorides. *Ind. Eng. Chem. Res.* 50, 849–855. doi:10.1021/ie101884h

Kong, J., He, M., Lercher, J. A., and Zhao, C. (2015). Direct production of naphthenes and paraffins from lignin. *Chem. Commun.* 51, 17580–17583. doi:10.1039/c5cc06828b

Laskar, D. D., Tucker, M. P., Chen, X., Helms, G. L., and Yang, B. (2014). Noble-metal catalyzed hydrodeoxygenation of biomass-derived lignin to aromatic hydrocarbons. *Green Chem.* 16, 897–910. doi:10.1039/c3gc42041h

Li, C., Zhao, X., Wang, A., Huber, G. W., and Zhang, T. (2015). Catalytic transformation of lignin for the production of chemicals and fuels. *Chem. Rev.* 21, 11559–11624. doi:10.1021/acs.chemrev.5b00155

Peters, J. E., Carpenter, J. R., and Dayton, D. C. (2015). Anisole and guaiacol hydrodeoxygenation reaction pathways over selected catalysts. *Energy Fuels* 29, 909–916. doi:10.1021/ef502551p

Ragauskas, A. J., Beckham, G. T., Biddy, M. J., Chandra, R., Chen, F., Davis, M. F., et al. (2014). Lignin valorization: improving lignin processing in the biorefinery. *Science* 344, 1246843. doi:10.1126/science.1246843

Scanion, J. T., and Willis, D. E. (1985). Calculation of flame ionization detector relative response factors using the effective carbon number concept. *J. Chromatogr. Sci.* 23, 333–340. doi:10.1093/chromsci/23.8.333

Singh, S. K., and Ekhe, J. D. (2014). Towards effective lignin conversion: HZSM-5 catalyzed one-pot solvolytic depolymerization/hydrodeoxygenation of lignin into value added compounds. *RSC Adv.* 4, 27971–27978. doi:10.1039/c4ra02968b

Singh, V. V., Jurado-Sánchez, B., Sattayasamitsathit, S., Orozco, J., Li, J., Galarnyk, M., et al. (2015). Multifunctional silver-exchanged zeolite micromotors for catalytic detoxification of chemical and biological threats. *Adv. Funct. Mater.* 25, 2147–2155. doi:10.1002/adfm.201500033

Song, Q., Wang, F., and Xu, J. (2012). Hydrogenolysis of lignosulfonate into phenols over heterogeneous nickel catalysts. *Chem. Commun.* 48, 7019–7021. doi:10.1039/c2cc31414b

Taarning, E., Osmundsen, C. M., Yang, X., Voss, B., Andersen, S. I., and Christensen, C. H. (2011). Zeolite-catalyzed biomass conversion to fuels and chemicals. *Energy Environ. Sci.* 4, 793–804. doi:10.1039/C004518G

Wang, H., Ruan, H., Feng, M., Qin, Y., Job, H., Luo, L., et al. (2017). One-pot process for hydrodeoxygenation of lignin to alkanes using Ru-based bimetallic and bifunctional catalysts supported on zeolite Y. *ChemSusChem* 10, 1846–1856. doi:10.1002/cssc.201700160

Wang, H., Ruan, H., Pei, H., Wang, H., Chen, X., Tucker, M. P., et al. (2015). Biomass-derived lignin to jet fuel range hydrocarbons via aqueous phase hydrodeoxygenation. *Green Chem.* 17, 5131–5135. doi:10.1039/C5GC01534K

Wang, H., Zhang, L., Deng, T., Ruan, H., Hou, X., Cort, J. R., et al. (2016). ZnCl₂ induced catalytic conversion of softwood lignin to aromatics and hydrocarbons. *Green Chem.* 18, 2802–2810. doi:10.1039/C5GC02967H

Xu, C., Arancon, R. A., Labidi, J., and Luque, R. (2014). Lignin depolymerization strategies: towards valuable chemicals and fuels. *Chem. Soc. Rev.* 43, 7485–7500. doi:10.1039/C4CS00235K

Yang, Y., Fan, H., Song, J., Meng, Q., Zhou, H., Wu, L., et al. (2015). Free radical reaction promoted by ionic liquid: a route for metal-free oxidation depolymerization of lignin model compound and lignin. *Chem. Commun.* 51, 4028–4031. doi:10.1039/c4cc10394g

Zakzeski, J., and Weckhuysen, B. M. (2011). Lignin solubilization and aqueous phase reforming for the production of aromatic chemicals and hydrogen. *ChemSusChem* 4, 369–378. doi:10.1002/cssc.201000299

Zhang, W., Chen, J., Liu, R., Wang, S., Chen, L., and Li, K. (2014a). Hydrodeoxygenation of lignin-derived phenolic monomers and dimers to alkane fuels over bifunctional zeolite-supported metal catalysts. *ACS Sustain. Chem. Eng.* 2, 683–691. doi:10.1021/sc400401n

Zhang, J., Teo, J., Chen, X., Asakura, H., Tanaka, T., Teramura, K., et al. (2014b). A series of NiM (M = Ru, Rh, and Pd) bimetallic catalysts for effective lignin hydrogenolysis in water. *ACS Catal.* 4, 1574–1583. doi:10.1021/cs401199f

Catalytic Oxidation and Depolymerization of Lignin in Aqueous Ionic Liquid

Lalitendu Das[1], Siquan Xu[1,2] and Jian Shi[1]*

[1] Biosystems and Agricultural Engineering, University of Kentucky, Lexington, KY, United States, [2] College of Chemical Engineering, Nanjing Forestry University, Nanjing, China

Lignin is an integral part of the plant cell wall, which provides rigidity to plants, also contributes to the recalcitrance of the lignocellulosic biomass to biochemical and biological deconstruction. Lignin is a promising renewable feedstock for aromatic chemicals; however, an efficient and economic lignin depolymerization method needs to be developed to enable the conversion. In this study, we investigated the depolymerization of alkaline lignin in aqueous 1-ethyl-3-methylimidazolium acetate [C_2C_1Im][OAc] under oxidizing conditions. Seven different transition metal catalysts were screened in presence of H_2O_2 as oxidizing agent in a batch reactor. $CoCl_2$ and Nb_2O_5 proved to be the most effective catalysts in degrading lignin to aromatic compounds. A central composite design was used to optimize the catalyst loading, H_2O_2 concentration, and temperature for product formation. Results show that lignin was depolymerized, and the major degradation products found in the extracted oil were guaiacol, syringol, vanillin, acetovanillone, and homovanillic acid. Lignin streams were characterized by Fourier transform infrared spectroscopy and gel permeation chromatography to determine effects of the experimental parameters on lignin depolymerization. The weight-average molecular weight (M_w) of liquid stream lignin after oxidation, for $CoCl_2$ and Nb_2O_5 catalysts were 1,202 and 1,520 g mol^{-1}, respectively, lower than that of Kraft lignin. Polydispersity index of the liquid stream lignin increased as compared with Kraft lignin, indicating wide span of the molecular weight distribution as a result of lignin depolymerization. Results from this study provide insights into the role of oxidant and transition metal catalysts and the oxidative degradation reaction sequence of lignin toward product formation in presence of aqueous ionic liquid.

Keywords: catalyst, depolymerization, ionic liquids, lignin, oxidation

INTRODUCTION

Lignin is the second most abundant terrestrial biopolymer on earth and is one of the three main building blocks of lignocellulosic biomass (Das et al., 2012). Depending on the biomass source, lignin accounts for approximately 10–30% of the biomass together with cellulose, hemicellulose, and other minor components (Chatel and Rogers, 2013). Lignin is a three dimensional polyphenolic biopolymer synthesized in plants mainly from coniferyl, sinapyl, and *p*-coumaryl alcohol (Brandt et al., 2015). These monomers give rise to guaiacyl (G), syringyl (S), and *p*-hydroxyphenyl (H)

subunits *via* free radical polymerization (Brandt et al., 2015). As projected by the 2009 Renewable Fuel Standard (RFS2) on basis of the 2007 Energy Independence and Security Act, the US alone will generate approximately 60 million dry tons of lignin annually from the capacity of cellulosic biorefineries by year 2022 (Tilman et al., 2009; Somerville et al., 2010; Brown and Brown, 2013). This quantity will add on top of the existing ~100 million dry tons of lignin from paper and pulping industry (Chakar and Ragauskas, 2004; Ragauskas et al., 2014). Despite its great potential to a wide range of chemicals, lignin is yet an underutilized substrate, and under the current biorefinery concept, lignin is commonly burned to generate steam and electricity. It is critical to convert lignin waste streams to high value-added chemicals to enable cost-competitive biofuels and chemicals production in a biorefinery (Ragauskas et al., 2014; Beckham et al., 2016; Mottiar et al., 2016).

Lignin's full potential as a renewable source for aromatic compounds can be, in part, unlocked only if an efficient and economic method for lignin depolymerization and valorization is developed (Prado et al., 2016a). The heterogeneity of lignin (both in its varied bond chemistry and its variability between plants), however, is the major hurdle to its targeted upgrading and reuse as a feedstock for chemicals and advanced materials (Das et al., 2012). The type and abundance of the inter-unit linkages (β-O-4, β-β, β-5, 5-5, and 5-O-4), as combinations of carbon–oxygen and carbon–carbon bonds, vary largely based on the plant type (Zakzeski et al., 2010a). Several lignin conversion methods are currently under investigation, inlcuding hydrolysis, hydrogenolysis, pyrolysis, catalytic oxidation, and biological depolymerization (Stärk et al., 2010). Among those, catalytic oxidation is one of the suitable routes as the side-chain aliphatic OH, the terminal phenolic OH groups, and the reactive benzylic positions in lignin can be selectively modified *via* oxidation. Lignin oxidation produces a suite of platform compounds with added functionalities, which can be subsequently separated through filtration or extraction (Crestini et al., 2010; Pandey and Kim, 2011).

Ionic liquids (ILs) have received increasing interest because of their high efficacy in fractionating and pretreating lignocellulosic biomass. ILs are defined as salts consisting of cations and anions, which typically melt at or below 100°C. ILs have wide range of applications due to their unique properties including negligible vapor pressure, thermal, electrochemical, and chemical stability, and versatile solvent power (Marszałł and Kaliszan, 2007). Several ILs, such as 1-ethyl-3-methylimidazolium acetate [C_2C_1Im][OAc], 1-butyl-3-methylimidazolium chloride [C_4C_1Im][Cl] (Kilpeläinen et al., 2007), 1,3-dimethylimidazolium methylsulfate [C_2C_1Im][$MeSO_4$] (Tan et al., 2009), and 1-butyl-3-methylimidazolium methylsulfate [C_4C_1Im][$MeSO_4$] (Pu et al., 2007) have proven their efficacy toward delignification of plant biomass and lignin depolymerization. The solvent property of an IL is the key for lignin solvation. It was suggested that the anion of IL is the dominating factor influencing lignin dissolution as compared with cation. The affinity in which anions intereacting with lignin is in the order of sulfate > lactate > acetate > chloride > phosphate (Prado et al., 2016a).

Despite the effectiveness of [C_2C_1Im][OAc] and similar ILs at reducing the recalcitrance of lignocellulosic biomass

and solubilizing lignin, the challenges associated with product recovery and IL recycling hinder the commercial scale-up of an IL-based technology (Datta et al., 2010; Klein-Marcuschamer et al., 2011; Gladden et al., 2014). In an aqueous IL pretreatment system, the majority of the lignin is extracted to the liquid phase (black liquor) and separation of lignin form this liquid system is however challenging. Hence, direct lignin valorization in aqueous (liquor) IL could offer a new strategy for selective lignin depolymerization meanwhile help to tackle the challenges associated with IL recycle and product recovery, thus improving the economics of an IL-based biorefining process.

Catalytic oxidation of lignin and lignin model compounds into aromatic chemicals in various solvent systems has been explored (Behling et al., 2016). Oxidative catalysts including inorganic metal-based catalysts, organocatalysts, and metallo-based complexes have been investigated for lignin oxidation to produce high value chemicals (Crestini et al., 2010). Transitional metals are known catalysts for oxidation reaction with several transition metals such as Cu^{II}, Fe^{III}, $Mn^{II,III}$, Co^{II}, and Zr^{IV} identified in enhancing product yields of lignin oxidation (Zakzeski et al., 2010a). Side-chain cleavage and ether bond hydrolysis are the predominant reactions during the oxidation of lignin model compounds (Zhang et al., 2016).

A few oxidizing agents such as H_2O_2 and oxygen have been demonstrated effective in lignin depolymerization when combined with metal oxide-based catalysts; however, most of the studies were carried out in organic solvents or water under basic/acidic conditions (Zakzeski et al., 2010b; Behling et al., 2016). Several studies have explored catalysis of lignin model compounds and technical lignin in 100% IL medium (Zakzeski et al., 2010b; Chatel and Rogers, 2013; Xu et al., 2014). Delignification of miscanthus and willow in [HC_4Im][HSO_4] and [Et_3NH][HSO_4] and subsequent lignin depolymerization in the black liquor using H_2O_2 in presence of TiO_2 catalyst were reported recently (Prado et al., 2016a,b). Despite many reports of using [C_2C_1Im][OAc] for biomass delignification, catalytic lignin depolymerization in aqueous [C_2C_1Im][OAc] has not been explored. There is a gap in our understanding of the interplay of catalyst, oxidizing agent, and product formation in an aqueous IL system (Zhang et al., 2016). Hence, the objectives of this study are to: (1) screen transition metal catalysts in aqueous [C_2C_1Im][OAc] IL system; (2) investigate the effects of catalyst loading, temperature, and H_2O_2 concentration on the production of aromatic compounds from alkaline (Kraft) lignin; (3) characterize the lignin before and after oxidation reaction. Results from this study provide insights into the oxidative degradation pathway of lignin in the presence of aqueous IL and the selectivity of catalyst/oxidizing agent toward the formation of desirable products.

MATERIALS AND METHODS

Materials

Transition metal salts Nb_2O_5 (99.9%), $CoCl_2 \cdot 6H_2O$ (98%), $CuSO_4$ (99%), $MnN_2O_6 \cdot 4H_2O$ (97%), TiO_2 (99.8%), $CrKO_8S_2 \cdot 12H_2O$ (98%), and $NiCl_2 \cdot XH_2O$ (99.9%) were obtained from Sigma Aldrich (St. Louis, MO, USA). The IL ([C_2C_1Im][OAc]), alkaline

(Kraft) lignin, 2-methyltetrahydrofuran (MeTHF, 99%), H_2O_2 (30%), guaiacol (98%), syringol (98%), vanillin (99%), acetovanillone (98%), and homovanillic acid (98%) were also procured from Sigma Aldrich (St. Louis, MO, USA).

Lignin Depolymerization, Extraction, and Analytical Method

Lignin oxidation reactions were performed in batch reactors. Prior to the reaction, lignin (10 wt%) was treated in $[C_2C_1Im]$ [OAc] for 3 h at 140°C by following a typical IL pretreatment condition shown elsewhere (Li et al., 2010); subsequently the IL–lignin mixtures were diluted by adding water at a mass ratio of 1:1 to a 2 mL total volume. To the above mixture, a predetermined amount of catalyst and H_2O_2 were added and the reaction was conducted at different temperatures (74–126°C) for 3 h with constant mixing by a magnetic stir bar at 200 rpm. The catalyst and hydrogen peroxide (commercially available 30% H_2O_2 solution) loadings were based on the total weight of IL and lignin. After reaction, residual lignin was precipitated by addition of 2 mL of water followed by centrifugation at 4,000 rpm for 15 min to separate solids from liquid stream. The liquid stream was subjected to a liquid–liquid extraction using MeTHF for three times. Finally, the MeTHF was evaporated to leave thick oil in a vacuum oven at 30°C for 24 h. The oil was re-dissolved in 750 µL of ethyl acetate and analyzed by GC/MS for monomeric compounds.

The solid stream (residual lignin) was washed by 5 mL warm water for four times and subsequently oven dried for 24 h at 70°C. Lignin conversion was calculated using Eq. 1

$$Conversion (\%) = \frac{\text{weight of initial lignin} - \text{weight of precipitated lignin}}{\text{weight of initial lignin}} \times 1 \quad (1)$$

Identification and quantification of the monomeric products from the depolymerization reaction were performed by Agilent 7890B GC coupled 5977B MS with an HP-5ms (60 m × 0.32 mm) capillary column. The temperature program started at 50°C and increased to 120°C at 10°C min^{-1} with a holding time of 5 min; then it was raised to 280°C at 10°C min^{-1} with a holding time of 8 min and to 300°C at 10°C min^{-1} with holding time of 2 min (Prado et al., 2016a). Helium was used as a carrier gas at a flow rate of 1.2 mL min^{-1}. Calibration curves were created using commercially available pure compounds: guaiacol, syringol, vanillin, acetovanillone, and homovanillic acid (Sigma Aldrich, St. Louis, MO, USA).

Screening of Catalysts

In a series of preliminary screening experiments, various transition metal catalysts including Nb_2O_5, $CoCl_2 \cdot 6H_2O$, $CuSO_4$, $MnN_2O_6 \cdot 4H_2O$, TiO_2, $CrKO_8S_2 \cdot 12H_2O$, and $NiCl_2 \cdot XH_2O$ were tested in batch reactors. Catalyst and H_2O_2 were both loaded at 5 wt% loading (IL + lignin); the screening experiments were conducted at 120°C and a reaction time of 3 h (Prado et al., 2016a). Identification and determination of product formation and concentration were performed according to the batch experiments mentioned in the Section "Lignin Depolymerization, Extraction, and Analytical Method."

Experimental Design

An orthogonal central composite design (CCD) (**Table 1**) was used to study the effect of H_2O_2 concentration, catalyst loading, and temperature on product concentration for selected catalysts. Levels for independent variables were selected to be, 1–5%, 1–5%, and 80–120°C for H_2O_2 concentration, catalyst loading, and temperature, respectively.

A CCD consists of 2^p factorial runs with $2p$ axial runs and P_c center runs. In this study, the independent variables were H_2O_2 concentration (X_1), catalyst loading (X_2), and temperature (X_3). For each independent variable, a 2^3 full factorial CCD for the three variables consisting of 8 factorial points, 6 axial points, and 3 replicates at the center points were employed, which accounted for a total of 17 experiments.

The center points were used to determine the experimental error and reproducibility of the data. Low and high levels of the independent variable were coded as −1 and +1. Axial points were located at ($\pm\alpha$, 0, 0), (0, $\pm\alpha$, 0), and (0, 0, $\pm\alpha$) where α is the distance of the axial point. In this study, α value was fixed at 1.287. The experimental sequence was randomized to minimize the effects of uncontrolled errors. The response variable for this study was product concentration (Y_1). Response was used to develop an empirical model corresponding to product concentration using a second-degree polynomial equation as given in Eq. 2:

$$\hat{Y} = \beta_0 + \sum_{i}^{n} \beta_i x_i + \sum_{ii}^{n} \beta_{ii} x_i^2 + \sum_{i=1}^{n-1} \sum_{j=i+1}^{n} \beta_{ij} x_i x_j \quad (2)$$

where $\hat{Y}$ is the response, β_0 is the intercept, β_i the linear coefficients, β_{ii} the quadratic coefficients, β_{ij} the interaction coefficients, and $x_i x_j$ are the coded values.

Lignin Characterization
Gel Permeation Chromatographic (GPC) Analysis

The weight-average molecular weight (M_w) and number-average molecular weight (M_n) of the residual lignin were measured by GPC after acetylation (Samuel et al., 2014). An Ultimate 3000 HPLC system (Dionex Corporation, Sunnyvale, CA, USA) equipped with an ultra violet (UV) detector was used. Separation was accomplished with a Mixed-D PLgel column (5 µm particle size, 300 mm × 7.5 mm i.d., linear molecular weight range of 200–400,000 µm, Polymer Laboratories, Amherst, MA, USA) at 80°C using a mobile phase of THF at a flow rate of 0.5 mL min^{-1}. Elution profile of materials eluting from the column was monitored by UV absorbance at 280 nm and calibrated using a polystyrene standards kit (Sigma-Aldrich).

TABLE 1 | Experimental factors and their coded levels of independent variables for central composite design.

Factors	Code	Coded variable levels				
		−α	−1	0	1	+α
H_2O_2 concentration (%)	X_1	0.43	1	3	5	5.57
Catalyst loading (%)	X_2	0.43	1	3	5	5.57
Temperature (°C)	X_3	74	80	100	120	126

Fourier Transform Infrared (FTIR)

Changes in the chemical structure of untreated lignin and residual lignin were performed using a Thermo Nicolet Nexus 870 FTIR-ATR spectroscopy. Spectra of the lignin samples were obtained using an average of 64 scans in the range of 700 and 4,000 cm⁻¹ with a spectral resolution of 1.928 cm⁻¹.

RESULTS AND DISCUSSION

Catalyst Selection and Model Development

Catalysts were screened based on the total product concentration and conversion. Results obtained from the screening experiments show that out of the seven catalysts used $CoCl_2$ and Nb_2O_5 gave the highest product concentration and conversion compared to the other catalysts (**Figure 1**). Subsequently, optimization of batch experiments was performed using these two catalysts. Cobalt (Co)-based catalysts have been used for oxidation of lignin model compounds and alcohols in 1-ethyl-3-methylimidazolium diethylphosphate ([C$_2$C$_1$Im][DEP]) (Zakzeski et al., 2010b, 2011). Co species facilitate the oxidation reaction by readily catalyzing the disproportionation of H_2O_2 to form O_2 and H_2O (Pokutsa et al., 2009). In addition, several studies reported niobium oxide as a selective and effective oxidation catalyst for a wide range of oxidation reactions (Wachs et al., 2000). Apart from acting as a strong Lewis acid, niobium oxide also has the capability to stabilize oxidation cation species, which could assist in the electrophilic attack of H_2O_2 on lignin (Fielicke et al., 2003; Nakajima et al., 2011).

Concentrations (mg L⁻¹) of five products: guaiacol, syringol, vanillin, acetovanillone, and homovanillic acid were determined by GC/MS for all the reaction conditions based on the central composite design. Results illustrate that the total product concentrations for $CoCl_2$ catalyst were in the range of 545.3–1,200.5 mg L⁻¹; whereas for Nb_2O_5 catalyst the total product concentrations fell into 340.7–1,325.6 mg L⁻¹ range (**Table 2**). In addition, obtained data were fitted to a polynomial model to optimize the reaction parameters for the formation of products from lignin using a desirability approach (JMP 12, SAS Institute, Inc., Cary, NC, USA). The suggested optimum levels for $CoCl_2$ catalyst were temperature of 120°C, catalyst loading of 1%, and H_2O_2 concentration of 1%, corresponding to a predicted total product concentration of 1,079.5 mg L⁻¹ at 95% confidence interval (989.0, 1,169.9). For Nb_2O_5 catalyst, the optimum reaction parameters were temperature of 120°C, catalyst loading of 4.45%, and H_2O_2 concentration of 3.08%, corresponding to a predicted total product concentration of 1,262.6 mg L⁻¹ at 95% confidence interval (1,182.8, 1,342.3). The quadratic regression models for the $CoCl_2$ and Nb_2O_5 catalysts were shown below:

$$\hat{Y}_{CoCl_2} = 718.91 - 37.43\,X_1 - 92.79\,X_2 + 155.90\,X_3 \\ + 14.71\,X_1^2 + 12.57\,X_2^2 + 111.19\,X_3^2 \qquad (3) \\ + 31.01\,X_1X_2 + 36.17\,X_1X_3 + 58.88\,X_2X_3$$

$$\hat{Y}_{Nb_2O_5} = 735.42 - 37.09\,X_1 + 104.98\,X_2 + 195.64\,X_3 \\ - 33.49\,X_1^2 - 84.95\,X_2^2 + 285.65\,X_3^2 \qquad (4) \\ - 6.65\,X_1X_2 + 45.10\,X_1X_3 + 19.73\,X_2X_3$$

where, X_1, X_2, and X_3 are H_2O_2 concentration, catalyst loading, and temperature, respectively. The linear effects were represented by the coefficients of one factor (X_1, X_2, X_3), while the coefficients
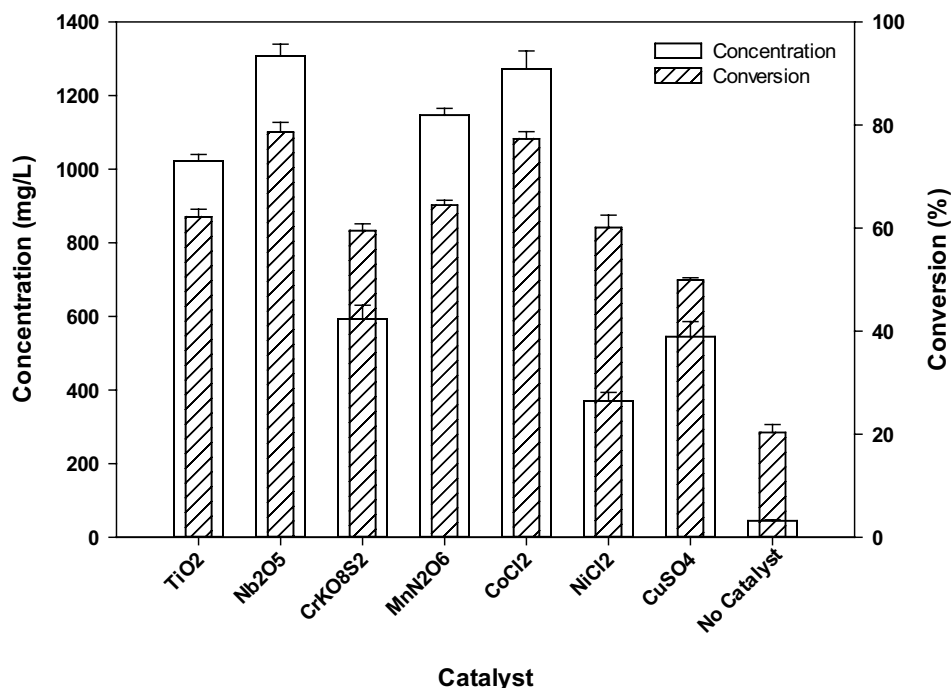
FIGURE 1 | Screening of transition metal catalysts.

TABLE 2 | Experimental conditions and corresponding product concentrations, conversion, and yield.[a]

ID	Pattern	Catalyst loading (%)	H$_2$O$_2$ conc. (%)	Temperature (°C)	CoCl$_2$ catalyst			Nb$_2$O$_5$ catalyst		
					Total product concentration (mg L^{-1})	Yield with respect to lignin (%)	Conversion (%)	Total product concentration (mg L^{-1})	Yield with respect to lignin (%)	Conversion (%)
1	000	3	3	100	765.2 (83.6)	0.6 (0.06)	40.3 (0.15)	758.7 (3.2)	0.6 (0.01)	41.7 (0.34)
2	+++	5	5	120	961.9 (7.2)	0.7 (0.01)	78.1 (0.52)	1,301.6 (36.9)	1.0 (0.03)	80.1 (0.26)
3	0A0	3	5.57	100	737.0 (29.5)	0.6 (0.02)	47.3 (0.18)	553.1 (8.5)	0.4 (0.01)	40.2 (0.72)
4	−−+	1	1	120	1,055.9 (17.1)	0.8 (0.01)	33.9 (0.38)	1,061.8 (1.1)	0.8 (0.00)	20.2 (0.44)
5	+−+	5	1	120	952.5 (26.5)	0.7 (0.02)	70.9 (1.00)	1,171.8 (40.2)	0.9 (0.03)	72.7 (0.05)
6	A00	0.43	3	100	864.1 (23.9)	0.7 (0.02)	20.8 (0.18)	340.7 (9.2)	0.3 (0.01)	32.2 (0.37)
7	++−	5	5	80	545.3 (25.0)	0.4 (0.02)	65.5 (0.50)	617.7 (7.3)	0.5 (0.01)	29.5 (0.52)
8	−+−	1	5	80	760.3 (2.3)	0.6 (0.01)	21.8 (1.35)	613.1 (12.4)	0.5 (0.01)	29.1 (1.20)
9	000	3	3	100	720.5 (70.6)	0.5 (0.01)	40.6 (0.47)	739.3 (8.6)	0.6 (0.01)	42.2 (0.78)
10	0a0	3	0.43	100	714.2 (14.5)	0.5 (0.01)	41.2 (0.08)	765.4 (13.9)	0.6 (0.01)	38.8 (1.22)
11	+−−	5	1	80	657.1 (10.0)	0.5 (0.01)	67.1 (4.06)	847.2 (35.3)	0.6 (0.03)	31.2 (0.20)
12	−−−	1	1	80	1,019.7 (14.3)	0.8 (0.01)	20.9 (0.96)	637.2 (27.6)	0.5 (0.02)	44.9 (0.68)
13	00A	3	3	126	1,200.5 (17.5)	0.9 (0.01)	52.8 (0.26)	1,325.6 (29.4)	1.0 (0.02)	43.5 (1.74)
14	00a	3	3	74	570.5 (24.9)	0.4 (0.02)	40.5 (0.01)	1,050.5 (36.5)	0.8 (0.03)	29.6 (0.30)
15	A00	5.57	3	100	580.0 (11.4)	0.4 (0.01)	80.4 (0.23)	807.3 (7.2)	0.6 (0.01)	29.6 (0.30)
16	−++	1	5	120	964.9 (4.8)	0.7 (0.01)	33.8 (0.39)	1,039.2 (29.8)	0.8 (0.02)	31.2 (0.20)
17	000	3	3	100	718.4 (15.2)	0.5 (0.05)	41.7 (0.10)	763.7 (3.3)	0.6 (0.01)	42.0 (2.28)

[a]The values in the parenthesis represent the standard deviations (SDs).
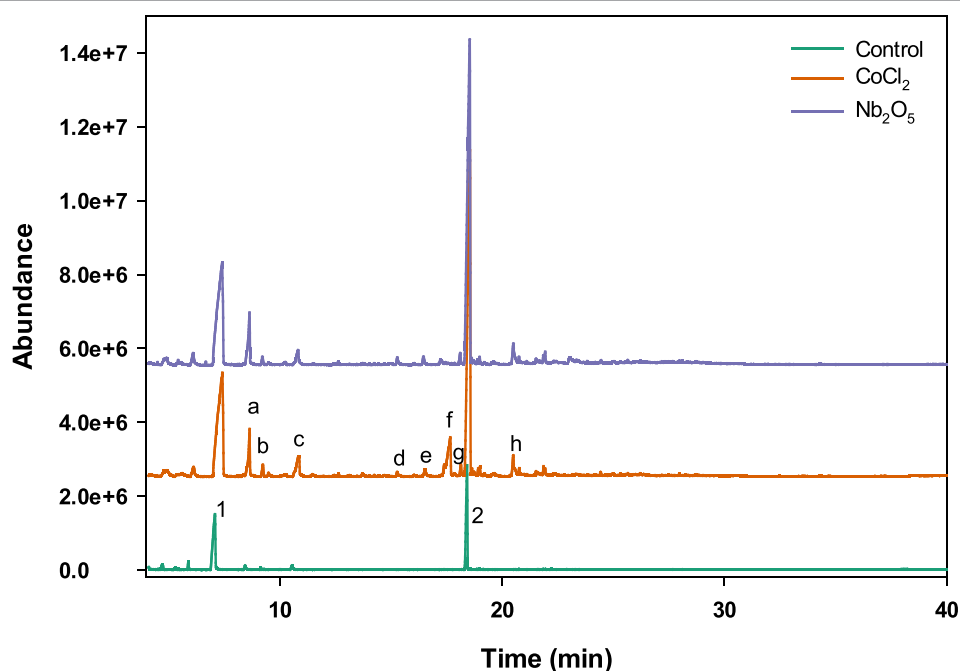
FIGURE 2 | Representative GC chromatography [peaks representing a: guaiacol, b: 4-methoxy-1,3-benzenediamine, c: 1,3,5-benzenetriol, d: syringol, e: vanillin, f: 1-methyl-4-thiouracil, g: acetovanillone, h: homovanillic acid, 1: 1-ethyl imidazole, and 2: butylated hydroxytoluene (stabilizer for MeTHF)]. Experimental conditions: temperature: 120°C, catalyst loading: 1%, and H$_2$O$_2$ concentration: 1%.

of the second-order term (X_1^2, X_2^2, X_3^2) and two-factor term (X_1X_2, X_1X_3, X_2X_3) represent the quadratic effects and interaction effects, respectively.

Lignin Breakdown Product Identification

Products obtained from the catalytic oxidation process were identified and quantified using GC/MS. **Figure 2** shows a GC chromatography representing the mixture of aromatic products derived from lignin after catalytic oxidation in aqueous IL. Several lignin derived monomers of commercial interest such as guaiacol, syringol, vanillin, acetovanillone, and homovanillic acid were determined quantitatively for both catalysts. Guaiacol was the major oxidation product followed by homovanillic acid, acetovanillone, vanillin, and syringol. For CoCl$_2$ catalyst, the

concentration of guaiacol was in a range of 265.0–536.9 mg L^{-1} whereas for Nb_2O_5 catalyst the concentration was in a range of 235.4–649.4 mg L^{-1}. The concentrations of homovanillic acid were in the range of 25.5–314.3 and 45.1–361.7 mg L^{-1}, for $CoCl_2$ and Nb_2O_5 catalysts, respectively. Other products such as syringol, vanillin, and acetovanillone were also present at small proportions. The alkaline lignin used in this study was derived from softwood, which contains primarily G-lignin and a small quantity of S-lignin in the original feedstock (Sigma-Aldrich, 2016). The fact that products obtained from oxidation reactions were mainly G-lignin derived compounds corroborates the G-lignin rich source. Similar profile of compounds were reported in a previous study using $[C_2C_1Im][OAc]$ IL for the pretreatment of switchgrass, eucalyptus, and Kraft lignin (Varanasi et al., 2013). In another study, Stärk et al. (2010) reported similar product profiles from the catalytic oxidation of organosolv beech wood lignin with guaiacol as the main product probably due to the cleavage of β-aryl ether bond.

Product formation during a catalytic oxidation process is partially dependent on the basicity or acidity of the reaction system. Formation of vanillin from Kraft lignin by different oxidants such as H_2O_2, O_2, and nitrobenzene in NaOH medium has been reported (Xiang and Lee, 2000; Rodrigues Pinto et al., 2010; Pandey and Kim, 2011). It was reported that the IL, $[C_2C_1im][OAc]$ possesses dual basic and acidic characteristics as a function of temperature (Varanasi et al., 2012). The hydrogen bond basicity (β) decreased by 1.4% with an increase in temperature from 120 to 160°C (Varanasi et al., 2012). In an aqueous IL system, the hydrogen bond basicity (β value) can be correlated with the disruption of the inter- and intramolecular hydrogen bondings in cellulose, hemicellulose, and lignin (Shi et al., 2014). It is likely that the G-lignin monomeric products obtained in this study were phenolic moieties of G-lignin caused by losing phenolic proton under alkaline conditions at low reaction temperatures (Varanasi et al., 2012). These results lead to the hypothesis that the temperature-dependent dual basic and acidic characteristics of an IL could serve as a design basis to tune the aqueous IL system for better lignin solubility and product selectivity (Park and Kazlauskas, 2003; Shi et al., 2014).

Effect of Reaction Parameters on Product Concentration and Yield

H_2O_2 Loading

The effect of H_2O_2 loading on total product concentration was optimized for both catalysts. **Figures 3A,C** illustrate the effect of H_2O_2 loading coupled with interactions of catalyst loading and reaction temperature for $CoCl_2$ catalyst. From the 3D response surface plot, it appeared that the overall product concentrations increased with the decrease in H_2O_2 loading, with 1% H_2O_2 giving the highest concentration. In addition, results from ANOVA (Tables S1 and S3 in Supplementary Material) indicate that H_2O_2 loading had a significant effect ($p = 0.020$) whereas interaction effect of H_2O_2 with catalyst loading and temperature were not significant ($p = 0.096$ and $p = 0.055$). **Figures 4A,C** illustrate the combined effect of H_2O_2 concentration with catalyst loading and temperature on product concentration for Nb_2O_5 catalyst. Results from ANOVA (Tables S1 and S4 in Supplementary Material) illustrate that H_2O_2 had less

significant effect ($p = 0.064$) on product formation in the experimental design specified levels. Furthermore, the interaction effects of H_2O_2 with catalyst loading and temperature were not significant ($p = 0.772$ and $p = 0.058$), which explain the lack of any particular trend in the 3D response surface plot.

For both catalysts, H_2O_2 concentration (in the design specified range) did not have a significant effect on product concentration. Results obtained from this study corroborate the findings by Das et al., using niobium oxalate catalyst in presence of H_2O_2 in an aqueous system where increasing H_2O_2 loading from 3 to 7% did not change the concentrations of vanillin and syringaldehyde significantly. In another study, Xiang and Lee (2000) demonstrated that doubling H_2O_2 loading from 0.56 to 1.12 g resulted in a total aromatics yield of 9.8 and 8.3%, respectively. The decrease in product yield could be explained by the decomposition of excess H_2O_2 before its reaction with lignin or over-oxidization to other intermediate compounds (Xiang and Lee, 2000).

Catalyst Loading

The effects of $CoCl_2$ catalyst loading combined with H_2O_2 concentration and temperature on the total quantified product concentration are shown in **Figures 3A,B**. From the 3D surface plots, it is evident that 1% of $CoCl_2$ catalyst loading gave the highest product concentration. ANOVA results (Tables S1 and S3 in Supplementary Material) demonstrate that catalyst loading alone and its interaction with temperature were significant ($p < 0.0001$ and $p = 0.003$, respectively); however, the interaction effect of catalyst loading with H_2O_2 concentration was not significant ($p = 0.096$). The effect of Nb_2O_5 catalyst loading was also evaluated for total product concentrations. The combined effects of catalyst loading with H_2O_2 concentration and temperature on total product concentration were illustrated in **Figures 4A,B**, respectively. Catalyst loading had a significant ($p < 0.0001$) effect, but the interaction effect of catalyst loading on H_2O_2 concentration and temperature were not significant ($p = 0.772$ and $p = 0.393$, respectively). Optimal catalyst loading was 4.48%, leading to a maximum predicted product concentration of 1,262.6 mg L^{-1}. Similar trends were reported for degradation of pine wood lignin using vanadium-based polyoxometalate (POM) in presence of an acidic IL, 1-butylimidazolium hydrogen sulfate, and H_2O_2 (Prado et al., 2016b). Increasing POM loading from 1 to 20% led to increases in vanillin yield from 0.01 to 0.22%, and the authors speculated that with increase in catalyst loading, more active sites became available for breaking down lignin to products. Taking together, results from this study suggest that catalyst loading is catalyst-dependent and critical to both lignin conversion and product yield.

Reaction Temperature

The combined effects of temperature with $CoCl_2$ catalyst loading and H_2O_2 concentration are illustrated in **Figures 3B,C**. Both temperature and temperature/catalyst loading interaction had significant ($p < 0.0001$ and $p = 0.003$) effects on total product concentration. Product concentration increased with increase in temperature and the highest product concentration was achieved at 120°C. Similarly, the combined effects of temperature with Nb_2O_5 catalyst loading and H_2O_2 concentration are shown in **Figures 4B,C**. Only temperature had significant ($p < 0.0001$)
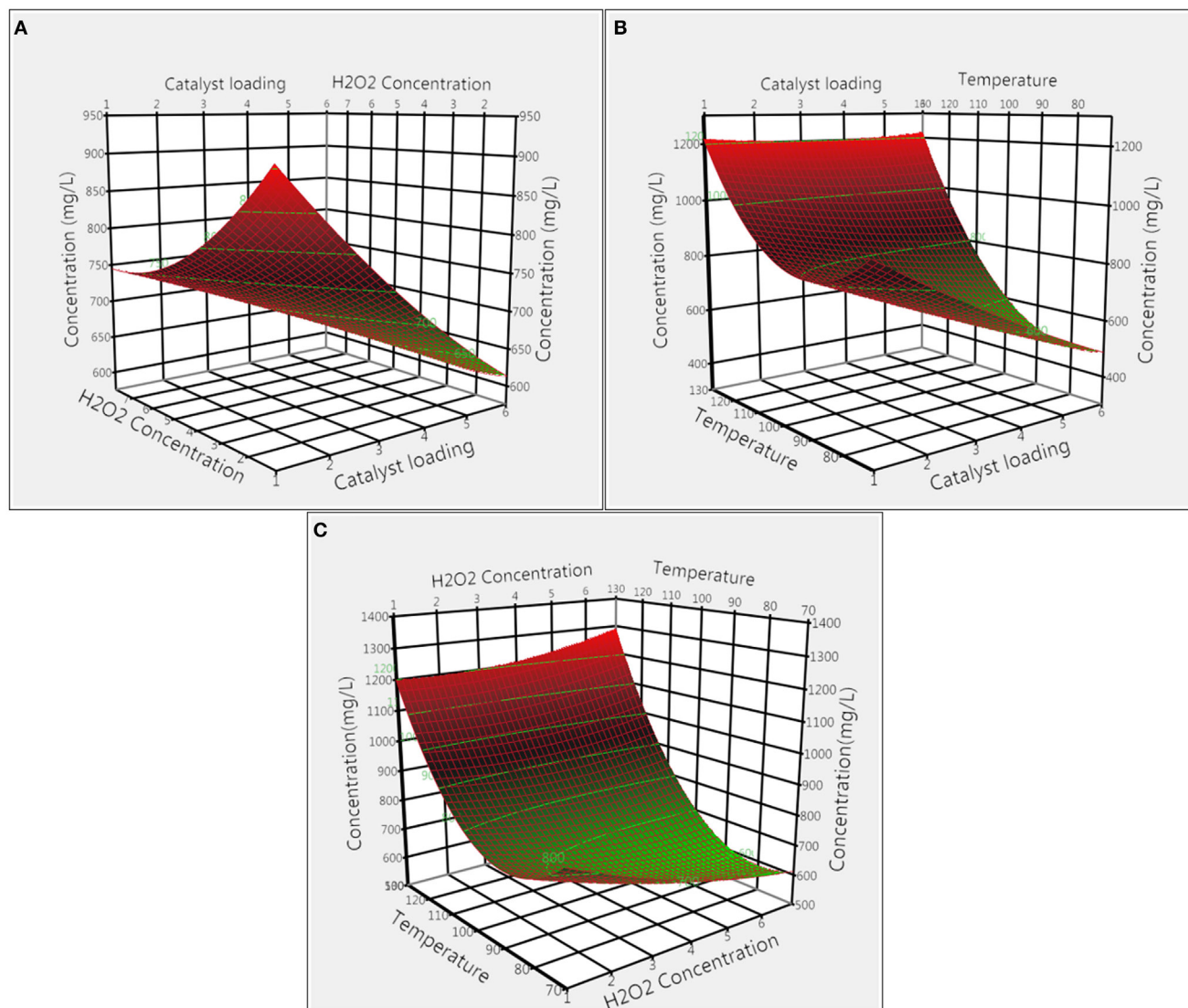
FIGURE 3 | Surface response plots showing the effect of CoCl₂ catalyst on product concentration: **(A)** catalyst loading and H₂O₂ concentration, **(B)** catalyst loading and temperature, and **(C)** temperature and H₂O₂ concentration.

effect on product concentration whereas its interactions with H₂O₂ concentration and catalyst loading were not significant. Pokutsa et al. (2009) reported that elevation of temperature from 80 to 120°C improved the conversion of precipitated hardwood lignin from 84.6 to 97.8% using H₂O₂ in a NaOH medium. In this study, for both catalysts, increasing temperature led to increases in product concentration, probably due to the formation of active hydroxyl and superoxide ions at higher temperatures as a result of hydrogen peroxide disintegration (Rodrigues Pinto et al., 2010).

Characterization of Lignin Streams
FTIR-ATR
The ATR-IR spectra of alkaline lignin and residual lignin (after oxidation) are shown in **Figure 5A**. All lignin samples showed a wide absorption band at 3,400 cm⁻¹, which is assigned to

the O–H stretching vibrations in aromatic and aliphatic O–H groups (Tejado et al., 2007). Bands around 2,930 and 2,840 cm⁻¹ can be assigned to C–H vibrations of CH₂ and CH₃ groups; while signals between 1,700 and 1,400 cm⁻¹ can be attributed to the aromatic skeletal vibrations (Cachet et al., 2014). The C=C of aromatic skeletal vibrations were reflected by peaks at 1,595 and 1,510 cm⁻¹ (Prado et al., 2016b); these two stretches showed decrease in intensity when compared to unreacted alkaline lignin, indicating the oxidation of lignin at tested conditions. The bands found at 1,460 and 1,420 cm⁻¹ can be assigned to the C–H deformation in CH₂ and CH₃ groups and C–H aromatic ring vibrations, respectively. Notable decreases in peak intensity at 1,420 cm⁻¹ for both catalysts were observed when compared to unreacted alkaline lignin, indicating possible breakdown of the CH₂ and
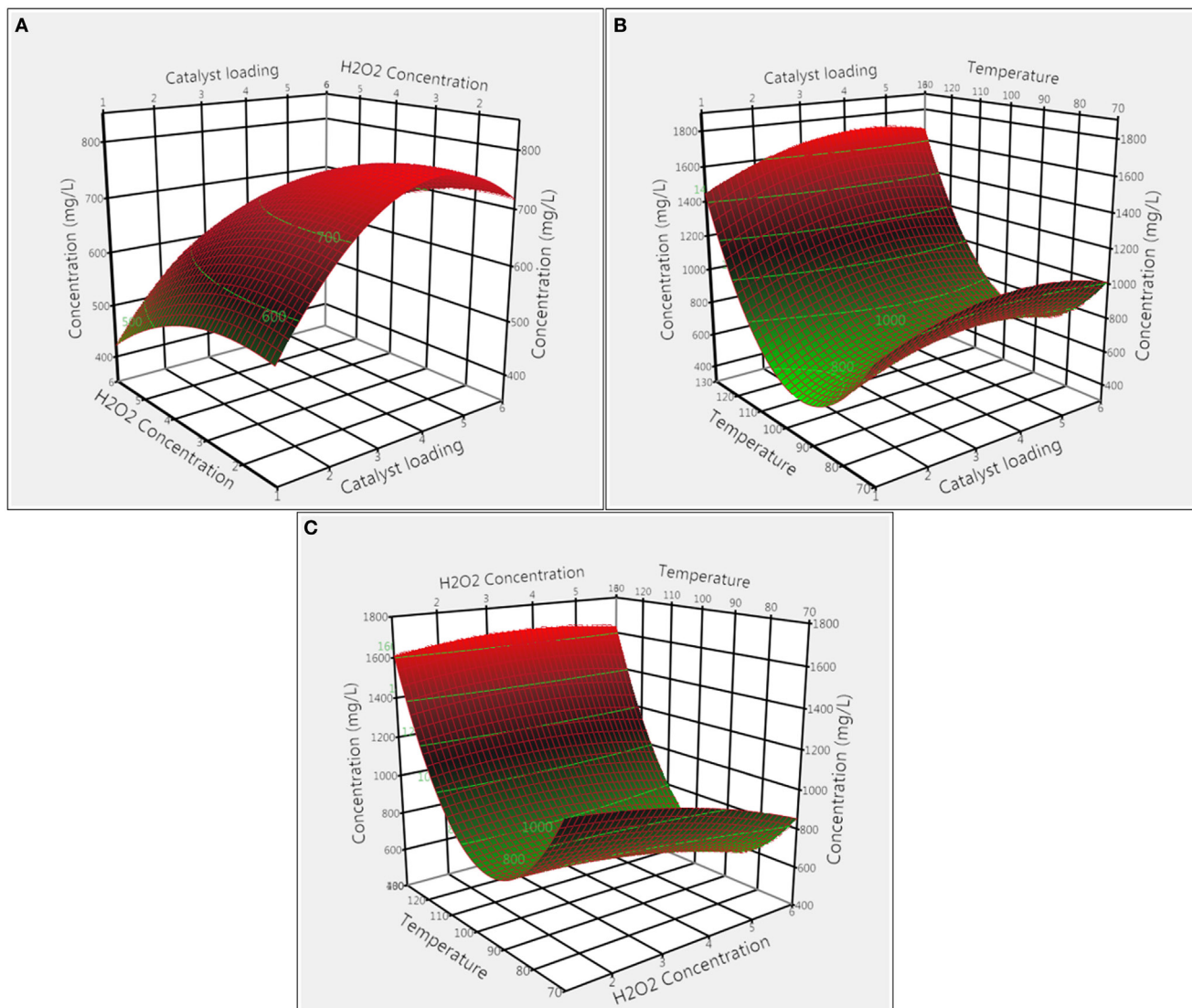
FIGURE 4 | Surface response plots showing the effect of Nb$_2$O$_5$ catalyst on product concentration: **(A)** catalyst loading and H$_2$O$_2$ concentration, **(B)** catalyst loading and temperature, and **(C)** temperature and H$_2$O$_2$ concentration.

CH$_3$ groups by oxidation. The bands associated with guaiacyl (G) and syringyl (S) units of lignin were detected at 1,220, 1,110, and 1,030 cm^{-1} (García et al., 2012; Gordobil et al., 2016). The band at 1,220 cm^{-1} corresponding to C–C, C–O, and C=O stretching (G) showed a decrease in intensity from untreated lignin compared to catalyzed lignin. The band at 1,110 cm^{-1} corresponding to aromatic C–H in plane deformation (S) also showed decrease in intensity as compared with unreacted alkaline lignin, possibly due to the reduced proportion of S-lignin in the residual lignin. Meanwhile, the band at 1,030 cm^{-1} assigning to aromatic C–H in plane deformation (G > S) remained constant for all the three peaks. Collectively, these observations supported the general fact that the lignin used in this study is dominated by G-units and indicated possible preferential breakdown of S-lignin as a result of its high chemical reactivity (Shi et al., 2016).

GPC Analysis

The M_w (weight-average molecular weight) and M_n (number-average molecular weight) of the alkaline lignin and residual lignin after oxidation reaction are shown in **Table 3** and the molecular weight distribution (MWD) profiles are depicted in **Figure 5B**. Comparing the MWD profiles of the unreacted alkaline lignin with residual lignins, the MWD curves of the residual lignins shifted to the right (translating to late elution time and lower M_w as shown in **Table 3**), indicating lignin depolymerization caused by oxidation. The extent of depolymerization was greater for Nb$_2$O$_5$ catalyst, as indicated by the slightly lower M_w and M_n when compared with that of CoCl$_2$ catalyst. This observation was further supported by the higher products concentration and greater conversion when comparing Nb$_2$O$_5$ catalyst with CoCl$_2$ catalyst. M_w of the lignin in liquid streams for CoCl$_2$ and Nb$_2$O$_5$ catalysts were 1,201.9 and 1,520.2 g mol^{-1},
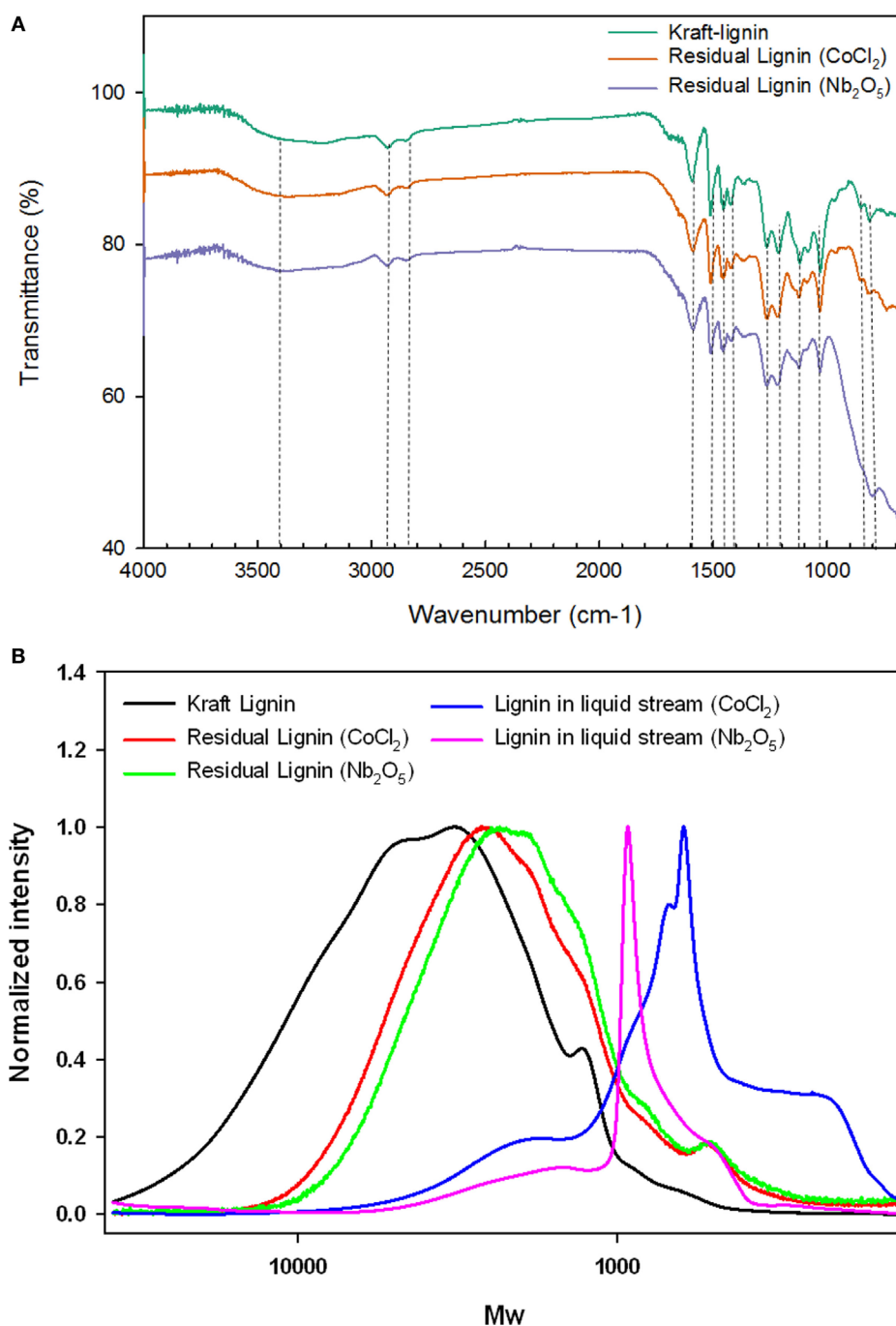
FIGURE 5 | (A) Fourier transform infrared spectra and (B) gel permeation chromatography of lignin streams before and after oxidation.

TABLE 3 | Molecular weight of untreated lignin and oxidized lignin residuals.

Source	M_w (g mol^{-1})	M_n (g mol^{-1})	Polydispersity index
Alkaline lignin	5,736.1	3,056.3	1.88
Residual lignin (CoCl$_2$)	2,897.7	1,600.8	1.81
Lignin in liquid stream (CoCl$_2$)	1,201.9	577.0	2.08
Residual lignin (Nb$_2$O$_5$)	2,602.1	1,424.3	1.83
Lignin in liquid stream (Nb$_2$O$_5$)	1,520.2	614.1	2.48

respectively; both were lower than the corresponding solids residues and untreated lignin. However, the M_n showed to be much lower as compared to solids residues and untreated lignin; this is in accordance to the increased polydispersity index, indicating a wide span of MW after oxidation. Taken together, these results suggest that lignin underwent significant depolymerization during the catalytic oxidation; however, the dissolved and depolymerized lignin might have underwent

repolymerization (Li et al., 2007; El Hage et al., 2009; Toledano et al., 2014).

Possible Reaction Sequence

Temperature and catalyst loading were the significant factors for both catalysts. Guaiacol, syringol, vanillin, acetovanillone, and homovanillic acid were the main compounds of the total quantified products (**Figure 6**). Yields of the total quantified products are detailed in Table S2 in Supplementary Material. Nb_2O_5 catalyst led to higher yield of products than that of $CoCl_2$ catalyst. Yield (%) with respect to the loaded lignin ranged from 0.26 to 0.99 for Nb_2O_5 catalyst and from 0.41 to 0.90 for $CoCl_2$ catalyst, respectively, under the tested conditions. The product yields obtained from this study were comparable with results from previous studies using vanadium-based POM in presence of IL 1-butylimidazolium hydrogen sulfate and H_2O_2 with a product (vanillin, syringaldehyde, and guaiacol) yield of 0.055% (De Gregorio et al., 2016; Prado et al., 2016a). Low product yield in this study may be due to repolymerization of depolymerized lignin and/or over-oxidization products to other intermediates which were not detected in the GC/MS. Based on the insight gained from this study, a few possible approaches to improve product yield could be (a) a better control of the reaction time and temperature of the oxidation reaction; (b) selection of more selective catalysts; and (c) *in situ* product recovery such as using a biphasic system or *via* continuous product separation.

Complexity of lignin structure hindered the understanding of the reaction mechanisms of the substrate under catalytic oxidation. Lignin model compounds (monomeric and oligomeric) have been investigated to understand the cleavage mechanism and parameters effecting the depolymerization product and yield (Xu et al., 2014). Depolymerization of organosolv lignin in ILs $[C_2C_1Im][OTf]$ and $[C_2C_1Im][Cl]$ under reductive conditions using Lewis and Brønsted acid catalysts showed low conversion despite the high yields obtained on lignin model compounds (Behling et al., 2016). On the other hand, catalytic oxidation of Kraft lignin, soda lignin, Alcell/organosolv lignin in ILs $[C_2C_1Im]$ [DEP], $[C_2C_1Im][MeSO_4]$, $[C_2C_1Im][CF_3SO_3]$, and $[C_2C_1Im]$

$[EtSO_4]$ involving various metal oxides such as Ni, Co, V, Cu, Fe, and Mn coupled with oxidants such as O_2 and H_2O_2 were effective on lignin conversion, however, did not lead to high product yield (Chatel and Rogers, 2013; Xu et al., 2014). Zakzeski et al. (2010b) studied the oxidation of organosolv lignin and soda lignin with 1-ethyl-3-methylimidazilium diethylphosphate, $[C_2C_1Im][DEP]$ IL in presence of transition metal catalysts; however, the study failed to detect any monomeric products *via* GC/MS. In another study, oxidation of lignin model compounds and lignin was investigated using dispersed metal nanoparticle catalyst in $[C_4C_1Im]$ $[MeSO_4]$ or $[C_4C_1Im][PF_6]$ (Zhu et al., 2012). It was postulated that there was insufficient disruption of lignin linkages to yield monomeric products or over-oxidation of monomeric product in the latter case.

Oxidation of lignin is a complex process, involving various kinds of reaction pathways. On the basis of previous literature (Zakzeski et al., 2011) and results obtained for the current study, we proposed a plausible reaction sequence for lignin oxidation in aqueous $[C_2C_1Im][OAc]$. Anion [OAc] from the IL coordinates to the Co or Nb, forming Co[OAc] or Nb[OAc] species. We hypothesize that at 120°C IL behaves as an alkaline medium and under these conditions hydrogen peroxide dissociates to perhydroxyl anion (HOO^-), an extremely strong nucleophile (Xiang and Lee, 2000; Pokutsa et al., 2009). Perhydroxyl anion (HOO^-) combines with Co[OAc] or Nb[OAc] species to cleave the aryl ether bonds of the phenolic moieties of the lignin to form lignin monomers (Varanasi et al., 2012).

CONCLUSION

The alkaline lignin was oxidized to aromatic compounds using transition metal catalysts in presence of H_2O_2 in an aqueous IL, $[C_2C_1Im][OAc]$. Among the seven tested transition metal catalysts, Nb_2O_5 and $CoCl_2$ proved to be the most effective catalysts. From the batch experiment results, catalyst loading and temperature were significant factors affecting lignin conversion and product yield. The highest product concentrations were obtained using Nb_2O_5 catalyst with the main lignin depolymerization products identified and quantified in the extracted oil as guaiacol, syringol, vanillin, acetovanillone, and homovanillic acid. For both catalysts, guaiacol was the major compound, and the formation of guaiacol can be attributed to the cleavage of β-aryl ether bond of the alkaline lignin derived from softwood. Molecular weights of the residual lignin (both M_w and M_n) were lower than untreated alkaline lignin indicating depolymerization of lignin to aromatic products *via* oxidation. Product yield could be further improved by selecting catalyst/IL pairs for better conversion efficacy and selectivity and by applying *in situ* product recovery to minimize lignin repolymerization or product over-oxidation.

AUTHOR CONTRIBUTIONS

LD and JS conceptualized the work, designed experiment, analyzed data, and wrote the manuscript. LD and SX conducted the experiment. All authors have approved the manuscript and agreed with submission to *Frontiers in Energy Research*.
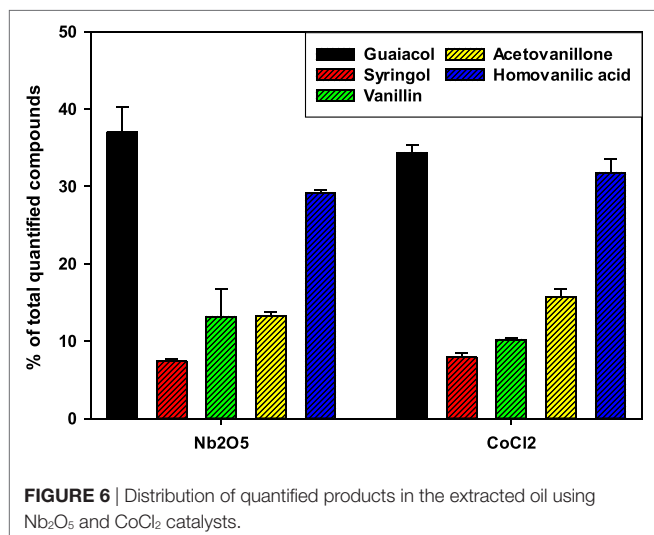
FIGURE 6 | Distribution of quantified products in the extracted oil using Nb_2O_5 and $CoCl_2$ catalysts.

ACKNOWLEDGMENTS

FUNDING

SUPPLEMENTARY MATERIAL

The Supplementary Material for this article can be found online at http://journal.frontiersin.org/article/10.3389/fenrg.2017.00021/full#supplementary-material.

REFERENCES

Beckham, G. T., Johnson, C. W., Karp, E. M., Salvachúa, D., and Vardon, D. R. (2016). Opportunities and challenges in biological lignin valorization. *Curr. Opin. Biotechnol.* 42, 40–53. doi:10.1016/j.copbio.2016.02.030

Behling, R., Valange, S., and Chatel, G. (2016). Heterogeneous catalytic oxidation for lignin valorization into valuable chemicals: what results? What limitations? What trends? *Green Chem.* 18, 1839–1854. doi:10.1039/C5GC03061G

Brandt, A., Chen, L., van Dongen, B. E., Welton, T., and Hallett, J. P. (2015). Structural changes in lignins isolated using an acidic ionic liquid water mixture. *Green Chem.* 17, 5019–5034. doi:10.1039/C5GC01314C

Brown, T. R., and Brown, R. C. (2013). A review of cellulosic biofuel commercial-scale projects in the United States. *Biofuels Bioprod. Biorefin.* 7, 235–245. doi:10.1002/bbb.1387

Cachet, N., Camy, S., Benjelloun-Mlayah, B., Condoret, J.-S., and Delmas, M. (2014). Esterification of organosolv lignin under supercritical conditions. *Ind. Crops Prod.* 58, 287–297. doi:10.1016/j.indcrop.2014.03.039

Chakar, F. S., and Ragauskas, A. J. (2004). Review of current and future softwood kraft lignin process chemistry. *Ind. Crops Prod.* 20, 131–141. doi:10.1016/j.indcrop.2004.04.016

Chatel, G., and Rogers, R. D. (2013). Review: oxidation of lignin using ionic liquids – an innovative strategy to produce renewable chemicals. *ACS Sustainable Chem. Eng.* 2, 322–339. doi:10.1021/sc4004086

Crestini, C., Crucianelli, M., Orlandi, M., and Saladino, R. (2010). Oxidative strategies in lignin chemistry: a new environmental friendly approach for the functionalisation of lignin and lignocellulosic fibers. *Catalysis Today* 156, 8–22. doi:10.1016/j.cattod.2010.03.057

Das, L., Kolar, P., and Sharma-Shivappa, R. (2012). Heterogeneous catalytic oxidation of lignin into value-added chemicals. *Biofuels* 3, 155–166. doi:10.4155/bfs.12.5

Datta, S., Holmes, B., Park, J. I., Chen, Z. W., Dibble, D. C., Hadi, M., et al. (2010). Ionic liquid tolerant hyperthermophilic cellulases for biomass pretreatment and hydrolysis. *Green Chem.* 12, 338–345. doi:10.1039/B916564a

De Gregorio, G. F., Prado, R., Vriamont, C., Erdocia, X., Labidi, J., Hallett, J. P., et al. (2016). Oxidative depolymerization of lignin using a novel polyoxometalate-protic ionic liquid system. *ACS Sustainable Chem. Eng.* 4, 6031–6036. doi:10.1021/acssuschemeng.6b01339

El Hage, R., Brosse, N., Chrusciel, L., Sanchez, C., Sannigrahi, P., and Ragauskas, A. (2009). Characterization of milled wood lignin and ethanol organosolv lignin from miscanthus. *Polym. Degrad. Stab.* 94, 1632–1638. doi:10.1016/j.polymdegradstab.2009.07.007

Fielicke, A., Meijer, G., and von Helden, G. (2003). Infrared spectroscopy of niobium oxide cluster cations in a molecular beam: identifying the cluster structures. *J. Am. Chem. Soc.* 125, 3659–3667. doi:10.1021/ja0288946

García, A., Erdocia, X., Alriols, M. G., and Labidi, J. (2012). Effect of ultrasound treatment on the physicochemical properties of alkaline lignin. *Chem. Eng. Process. Process Intensif.* 62, 150–158. doi:10.1016/j.cep.2012.07.011

Gladden, J. M., Park, J. I., Bergmann, J., Reyes-Ortiz, V., D'haeseleer, P., Quirino, B. F., et al. (2014). Discovery and characterization of ionic liquid-tolerant thermophilic cellulases from a switchgrass-adapted microbial community. *Biotechnol. Biofuels* 7, 15. doi:10.1186/1754-6834-7-15

Gordobil, O., Moriana, R., Zhang, L., Labidi, J., and Sevastyanova, O. (2016). Assessment of technical lignins for uses in biofuels and biomaterials: structure-related properties, proximate analysis and chemical modification. *Ind. Crops Prod.* 83, 155–165. doi:10.1016/j.indcrop.2015.12.048

Kilpeläinen, I., Xie, H., King, A., Granstrom, M., Heikkinen, S., and Argyropoulos, D. S. (2007). Dissolution of wood in ionic liquids. *J. Agric. Food Chem.* 55, 9142–9148. doi:10.1021/jf071692e

Klein-Marcuschamer, D., Simmons, B. A., and Blanch, H. W. (2011). Techno-economic analysis of a lignocellulosic ethanol biorefinery with ionic liquid pre-treatment. *Biofuels Bioprod. Biorefin.* 5, 562–569. doi:10.1002/bbb.303

Li, C., Knierim, B., Manisseri, C., Arora, R., Scheller, H. V., Auer, M., et al. (2010). Comparison of dilute acid and ionic liquid pretreatment of switchgrass: biomass recalcitrance, delignification and enzymatic saccharification. *Bioresour. Technol.* 101, 4900–4906. doi:10.1016/j.biortech.2009.10.066

Li, J., Henriksson, G., and Gellerstedt, G. (2007). Lignin depolymerization/repolymerization and its critical role for delignification of aspen wood by steam explosion. *Bioresour. Technol.* 98, 3061–3068. doi:10.1016/j.biortech.2006.10.018

Marszałł, M. P., and Kaliszan, R. (2007). Application of ionic liquids in liquid chromatography. *Crit. Rev. Anal. Chem.* 37, 127–140. doi:10.1080/10408340601107847

Mottiar, Y., Vanholme, R., Boerjan, W., Ralph, J., and Mansfield, S. D. (2016). Designer lignins: harnessing the plasticity of lignification. *Curr. Opin. Biotechnol.* 37, 190–200. doi:10.1016/j.copbio.2015.10.009

Nakajima, K., Baba, Y., Noma, R., Kitano, M., Kondo, J. N., Hayashi, S., et al. (2011). $Nb_2O_5 \cdot nH_2O$ as a heterogeneous catalyst with water-tolerant Lewis acid sites. *J. Am. Chem. Soc.* 133, 4224–4227. doi:10.1021/ja110482r

Pandey, M. P., and Kim, C. S. (2011). Lignin depolymerization and conversion: a review of thermochemical methods. *Chem. Eng. Technol.* 34, 29–41. doi:10.1002/ceat.201000270

Park, S., and Kazlauskas, R. J. (2003). Biocatalysis in ionic liquids-advantages beyond green technology. *Curr. Opin. Biotechnol.* 14, 432–437. doi:10.1016/S0958-1669(03)00100-9

Pokutsa, A., Makitra, R., Maksim, D., and Pal'chikova, E. Y. (2009). Quantitative accounting for the medium effect at the catalytic decomposition of H_2O_2 in hydrophilic solvents. *Russ. J. Gen. Chem.* 79, 1425–1429. doi:10.1134/S1070363209070032

Prado, R., Brandt, A., Erdocia, X., Hallet, J., Welton, T., and Labidi, J. (2016a). Lignin oxidation and depolymerisation in ionic liquids. *Green Chem.* 18, 834–841. doi:10.1039/C5GC01950H

Prado, R., Erdocia, X., De Gregorio, G. F., Labidi, J., and Welton, T. (2016b). Willow lignin oxidation and depolymerization under low cost ionic liquid. *ACS Sustain Chem. Eng.* 4, 5277–5288.

Pu, Y., Jiang, N., and Ragauskas, A. J. (2007). Ionic liquid as a green solvent for lignin. *J. Wood Chem. Technol.* 27, 23–33. doi:10.1080/02773810701282330

Ragauskas, A. J., Beckham, G. T., Biddy, M. J., Chandra, R., Chen, F., Davis, M. F., et al. (2014). Lignin valorization: improving lignin processing in the biorefinery. *Science* 344, 1246843. doi:10.1126/science.1246843

Rodrigues Pinto, P. C., Borges da Silva, E. A., and Rodrigues, A. E. (2010). Insights into oxidative conversion of lignin to high-added-value phenolic aldehydes. *Ind. Eng. Chem. Res.* 50, 741–748. doi:10.1021/ie102132a

Samuel, R., Pu, Y., Jiang, N., Fu, C., Wang, Z.-Y., and Ragauskas, A. (2014). Structural characterization of lignin in wild-type versus COMT down-regulated switchgrass. *Front. Energy Res.* 1:14. doi:10.3389/fenrg.2013.00014

Shi, J., Balamurugan, K., Parthasarathi, R., Sathitsuksanoh, N., Zhang, S., Stavila, V., et al. (2014). Understanding the role of water during ionic liquid pretreatment of lignocellulose: co-solvent or anti-solvent? *Green Chem.* 16, 3830–3840. doi:10.1039/c4gc00373j

Shi, J., Pattathil, S., Parthasarathi, R., Anderson, N. A., Im Kim, J., Venketachalam, S., et al. (2016). Impact of engineered lignin composition on

biomass recalcitrance and ionic liquid pretreatment efficiency. *Green Chem.* 18, 4884–4895. doi:10.1039/C6GC01193D

Sigma-Aldrich. (2016). *Certification of Origin.* Available at: http://www.sigmaaldrich.com/catalog/CertOfOriginPage.do?symbol=471003&brand=ALDRICH&LotNo=04414PEV&brandTest=ALDRICH

Somerville, C., Youngs, H., Taylor, C., Davis, S. C., and Long, S. P. (2010). Feedstocks for lignocellulosic biofuels. *Science* 329, 790–792. doi:10.1126/science.1189268

Stärk, K., Taccardi, N., Bösmann, A., and Wasserscheid, P. (2010). Oxidative depolymerization of lignin in ionic liquids. *ChemSusChem* 3, 719–723. doi:10.1002/cssc.200900242

Tan, S. S., MacFarlane, D. R., Upfal, J., Edye, L. A., Doherty, W. O., Patti, A. F., et al. (2009). Extraction of lignin from lignocellulose at atmospheric pressure using alkylbenzenesulfonate ionic liquid. *Green Chem.* 11, 339–345. doi:10.1039/b815310h

Tejado, A., Pena, C., Labidi, J., Echeverria, J., and Mondragon, I. (2007). Physico-chemical characterization of lignins from different sources for use in phenol-formaldehyde resin synthesis. *Bioresour. Technol.* 98, 1655–1663. doi:10.1016/j.biortech.2006.05.042

Tilman, D., Socolow, R., Foley, J. A., Hill, J., Larson, E., Lynd, L., et al. (2009). Beneficial biofuels – the food, energy, and environment trilemma. *Science* 325, 270–271. doi:10.1126/science.1177970

Toledano, A., Serrano, L., and Labidi, J. (2014). Improving base catalyzed lignin depolymerization by avoiding lignin repolymerization. *Fuel* 116, 617–624. doi:10.1016/j.fuel.2013.08.071

Varanasi, P., Singh, P., Arora, R., Adams, P. D., Auer, M., Simmons, B. A., et al. (2012). Understanding changes in lignin of *Panicum virgatum* and *Eucalyptus globulus* as a function of ionic liquid pretreatment. *Bioresour. Technol.* 126, 156–161. doi:10.1016/j.biortech.2012.08.070

Varanasi, P., Singh, P., Auer, M., Adams, P. D., Simmons, B. A., and Singh, S. (2013). Survey of renewable chemicals produced from lignocellulosic biomass during ionic liquid pretreatment. *Biotechnol. Biofuels* 6, 1. doi:10.1186/1754-6834-6-14

Wachs, I. E., Briand, L. E., Jehng, J.-M., Burcham, L., and Gao, X. (2000). Molecular structure and reactivity of the group V metal oxides. *Catalysis Today* 57, 323–330. doi:10.1016/S0920-5861(99)00343-0

Xiang, Q., and Lee, Y. (2000). Oxidative cracking of precipitated hardwood lignin by hydrogen peroxide. *Appl. Biochem. Biotechnol.* 84, 153–162. doi:10.1385/ABAB:84-86:1-9:153

Xu, C., Arancon, R. A. D., Labidi, J., and Luque, R. (2014). Lignin depolymerisation strategies: towards valuable chemicals and fuels. *Chem. Soc. Rev.* 43, 7485–7500. doi:10.1039/c4cs00235k

Zakzeski, J., Bruijnincx, P. C., Jongerius, A. L., and Weckhuysen, B. M. (2010a). The catalytic valorization of lignin for the production of renewable chemicals. *Chem. Rev.* 110, 3552–3599. doi:10.1021/cr900354u

Zakzeski, J., Jongerius, A. L., and Weckhuysen, B. M. (2010b). Transition metal catalyzed oxidation of Alcell lignin, soda lignin, and lignin model compounds in ionic liquids. *Green Chem.* 12, 1225–1236. doi:10.1039/c001389g

Zakzeski, J., Bruijnincx, P. C., and Weckhuysen, B. M. (2011). In situ spectroscopic investigation of the cobalt-catalyzed oxidation of lignin model compounds in ionic liquids. *Green Chem.* 13, 671–680. doi:10.1039/c0gc00437e

Zhang, Z., Song, J., and Han, B. (2016). Catalytic transformation of lignocellulose into chemicals and fuel products in ionic liquids. *Chem. Rev.* 117, 6834–6880. doi:10.1021/acs.chemrev.6b00457

Zhu, Y., Chuanzhao, L., Sudarmadji, M., Hui Min, N., Biying, A. O., Maguire, J. A., et al. (2012). An efficient and recyclable catalytic system comprising nanopalladium (0) and a pyridinium salt of iron bis (dicarbollide) for oxidation of substituted benzyl alcohol and lignin. *ChemistryOpen* 1, 67–70. doi:10.1002/open.201100014

Conflict of Interest Statement: The authors declare that the research was conducted in the absence of any commercial or financial relationships that could be construed as a potential conflict of interest.

Characteristics of Lignin Fractions from Dilute Acid Pretreated Switchgrass and Their Effect on Cellobiohydrolase from *Trichoderma longibrachiatum*

Lan Yao[1,2,3], Haitao Yang[1,2], Chang Geun Yoo[4], Xianzhi Meng[3], Yunqiao Pu[3], Naijia Hao[3] and Arthur J. Ragauskas[3,4,5]*

[1] Hubei Provincial Key Laboratory of Green Materials for Light Industry, Hubei University of Technology, Wuhan, China, [2] State Key Laboratory of Pulp and Paper Engineering, South China University of Technology, Guangzhou, China, [3] Department of Chemical and Biomolecular Engineering, The University of Tennessee, Knoxville, TN, United States, [4] Joint Institute for Biological Sciences, Biosciences Division, Oak Ridge National Laboratory (ORNL), Oak Ridge, TN, United States, [5] Department of Forestry, Wildlife and Fisheries, Center for Renewable Carbon, Institute of Agriculture, The University of Tennessee, Knoxville, TN, United States

To investigate the interactions between acid pretreated switchgrass lignin and cellobio-hydrolase (CBH), three different lignin fractions were isolated from dilute acid pretreated switchgrass by (i) ethanol extraction, followed by (ii) dioxane/H_2O extraction, and (iii) cellulase treatment, respectively. Structural properties of each lignin fraction were eluci-dated by GPC, ^{13}C-NMR, and 2D-HSQC NMR analyses. The adsorptions of CBH to the isolated lignin fractions were also studied by Langmuir adsorption isotherms. Ethanol-extractable lignin fraction, mainly composed of syringyl (S) and guaiacyl (G) units, had the lowest molecular weight, while dioxane/H_2O-extracted lignin fraction had the lowest S/G ratio with higher content of *p*-coumaric acid (*p*CA) unit. The residual lignin fraction after enzymatic treatment had the highest S/G ratio without hydroxyphenyl (H) unit. Strong associations were found between lignin properties such as lignin composition and S/G ratio and its non-productive enzyme adsorption factors including the maximum adsorption capacity and binding strength.

Keywords: characterization, lignin, dilute acid pretreatment, switchgrass, cellobiohydrolase

INTRODUCTION

Rapid population growth and energy security concerns associated with fossil fuels have led to the development in alternative energy resources like biofuels (Cao et al., 2012). Second-generation bio-fuel produced from energy crops, agricultural, and forestry residues can avoid competition with food resources, thus it is a promising alternative fuel technology (Yan et al., 2010). Switchgrass has been considered as a potential feedstock for bioethanol production due to its high net energy content, low production costs, low nutrient necessity, high water utilization efficiency, and high pests and diseases tolerance (Samuel et al., 2010).

Pretreatment is an essential step for effective biological conversion of biomass to bioethanol. Diverse pretreatment technologies have been introduced to reduce biomass recalcitrance (Li et al., 2014). Among various pretreatment methods, dilute acid pretreatment has been widely investi-gated and applied, which typically employing a low concentration of H_2SO_4 (<4%) at moderate

temperatures (140–220°C) (Galbe and Zacchi, 2007; Yao et al., 2010). Compared to other pretreatment methods, by now, this pretreatment method is close to practical application in industrial production due to low chemical cost and utilization with diverse biomass feedstocks including hardwood and agricultural residues (Benjamin et al., 2013; Mesa et al., 2017). Typically, pretreated biomass is then subjected to enzymatic hydrolysis to produce glucose *via* a mixture of enzymes such as endoglucanase (EG), exoglucanase or cellobiohydrolases (CBHs), and β-glucosidase (Abraham et al., 2014). CBHs are a group of cellulases that can hydrolyze glycosidic linkages at a crystalline surface of cellulose (Igarashi et al., 2009). In particular, CBH I (TrCel7A) is one of the most abundant enzymes secreted by *Trichoderma reesei*. It was reported that Cel7A showed higher hydrolytic power than other *T. reesei* enzymes involving cellulose hydrolysis (Yan et al., 2011). In recent years, researches have focused on CBH binding to lignin. Palonen et al. found that CBH I exhibited a higher adsorption affinity to lignin than EG II from *T. reesei* (Palonen et al., 2004). Strong bindings of *Trichoderma reesei* CBH-I and EG-I to both cellulose and lignin were observed using quartz crystal microgravimetry (Martín et al., 2013). Other studies reported that the cellulose binding domain of the effluent enzyme played a significant role in the unspecific binding of cellulases to lignin (Palonen et al., 2004; Rahikainen et al., 2013; Strobel et al., 2015, 2016). *T. longibrachiatum*, which are taxonomically separable from *T. reesei*, could also act as a potential cellulase candidate with high activities (Kubicek et al., 1996).

Lignin is the most abundant non-carbohydrate component in plant cell walls and is considered a leading contributor involved in biomass recalcitrance. Lignin is typically derived from three hydroxycinnamyl alcohols (monolignols) that include *p*-coumaryl, coniferyl, and sinapyl alcohols which are connected *via* various types of linkages including aryl ether and carbon–carbon bonds (Ralph et al., 2004; Ragauskas et al., 2014). It is widely accepted that lignin inhibits enzymatic hydrolysis of lignocellulosic biomass (Zeng et al., 2014; Lu et al., 2016; Saini et al., 2016; Yang et al., 2016). The adsorption of enzymes onto isolated lignins from dilute acid or hot water pretreated biomass has been studied (Zheng et al., 2013; Yu et al., 2014; Li et al., 2016; Lu et al., 2016; Sun et al., 2016). They reported key lignin-enzyme binding effects including the effects of condensed phenolic OH groups, methoxy groups, and the degree of lignin condensation on cellulase binding.

The difficulty in elucidating the mechanism of cellulase adsorption to lignin is partly due to the structural complexity of lignin. Thus, a method to fractionate lignin and get lignin fractions with distinctive structure is needed. Lignin fractionation using different hydrogen-bonding capacity organic solvents was introduced to elucidate structural properties of lignin (Mörck et al., 1986, 1988; Yuan et al., 2009). In order to fractionate lignin with various properties that might affect its adsorption capabilities to enzymes, in this study, three different lignin fractions were separated from the dilute acid pretreated switchgrass using ethanol extraction (Fraction NO.1 lignin), followed by 96% dioxane extraction (Fraction NO.2 lignin), and then overloading with cellulase to recover lignin residue (Fraction NO.3 lignin). Characteristics of each lignin fraction were analyzed by gel

permeation chromatography (GPC), ^{13}C-nuclear magnetic resonance (NMR) and 2D-heteronuclear single quantum coherence (HSQC) NMR. Non-productive enzyme adsorption factors of lignin were evaluated by measuring the adsorption of CBHs to lignin samples. The correlations between physicochemical characteristics of lignin and lignin-enzyme adsorption parameters were also discussed.

EXPERIMENTAL

Materials

Samples of the lowland cultivar Alamo switchgrass (*Panicum virgatum*), which were grown in 2011 and harvested in 2012 were provided by the Samuel Roberts Noble Foundation in Ardmore, OK. The chemical reagents were purchased from Fisher Scientific (USA) and used as received without further purification unless otherwise specified. Protease (Cat. No. 10165921001) was purchased from Sigma Chemical Company (USA), and CBH (Cat. No. 37329-65-0) was purchased from Megazyme (Ireland).

Dilute Acid Pretreatment of Switchgrass

The biomass sample was Wiley-milled through a 2 mm screen and then extracted by toluene/ethanol (2:1, *v/v*) for 8 h, followed by water and acetone for 3 h per each extraction to remove extractives (Hao et al., 2017). The extractive-free material was loaded to a 1 L 4560 Parr reactor (Parr Instrument Company, Moline, IL, USA) with 1% sulfuric acid (*v/v*) solution at a 10% solid loading (*w/w*). The pretreatment temperature was set at 150 ± 2°C and kept for 10 min (±0.5 min), which was the optimum dilute-acid pretreatment condition for switchgrass in the previous study (Zhou et al., 2012). The stirring speed was 2.5 Hz and the heating rate was 3°C/min. To stop the pretreatment process, the Parr reactor was quenched in an ice water bath. The pretreated switchgrass was seperated and washed with deionized water until the effluent pH was neutral, then the biomass was air-dried overnight. The yield for pretreatment was 43% by mass of the initial substrate.

Fractionation of Lignin from Pretreated Switchgrass

Lignin fractions were separated from dilute acid pretreated switchgrass as shown in **Figure 1**. The detailed method was the same as described in a previous study (Yao et al., 2017). In brief, the pretreated switchgrass was first extracted with anhydrous ethanol (liquid:solid = 10:1) for 24 h (×2) and ethanol-solved lignin fraction was purified as NO.1 lignin. The air-dried solid residues after ethanol extraction was treated by 96% dioxane (*v/v*) to get the dioxane-water soluble lignin (NO.2 lignin). The last lignin fraction was obtained by over-loading cellulase hydrolysis of the solid residues followed by 96% dioxane (*v/v*) extraction. Each lignin fraction was purified according to the milled wood lignin method (Björkman, 1956). The relative quantity of each lignin fraction was 62.6, 35.4, and 2.0%.

Analysis Procedures
Chemical Composition Analysis
Lignin and carbohydrate contents were determined according to the National Renewable Energy Laboratory procedure (Sluiter

FIGURE 1 | Fractionation of lignin from dilute-acid pretreated switchgrass.

TABLE 1 | Weight-average (M_w), number-average (M_n) molecular weights and polydispersity indexes (M_w/M_n) of the three lignin samples.

Samples	M_n g/mol	M_w g/mol	M_w/M_n
NO.1 lignin	1,511 ± 50	2,277 ± 75	1.51 ± 0.00
NO.2 lignin	2,177 ± 71	3,551 ± 85	1.63 ± 0.01
NO.3 lignin	2,187 ± 74	3,284 ± 93	1.51 ± 0.01

TABLE 2 | Chemical composition of three lignin samples.

Samples	Acid insoluble lignin %	Glucose%	Total%
NO.1 lignin	89.35	0.20	89.55
NO.2 lignin	90.20	0.15	90.35
NO.3 lignin	90.02	0.20	90.22

et al., 2008) and analyzed by a high-performance anion exchange chromatography (Dionex, ICS 3000, Sunnyvale, CA, USA), as described in a previous study (Meng et al., 2013).

GPC Analysis

The molecular weights of each lignin fraction was measured with GPC analysis after acetylation of lignins (Kumar et al., 2013). GPC was performed on an Agilent 1200 HPLC system (Agilent Technologies, Inc, Santa Clara, CA, USA).

NMR Analysis

About 50 mg of lignin samples were dissolved in deuterated dimethyl sulfoxide (DMSO-d_6, 0.4 mL). Two-dimensional (2D) ^{1}H–^{13}C HSQC NMR experiment was conducted at 298 K using a Bruker Advance III 400-MHz spectroscopy (5-mm BBO 400 MHz W1 with Z-gradient probe, Bruker). A Bruker standard pulse sequence ("hsqcetgpsi2") was used. Operation parameters were obtained from a previous study (Yoo et al., 2017).

^{31}P NMR spectra were obtained after derivatization of the lignin fractions by 2-chloro-4,4,5,5-tetramethyl-1,3,2-dioxaphospholane. Endo N-hydroxy-5-norbene-2,3-dicarboxylic acid imide was prepared as the internal standard. The spectral acquistion parameters for ^{31}P NMR spectra were as follows: a 90° pulse angle, 25-s pulse delay, and 256 transients at room temperature.

Adsorption of CBH to Lignin

Prior to conducting the adsorption test, soluble impurities in the lignin fraction was removed with acetate buffer (50 mM, pH 4.8) at 50°C for 12 h. CBH (Megazyme, Wicklow, Ireland), from *Trichoderma longibrachiatum*, was supplied at 10 mg protein/mL. The adsorption of CBH to the lignins was measured by the Langmuir isotherm. A range concentration of CBH (0.1–10.0 mg/mL) was mixed with lignin fractions (2%, *w/v*) suspended in 50 mM sodium acetate buffer (pH 4.8). The mixture was kept at 50°C with 150 rpm shaking for 4 h to reach the equilibrium. Lignin in acetate buffer (2%, *w/v*) and the same concentration of CBH were used as the controls. The protein concentration was determinated by Pierce™ bicinchoninic acid protein assay from Thermo scientific. The adsorption parameters, such as E_{max} and

K_{ads} were obtained by linear regression of the adsorption data by the following Equation.

$$\frac{[E_f]}{[E]} = \frac{1}{K_{ads}[E_{max}]} + \frac{[E_f]}{[E_{max}]}$$

where $[E_f]$ (mg/mL) is the free protein concentration at equilibrium, $[E]$ (mg/mg) is the amount of protein adsorbed by lignin, K_{ads} is Langmuir adsorption constant, and $[E_{max}]$ is the maximum amount of adsorbed protein.

RESULTS AND DISCUSSION

Molecular Weight and Chemical Composition of Lignin

Table 1 presents molecular weights of three lignin fractions isolated from dilute acid pretreated switchgrass. Molecular weights of these lignins were lower than the values of untreated switchgrass in the previous study [5,000 g/mol of weight average molecular weight (M_w) and 2,940 g/mol of number average molecular weight (M_n), respectively] (Samuel et al., 2010). It indicated that these lignin fractions extracted was depolymerized during the dilute acid pretreatment. In addition, slightly lower polydispersity indexes of the three lignin samples (1.51–1.63) were observed as compared to that of initial lignin from untreated sample (1.70), suggesting a narrower molecular weight distribution of these lignins. In specific, the weight average molecular weight of the NO.1 lignin extracted by ethanol was 2,277 g/mol, which represents the lowest molecular weight among all three fractions, while the NO.2 and NO.3 lignin fractions had higher Mw (3,551 and 3,284 g/mol, respectively).

The carbohydrate and lignin content of the three lignin fractions are presented in **Table 2**. The results showed that the acid insoluble lignin contents were 90% for all three lignin samples with small quantity of glucose. There were no significant compositional differences among the three lignin fractions.

^{13}C NMR Analysis

NMR is a well-established analytical tool to observe lignin structures (Capanema et al., 2004). To compare the characteristic
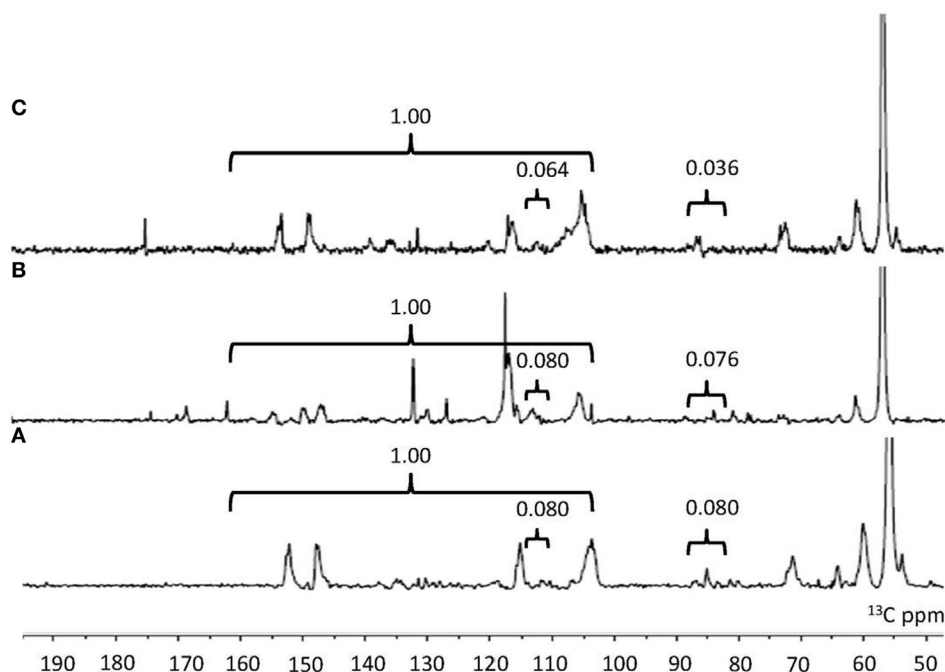
FIGURE 2 | ^{13}C-NMR spectra and integration value of lignin samples **(A)** NO.1 lignin. **(B)** NO.2 lignin. **(C)** NO.3 lignin. 160–102 ppm in the quantitative ^{13}C nuclear magnetic resonance was representative of the total carbon atoms from all aromatic rings within the lignin. 119–113 and 88–82 ppm was used as internal standard in the aromatic and aliphatic region.

of the isolated lignin samples, quantitative ^{13}C NMR was carried out. ^{13}C-NMR spectra of lignin samples are shown in **Figure 2**. The assignments of signals are listed in **Table 3**. In the aromatic region, the signals were mainly from guaiacyl (G), syringyl (S) and *p*-hydroxyphenyl (H). It was facile to assign signals for these three substructures in NO.1 and NO.2 lignin at 128.9 ppm ($C_{2/6}$ in *p*-hydroxyphenyl), 115.0 ppm (C_5 in guaiacyl), and 104.0 ppm ($C_{2/6}$ in syringyl) (Yang et al., 2016). The signal at ~173.9 ppm assigned for C = O was absent in NO. 1 and 2 lignin. In the aliphatic region, the signals from –OCH$_3$ at 55.8 ppm, β-O-4′ at around 72.3 ppm (Cα in β-O-4′), 85.2 ppm (Cβ in S type β-O-4′) and 60.1 ppm (Cγ in β-O-4′), β-5 at about 86.8 ppm (Cα) and Cγ in β-β′ at ~71.7 ppm (Samuel et al., 2010; Strobel et al., 2016) were readily assigned.

Structural Information of Lignin Fractions using 2D-HSQC NMR Analysis

HSQC is the most applied 2D NMR techniques for the structure determination of lignin samples with enhanced spectral resolution. HSQC spectra of aromatic and aliphatic regions of each lignin fraction from dilute acid pretreated switchgrass are shown in **Figure 3**. The cross peaks were assigned according to previous studies (Samuel et al., 2010; Hu et al., 2012; Zeng et al., 2013; Yang et al., 2016).

In aromatic region, lignin subunits such as G, S, and H units were observed. The spectra indicated that the lignin fractions were mainly enriched in G and S units with small contents of H unit in NO.1 and NO.2 lignin. The ^{13}C–^{1}H correlation for

TABLE 3 | Signal assignments for the ^{13}C-NMR spectra of three lignin samples from dilute acid pretreated switchgrass.

Assignments	Chemical shift (ppm)		
	NO.1 lignin	**NO.2 lignin**	**NO.3 lignin**
C = O	–	–	173.9
$C_{3/5}$ in syringyl	152.5	152.7	152.2
C_3 in guaiacyl	147.8	148.0	147.5
$C_{2/6}$ in *p*-hydroxyphenyl	128.9	128.9	–
C_6 in guaiacyl	–	111.8	119.1
C_5 in guaiacyl	115.4	115.1	115.9
C_2 in guaiacyl	111.8	111.4	–
$C_{2/6}$ in syringyl	104.1	104.1	104.0
$C_α$ in β-5	86.8	86.8	87.1
$C_β$ in S type β-O-4′	85.2	85.1	85.3
$C_α$ in β-O-4′	72.3	72.3	72.2
$C_γ$ in β-β′	71.7	71.6	71.4
$C_γ$ in β-O-4′	60.1	60.0	59.7

$S_{2/6}$ was found at δ_C/δ_H 103.0/6.6 ppm. Cross peak from $C_{2/6}$/$H_{2/6}$ in oxidized Cα = O was shifted to δ_C/δ_H 106.0/7.3 ppm. Condensed S (δ_C/δ_H106.6/6.5 ppm) unit was observed in NO.1 and NO.3 lignin fractions, while the signal from condensed G (δ_C/δ_H113.4/6.7 ppm) was found only in ethanol-extractable lignin fraction. For relative abundance analysis of the lignin subunits in this region, the range of δ_C/δ_H 113–109/7.6–6.8 ppm was used as the internal standard (Zeng et al., 2013). The ^{13}C–^{1}H correlation for $S_{2/6}$ at δ_C/δ_H 103.0/6.6 ppm, G_2 at δ_C/δ_H 111.0/6.9 ppm, $H_{2/6}$ at δ_C/δ_H 128.0/7.2 ppm, and *p*CA$_{2/6}$ at δ_C/δ_H130.0/7.4 ppm were used for volume integration of the S,
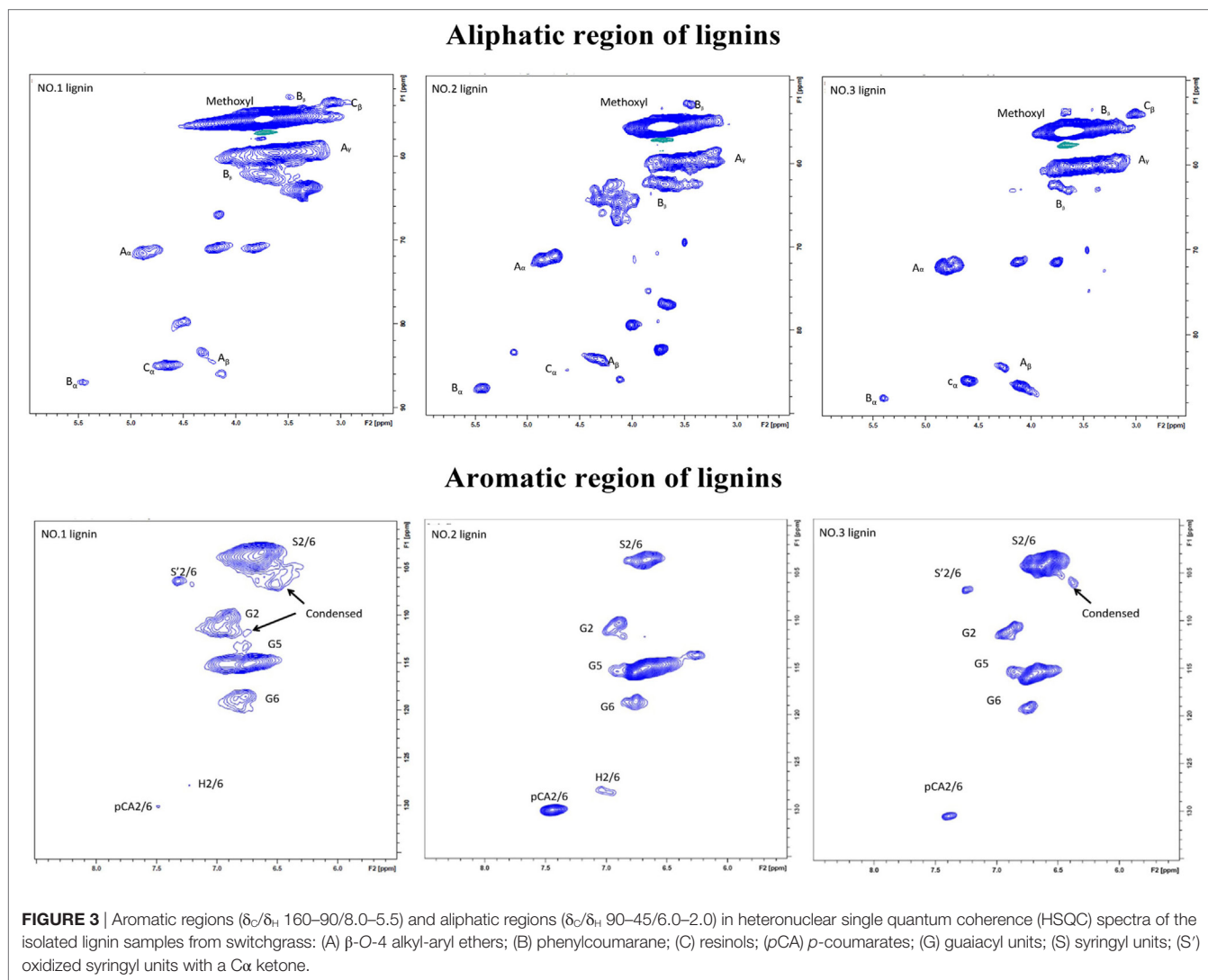
FIGURE 3 | Aromatic regions (δ_C/δ_H 160–90/8.0–5.5) and aliphatic regions (δ_C/δ_H 90–45/6.0–2.0) in heteronuclear single quantum coherence (HSQC) spectra of the isolated lignin samples from switchgrass: (A) β-*O*-4 alkyl-aryl ethers; (B) phenylcoumarane; (C) resinols; (*p*CA) *p*-coumarates; (G) guaiacyl units; (S) syringyl units; (S′) oxidized syringyl units with a Cα ketone.

G, H, and *p*-coumaric acid (*p*CA) moieties. Analysis results by a combination of ^{13}C NMR and 2D-HSQC NMR were also shown and the results were expressed as number of specific subunit per 100 aromaitc rings (Ar). As presented in **Table 4**, the relative content of S unit was the highest in NO.3 lignin (62.8/100 Ar and 74.8%) and the lowest in NO.2 lignin (22.0/100 Ar and 36.6%), while the relative content of G unit in those samples was decreased in the order of NO.1 lignin (34.6/100 Ar) > NO.2 lignin (28.2/100 Ar) > NO.3 lignin (23.1/100 Ar). The S/G ratios of the three lignin fractions were 1.4, 0.7, and 2.9 for NO.1 lignin, NO.2 lignin, and NO.3 lignin, respectively. H units were mainly found in NO.2 lignin fraction (96% dioxane extraction). Previous studies showed that *p*CA was formed *via* lignification of *p*-coumarolyated monolignols and acylated at γ-OH (Del et al., 2012; Zeng et al., 2013), which was mostly contained in NO.2 lignin (12.0/100 Ar), followed by NO.3 (3.1/100 Ar) and NO.1 (0.4/100 Ar) lignin.

The C–H correlations of methoxyl group (–OCH$_3$), β-*O*-4, β-5, and β-β were observed in the aliphatic region. For the quantitative analysis of the lignin subunits in this region, the

range of δ_C/δ_H 88–82/5.6–3.9 ppm was used as the internal standard (Zeng et al., 2013). Signals from Cα/Hα in β-*O*-4 linkage at δ_C/δ_H 72.0/4.8 ppm, Cα/Hα in phenylcoumaran (β-5) substructure at δ_C/δ_H 87.0/5.4 ppm, Cα/Hα in resinol (β-β) substructure at δ_C/δ_H 85.0/4.6 ppm were used to represent the total linkages. The analysis results showed that β-*O*-4 was the dominant interunit linkages in the lignin fractions, which accounted for 61.7, 73.1, and 76.4% for NO.1, NO.2, and NO.3 lignin fraction, respectively. NO.2 lignin had the highest β-*O*-4 content (18.6/100 Ar), while NO.3 lignin had the lowest (8.6/100 Ar). The same trend could also be found in the content of phenylcoumaran linkages. More resinol linkages were observed than phenylcoumaran linkages in NO.1 and NO.3 lignin fractions, while phenylcoumaran linkages were more abundant than resinol in NO.2 lignin.

^{31}P-NMR Determination

For the quantitative analysis of hydroxyl group (–OH) in each lignin fraction, ^{31}P NMR analysis was conducted as described in previous study (Pu et al., 2011). Quantitative analysis results of

TABLE 4 | Nuclear magnetic resonance analysis results of three lignin samples fractionated from dilute acid pretreated switchgrass.

Lignin substructure	NO.1 lignin		NO.2 lignin		NO.3 lignin	
	Ar[a]	%[b]	Ar[a]	%[b]	Ar[a]	%[b]
S	48.5 ± 0.01	58.0 ± 0.03	22.0 ± 0.04	36.6 ± 0.02	64.8 ± 0.24	74.8 ± 0.02
G	34.6 ± 0.05	41.7 ± 0.03	28.2 ± 0.03	53.2 ± 0.04	23.1 ± 0.63	25.2 ± 0.02
H	0.3 ± 0.01	0.3 ± 0.00	6.4 ± 0.04	0.11 ± 0.01	0	0
p-coumaric acid (pCA)	0.4 ± 0.00	0.7 ± 0.00	12.0 ± 0.08	21.9 ± 0.01	3.1 ± 0.02	3.7 ± 0.00
S/G	1.4 ± 0.01	1.4 ± 0.08	0.8 ± 0.01	0.7 ± 0.00	2.8 ± 0.06	2.9 ± 0.07
β-O-4	10.4 ± 0.01	61.7 ± 0.01	18.6 ± 0.04	73.1 ± 0.04	8.6 ± 0.10	76.4 ± 0.02
β-5	1.7 ± 0.03	11.0 ± 0.01	8.3 ± 0.01	25.4 ± 0.02	1.1 ± 0.04	9.1 ± 0.02
β-β	4.5 ± 0.01	27.3 ± 0.01	0.6 ± 0.03	1.5 ± 0.01	1.7 ± 0.03	14.5 ± 0.01

[a]Amount of specific functional group was expressed as number per 100 Ar.
[b]Amount of specific functional group was expressed as percentage of S + G + H for S, G, H, and pCA, of total side chain for β-O-4, β-5, and β-β.

FIGURE 4 | ^{31}P-NMR spectra analysis results of lignin fractions from dilute acid pretreated switchgrass.

TABLE 5 | Langmuir adsorption isotherm parameters from CBH adsorption to lignins.

	E_{max} mg/g	K_{ads} ml/mg	Binding strength ml/g lignin	R^2
NO.1 lignin	7.63	4.08	31.13	0.94
NO.2 lignin	5.53	3.34	18.47	0.99
NO.3 lignin	12.32	4.92	60.61	0.99

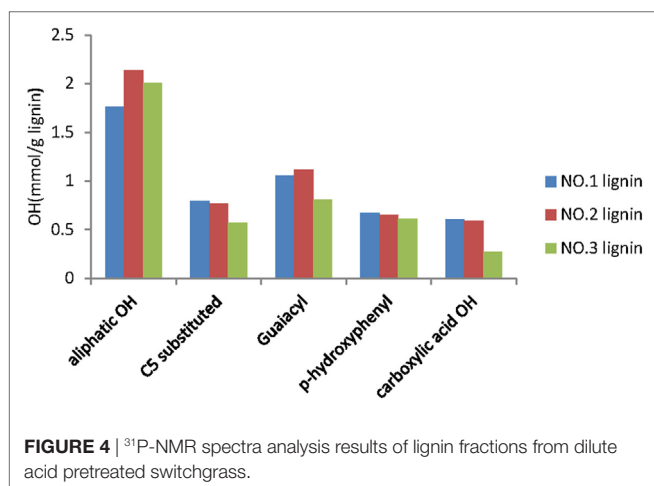OH groups in the lignin fractions were presented in **Figure 4**. The results clearly showed that the aliphatic hydroxyl group was a major hydroxyl group in the three lignin fractions. This was in accordance with the previously reported results, which stated that the dominant hydroxyl groups from lignin of switchgrass after acidic pretreatment were at aliphatic site (Samuel et al., 2010). The NO.2 lignin fraction has the most aliphatic OH content (2.14 mmol/g) and the least C5 substituted OH (0.57 mmol/g), while the NO.1 fraction has the least aliphatic OH content (1.76 mmol/g) and the most C5 substituted OH content (0.79 mmol/g). The contents of other groups from the three lignin fractions were similar, except that the carboxylic acid OH in the NO.3 lignin was only half of that in the other two lignin fractions. Similar results have been previously reported, which indicated that lignin fraction with high molecular weight contains high aliphatic OH and low phenolic OH (Sadeghifar et al., 2017).

CBH Adsorption to Lignins by Langmuir Equation

It was reported that binding ability of lignin to enzymes can represent the binding capacity of lignin in the biomass (Sun et al., 2016). In this study, the binding ability between the isolated lignin fractions and CBH was measured by determining the Langmuir

adsorption isotherms of CBH onto the isolated lignins. The results are shown in **Table 5**. The adsorption data fitted well with the Langmuir isotherm. The maximum adsorptions of CBH were 7.63, 5.53, and 12.32 mg/g for the three lignin fractions, which were similar to the literature (Pareek et al., 2013; Zheng et al., 2013; Machado et al., 2015; Lu et al., 2016; Sun et al., 2016). It should be noted that the binding results could be affected by the different lignin isolation/pretreatment conditions, enzyme and test conditions (temperatures, lignin loading) used for determination. The highest binding strength was observed for NO.3 lignin (60.61 ml/g), followed by NO.1 (31.13 ml/g) lignin and NO.2 lignin (18.47 ml/g). The variations in the adsorption results for the lignin faction samples might be due to the different structural characteristics.

The Relationship between Lignin Structural Characteristic and Non-Productive Enzyme Adsorption Factors

In order to identify the responsible functional groups for the adsorption ability of different lignin samples, the content of different specific groups in lignins was correlated with the corresponding adsorption results. Positive associations were observed between the percentage of S units and the adsorption capacity ($y = 0.1493x + 2.8231$, $R^2 = 0.99$), K_{ads} ($y = 0.0509x + 1.4104$, $R^2 = 0.90$) and binding strength ($y = 1.2773x - 31.129$, $R^2 = 0.76$). Similar correlations was also found between number of S units/100 Ar and binding parameters, suggesting that higher content of S unit in isolated lignin resulted in more adsorbed CBH. In contrast, negative correlations were observed between the content of G unit and the adsorption parameters (E_{max}: $y = -0.725x + 28.745$, $R^2 = 0.92$; K_{ads}: $y = -0.056x + 6.357$, $R^2 = 0.99$; binding

strength: $y = -1.5246x + 97.77$, $R^2 = 0.98$). For the S/G ratio, we also observed positive correlations with maximum adsorption capacity ($y = 3.1233x + 3.7043$, $R^2 = 0.99$), K_{ads} ($y = 0.6931x + 2.9581$, $R^2 = 0.97$), and binding strength ($y = 19.234x + 4.6808$, $R^2 = 0.99$). Similarly, Tan and coworkers (Tan et al., 2015) observed that the milled wood lignin from bisulfite pretreated oil palm empty fruit bunch with a higher S/G ratio showed higher enzyme adsorption. In addition, negative correlations of guaiacyl OH content with maximum adsorption capacity ($y = -21.135x + 29.475$, $R^2 = 0.98$), K_{ads} ($y = -4.6209x + 8.7006$, $R^2 = 0.91$) and binding strength ($y = -131.61x + 167.39$, $R^2 = 0.99$) were found.

The effect of molecular weights and uniformity in lignin fragment size on the cellulase binding has been studied before (Guo et al., 2014; Tan et al., 2015). Among the three lignin fractions from dilute acid pretreated switchgrass, lignin with higher PDI absorbed less CBH during the binding process. It indicated that lignin with more uniform fragment size tends to have stronger binding ability on cellulase. Previous research also reported that PDI was inversely related to the interaction of the lignin with the cellulase (Berlin et al., 2006; Pareek et al., 2013).

Better understanding of the mechanism of cellulase adsorption to lignin is beneficial to the bioethanol production process. It is possible to make modification to lignin accordingly and choose proper pretreatment techniques to reduce the non-productive binding of cellulase to lignin and make the whole process economically feasible. The results indicates that lower S/G ratio in the the pretreated switchgrass lignin has lower non-productive enzyme binding, which could be favorable for enzymatic hydrolysis.

CONCLUSION

To obtain lignin with different physicochemical characteristics, three lignin fractions were extracted from diluted acid pretreated switchgrass. Each lignin fraction was found to have different structural characteristic and adsorption ability to CBH from *Trichoderma longibrachiatum*. It was found that the monolignol composition of syringyl, guaiacyl units, and S/G ratio in switchgrass lignin had correlation with the adsorption ability of lignin and binding strength of CBH. Lignin with lower S/G ratio appeared to have less effect on the CBH adsorption.

REFERENCES

Abraham, R., Verma, M., Barrow, C., and Puri, M. (2014). Suitability of magnetic nanoparticle immobilized cellulases in enhancing enzymatic saccharification of pretreated hemp biomass. *Biotechnol. Biofuels* 7, 90–101. doi:10.1186/1754-6834-7-90

Benjamin, Y., Cheng, H., and Görgens, J. (2013). Evaluation of bagasse from different varieties of sugarcane by diluteacid pretreatment and enzymatic hydrolysis. *Ind. Crops Prod.* 51, 7–18. doi:10.1016/j.indcrop.2013.08.067

Berlin, A., Balakshin, M., Gilkes, N., Kadla, J., Maximenko, V., Kubo, S., et al. (2006). Inhibition of cellulase, xylanase and β-glucosidase activities by softwood lignin preparations. *J. Biotechnol.* 125, 198–209. doi:10.1016/j.jbiotec.2006.02.021

Björkman, A. (1956). Studies on finely divided wood. Part 1.-Extraction of lignin with neutral solvent. *Sven. Papperstidn* 59, 477–485.

Cao, S., Pu, Y., Studer, M., Wyman, C., and Ragauskas, A. J. (2012). Chemical transformations of *Populustrichocarpa* during dilute acid pretreatment. *RSC Adv.* 29, 10925–10936. doi:10.1039/c2ra22045h

Capanema, E., Balakshin, M., and Kadla, J. (2004). A comprehensive approach for quantitative lignin characterization by NMR spectroscopy. *J. Agric. Food Chem.* 52, 1850–1860. doi:10.1021/jf035282b

Del, J., Rencoret, J., Prinsen, P., Martinez, A., Ralph, J., and Gutierrez, A. (2012). Structural characterization of wheat straw lignin as revealed by analytical pyrolysis, 2D-NMR, and reductive cleavage methods. *J. Agric. Food Chem.* 60, 5922–5935. doi:10.1021/jf301002n

Galbe, M., and Zacchi, G. (2007). Pretreatment of lignocellulosic materials for efficient bioethanol production. *Adv. Biochem. Eng. Biotechnol.* 108, 41–65. doi:10.1007/10_2007_070

Guo, F., Shi, W., Sun, W., Li, X., Wang, F., Zhao, J., et al. (2014). Differences in the adsorption of enzymes onto lignins from diverse types of lignocellulosic

biomass and the underlying mechanism. *Biotechnol. Biofuels* 7, 38–47. doi:10.1186/1754-6834-7-38

Hao, N., Lu, K., Ben, H., Adhikari, S., Lacerda, B., and Ragauskas, A. J. (2017). Effect of autohydrolysis pretreatment conditions on sugarcane bagasse structures and product distribution resulting from pyrolysis. *Energy Technol.* 5, 1–10. doi:10.1002/ente.201700490

Hu, G., Cateto, C., Pu, Y., Samuel, R., and Ragauskas, A. (2012). Structural characterization of switchgrass lignin after ethanol organosolv pretreatment. *Energy Fuels* 26, 740–745. doi:10.1021/ef201477p

Igarashi, K., Koivula, A., Wada, M., Kimura, S., Penttilä, M., and Samejima, M. (2009). High speed atomic force microscopy visualizes processive movement of *Trichoderma reesei* cellobiohydrolase I on crystalline cellulose. *J. Biol. Chem.* 284, 36186–36190. doi:10.1074/jbc.M109.034611

Kubicek, C., Bölzlbauer, U., Kovacs, W., Mach, R., Kuhls, K., Lieckfeldt, E., et al. (1996). Cellulase formation by species of *Trichoderma sect. Longibrachiatum* and of *Hypocrea* spp. with anamorphs referable to *Trichoderma sect. Longibrachiatum*. *Fungal Genet. Biol.* 20, 105–114. doi:10.1006/fgbi.1996.0025

Kumar, R., Hu, F., Hubbell, C. A., Ragauskas, A. J., and Wyman, C. E. (2013). Comparison of laboratory delignification methods, their selectivity, and impacts on physiochemical characteristics of cellulosic biomass. *Bioresour. Technol.* 130, 372–381. doi:10.1016/j.biortech.2012.12.028

Li, H., Pu, Y., Kumar, R., Ragauskas, A., and Wyman, C. (2014). Investigation of lignin deposition on cellulose during hydrothermal pretreatment, its effect on cellulose hydrolysis, and underlying mechanisms. *Biotechnol. Bioeng.* 111, 485–492. doi:10.1002/bit.25108

Li, P., Liu, Y., Lu, J., Yang, R., Li, H., and Wang, H. (2016). Structural characterization and effect on enzymatic hydrolysis of milled wood lignin isolated from reed straw and corn stover pretreated with liquid hot water. *BioResources* 11, 8777–8790. doi:10.15376/biores.11.4.8777-8790

Lu, X., Zheng, X., Li, X., and Zhao, J. (2016). Adsorption and mechanism of cellulase enzymes onto lignin isolated from corn stover pretreated with liquid hot water. *Biotechnol. Biofuels* 9, 118–129. doi:10.1186/s13068-016-0531-0

Machado, D., NetoJoão, M., Pradella, J., Bonomi, A., and Aline, C. (2015). Adsorption characteristics of cellulase and β-glucosidase on Avicel, pretreated sugarcane bagasse, and lignin. *Biotechno. Appl. Biochem.* 62, 681–689. doi:10.1002/bab.1307

Martín, R., Rahikainen, J., Johansson, L., Marjamaa, K., Laine, J., Kruus, K., et al. (2013). Preferential adsorption and activity of monocomponent cellulases on lignocellulose thin films with varying lignin content. *Biomacromolecules* 14, 1231–1239. doi:10.1021/bm400230s

Meng, X., Foston, M., Leisen, J., DeMartini, J., Wyman, C. E., and Ragauskas, A. J. (2013). Determination of porosity of lignocellulosic biomass before and after pretreatment by using Simons' stain and NMR techniques. *Bioresour. Technol.* 144, 467–476. doi:10.1016/j.biortech.2013.06.091

Mesa, L., Martínez, Y., Barrio, E., and González, E. (2017). Desirability function for optimization of dilute acid pretreatment of sugarcane straw for ethanol production and preliminary economic analysis based in three fermentation configurations. *Appl. Energ.* 198, 299–311. doi:10.1016/j.apenergy.2017.03.018

Mörck, R., Reimann, A., and Kringstad, K. (1988). Fractionation of kraft lignin by successive extraction with organic solvents. III. Fractionation of kraft lignin from birch. *Holzforschung* 42, 111–116. doi:10.1515/hfsg.1988.42.2.111

Mörck, R., Yoshida, H., and Kringstad, K. (1986). Fractionation of kraft lignin by successive extraction with organic solvents. 1. Functional groups, ^{13}C-NMR-spectra and molecular weight distributions. *Holzforschung* 42, 51–60.

Palonen, H., Tjerneld, F., Zacchi, G., and Tenkanen, M. (2004). Adsorption of *Trichoderma reesei* CBH I and EG II and their catalytic domains on steam pretreated softwood and isolated lignin. *J. Biotechnol.* 107, 65–72. doi:10.1016/j.jbiotec.2003.09.011

Pareek, N., Gillgren, T., and Jönsson, L. (2013). Adsorption of proteins involved in hydrolysis of lignocellulose on lignins and hemicelluloses. *Bioresour. Technol.* 148, 70–77. doi:10.1016/j.biortech.2013.08.121

Pu, Y., Cao, S., and Ragauskas, A. J. (2011). Application of quantitative ^{31}P NMR in biomass lignin and biofuel precursors characterization. *Energy Environ. Sci.* 4, 3154–3166. doi:10.1039/C1EE01201K

Ragauskas, A., Beckham, G., Biddy, M., Chandra, R., Chen, F., Davis, M., et al. (2014). Lignin valorization: improving lignin processing in the biorefinery. *Science* 344, 709–718. doi:10.1126/science.1246843

Rahikainen, J., Evans, J., Mikander, S., Kalliola, A., Puranen, T., Tamminen, T., et al. (2013). Cellulase-lignin interactions—the role of carbohydrate-binding module and pH in non-productive binding. *Enzyme Microb. Technol.* 53, 315–321. doi:10.1016/j.enzmictec.2013.07.003

Ralph, J., Bunzel, M., Marita, J., Hatfield, R., Lu, F., Kim, H., et al. (2004). Peroxidase-dependent cross-linking reactions of phydroxycinnamates in plant cell walls. *Phytochem. Rev.* 3, 79–96. doi:10.1023/B:PHYT.0000047811.13837.fb

Sadeghifar, H., Wells, T., Le, R., Sadeghifar, F., Yuan, J., and Ragauskas, A. (2017). Fractionation of organosolv lignin using acetone: water and properties of the obtained fractions. *ACS Sustainable Chem. Eng.* 5, 580–587. doi:10.1021/acssuschemeng.6b01955

Saini, J., Patel, A., Adsul, M., and Singhania, R. (2016). Cellulase adsorption on lignin: a roadblock for economic hydrolysis of biomass. *Renew. Energy* 98, 29–42. doi:10.1016/j.renene.2016.03.089

Samuel, R., Pu, Y., Raman, B., and Ragauskas, A. J. (2010). Structural characterization and comparison of switchgrass ball-milled lignin before and after dilute acid pretreatment. *Appl. Biochem. Biotechnol.* 162, 62–74. doi:10.1007/s12010-009-8749-y

Sluiter, A., Hames, B., Ruiz, R., Scarlata, C., Sluiter, J., Templeton, D., et al. (2008). *Determination of Structural Carbohydrates and Lignin in Biomass*. Technical Report No. TP-510-42618. Golden, CO: National Renewable Energy Laboratory. Available at: https://www.nrel.gov/docs/gen/fy13/42618.pdf

Strobel, K., Pfeiffer, K., Blanch, H., and Clark, D. (2015). Structural insights into the affinity of Cel7a carbohydrate-binding module for lignin. *J. Biol. Chem.* 290, 22818–22826. doi:10.1074/jbc.M115.673467

Strobel, K., Pfeiffer, K., Blanch, H., and Clark, D. (2016). Engineering Cel7A carbohydrate binding module and linker for reduced lignin inhibition. *Biotechnol. Bioeng.* 113, 1369–1374. doi:10.1002/bit.25889

Sun, S., Huang, Y., Sun, R., and Tu, M. (2016). Strong association of condensed phenolic moieties in isolated lignins with their inhibition of enzymatic hydrolysis. *Green Chem.* 18, 4276–4286. doi:10.1039/C6GC00685J

Tan, L., Sun, W., Li, X., Zhao, J., Qu, Y., Choo, Y., et al. (2015). Bisulfite pretreatment changes the structure and properties of oil palm empty fruit bunch to improve enzymatic hydrolysis and bioethanol production. *Biotechnol. J.* 10, 915–925. doi:10.1002/biot.201400733

Yan, J., Hu, Z., Pu, Y., Brummer, C., and Ragauskas, A. J. (2010). Chemical compositions of four switchgrass populations. *Biomass Bioenergy* 34, 48–53. doi:10.1016/j.biombioe.2009.09.010

Yan, S., Li, T., and Yao, L. (2011). Mutational effects on the catalytic mechanism of cellobiohydrolase I from *Trichoderma reesei*. *J. Phys. Chem. B* 115, 4982–4989. doi:10.1021/jp200384m

Yang, H., Xie, Y., Zheng, X., Pu, Y., Huang, F., Meng, X., et al. (2016). Comparative study of lignin characteristics from wheat straw obtained by soda-AQ and kraft pretreatment and effect on the following enzymatic hydrolysis process. *Bioresour. Technol.* 207, 361–369. doi:10.1016/j.biortech.2016.01.123

Yao, L., Yang, H., Yoo, C. G., Meng, X., Li, M., Pu, Y., et al. (2017). Adsorption of cellobiohydrolases I onto lignin fractions from dilute acidpretreated *Broussonetia papyrifera*. *Bioresour. Technol.* 244, 957–962. doi:10.1016/j.biortech.2017.08.024

Yao, L., Yue, J., Zhao, J., Dong, J., Li, X., and Qu, Y. (2010). Application of acidic wastewater from monosodium glutamate process in pretreatment and cellulase production for bioconversion of corn stover feasibility evaluation. *Bioresour. Technol.* 101, 8755–8761. doi:10.1016/j.biortech.2010.04.104

Yoo, C., Li, M., Meng, X., Pu, Y., and Ragauskas, A. J. (2017). Effects of organosolv and ammonia pretreatments. *Green Chem.* 19, 2006–2016. doi:10.1039/C6GC03627A

Yu, Z., Gwak, K., Treasure, T., Jameel, H., Chang, H., and Park, S. (2014). Effect of lignin chemistry on the enzymatic hydrolysis of woody biomass. *Chem. Sus. Chem.* 7, 1942–1950. doi:10.1002/cssc.201400042

Yuan, T., He, J., Xu, F., and Sun, R. (2009). Fractionation and physico-chemical analysis of degraded lignins from the black liquor of Eucalyptus pellita KP-AQ pulping. *Polym. Dgrade. Stabil.* 94, 1142–1150. doi:10.1016/j.polymdegradstab.2009.03.019

Zeng, J., Helms, G., Gao, X., and Chen, S. (2013). Quantification of wheat straw lignin structure by comprehensive NMR analysis. *J. Agric. Food Chem.* 61, 10848–10857. doi:10.1021/jf4030486

Zeng, Y., Zhao, S., Yang, S., and Ding, S. (2014). Lignin plays a negative role in the biochemical process for producing lignocellulosic biofuels. *Curr. Opin. Biotechnol.* 27, 38–45. doi:10.1016/j.copbio.2013.09.008

Zheng, Y., Zhang, S., Miao, S., Su, Z., and Wang, P. (2013). Temperature sensitivity of cellulase adsorption on lignin and its impact on enzymatic hydrolysis of lignocellulosic biomass. *J. Biotechnol.* 166, 135–143. doi:10.1016/j.jbiotec.2013.04.018

Zhou, X., Xu, J., Wang, Z., Cheng, J., Li, R., and Qu, R. (2012). Dilute sulfuric acid pretreatment of transgenic switchgrass for sugar production. *Bioresour. Technol.* 104, 823–827. doi:10.1016/j.biortech.2011.11.051

Enzymatic Processes to Unlock the Lignin Value

Veera Hämäläinen, Toni Grönroos, Anu Suonpää, Matti Wilhem Heikkilä, Bastiaan Romein, Petri Ihalainen, Sara Malandra and Klara R. Birikh*

MetGen Oy, Kaarina, Finland

Main hurdles of lignin valorization are its diverse chemical composition, recalcitrance, and poor solubility due to high-molecular weight and branched structure. Controlled fragmentation of lignin could lead to its use in higher value products such as binders, coatings, fillers, etc. Oxidative enzymes (i.e., laccases and peroxidases) have long been proposed as a potentially promising tool in lignin depolymerization. However, their application was limited to ambient pH, where lignin is poorly soluble in water. A Finnish biotechnology company, MetGen Oy, that designs and supplies industrial enzymes, has developed and brought to market several lignin oxidizing enzymes, including an extremely alkaline lignin oxidase MetZyme® LIGNO™, a genetically engineered laccase of bacterial origin. This enzyme can function at pH values as high as 10–11 and at elevated temperatures, addressing lignin at its soluble state. In this article, main characteristics of this enzyme as well as its action on bulk lignin coming from an industrial process are demonstrated. Lignin modification by MetZyme® LIGNO™ was characterized by size exclusion chromatography, UV spectroscopy, and dynamic light scattering for monitoring particle size of solubilized lignin. Under highly alkaline conditions, laccase treatment not only decreased molecular weight of lignin but also increased its solubility in water and altered its dispersion properties. Importantly, organic solvent-free soluble lignin fragmentation allowed for robust industrially relevant membrane separation technologies to be applicable for product fractionation. These enzyme-based solutions open new opportunities for biorefinery lignin valorization thus paving the way for economically viable biorefinery business.

Keywords: oxidoreductase, laccase, lignin, biomass, lignocellulosic, enzyme

INTRODUCTION

In the biorefinery context, lignin is often mostly regarded as a recalcitrance factor, fermentation inhibitor, sugar stream contaminant, etc. Broader view to the biorefinery, however, considers valorization of lignin a vital component of the economics of the entire concept.

Today, the commercial sales of lignin are limited but growing. Even though the pulp and paper industry produces about 50 million tons of lignin in a year, as defined by Lux Research (Essery, 2017), most of this is burned for power; only 1 million ton reaches the chemicals market. Lignin is currently being used for low- and medium-value applications (e.g., binding and dispersing agents), representing a market of $730 million. As detailed by Lux Research report (Lux, 2014), the total market value for lignin-derived product is at $3.3B, with energy capturing about 89% of the market. Other markets include vanillin production ($192M) and cement additives ($176M). The market has

both high-value applications, such as carbon fibers and phenols, as well as lower value applications such as binders and activated carbon. The lowest value use of lignin is its use as solid fuel as energy content of the lignin is in the range of 22 MJ/kg.

The growing need for lignin to produce renewable biochemicals from lignocellulosic feedstocks alone is projected to grow up to 2.9 million Mton in 2017. Potential market value of new lignin-based products is estimated to be about \$13.9B by 2020–2025, with lignin-based phenols and carbon fiber poised to capture the largest market potential in the future (Frost and Sullivan, 2014; Smith et al., 2016).

Main hurdles of lignin valorization are its diverse structure and poor solubility. Liquefaction of lignin would allow its use as fuel, as it is reached in high-energy chemical structures. More precise depolymerization or fragmentation of lignin may enable higher value products for various industries from construction to high-performance materials. Notwithstanding the fact that lignin-based replacement products have already been reported (Gandini and Belgacem, 2008; Kim and Kadla, 2010; Laurichesse and Avérous, 2014; Xing et al., 2017) to be useful as binders, coatings, and fillers and others, these applications are not yet widely industrially implemented. Some of the main challenges for full valorization of lignin are the economical production of suitable lignin and maintaining consistent quality throughout different batches.

To achieve desirable properties for the industrial application, lignin usually needs to be fragmented to a lower molecular weight and often chemically modified as well. Some chemo-mechanical methods for lignin depolymerization have been reported (Rinaldi et al., 2016). Different ways to convert lignin to phenolics compounds are liquefaction (Kang et al., 2013), oxidation (Ma et al., 2014), solvolysis (Kleinert and Barth, 2008), hydrocracking (Yoshikawa et al., 2013), and hydrolysis (Roberts et al., 2011). The challenge, however, is that lignin is very difficult to decompose and these processes generate high amounts of solid residue.

Enzymatic degradation of lignin, which occurs in nature, was speculated for a long time to be applicable in the industry (Wong, 2009). This approach seems attractive due to the fact that the catalysis takes place in water and under mild conditions avoiding high pressure, temperatures, and hazardous and expensive chemical catalysts, thus saving CAPEX and lowering environmental impact.

Research efforts for enzymatic lignin depolymerization were especially focusing on laccases (copper oxidases), as these enzymes require no cofactors or cosubstrates (such as hydrogen peroxide), they use oxygen as an electron acceptor and produce water as the only by-product. Prospective and challenges of laccase application in biotechnology were recently reviewed (Roth and Spiess, 2015; Mate and Alcalde, 2017).

Industrially available and most studied laccases are fungal enzymes. These enzymes, however, efficient, mostly work in acidic pH (Rodgers et al., 2010), at which lignin is hardly soluble in water. In addition, fungal enzymes lack the needed thermostability and robustness.

Some studies addressed the feasibility of using these laccases for lignin depolymerization (Munk et al., 2015); however, special measures need to be taken to bring lignin into the soluble state. To this end, laccases were evolved to be used in solvent containing mixtures, ionic liquids, and other technically and economically challenging environments (Mate and Alcalde, 2014; Rehmann et al., 2014). To the best of our knowledge, none of these studies led to an industrially viable enzymatic process for lignin valorization. Alternatively, lignin can be efficiently solubilized in water under alkaline pH. The higher the pH, the higher the lignin solubility. This phenomenon could be exploited in enzymatic depolymerization, where laccases able to function under these conditions.

Bacterial laccases are rather overlooked by the industries due to challenges in their production and lower redox potential as compared to fungal laccases. However, they are also known for larger diversity in operation conditions, including higher thermostability and extended pH range (Santhanam et al., 2011; Rosado et al., 2012). In this respect, they may represent an alternative route to lignin depolymerization—that is by carrying out the process under alkaline conditions.

One of the challenges in laccase application for lignin depolymerization as noted by many experts is the fact that the strong polymerization activity of laccase counters the decomposition of lignin by re-polymerizing the degradation products (Roth and Spiess, 2015). It was postulated (Hahn et al., 2014) that the balance between polymerization and cleavage reactions depend on the structure and redox potential of the laccase, structure and redox potential of the substrate, pH value of the buffer used, incubation temperature, and solvent concentration. Thus, thorough process development is required for directing the reaction into the desired path (Santhanam et al., 2011; Singh et al., 2015). This notion also implies that finding a laccase highly efficient in oxidizing phenolic compounds is not necessarily instrumental for lignin depolymerization. In our experience, highly alkaline pH is more favorable for depolymerization, than acidic conditions.

It has to be noted that even in alkaline conditions lignin may have limited solubility which results in relatively low product titer when compared with chemical processes. Besides, timescale of the enzymatic oxidation poses a challenge, which may be eventually overcome by a continuous process setup with reusable enzyme. Application testing in relevant experimental setup is necessary to evaluate the industrial relevance.

In this study, we present a genetically engineered commercially produced bacterial laccase which is functional and stable at pH as high as 10–11 and demonstrate its use in reactor-scale lignin depolymerization.

MATERIALS AND METHODS

Enzyme Activity Testing with Standard Substrates

Relative laccase activity at different pH with standards substrates, 2,2′-Azino-bis(3-ethylbenzthiazoline-6-sulfonic acid) (ABTS), syringaldazine (SGZ), and 2,6-dimethylphenol (DMP), were determined as follows. Substrates were prepared as 10× stock solutions: 50 mM ABTS and 10 mM DMP in water and 250 µM

SGZ in methanol. Enzyme was diluted to provide linear product accumulation during the reaction time. Reaction mixtures were prepared by adding 10 µl of enzyme to 170 µl of 30 mM Britton & Robinson buffer (pH 2–11) and equilibrated to room temperature in a 96-well microtiter plate. The enzymatic reactions were initiated by adding 20 µl of substrates solutions and oxidation of substrates was followed by monitoring absorbance at 405 nm for ABTS, 450 nm for DMP, and 530 nm SGZ. Relative reaction rates were calculated from the absorbance increase vs time.

Specific enzyme activity was determined using ABTS as substrate. Reaction mixture was prepared by mixing 20 µl of diluted enzyme with 430 µl of 100 mM sodium acetate pH 4.5 in 1-cm light-path spectrophotometer cuvette, the mixture was equilibrated to 60 C; the reaction was initiated by adding 50 µl of ABTS solution and incubated at 60 C; UV measurements at 405 nM were performed every 2 min. One unit of laccase activity was defined as the enzyme amount oxidizing 1 µmol of ABTS per minute under these conditions (whereas extinction coefficient of ABTS at 405 nm is 36,800 M^{-1} cm^{-1}). One microkatal is the amount of enzyme oxidizing 1 µmol of substrate per second, hence 1 µkat equals to 60 U.

Laccase Stability Testing

Laccase stability at different pH was determined by pre-incubation of the enzyme at a certain temperature and pH, followed by measurement of residual activity.

For this, 20 µl of enzyme was added to 180 µl of 150 mM Britton & Robinson buffers with the desired pH (9–11) pre-equilibrated to the desired temperature, incubation was continued for the desired time. Samples of 10 µl were taken at certain time points (starting from time 0) and immediately added to 170 µl of 100 mM sodium acetate buffer pH 4.5 in a 96-well microtiter plate and kept on ice. When all the time-point samples were collected, enzymatic reactions in the microtiter plate were started by adding 20 µl of 50 mM ABTS solution, and relative reaction rates were determined by monitoring absorbance at 405 nm vs time.

Alkali Soluble Lignin Preparation

Hardwood lignin extracted by extrusion-based process was obtained from an industrial source (http://sweetwater.us/process/). As reported by the manufacturer, the molecular weight is Mn = 2,700–4,000 g/mol, M_w = 7,500–8,280 g/mol, PDI = 2.2–3.0, and the hydroxyl content is 2.85 mmol/g aliphatic -OH (possibly carbohydrates), 0.9 mmol/g syringyl -OH, 0.53 mmol/g guaiacyl OH, 0.1 mmol/g phenolic OH.

Alkali soluble lignin was prepared as follows: lignin was solubilized at 100 g/l in 0.25 M NaOH, mixed for 30 min at room temperature, centrifuged at 6,000 *g* for 20 min, supernatant was dried in oven at 105 C, and stored at room temperature until used. Drying of lignin after alkaline solubilization was not essential for laccase oxidation, it was performed for convenience in storage and obtaining reproducible results with different batches of lignin. For the laccase treatment, dried alkaline soluble lignin was dissolved at 25 g/l in water (solubilization was complete) and pH adjusted to 10.5.

Lignin Depolymerization with Laccase MetZyme® LIGNO™

Alkaline soluble lignin prepared as described earlier was dissolved in water to the final concentration 25 g/l. The reactions were run in 1 l twin-pot bioreactor (BIOSTAT® B plus twin from Sartorius Stedim Biotech). Mediator syringaldehyde was added 0.1% w/w in respect to lignin and the reactor equilibrated to 50°C, and pH 10.5 with aeration 0.16 l/min. After that, the enzyme was added 80 nkat/g of lignin (~5 U/g of lignin). Control reaction was run without the enzyme—further throughout the text referred to as "Control lignin" or "Control sample." Reaction was continued for 21 h with constant aeration (0.16 l/min, dissolved oxygen level was remaining constant from the time of enzyme addition), pH was controlled with NaOH to remain 10.5 throughout the reaction.

Size Exclusion Chromatography

Size exclusion chromatography for lignin samples and molecular weight standards was performed using HPLC chromatographer 120 CompactLC with UV detector (Agilent Technologies), equipped with size exclusion column MCX 1,000 Å 5 µm, 8 mm × 300 mm and with pre-column MCX 5 µm, 8 mm × 50 mm (Polymer Standards Service). Isocratic mode with 0.1 M NaOH eluent flow 0.5 ml/min at RT was used; run time was 40 min. Lignin samples were monitored at 280 nm. Molecular mass standards (polystyrene sulfonate sodium salt standards Mp = ~0.9 to ~65 kDa, Polymer Standards Service) were monitored at 254 nm. Data were acquired using the EzChrom Elite Compact software.

Primary HPLC traces acquired using the Agilent EZChrom Elite software were transferred to tailor-made MS Excel(R) spreadsheets for further processing. Signal vs retention time graphs were produced from 1 Hz time series to depict the chromatography traces.

Polystyrene sulfonate molecular mass standards (Polymer Standards Service), ranging in mass at peak maximum from M_W = ~900 to ~65,000, and syringaldehyde (M_W 182) were used for calibration of molecular weights.

Based on HPLC profiles, average molecular weights—number average molecular weight (M_n) and the weight average molecular weight (M_w), which emphasizes the contribution of polymers with larger molecular weights, were calculated for lignin fractions.

The M_n was calculated by dividing the total relative polymer weight by the total number of polymer molecules, using the following equation:

$$M_n = \frac{W}{\sum N_i} = \frac{\sum (M_i N_i)}{\sum N_i} = \frac{\sum (H_i)}{\sum (H_i / N_i)}.$$

The M_w was calculated using the equation:

$$M_w = \frac{\sum (W_i M_i)}{W} = \frac{\sum (H_i M_i)}{\sum H_i}$$

where W—total weight of polymers, W_i—weight of i-th polymer, M_i—molecular weight of the i-th elution time, N_i—number of molecules with molecular weight M_i, H_i—height of i-th elution time.

Demethylation Detection

Demethylation of lignin was followed by monitoring methanol in the reaction mixture after completion of the oxidation. Purpald method adapted from Anthon and Barrett (2004) was used for detecting methanol. The method is based on conversion of methanol to formaldehyde by alcohol oxidase enzyme and subsequent spectrophotometric quantification of the formaldehyde. Alcohol oxidase from *Pichia pastoris* and Purpald reagent (4-amino-3-hydrazino-5-mercapto-1,2,4-triazole) were purchased from Sigma Aldrich.

Purpald method was adapted to 96-microwell plate (Spectra Plate, Cat. 6005640, Perkin Elmer). Lignin samples were adjusted to pH 7.0 with HCl and diluted 1:25 with water. Methanol standards (0–0.5 mM) were used. For all lignin samples, negative controls were prepared by adding buffer without alcohol oxidase. Diluted lignin samples (28 µl) or methanol standards were pipetted as triplicates into 96-well plate, and 28 µl of 100 mM sodium phosphate buffer pH 7 containing 1 U/ml alcohol oxidase (solution prepared just before use) was added to the wells. The mixtures were incubated at 30°C for 10 min with 250 rpm shaking (MaxQ 4450, Thermo Scientific). Purpald reagent (34 mM in 0.5 M NaOH) was prepared just before use, and 56 µl of Purpald reagent was added to the reactions; the samples were further incubated at 30°C for 30 min with 250 rpm shaking. After that, 168 µl of water was added to the wells, mixed for a minute, and absorbance measured at 560 nm using spectrophotometer (Multiscan Go, Thermo Scientific). The methanol concentrations in the lignin samples were calculated using absorbance values obtained from the calibration curve of methanol standard solutions.

Lignin Solubility Assessment

Lignin sample after enzyme treatment (or control sample, run without the enzyme) was equilibrated to room temperature and showed initial pH 10.8 (as depolymerization was carried out at 50°C at pH 10.5). Sample was slowly titrated with HCl to allow the pH to stabilize at integer values (10.0, 9.0, 8.0, and so on); aliquots were taken at each of these pH and frozen. After completing the titration, all samples were thawed at room temperature and allowed to stand for 1 h, after which samples were centrifuged at 18,000 *g* for 30 min and UV absorption was measured in the supernatant to determined soluble fraction. Relative values to the starting material were plotted against the pH.

Lignin Fractions Separation

For lignin fractions separation, ultrafiltration was performed using tangential flow membrane units Vivaflow 200 (Sartorius) with polyethersulfone membranes with 10- and 2-kDa cutoff values. The units were used according to the manufacturer's protocol (2.5 bar pressure, 200–400 ml/min retentate flow/module). The ultrafiltration was carried on until penetrate volume reached 90% of the starting material volume.

Lignin Particles Measurement

Dynamic light scattering (DLS) measurements were performed at 298 K using a zetasizer equipment (Model Nano ZS, Malvern, Worcestershire, UK) equipped with a red laser operating at 632.8 nm (He/Ne laser) and the detector positioned at 173° (non-invasive back scattering technology). The measuring size range of 0.1 nm to 10 µm was applied. The data were analyzed using the Malvern Zetasizer Software v. 7.12. Soluble lignin samples were prepared and treated with the enzyme as described above and diluted 1:100 with 150 mM Britton and Robinson buffer pH 10.5 for the measurement.

RESULTS

Alkaline Laccase MetZyme® LIGNO™

New commercially available genetically engineered bacterial laccase MetZyme® LIGNO™ (MetGen) was tested with following standard laccase substrates: 2,2′-Azino-bis(3-ethylbenzthiazoline-6-sulfonic acid) (ABTS), SGZ, and DMP. Laccase efficiency in oxidizing different substrates depends on both—laccase properties and substrate properties (Rosado et al., 2012), thus optimal pH needs to be determined for a particular laccase with each substrate. As seen from **Figure 1A**, the enzyme is able to oxidase phenolic substrate (DMP) at extremely alkaline pH, as high as 11.

Enzyme stability may be severely compromised in alkaline pH, and standard activity measurements can be misleading, as they are performed in short-time reactions. Enzyme stability at alkaline pH was evaluated by pre-incubation of the enzyme in a buffer with desired pH and further testing the residual activity after readjusting the pH (**Figures 1B–D**). ABTS was used for residual activity measurement as it provides the highest sensitivity and dynamic range. The enzyme was found to be fairly stable in the tested pH range at 50°C, therefore pre-incubation at this temperature was carried out over an extended period of time—24 h (**Figure 1B**); in other temperatures 1 h pre-incubation was used.

Treatment of Alkali Soluble Industrial Lignin with MetZyme® LIGNO™

Industrial biorefinery lignin obtained from extrusion pretreatment method was used in these experiments. Experiments were performed in a reactor scale and final samples were analyzed by size exclusion chromatography with UV detector set to 280 nm (**Figure 2A**). Based on the HPLC profile, molecular weight distribution was obtained using molecular weight standards (**Figure 2B**). The results show a substantial transformation of the molecular weight distribution toward lower molecular weights.

Properties of Enzyme-Treated Lignin

Enzyme-treated lignin and control sample were subjected to titration with hydrochloric acid and the acid consumption was recorded throughout the course of the titration (**Figure 3A**). Enzyme-treated sample showed more extensive buffering in the range of pH 9–11, corresponding to protonation of phenolic hydroxyls, and an additional buffering range around pH 8–9, likely to reflect the presence of C-alpha oxidized phenolic groups as pictured on the graph of **Figure 3A** (see Discussion).

During the titration, it was observed that enzyme-treated lignin starts to precipitate at much more acidic pH than control sample. To evaluate this phenomenon, we prepared lignin samples
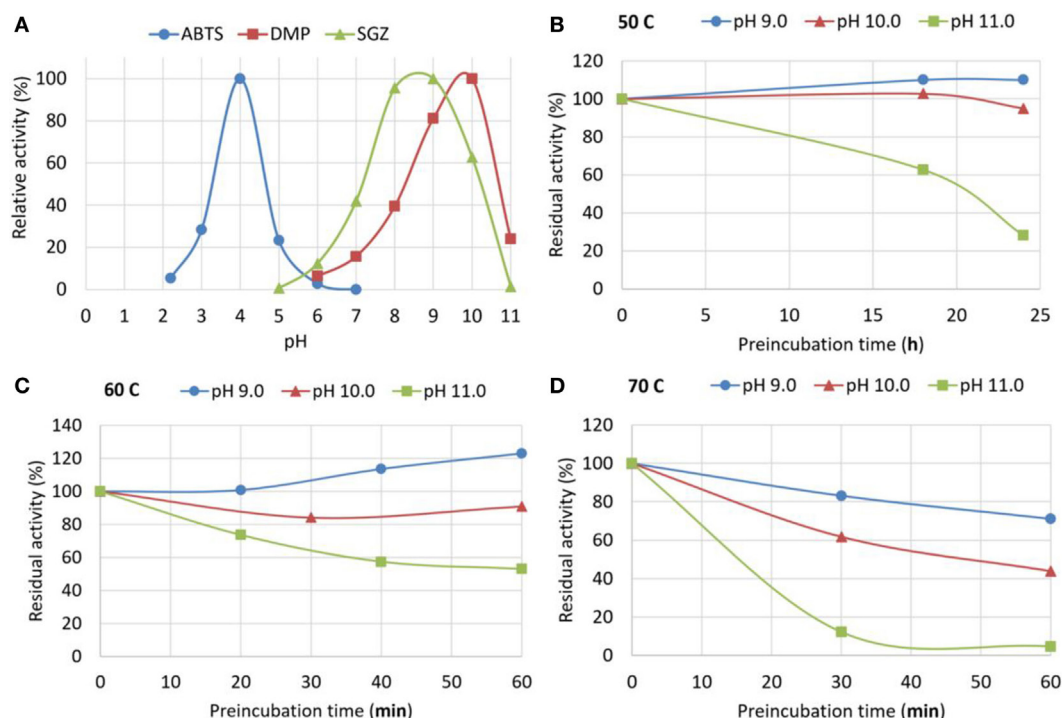
FIGURE 1 | Standard activity and stability of MetZyme® LIGNO™. **(A)** pH dependence of MetZyme® LIGNO™ activity toward standard low-molecular weight substrates: 2,2′-Azino-bis(3-ethylbenzthiazoline-6-sulfonic acid) (ABTS), syringaldazine (SGZ), and 2,6-dimethylphenol (DMP). **(B–D)** Stability of MetZyme® LIGNO™ at various pH (9–11) and temperatures (50, 60, and 70°C); pre-incubation time at indicated conditions is plotted against residual activity measured after pre-incubation. Pre-incubation at 50°C was carried out over a span of 24 h, at 60 and 70°C—over 1 h; temperatures and pH are indicated over the graphs. The curves do not represent a model fit, they are line interpolations that Microsoft excel provides as a default and they are added only for convenience.

by adjusting the pH of control and enzyme-treated preparations (25 g/l) to different pH values, and monitored lignin precipitation (**Figure 3B**). Enzyme-treated lignin remained fully soluble even at pH 5.0, whereas in control sample at this pH only 35% of lignin remained in solution.

Oxidative demethylation of lignin is cleavage of aryl ether between phenolic oxygens and methoxy carbons, resulting in formation of a methanol molecule and a new phenolic hydroxyl group. It is a desirable process in lignin upgrade, as it increases the number of hydroxyls and thus results in activation of lignin. Demethylation was monitored by measuring MeOH in the reaction mixture after depolymerization. The enzyme-treated sample showed 0.47 mmol of MeOH per gram of lignin as opposed to 0.11 mmol/g in the control sample. This corresponds to a 30% increase of total number of phenolic hydroxyls when compared with the starting material as of manufacturer specification (1.5 mmol/g). It has to be noted that this method may result in some underestimation of the degree of demethylation, as MeOH is likely to be evaporated during the course of lignin depolymerization in spite of the water condensation unit present in the reactor. Nevertheless, this result confirms an important notion that significant demethylation does take place during this process.

Dynamic Light Scattering

As it has been shown previously, lignin tends to be dispersed in aqueous medium and the particle size depends on its chemical

composition, solubility, pH, and other factors (Nistor et al., 2014). This property is important for evaluating lignin as potential dispersant for industrial applications.

The particle size distribution curves show a clear differentiation between untreated and enzymatically treated lignin (**Figure 4**). Particle size distribution curve is multimodal in the case of unmodified lignin sample, showing relatively broad main peak at 459 nm and two other peaks at 68 and 5,560 nm. On the other hand, the enzymatically treated sample shows bimodal distribution with main peak at 142 nm and lower intensity peak at 28 nm. In addition, the peaks are clearly narrower than those for untreated lignin, suggesting less polydispersity.

The observed differences in the particle size distribution and polydispersity between untreated and enzymatically treated lignin samples indicate an increased solubility and better dispersibility for the latter.

Fractionation of Enzyme-Treated Lignin

Enzyme-treated lignin was further subjected to ultrafiltration to separate fractions of different molecular weight. The experiment flow chart is depicted in **Figure 5A**. Fractions were designated with codes (L0 for the extrusion lignin, L1—for alkaline soluble fraction, and so on according to the **Figure 5**). Further mentioning of these codes refers to the corresponding lignin fractions.

As seen on the photographs (**Figure 5A**), dried lignin fractions have different color and morphology. Lignin fractions were

FIGURE 2 | Molecular weight distribution of enzyme-treated lignin sample and control sample (the same process run without the enzyme). **(A)** Elution profiles of size exclusion chromatography, profiles were area-normalized to reflect the same total mass; **(B)** molecular weight distribution calculated based on HPLC profile using molecular weight standards.

FIGURE 3 | Properties of enzyme-treated lignin revealed from acid titration. **(A)** Acid titration curve of enzyme-treated and control lignin; highlighted areas indicate pH ranges of deprotonation of phenolic hydroxyls (pH 9–11) and phenolic hydroxyls of lignin units with keto group at alpha-carbon (see Discussion), deprotonating hydroxyls in the molecules are outlined with solid line, substituent at alpha-carbon is outlined with dotted line; **(B)** solubility of enzyme-treated and control lignin at different pH. The results are average of three independent titrations.

analyzed by size exclusion chromatography and showed good separation and low dispersity (**Figure 5B**). Average molecular weights M_n, and M_w were calculated for selected fractions. Notably, from this analysis L4 fraction contains predominantly molecules no bigger than trimers. More precise determination of molecular weights of this smallest fraction requires different type of column.

DISCUSSION

In the view of rising BioEconomy, proper exploitation of lignin through more noble applications than fuel are of vital importance.

The key characteristics of lignin that need to be achieved are unification of its molecular weight and increased reactivity. In addition, the material needs to be transformed to a more manageable form—soluble or melting. These characteristics largely depend on the lignin origin and preparation methods and can be further tuned after lignin separation (Abdelaziz et al., 2016; Rinaldi et al., 2016); this is often referred to as lignin upgrade.
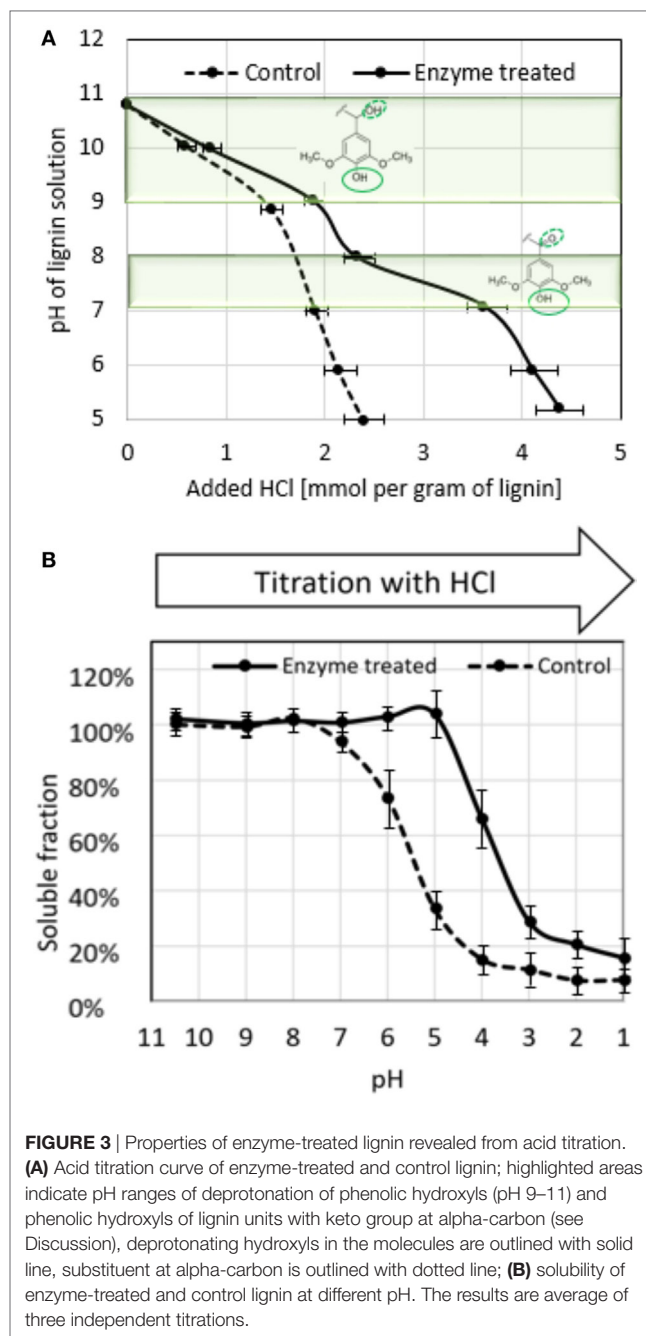
Methods for isolation and chemical oxidative upgrade of lignin were recently reviewed by Lange et al. (2013). It is evident that different strategies of lignin valorization have been exploited from trying to preserve its native structure and high-molecular weight to depolymerizing it to monomers (Gouveia et al., 2012; Picart et al., 2017).

It is important to understand that lignin preparations of different molecular weight can be further valorized and utilized in various industrial applications (Gandini and Belgacem, 2008; Laurichesse and Avérous, 2014) as long as chemical/physical properties are matching the requirements (Passoni et al., 2016). Thus, the target of lignin depolymerization is to create lignin fractions
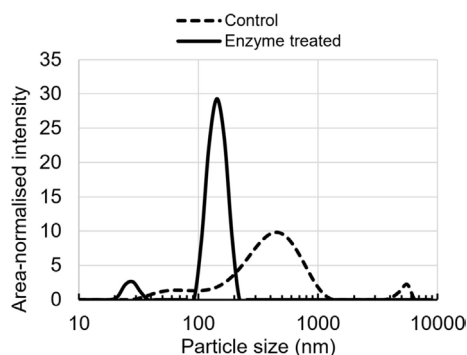
FIGURE 4 | Colloidal particle size distribution of enzyme-treated and control lignin in a buffer at pH 10.5.

that are bioequivalent, for example, to oil-based compounds used as resins, adhesives, composites, and foams (**Table 1**). Generally, if higher value chemicals are wanted to be replaced, stricter molecular weight distributions are required—reachable *via* enzymatic lignin depolymerization. In this view, it is not necessarily desirable to depolymerize lignin to monomers in its entirety. We believe that it is beneficial from the economic and environmental point of view to pursue a less energy intensive transformation of the starting material, followed by efficient separation, which will provide valuable fractions for various applications. In this view, enzymatic approach seems very attractive.

In this study, for the first time, enzymatic treatment of bulk industrial lignin was demonstrated at extremely alkaline conditions, where lignin is soluble in water.

This has become possible due to a new industrial genetically evolved laccase of bacterial origin with exceptional properties. As demonstrated in Section "Results," the enzyme retains full activity after 24 h incubation at 50°C at pH 10 and 30% activity at pH 11.

In a one-liter bioreactor scale, extensive lignin depolymerization was observed, accompanied by chemical activation *via* demethylation and benzylic oxidation as well as increased solubility in neutral and acidic pH and altered colloidal behavior. In the view of recent advancements in using lignin nanoparticles for grafting synthetic polymers and manufacturing thermoplastic composites, the particle size decrease and unification that we observed in enzyme-treated samples may be advantageous for this technology (Hilburg et al., 2014).

In the course of process optimization, we observed that the balance between polymerization and depolymerization reactions is pH and aeration dependent. Under highly alkaline conditions and strong aeration, depolymerization prevailed over polymerization (data not shown).

We were further able to separate lignin fractions with defined molecular weight and low dispersity. Dried lignin fractions have district appearances. Notably, lignin fraction of >10-kDa molecular weight (L2.1 in **Figure 5**) shows a clear directional drying pattern and appears as stripes and elongated flakes, as opposed to the full sample (L2 in **Figure 5**), which dries as small rounded grains. Our results also show that 2-kDa cutoff

membrane allows for separation of predominantly monomeric lignin.

Importantly, the absence of organic solvents in the reaction mixture allowed for utilization of polymer-based ultrafiltration membranes, which are widely used in food industry, making scalable and economically feasible. Ultrafiltration membranes of different cutoff are available and widely used in industry. The choice of membranes used in this study was rather arbitrary and can be tuned to the targeted lignin size.

The mechanism of lignin oxidation by bacterial laccases was thoroughly described by Rosado et al. (2012). As opposed to fungal laccases that oxidize the phenolic substrates in the phenolic form, bacterial laccases oxidize them optimally in the phenolate form, i.e., after deprotonation of the phenolic group. Structurally, this is due to the fact that bacterial laccases (such as COTA) do not contain any negatively charged residue in the vicinity of the substrate binding site, and the efficiency of the oxidation of phenols rely mostly on the protonation/deprotonation state equilibria of the compounds themselves. Thus, oxidation is strictly dependent on the chemical nature of the substrates themselves, i.e., on their pKa values.

The pKa values of phenolic mediators such as syringaldehyde, acetosyringone, and methyl syringate lie between 7 and 9. This outlines the range where bacterial laccases could be effective in oxidizing lignin *via* a mediator. However, pKa of phenolic groups in lignin itself is in the range of 10–11. This makes lignin poorly soluble at pH values substantially lower than this range and also prevents or largely impedes direct oxidation of lignin phenolics by a bacterial laccase. Therefore, reaction conditions exploited in this study open a whole new mode of operation for enzymatic lignin oxidation.

Another important aspect of laccase-mediated oxidation of lignin is that not only it considerably changes molecular weight of the molecules but also changes its properties. Significant increase in water solubility of enzyme-treated lignin was observed even at neutral and acidic pH as illustrated in **Figure 3B**. Paralleled to this, enzyme-treated lignin demonstrated altered behavior of in acid titration. It showed a specific span of buffering capacity at pH 7–8, that was absent in the control sample, indicating the appearance of new moieties with pKa in this range.

To interpret this observation, one has to revert to the reaction mechanism of enzymatic lignin oxidation. According to various scenarios following the radical transfer from the mediator to a lignin unit (phenolic or non-phenolic), reported in previous works, one of the major outcomes of this process is benzylic oxidation resulting in a ketone (or aldehyde) groups at the alpha-carbon of the lignin unit (**Figure 6**). Further chemical scenarios elucidated from the experiments with lignin model compounds mainly revolve around the spacer between benzylic units where the oxidized alpha-carbon is residing (Lahtinen et al., 2009; Ohashi et al., 2011) and little attention is paid to the para-position of the phenyl group connected to this alpha-carbon (C4 position of the same benzene ring). Rightfully so, as in acidic pH, where conventional laccases are operating, that position is not yielding any pathways of interest. However, in alkaline pH, this position gains importance.
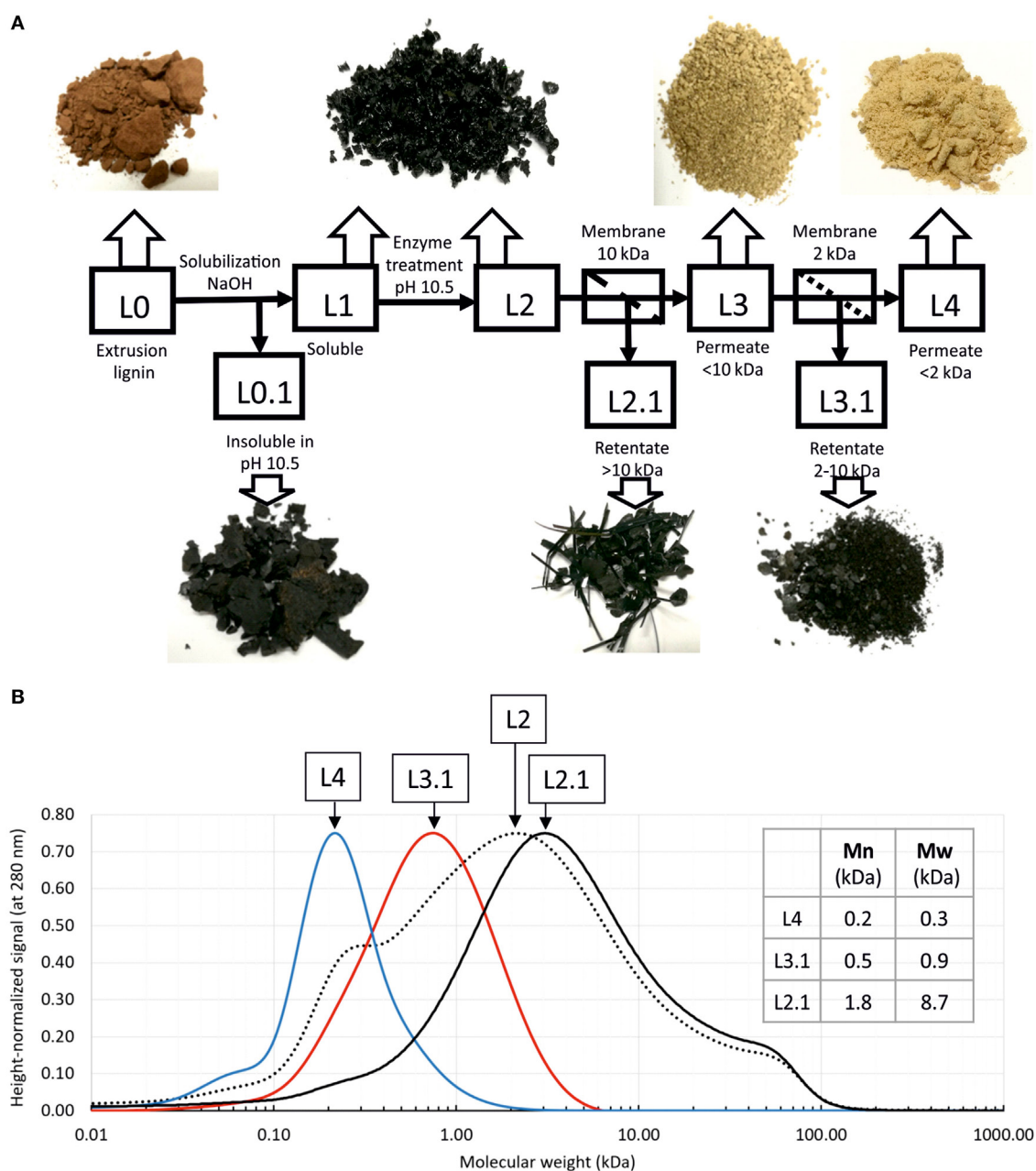
FIGURE 5 | Fractionation of enzyme-treated lignin. **(A)** Experiment flow chart and lignin fractions (dried); **(B)** analysis of lignin fractions by size exclusion chromatography. Calculated average molecular weights are given in the table. Since claimed column resolution range is 100–100,000 Da, and molecular weight standards range starts from 600 Da, smaller molecular weights may not be calculated correctly.

TABLE 1 | Valorization of lignin by oxidative upgrade and fractionation.

	Molecular weight	Reactivity and solubility	Application	Bioequivalent of	Approximate of the oil-based chemical
Pulp and paper lignin	5–100 kDa	Poor	Burning	Oil/electricity	50–150 €/ton
Dissolved lignin/biorefinery lignin	3–50 kDa	Medium	Resins and adhesives	Formaldehyde	400–500 €/ton
Enzyme oxidized lignin	Custom	Good	Composites	Polymers	>1,000 €/ton
Enzyme depolymerized lignin	0.3–2 kDa	Good	Foams and composites	PVA	1,000–1,500 €/ton
Enzyme depolymerized fractions	0.3, 0.5, 0.7, …, 2 kDa	Very good	New materials	Specialty chemicals and polymers	>1,500 €/ton
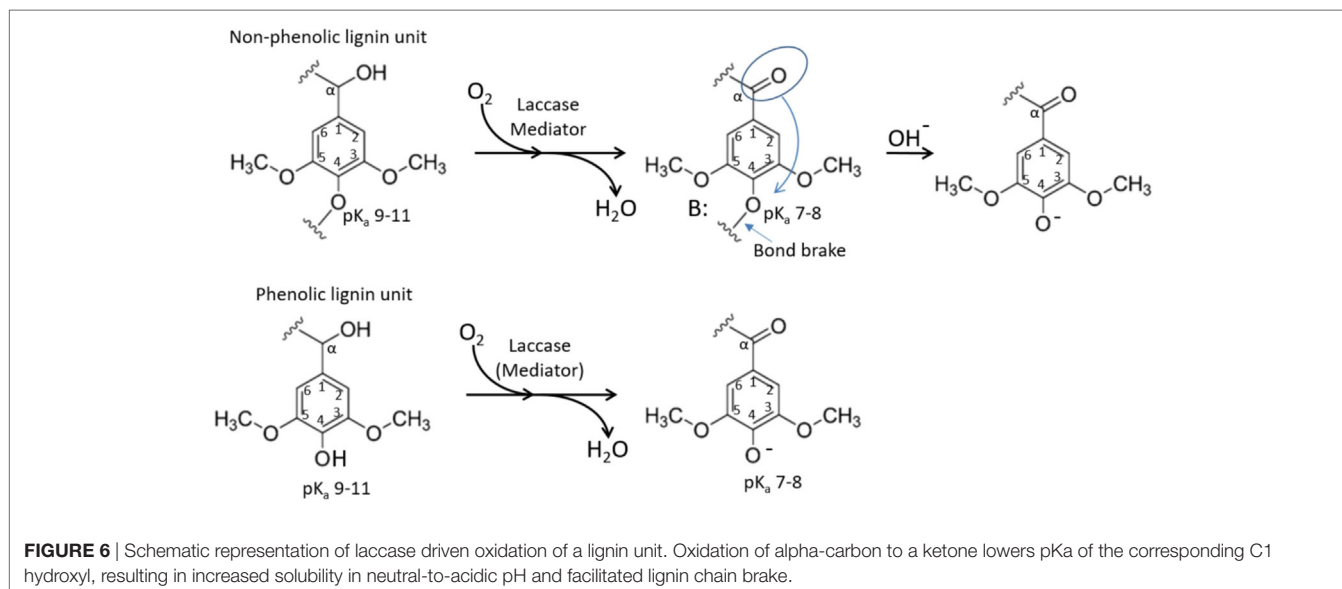
FIGURE 6 | Schematic representation of laccase driven oxidation of a lignin unit. Oxidation of alpha-carbon to a ketone lowers pKa of the corresponding C1 hydroxyl, resulting in increased solubility in neutral-to-acidic pH and facilitated lignin chain brake.

Ragnar et al. (2000) reported pKa values for phenolic C4 hydroxyls for over 50 different lignin model compounds including monomers and dimers with various substituents at C1. This remarkable data collection clearly shows that pKa of the C4 phenolic hydroxyl remains in very alkaline region (between 9.5 and 11) practically in any environment of the corresponding C1 atom, apart from alpha-carbon being in the form of a ketone or aldehyde (which is the case upon laccase oxidation). In the later situation, pKa of C4 hydroxyl drops to a value between 7 and 8. This could explain the buffering of oxidized lignin at this pH range as well as increased solubility at neutral-to-acidic pH. This is because in oxidized phenolic units, C4 hydroxyl would tend to remain deprotonated at lower pH (**Figure 6**). Another implication of this shift in pKa is that the corresponding alpha-carbon oxidized non-phenolic unit with an ether bond at C4 carbon (**Figure 6** top) represents a good leaving group (Boyd, 1985) and may promote lignin chain brake (**Figure 6** top, right) or demethylation event.

At the same time, increased number of other types of phenolic units in the oxidized lignin is reflected by the expanded buffering capacity at pH 9–11 (**Figure 3A**). In the enzyme-treated sample, the acid consumption in this pH range was increased by 0.5 mmol/g of lignin, which coincides with the degree of demethylation determined by methanol detection. In this respect, titration curve of the control sample is in agreement with lignin specification obtained from the manufacturer (1.5 mmol/g of total aromatic hydroxyls), confirming our interpretation.

This study is not focusing on polymerization of lignin using laccase; however, we did observe re-polymerization of the shorter molecules when pH is lowered, especially under limiting aeration. Under these conditions, the reaction was apparently driven more toward polymerization. This also represents an industrial opportunity, as chemically activated high-molecular weight lignin is highly desirable for some high-end bio-based materials. In addition, polymerization may provide a tool for removing small lignins from the process by polymerization followed by sedimentation or filtration. This is certainly an important aspect for future investigation.

Further studies need to be conducted to fully characterize the enzyme-treated lignin in terms of chemical composition and reactive groups as well as its applicability in industrial processes.

AUTHOR CONTRIBUTIONS

KB, VH, and AS contributed to enzyme discovery engineering and characterization. TG and MH contributed to lignin treatment, characterization, and separation. SM contributed in size exclusion chromatography analysis. PI contributed to colloidal particles analysis. BR implemented computational analysis of HPLC data and contributed to enzyme production. KB wrote the manuscript with support of all the coauthors and offered the interpretation of the results. All authors discussed the results and contributed to the final manuscript.

FUNDING

REFERENCES

Abdelaziz, O. Y., Brink, D. P., Prothmann, J., Ravi, K., Sun, M., García-Hidalgo, J., et al. (2016). Biological valorization of low molecular weight lignin. *Biotechnol. Adv.* 34, 1318–1346. doi:10.1016/j.biotechadv.2016.10.001

Anthon, G. E., and Barrett, D. M. (2004). Comparison of three colorimetric reagents in the determination of methanol with alcohol oxidase. Application to the assay of pectin methylesterase. *J. Agric. Food Chem.* 52, 3749–3753. doi:10.1021/jf035284w

Boyd, D. B. (1985). Leaving group ability and pKa, in elimination reactions. *J. Org. Chem.* 50, 885–886. doi:10.1021/jo00206a033

Essery, M. (2017). *First Higher-Value Chemical Derived from Lignin to Hit Market in 2021*. Lux Research. Available at: http://www.luxresearchinc.com/news-and-events/press-releases/read/first-higher-value-chemical-derived-lignin-hit-market-2021

Frost and Sullivan. (2014). *High-Value Opportunities for Lignin: Ready for Liftoff*. Available at: http://www.frost.com/sublib/display-market-insight.do?id=290584392

Gandini, A., and Belgacem, M. N. (2008). "Lignins as components of macromolecular materials," in *Monomers, Polymers and Composites from Renewable Resources*, eds A. Gandini and M. N. Belgacem (Elsevier Science), 243–271. Available at: https://www.elsevier.com/books/monomers-polymers-and-composites-from-renewable-resources/belgacem/978-0-08-045316-3

Gouveia, S., Fernández-Costas, C., Sanromán, M. A., and Moldes, D. (2012). Enzymatic polymerisation and effect of fractionation of dissolved lignin from *Eucalyptus globulus* Kraft liquor. *Bioresour. Technol.* 121, 131–138. doi:10.1016/j.biortech.2012.05.144

Hahn, V., Mikolasch, A., and Schauer, F. (2014). Cleavage and synthesis function of high and low redox potential laccases towards 4-morpholinoaniline and aminated as well as chlorinated phenols. *Appl. Microbiol. Biotechnol.* 98, 1609–1620. doi:10.1007/s00253-013-4984-9

Hilburg, S. L., Elder, A. N., Chung, H., Ferebee, R. L., Bockstaller, M. R., and Washburn, N. R. (2014). A universal route towards thermoplastic lignin composites with improved mechanical properties. *Polymer* 55, 995–1003. doi:10.1016/j.polymer.2013.12.070

Kang, S., Li, X., Fan, J., and Chang, J. (2013). Hydrothermal conversion of lignin: a review. *Renewable Sustainable Energy Rev.* 27, 546–558. doi:10.1016/J.RSER.2013.07.013

Kim, Y. S., and Kadla, J. F. (2010). Preparation of a thermoresponsive lignin-based biomaterial through atom transfer radical polymerization. *Biomacromolecules* 11, 981–988. doi:10.1021/bm901455p

Kleinert, M., and Barth, T. (2008). Towards a lignincellulosic biorefinery: direct one-step conversion of lignin to hydrogen-enriched biofuel. *Energy Fuels* 22, 1371–1379. doi:10.1021/ef700631w

Lahtinen, M., Kruus, K., Heinonen, P., and Sipilä, J. (2009). On the reactions of two fungal laccases differing in their redox potential with lignin model compounds: products and their rate of formation. *J. Agric. Food Chem.* 57, 8357–8365. doi:10.1021/jf901511k

Lange, H., Decina, S., and Crestini, C. (2013). Oxidative upgrade of lignin – recent routes reviewed. *Eur. Polym. J.* 49, 1151–1173. doi:10.1016/j.eurpolymj.2013.03.002

Laurichesse, S., and Avérous, L. (2014). Chemical modification of lignins: towards biobased polymers. *Prog. Polym. Sci.* 39, 1266–1290. doi:10.1016/j.progpolymsci.2013.11.004

Lux. (2014). *Finding Untapped Value: Converting Lignin to Higher Value Chemicals*. Available at: https://members.luxresearchinc.com/research/report/14807

Ma, R., Hao, W., Ma, X., Tian, Y., and Li, Y. (2014). Catalytic ethanolysis of Kraft lignin into high-value small-molecular chemicals over a nanostructured α-molybdenum carbide catalyst. *Angew. Chem. Int. Ed. Engl.* 53, 7310–7315. doi:10.1002/anie.201402752

Mate, D. M., and Alcalde, M. (2014). Laccase engineering: from rational design to directed evolution. *Biotechnol. Adv.* 33, 25–40. doi:10.1016/j.biotechadv.2014.12.007

Mate, D. M., and Alcalde, M. (2017). Laccase: a multi-purpose biocatalyst at the forefront of biotechnology. *Microb. Biotechnol.* 10, 1457–1467. doi:10.1111/1751-7915.12422

Munk, L., Sitarz, A. K., Kalyani, D. C., Mikkelsen, J. D., and Meyer, A. S. (2015). Can laccases catalyze bond cleavage in lignin? *Biotechnol. Adv.* 33, 13–24. doi:10.1016/j.biotechadv.2014.12.008

Nistor, M., Chirila, O., Cazacu, G., Totolin, M. I., and Vasile, C. (2014). Solution properties of some modified lignins. *Cell. Chem. Technol.* 48, 855–862.

Ohashi, Y., Uno, Y., Amirta, R., Watanabe, T., Honda, Y., and Watanabe, T. (2011). Alkoxyl- and carbon-centered radicals as primary agents for degrading non-phenolic lignin-substructure model compounds. *Org. Biomol. Chem.* 9, 2481–2491. doi:10.1039/c0ob00797h

Passoni, V., Scarica, C., Levi, M., Turri, S., and Griffini, G. (2016). Fractionation of industrial softwood Kraft lignin: solvent selection as a tool for tailored material properties. *ACS Sustainable Chem. Eng.* 4, 2232–2242. doi:10.1021/acssuschemeng.5b01722

Picart, P., Liu, H., Grande, P. M., Anders, N., Zhu, L., Klankermayer, J., et al. (2017). Multi-step biocatalytic depolymerization of lignin. *Appl. Microbiol. Biotechnol.* 101, 6277–6287. doi:10.1007/s00253-017-8360-z

Ragnar, M., Lindgren, C. T., and Nilvebrant, N.-O. (2000). pKa-values of guaiacyl and syringyl phenols related to lignin. *J. Wood Chem. Technol.* 20, 277–305. doi:10.1080/02773810009349637

Rehmann, L., Ivanova, E., Gunaratne, H. Q. N., Seddon, K. R., and Stephens, G. (2014). Enhanced laccase stability through mediator partitioning into hydrophobic ionic liquids. *Green Chem.* 16, 1462–1469. doi:10.1039/c3gc42189a

Rinaldi, R., Jastrzebski, R., Clough, M. T., Ralph, J., Kennema, M., Bruijnincx, P. C. A., et al. (2016). Paving the way for lignin valorisation: recent advances in bioengineering, biorefining and catalysis. *Angew. Chem. Int. Ed. Engl.* 55, 8164–8215. doi:10.1002/anie.201510351

Roberts, V. M., Stein, V., Reiner, T., Lemonidou, A., Li, X., and Lercher, J. A. (2011). Towards quantitative catalytic lignin depolymerization. *Chemistry* 17, 5939–5948. doi:10.1002/chem.201002438

Rodgers, C. J., Blanford, C. F., Giddens, S. R., Skamnioti, P., Armstrong, F. A., and Gurr, S. J. (2010). Designer laccases: a vogue for high-potential fungal enzymes? *Trends Biotechnol.* 28, 63–72. doi:10.1016/j.tibtech.2009.11.001

Rosado, T., Bernardo, P., Koci, K., Coelho, A. V., Robalo, M. P., and Martins, L. O. (2012). Methyl syringate: an efficient phenolic mediator for bacterial and fungal laccases. *Bioresour. Technol.* 124, 371–378. doi:10.1016/j.biortech.2012.08.023

Roth, S., and Spiess, A. C. (2015). Laccases for biorefinery applications: a critical review on challenges and perspectives. *Bioprocess Biosyst. Eng.* 38, 2285–2313. doi:10.1007/s00449-015-1475-7

Santhanam, N., Vivanco, J. M., Decker, S. R., and Reardon, K. F. (2011). Expression of industrially relevant laccases: prokaryotic style. *Trends Biotechnol.* 29, 480–489. doi:10.1016/j.tibtech.2011.04.005

Singh, G., Kaur, K., Puri, S., and Sharma, P. (2015). Critical factors affecting laccase-mediated biobleaching of pulp in paper industry. *Appl. Microbiol. Biotechnol.* 99, 155–164. doi:10.1007/s00253-014-6219-0

Smith, P., Chen, M., and Cline, S. (2016). *Biorefinery Value Chain Outputs*. Available at: https://nararenewables.org/documents/2017/02/155205-nara-biorefinery-value-chain-outputs-vcea-b-p2.pdf

Wong, D. W. S. (2009). Structure and action mechanism of ligninolytic enzymes. *Appl. Biochem. Biotechnol.* 157, 174–209. doi:10.1007/s12010-008-8279-z

Xing, Q., Ruch, D., Dubois, P., Wu, L., and Wang, W.-J. (2017). Biodegradable and high-performance poly(butylene adipate-*co*-terephthalate)–lignin UV-blocking films. *ACS Sustainable Chem. Eng.* 5, 10342–10351. doi:10.1021/acssuschemeng.7b02370

Yoshikawa, T., Taichi, Y., Satoshi, S., Tetsuya, F., Yuta, N., Teruoki, T., et al. (2013). Production of phenols from lignin via depolymerization and catalytic cracking. *Fuel Process. Technol.* 108, 69–75. doi:10.1016/j.fuproc.2012.05.003

The Effect of Plant Source on the Properties of Lignin-Based Polyurethanes

Jason M. Lang[1], Umesh M. Shrestha[1] and Mark Dadmun[1,2]*

[1] Department of Chemistry, University of Tennessee, Knoxville, TN, United States, [2] Chemical Sciences Division, Oak Ridge National Laboratory, Oak Ridge, TN, United States

This work increases our understanding of the effect of plant source on the mechanical and morphological properties of lignin-based polyurethanes (PUs). Lignin is a polymer that is synthesized inside the plant cell wall and can be used as a polyol to synthesize PUs. The specific aromatic structure of the lignin is heavily reliant on the plant source from which it is extracted. These results show that the mechanical properties of lignin-based PUs differ based on lignin's plant source. The morphology of lignin-based PUs was examined using atomic force microscopy and scanning electron microscopy and the mechanical properties of lignin-based PU samples were measured using dynamic mechanical analysis and shore hardness (Type A). The thermal analysis and morphology studies demonstrate that all PUs prepared form a multiphase morphology. In these PUs, better mixing was observed in the wheat straw lignin PU samples leading to higher moduli than in the hardwood lignin and softwood lignin PUs whose morphology was dominated by larger aggregates. Independent of the type of the lignin used, increasing the fraction of lignin increased the rigidity of PU. Among the different types of lignin studied, PU with wheat straw soda lignin exhibited storage moduli ~2-fold higher than those of PUs incorporating other lignins. This study also showed that during synthesis all hydroxyl groups in the lignin are not available to react with isocyanates, which alters the number of cross-links formed within the PU and impacts the mechanical properties of the material.

Keywords: plant source, lignin, polyol, polyurethane, hardwood, softwood, wheat straw, mechanical properties

INTRODUCTION

Over the past few decades, polymer materials have become important industrially produced materials due to their wide range of physical and chemical properties. These polymer materials have found use in a vast array of technologies ranging from wiring, coatings, sports, and medical devices to cell phones, houses, automobiles, and planes. However, the demand for new and more elaborate technologies that are more robust than their predecessors will continue to increase. For instance, according to Grand View Research, Inc., the polyurethane market was estimated at ~$54 billion in 2015 and is projected to grow to ~$105 billion by the year 2025 due to recent high demands for applications in furniture, automotive, electronic devices, and footwear (Grand View Research, 2017). Therefore, further research is needed to synthesize and understand new polymer materials that will allow the advancement of modern technology into the future.

Polyurethane (PU)

Polyurethanes were first discovered by Otto Bayer and his colleagues in 1937 (Seymour and Kauffman, 1992). PUs are known for their wide range of properties including high tensile strength, abrasion resistance, and chemical resistance (Saraf and Glasser, 1984, Sarkar and Adhikari, 2001). These properties, among others, make PUs an important commercial polymer for use as flexible or rigid foams, solid elastomers, coatings, and adhesives among other applications (Stevens, 1999, Szycher, 1999, Akindoyo et al., 2016).

Polyurethanes are polymers that are derived from monomer units joined together by carbamate (urethane) linkages. The most common pathway to synthesize a urethane linkage is to react an isocyanate functional group (R-N=C=O) with a hydroxyl functional group (R-OH). For a PU to be successfully synthesized using this method, a polyisocyanate that contains two or more isocyanate groups per molecule, reacts with a polyol, a compound that contains two or more hydroxyl groups per molecule, as shown in **Figure 1**. In some circumstances, an organic or inorganic catalyst or ultraviolet light is needed for the urethane reaction to take place (Silva and Bordado, 2004, Soto et al., 2014).

Isocyanate is the more reactive group than hydroxyl group in PU synthesis. The majority of isocyanates used such as toluene-2,4-diisocyanate, isophorone diisocyanate, and 4,4-methylene diphenyl diisocyanate are aromatic in structure while aliphatic isocyanates, such as hexamethylene diisocyanate (HMDI), are also used (Teo et al., 1997, Chan-Chan et al., 2010, Prisacariu, 2011, Chung and Washburn, 2012, Zhang et al., 2015). Polyols are usually the more flexible of the two components which allows the formation of flexible PU materials and usually consist of polyesters, polyethers, or glycols such as polyethylene glycol (PEG), 1,4-butanediol, and polypropylene glycol (PPG) (Grassie and Zulfiqar, 1978; Wen et al., 2001; Oprea, 2010; Nozaki et al., 2017). The structure of these compounds is presented in **Figure 2**. The properties of PU depend on the structure and length of polyisocyanate and polyol monomers used during synthesis. Addition of polyisocyanate with aromatic monomer as well as short polyol chains increases the rigidity of the PU backbone which affects the mechanical properties such as Young's modulus. On the contrary, addition of long aliphatic monomer units, most often as part of the polyol, has the opposite affect and allows the PU to have more rubbery characteristics (Yoshida et al., 1990, Bharadwaj et al., 2002). However, addition of too many aromatic or aliphatic units can produce material that is too brittle or rubbery in character for use. Therefore, a balance between these two traits must be met for a PU to be useful.

Another way to increase the structural rigidity of a PU is through cross-linking, as seen in **Figure 3**, which decreases the molecular freedom of the polymer chains. This increases mechanical properties, such as tensile modulus and decreases elongation. PU film that is cross-linked will provide higher chemical and abrasion resistance due to the formation of a tightly packed network. Cross-linking can occur *via* chemical reactions when at least one of the monomer units contains three or more reactive sites, addition of additives, or can be brought on through the use of radiation (Chen and Rånby, 1989; Basfar et al., 2003; Dong et al., 2012; Iype et al., 2016). PUs have another unique way to cross-link by the reaction of an isocyanate with an already formed urethane linkage to create an allophanate linkage, as shown in **Figure 4**. Even though the positive impacts that cross-linking has on the properties of PU is attractive, there are some drawbacks as
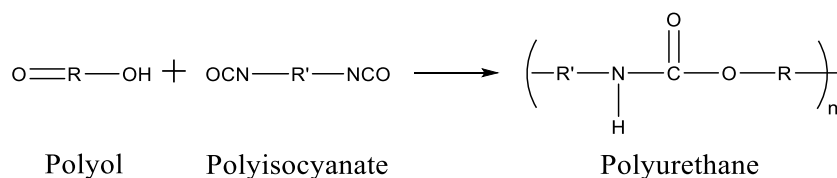
FIGURE 1 | Reaction of a polyol with a polyisocyanate to synthesize a polyurethane.
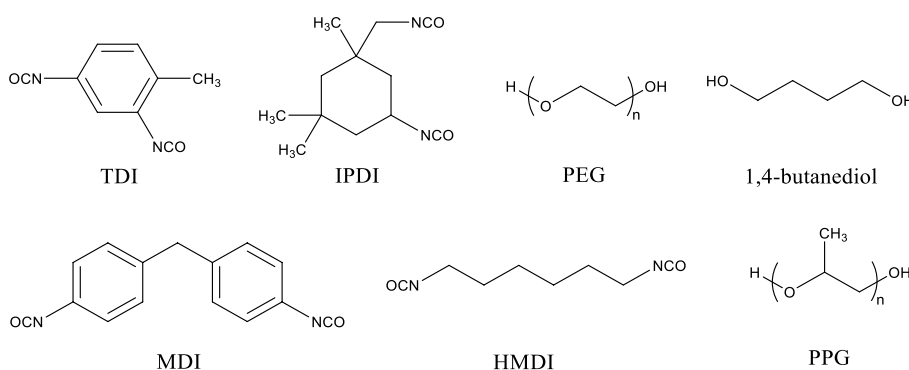
FIGURE 2 | Structures of a select few isocyanate compounds and polyol compounds.

well. One such setback is that cross-links are, for the most part, irreversible and products that have undergone cross-linking are difficult to recycle.

Over the last decade, there has been an increase in interest in deriving polymers from a renewable resource such as biomass, due to their renewability and biodegradability (Noreen et al., 2016, Gang et al., 2017). Among many renewable resources, one bio-based polymer that is of current interest to scientists and

industry is lignin due to its highly aromatic structure, natural abundance, and ability to form lignin-based PU materials.

Lignin

Lignin is a bio-based polyol and the second most naturally occurring polymer on Earth, behind cellulose, and makes up 18–35% of wood (Hon, 1996). Lignin is a highly aromatic polymer found in all plant cell wall alongside cellulose and hemicellulose. It provides structural support as well as a defense mechanism against parasites and diseases (Saito et al., 2013).

Although there is no precise definition of 3D structure of lignin, the structure consists of three-main monomer building blocks. The highly aromatic nature of lignin, shown in **Figure 5A**, is due to the enzyme initiated dehydrogenation polymerization and radical coupling reactions of three basic monomers or monolignols p-coumaryl alcohol, coniferyl alcohol, and syringyl alcohol shown in **Figure 5B** (Suhas and Ribeiro, 2007, Chatterjee and Saito, 2015). These three monolignols are very similar in structure consisting of a phenolic ring with an aliphatic side chain that includes an alkene and an alcohol functional group. Structurally they differ in the number of methoxy groups found at

FIGURE 3 | Representation of non-cross-linked polymer chains (left) and polymer chains that are cross-linked (right). The blue lines represent polymer chains and the red lines represent the cross-links.

Isocyanate   Urethane Linkage   Allophanate Linkage

FIGURE 4 | Scheme of the reaction between an isocyanate group and a urethane linkage to form an allophanate linkage.

p-Coumaryl Alcohol   Coniferyl Alcohol   Syringyl Alcohol

FIGURE 5 | **(A)** Theoretical representation of the structure of a lignin molecule and **(B)** the structures of the monolignol units used to polymerize lignin.

each ortho position relative to the phenolic hydroxyl group. These methoxy groups play a key role in the physical characteristics and construction of the lignin molecule.

The amounts of each monolignol used to form the lignin molecule depend on the type of plants (hardwood, softwood, and grass) from which lignin is extracted. Lignins extracted from hardwood sources contain the highest amounts of syringyl alcohol amongst the three classes of lignins with smaller amounts of coniferyl alcohol monolignols. Softwood lignins, also called coniferous or guaiacyl lignins, are solely made up of coniferyl alcohol monolignols. Lignins that are extracted from grasses, also called non-wood lignin, contain all three monolignols; however, this class of lignins contains the highest amount of p-coumaryl alcohol monolignols. The amount of methoxy groups in the monolignol is important due to the steric hindrance they provide to the phenolic hydroxyl group of the monolignol. This is because the enzyme catalyzed polymerization of the monolignol units heavily targets the two hydroxyl groups connecting the monomers together to form the polymer chain. An increase in steric hindrance leads to a decreased ability for the phenolic site to react with another monomer lowering the amount of cross-linking within the overall lignin structure. From the structure of lignin internal cross-linking, it is understood that hardwood lignin that consists of the highest amount of syringyl alcohol monolignol units possess the least internally cross-linked structure, while grasses that possess the highest amount of p-coumaryl alcohol monolignol have more internally cross-linked structure compared to other classes of lignins. This internal cross-linking affects not only lignin molecule but also the properties of lignin-based materials.

Lignin has gained significant attraction in the scientific community due to its potential use to produce polymer materials. One of the largest processes where lignin is extracted from plants is during the chemical pulping processes at paper mills as by-product (Chakar and Ragauskas, 2004). The main product for this process is cellulose to produce paper. Up until recently, lignin was viewed as waste that was only used as fuel to power the boilers during the paper-making process. In 2010, it was estimated that the paper and pulping industry alone extracted 50 million tons of lignin (Gosselink et al., 2004, Laurichesse and Avérous, 2014). Biorefineries increase that amount making lignin very economical. With lignin being highly abundant, including an estimated 300 billion tons of lignin available in the biosphere with a steady yearly increase of 20 billion tons. The high availability of lignin and its low cost further increases its attraction to be used as a starting material for producing polymer products (Gregorová et al., 2006, Laurichesse and Avérous, 2014).

Other than the plant source they are extracted from, another important classification of lignins is by the extraction process employed. There are several extraction processes that allow the separation of lignin from the lignocellulosic base. The most dominant processes used are the Kraft, sulfite, organosolv, and soda processes. The Kraft process makes up approximately 85% of the total lignin production throughout the world (Tejado et al., 2007). During this process, the wood is dissolved in an aqueous medium of sodium hydroxide and sodium sulfide and is cooked under pressure at 170°C for a couple of hours (Chakar and

Ragauskas, 2004, Fatechi and Chen, 2016). During the cooking process, hydroxide and hydrosulfide anions react with the lignin and cleaves α-aryl ether and β-aryl ether bonds producing lignin with higher amounts of phenolic hydroxyl groups and a small amount of sulfur in the form of thiol groups (−SH) (Smook, 1992, Chakar and Ragauskas, 2004, Wang et al., 2016).

In sulfite pulping, lignin is extracted in the form of lignosulfonates due to sulfonic groups ($-SO_3^-$) being introduced into the structural network of the lignin molecules (Fan and Zhan, 2008). The sulfite process uses sulfurous acid and its alkali salt versions to extract the lignin from wood chips by breaking α-O-4 ether linkages under high pressure at approximately 150°C (Qui et al., 2010, Wang et al., 2016). The attached sulfonic groups also cause lignosulfonate to act as a polyelectrolyte allowing it to be water soluble even though the backbone is composed of a hydrophobic aromatic skeleton. Lignosulfonates contain the highest amount of sulfur among all types of lignins. Although the polydispersity of lignin in general is usually high, lignosulfonates typically have the highest polydispersity among all types of lignins which can be a drawback in material production (Madad et al., 2013).

The organosolv process is a sulfur free pulping process that uses a mixture of solvents such as methanol, ethanol, acetic acid, formic acid, and peroxy-organic acids to cook the wood and separate lignin from the other wood constituents (Xu et al., 2006, Tian et al., 2017). During the organosolv process, lignin becomes solubilized by solvent or solvents used through acido-lytic or alkaline cleavage of aryl ether linkages resulting in an increased number of phenolic functionalities. Due to the use of organic solvents and organic acids as the reactants, organosolv lignins have no added functionalities like thiols or sulfonic groups found in Kraft lignins and lignosulfonates (Duval and Lawoko, 2014).

Another pulping process used to extract lignin is the soda process. Like the organosolv process, it is sulfur free and does not include side reactions that add extra functionalities onto the structure. However, in the soda process, alkaline materials without sodium sulfide is used to break down the lignin. The soda process is mainly used for the degradation of grass sources such as wheat straw, hemp, switchgrass, and bagasse and the absence of sulfur content makes it very attractive for polymer applications (Doherty et al., 2011, Laurichesse and Avérous, 2013).

Due to the highly aromatic structure of lignin, different processes have been developed that break down lignin molecules to produce other valuable aromatic chemicals, such as benzene, toluene, xylene, styrene, phenols, cyclohexane, aromatic alde-hydes, vanillin, and vanillic acid (da Silva et al., 2009; Varanasi et al., 2013; Yamaguchi et al., 2017). Since lignin is a polyol, different synthesis techniques have also been used to study the effect of lignin incorporation on the properties of biodegradable polymer materials. Due to the heterogeneous nature of lignin and its tendency to aggregate, homogeneous blends of lignin with other polymers are difficult to fabricate and usually results in poor mechanical properties when compared to the pure polymer counterpart (Alexy et al., 2000, Kadla and Kubo, 2004, Chung et al., 2013). However, modification of lignin, such as acetylation and grafting to/from, has been used to disrupt lignin aggregation. Resulting more homogeneous blend of lignin and polymers, as

well as an improvement in physical properties (Chung et al., 2013; Sen et al., 2015; Dehne et al., 2016).

The highly aromatic structure of lignin and its ability to act as a polyol have made it a desired building block to produce lignin-based PUs. Some of the more common lignin-based polymeric materials are soft or rigid PU foams, epoxy resins, lignin-grafted-polycaprolactone copolymers, and carbon fiber (Li and Ragauskas, 2012, Baker and Rials, 2013, Laurichesse and Avérous, 2013, Zhao and Abu-Omar, 2015). For most systems, it is desired to employ as much lignin into the polymeric material as possible to further increase targeted properties, use less petroleum-based chemicals, improve economics, and increase the biocompatibility of the material. However, too much lignin incorporated into a system usually leaves the material too brittle to be useful (Saito et al., 2013). Most of the results reported with higher loading of modified lignin-based PUs were too brittle to be studied for their properties; therefore, a compromise must be found between the amount of lignin content and rubbery content used to optimize economics, renewability, and mechanical properties.

Various studies have been carried out to understand the effects on the mechanical and thermal properties of PUs incorporating lignin from hard wood or soft wood or non-wood separately. However, to the best of our knowledge, no study has been done to investigate the effect of lignin from different plant source on the properties of PU. In this study, for the first time, the mechanical, thermal properties and morphology of the PU thermoplastic incorporating lignin extracted from different plant source, hard, soft and wheat straw is studied. Different studies have been carried out to maximize the incorporation of lignin in PU by modifying the lignin with different functionalities. Here, we studied a range of fraction of unmodified lignins from each plant source to understand the balance between the maximum amount of lignin that can be incorporated as polyols to synthesize PU while maintaining flexibility in the material. The results obtained from this study will provide insight into the different parameters that influence the properties of PU. With the understanding of the parameters will allow to develop materials with desired properties.

MATERIALS AND METHODS

Synthesis of Lignin-Based PU Elastomers

Three different lignins, each from different plant source, were used in this study: a Kraft processed lignin from a softwood source, a lignosulfonate lignin from a hardwood source, and a soda processed lignin from a wheat straw source. The softwood Kraft lignin (SWKL) was purchased from TCI America. The hardwood lignosulfonate lignin (HWLS) was supplied by Borregaard Lignntech and the wheat straw soda lignin (WSSL), also called Protobind 1000, was supplied by GreenValue LLC. The HWLS and the WSSL were used as received while the SWKL was subjected to an acid wash for further purification. The purification was carried out by adding approximately 10 g of SWKL to 300 mL of 2 M hydrochloric acid (HCl) and then SWKL/HCl solution was allowed to stir for 3 h open at ambient temperature and open to air. The mixture solution was then filtered using a

fritted funnel with a porosity of 4–5.5 μm to obtain the SWKL particles from the solution. This step was repeated twice and then the SWKL was washed few times with deionized water to remove any leftover HCl. Thus, obtained SWKL was dried overnight in vacuum oven under vacuum strength of 30 mmHg at 60°C. The dried SWKL powder was then stored in a desiccator.

Polypropylene glycol (PPG) (M_N = 2,300 g/mol) end-capped on both ends with toluene-2,4-diisocyanate (TDI) (purchased from Sigma-Aldrich) was used as isocyanate cross-linker during PU synthesis. Before synthesis, the lignin being used was heated and dried under full vacuum overnight to remove any residual moisture. All steps for the reaction of lignin with TDI–PPG–TDI to synthesize lignin-based PUs were performed in the nitrogen glove box.

PU Synthesis

2 g of isocyanate was weighed in a 50 mL beaker and allowed to mechanically stir on a hotplate at 100°C for a few minutes. Eight drops of dibutyltin dilaurate (DBTDL) purchased from Sigma-Aldrich was then added as a catalyst and isocyanate/DBTDL mixture was mechanically stirred at 100°C for 10 min to produce a homogeneous mixture. A precise amount of lignin that gave the desired lignin weight percent (wt%) was weighed out and added to isocyanate/DBTDL mixture. The lignin/isocyanate/DBTDL mixture was then allowed to stir on a hotplate at 100°C until the viscosity of the mixture increased due to the progress of the polymerization. The mixture was then poured into a Teflon® mold and allowed to cure at room temperature overnight inside the nitrogen glove box. The dimensions of the mold allowed the formation of samples appropriate as a dual-cantilever sample for the dynamic mechanical analysis (DMA). A range of lignin contents (20, 30, 40, 50, and 60 wt%) were used to synthesize lignin-based PUs. A reference PU sample was also synthesized using the same method as described for the lignin-based PU samples with a hydroxy-terminated PPG (M_N = 2,000 g/mol) as the polyol.

Characterization

Dynamic Mechanical Analysis (DMA)

Mechanical properties measurements were performed using a DMA Q800 (TA Instruments) with the dual cantilever geometry and calibrated using the TA Instruments calibration kit. Samples were made by curing in a Teflon® mold with the dimensions 57 mm × 12.5 mm × 3.5 mm (L × W × H). The measurement was carried out at 30°C and 0.1% strain with a frequency of 1 Hz.

Shore Hardness

The shore hardness of all lignin-based PU samples were measured according to the ASTM D2240-15 standard procedure with a Type A Model 2000 Durometer made by Rex Gauge Company. Since all lignin-based PU samples did not have a thickness of 6 mm, samples of the same lignin plant source and lignin wt% were piled together to create a sample with the appropriate thickness. Piled samples were measured in three separate areas.

Differential Scanning Calorimeter (DSC)

Thermal properties of the samples were measured using a DSC Q2000 (TA Instruments), where an Indium standard was used

for the calibration. Samples weighing between 5 and 10 mg were cut from DMA samples and weighed using a Cahn C-33 microbalance. The samples were then placed in a pre-weighed aluminum standard DSC pan and heated at 10°C per minute over the temperature range of −80–150°C in nitrogen environment.

Phosphorus-31 Nuclear Magnetic Resonance (^{31}P-NMR)

Phosphorus-31 nuclear magnetic resonance spectroscopy was used to determine hydroxyl group content of lignins used. All lignin samples were dried before use to remove any moisture content due to its high reactivity with phospholane reagent. 20 mg of dried lignin sample was added to a 400 µL dimethylformamide/pyridine (1:1, v/v) solution and 200 µL of internal standard (ISTD) solution in a NMR tube. The ISTD was prepared by mixing 75 mg cyclohexanol (CH) (Sigma-Aldrich, 99%) as a standard with 10.084 g deuterated chloroform ($CDCl_3$) and 20 mg chromium (III) acetylacetonate as a relaxation reagent. The sample solution was then derivatized with 100 µL of the phospholane reagent 2-chloro-4,4,5,5-tetramethyl-1,3,2-dioxaphospholane (TMDP) (Sigma-Aldrich, 95%). The sample mixtures were analyzed using a JEOL 400 MHz NMR spectrometer over 128 scans with inverse-gated decoupling, a 90° pulse, and a 25 s pulse delay.

A total of five ^{31}P-NMR samples for each lignin source were run to determine an average hydroxyl group concentration and a standard deviation (SD) based on lignin source. Mestrenova software was used to integrate all ^{31}P-NMR data. The following equations were used to calculated the concentrations of each hydroxyl group type (Olarte et al., 2016).

$$\text{mmol CH} = \frac{CH_{mass}\,(g)}{100.158\,\frac{g}{mol}\,CH} \times \frac{\text{CH purity}}{100} \times 1000,$$

$$[CH] = \frac{\left(\dfrac{\text{mmol CH}}{\text{ISTD Stock Solution}_{total\ mass}\,(g)}\right) \times \text{ISTD Aliquot}(g)}{\text{NMR sample}_{total\ mass}\,(g)},$$

$$\frac{I_i}{I_{CH}} = \frac{\text{integration of spectral region of interest}}{\text{integration of Cyclohexanol region}},$$

$$\frac{\text{mmol OH}}{\text{g Lignin}} = \frac{\left(\dfrac{I_i}{I_{CH}}\right) \times [CH] \times \text{NMR sample}_{total\ mass}\,(g)}{\text{Lignin}_{mass}\,(g)}.$$

Scanning Electron Microscope (SEM)

The morphologies of lignin-based PU samples were investigated using a Zeiss Auriga 40 field emission SEM. Samples were cut from bulk material and were not coated during sample preparation. Images were captured using a secondary electron detector lens and a voltage level of 1.00 kV.

Atomic Force Microscope (AFM)

Images of the phase morphology of lignin-based PU samples were scanned using an Asylum Research MFP-3D Infinity AFM. Samples were cut from bulk material and were imaged

under tapping mode. The uncoated silicon cantilevers with a resonant frequency range or 200–400 kHz and a spring constant of 13–77 N/m from AppNano were used for scanning. The AFM images were analyzed using the WSxM 5.0 software (Horcas et al., 2007).

RESULTS AND DISCUSSION

In this study, lignin extracted from a hardwood source, a softwood source, and a non-wood source were used to study the effects that the plant source of lignin has on targeted mechanical properties of lignin-based PUs. As previously discussed, lignin is used as a polyol and reacted with a rubbery cross-linker to synthesize lignin-based PU samples with multiple wt% of lignin loadings. The use of the rubbery cross-linker allows the synthesis of cohesive samples that are not too brittle to be tested. The synthesis of lignin-based PUs with varying lignin loadings provides a pathway to monitor the correlation between targeted mechanical properties and lignin loading and correlate these changes to lignin plant source.

Mechanical Properties

Dynamic mechanical analysis provides information on the influence of lignin source on the mechanical properties of lignin-based PU samples. **Figures 6** and **7** show the storage and loss modulus of PUs as a function of lignin content ranging from 10 to 60 wt%. It is evident from **Figure 6** that, for all three lignin sources, the storage modulus increases with lignin loading. This can be explained as lignin is the rigid component in PU, while diisocyanate PPG is the rubbery component. Thus, the rigid lignin provides mechanical strength to the system while PPG brings a more viscous response to the sample (Saito et al., 2013). As the ratio between rigid and rubbery component increases, the mechanical stiffness increases, resulting in a higher storage modulus. **Figure 6** also shows that the lignin-based PU samples that were synthesized using WSSL provided the highest storage modulus at all lignin loadings, while HWLS provided the lowest storage moduli.

The storage moduli of softwood Kraft lignin and hardwood lignosulfonate lignin based PUs exhibited similar storage moduli.
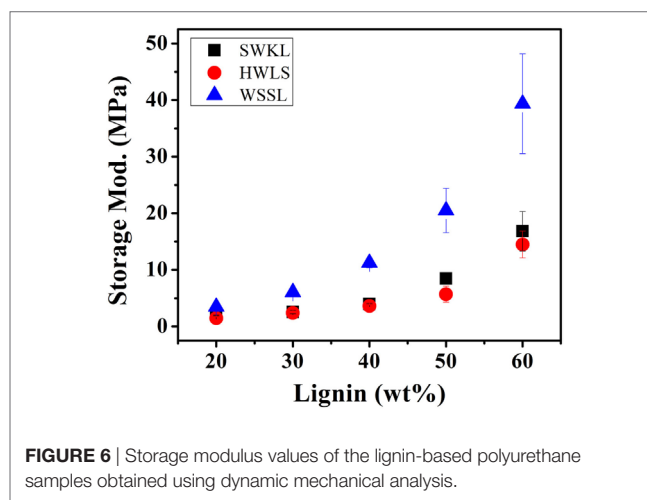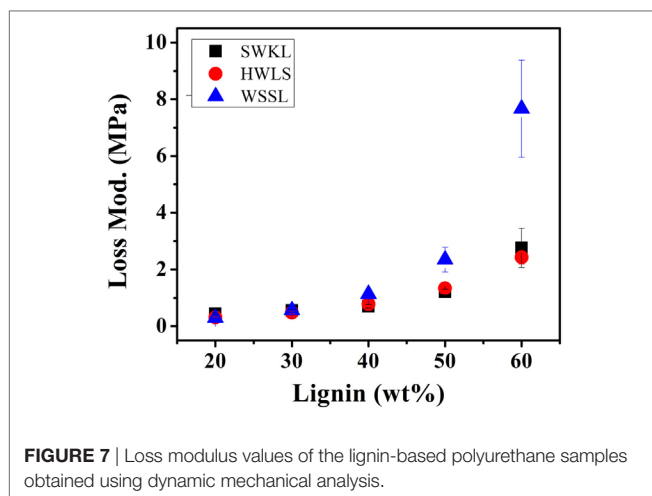

FIGURE 6 | Storage modulus values of the lignin-based polyurethane samples obtained using dynamic mechanical analysis.

FIGURE 7 | Loss modulus values of the lignin-based polyurethane samples obtained using dynamic mechanical analysis.

FIGURE 8 | Shore hardness (Type A) results for all lignin-based polyurethane samples.

At lower lignin loadings (20, 30, and 40 lignin wt%), the difference between the storage moduli of these two samples is minimal. However, the difference between the storage moduli increases at higher lignin loadings (50 and 60 lignin wt%). Even though the storage moduli of SWKL and HWLS samples are similar, SWKL samples consistently exhibited higher moduli than HWLS samples at all lignin loadings. The loss modulus (elastic response) in **Figure 7** showed the similar trend as the storage modulus for lignin with different plant source and lignin loading.

Figure 8 shows the shore hardness (Type A) of all lignin-based PU samples, which generally agree with the storage moduli obtained *via* DMA. All three lignin sources show an increase in hardness as lignin loading increases. This is again due to the increased rigidity that results from the higher lignin content. The increased rigidity resulted from the incorporation of more lignin also increases the resistance to deformation under a compressive force, due to the decrease in molecular mobility with added cross-linking (Saito et al., 2013; Wang et al., 2013; Llovera et al., 2016).

Lignin-based PU samples synthesized using wheat straw soda lignin show a higher shore hardness at all lignin loadings than softwood Kraft lignin and hardwood lignosulfonate lignin samples, while SWKL samples show a higher shore hardness at all lignin loadings than HWLS samples. This trend is also in agreement with dynamic mechanical analysis results depicting a more cross-linked material for WSSL samples. At higher lignin loading, the hardness values for the WSSL samples deviate from a linear trend due to the hardness value reaching the limits of the Type A durometer used for testing. Values that are close to the limits of the durometer used are considered to have more uncertainty.

To fully understand the mechanical testing results, it is important to determine the nano- and microscale structure of these materials, as these length scales highly influences the mechanical properties of a polymer material. This information will also offer a more thorough explanation on why WSSL samples provided higher storage modulus values relative to the SWKL and HWLS samples. Atomic Force Microscopy and SEM, along with DSC, were used to study the thermal and phase
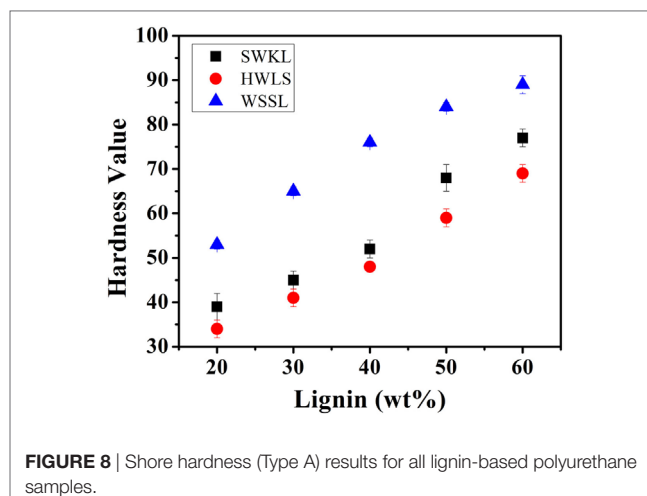
TABLE 1 | T_g values obtained from differential scanning calorimeter scans of lignin-based polyurethane samples of 20, 40, and 60 wt% lignin.

Sample	T_g (°C)		
	HWLS	**SWKL**	**WSSL**
Pure lignin	47	91	116
20 wt% Lignin	−52	−52	−48
40 wt% Lignin	−51, 26	−50	−45
60 wt% Lignin	−51, 2, 26	−46	−42, 10, 110
Pure polypropylene glycol PU		−53	

HWLS, hardwood lignosulfonate; SWKL, softwood Kraft lignin; and WSSL: wheat straw soda lignin.

behavior, as well as the morphology of lignin PUs with 20, 40, and 60 wt% lignin loading.

Thermal Properties

The thermal response of the pure lignins and lignin-based PU samples were obtained using DSC. The glass transition temperature (T_g) of the select PUs are shown in **Table 1** and the DSC scans are presented in Figures S1–S3 in Supplementary Material in the supplementary material. The thermal properties of the pure lignins show that the WSSL has the highest T_g while HWLS displays the lowest T_g. This is a result of the variation in monolignol content in lignins from various plant sources. Among three types of lignin, WSSL have the highest internal cross-linking due to the presence of the highest amount of p-coumaryl alcohol whereas HWLS have the lowest internal cross-linking. Increase in cross-linking makes molecule less mobile resulting higher T_g. All lignin-based PU samples show multiple T_gs, which is indicative of the presence of multiple phases (Saito et al., 2013, Sen et al., 2015). At low lignin loadings, only one T_g is observed for all lignin sources and is associated with the PPG-dominant domain. As lignin loading increases, a second T_g at a higher temperature is observed for HWLS and WSSL samples and is associated with a lignin-rich phase. Samples synthesized with SWKL did not show an observable second T_g, which we attribute to the faint nature of the T_g of the pure SWKL.

Nano and Microscale Morphology

Phase images obtained *via* AFM of the various lignin PUs are shown in **Figure 9**, while the microscopic structure of these samples as determined by SEM are shown in **Figure 10**. Both of these sets of images show multiphase morphology confirming presence of multi domain in the sample which is clearly visible in HWLS and SWKL samples. Figure S4 in Supplementary Material, in the supplementary material, provides SEM images of pure dry lignins before PU synthesis. Aggregation is observed in both AFM and SEM images for the HWLS-based PU samples at all lignin loadings which become more abundant on both the nanoscale and microscale as lignin loading increases in PUs. The aggregates observed are similar in size to those observed in the SEM images of the pure HWLS, indicating a modest level of mixing between PPG and HWLS during the synthesis. Voids between the aggregates and the surrounding matrix observed in the SEM also indicate that HWLS and PPG do not mix as well as the other lignins do. The size of HWLS particles, along with the minimal level of mixing inhibits the homogeneous dispersion of HWLS in the final PU, detrimentally affecting the mechanical properties. This modest level of mixing is also consistent with the glass transition behavior of the samples, where the T_g of the soft phase (-51 to $-53°C$) does not vary much from the T_g of the PPG precursor ($-53°C$).

The AFM images of SWKL-based PU samples do not show the presence of aggregates indicating better mixing on this length scale. As the result of this improved dispersion of SWKL small distinct domains of a continuous phase are formed, as seen in AFM images, and become more prominent at 60 wt% SWKL loading.

The scanning electron microscopy images show a poor level of mixing on the microscale with the appearance of large particles similar in size to those observed in pure softwood Kraft lignin. Voids are also observed between the particles and the surrounding matrix indicating poor interfacial adhesion between these phases. These particles and voids deteriorate the mechanical properties of the SWKL-based PU samples, similar to hardwood lignosulfonate lignin samples. However, the improved mixing observed at the nanoscale improves the mechanical properties of the material relative to that of the HWLS samples, resulting in higher storage moduli.

For WSSL-based PU samples, the AFM images show improved mixing relative to that of the SWKL and HWLS samples. As WSSL lignin loading increases, the AFM images show the formation of large continuous domains that are considerably larger than those found in SWKL samples. These continuous domains are a result of better mixing of lignin and PPG in WSSL samples. In the SEM images of the pure WSSL lignins, large particles are not observed. The smaller WSSL particles provide a pathway for better dispersion throughout the PU material leading to more enhanced mechanical properties. The SEM images of the WSSL PUs show areas with a smooth surface and some with rough surfaces indicating multiple domains in the sample. However, unlike SWKL samples and HWLS samples, there are no voids between these
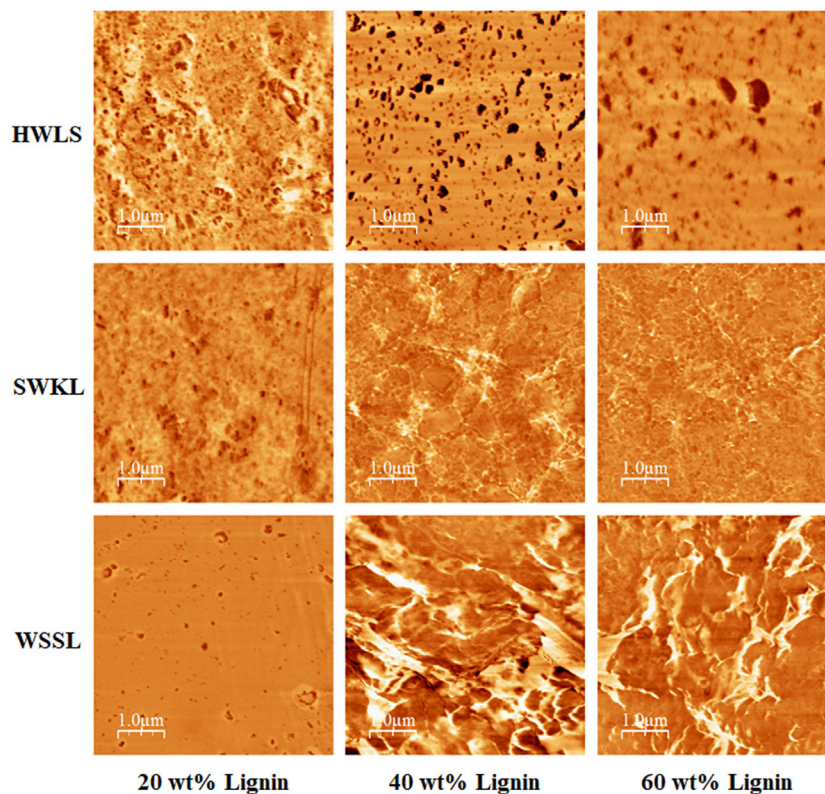

FIGURE 9 | Atomic force microscope phase images of lignin-based polyurethane samples at 20, 40, and 60 wt% lignin loading.
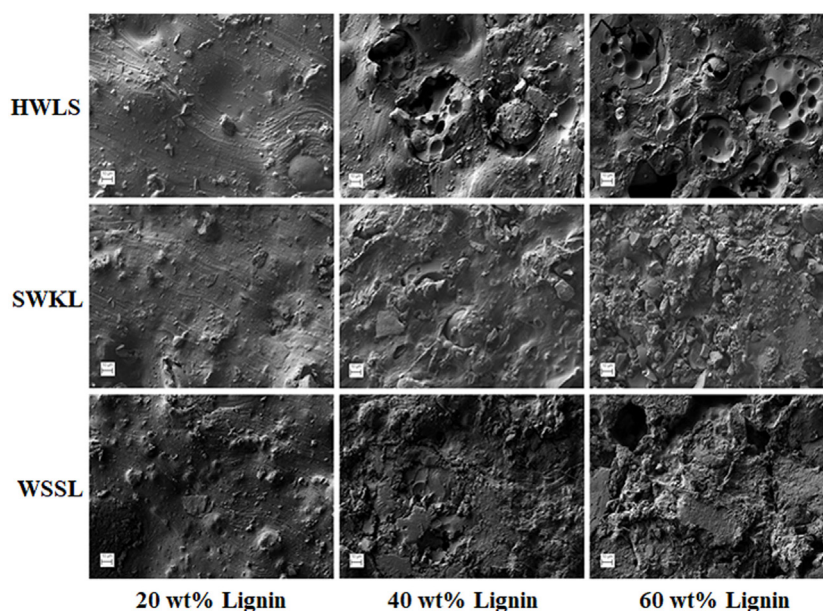
FIGURE 10 | Scanning electron microscope images of lignin-based polyurethane samples with 20, 40, and 60 wt% lignin loading.

domains, indicating strong adhesion between domains. Because of the improved mixing, the absence of large lignin particles, and strong adhesion between domains, WSSL samples attain a higher modulus than the other lignin samples at all lignin loadings.

These differing levels of mixing also correlate to the observed thermal behavior of PUs determined from differential scanning calorimeter. The T_g corresponding to the PPG-rich phase increases with lignin loading for all lignins, indicating the incorporation of lignin into these phases. Moreover, the amount of increase in the T_g of this rubbery phase corresponds to the extent of mixing of polypropylene glycol (PPG) and lignin in this phase. For the hardwood lignosulfonate lignin, the T_g increases from −53°C to −51°C, indicating poor mixing between HWLS and PPG. The T_g of the PPG-rich domain is −46°C for the 60 wt% softwood Kraft lignin sample and −42°C for wheat straw soda lignin sample; changes of +7°C and +11°C, respectively. These indicate better mixing between SWKL and WSSL lignins and PPG, in qualitative agreement with the microscopic images, particularly for the WSSL samples. These results also correlate to the mechanical properties of PUs, where the formation of continuous domains in WSSL samples, the better mixing of PPG and lignins in the rubbery phase, and improved adhesion between the domains inhibits the rubbery behavior of the PPG chains enhancing the storage modulus of the material. An opposite effect is evident in HWLS samples where the limited miscibility between the lignin and PPG offer minimal improvement in the storage modulus with addition of lignin.

Correlation to Molecular Level Structure

Correlating the molecular level structure of lignins to the morphology and mechanical properties provides further insight into the effect of plant source on the properties of the synthesized

TABLE 2 | Hydroxyl group type concentrations for each lignin source determined by ^{31}P-NMR.

Hydroxyl group type	Hydroxyl group type concentration (mmol OH/g lignin)		
	Hardwood lignosulfonate lignin (HWLS)	Softwood Kraft lignin (SWKL)	Wheat straw soda lignin (WSSL)
Aliphatic:	5.71 (± 0.04)	1.45 (± 0.12)	1.30 (± 0.12)
C_5-condensed:	0.12 (± 0.02)	0.69 (± 0.05)	0.55 (± 0.04)
(S) Syringyl:	0.35 (± 0.01)	–	0.54 (± 0.02)
(G) Guaiacyl:	0.28 (± 0.01)	1.17 (± 0.11)	0.80 (± 0.05)
(H) p-Coumaryl:	–	0.11 (± 0.02)	0.30 (± 0.03)
Carboxylic Acid:	0.32 (± 0.07)	0.60 (± 0.07)	0.70 (± 0.08)
Total:	6.86 (± 0.1)	4.02 (± 0.23)	4.19 (± 0.1)

lignin-based PUs. As mentioned earlier, ^{31}P-NMR provides hydroxyl group concentration of each lignin with the ability to distinguish between hydroxyl group types. Therefore, ^{31}P-NMR was used to obtain a better understanding of the structure and reactivity of each lignin by source.

The analysis of the ^{31}P-NMR data is shown in **Table 2** and hydroxyl group to isocyanate group ratios (OH:NCO) of each lignin-based PU are given in **Table 3**. Examples of the ^{31}P-NMR data for all three lignin sources are shown in Figure S5 in Supplementary Material in the supplementary material. Overall, HWLS lignin contains a higher total hydroxyl group content while SWKL and WSSL have approximately the same hydroxyl content. The NMR data also show that HWLS contains approximately four times more aliphatic hydroxyl groups than SWKL and WSSL while the SWKL and WSSL contain more phenolic groups. Based on this hydroxyl content, it would be expected that samples synthesized using HWLS would produce a more cross-linked

TABLE 3 | Calculated OH:NCO ratios for lignin-based PU samples with 20, 40, and 60 wt% lignin loadings.

Lignin wt%	Lignin source	OH:NCO ratio's			
		Total	Aromatic	Aliphatic	Carb. acid
20	Hardwood lignosulfonate lignin (HWLS)	1.97	0.24	1.64	0.09
	Softwood Kraft lignin (SWKL)	1.16	0.57	0.42	0.17
	Wheat straw soda lignin (WSSL)	1.20	0.63	0.37	0.20
40	HWLS	5.26	0.64	4.38	0.25
	SWKL	3.08	1.51	1.11	0.46
	WSSL	3.21	1.68	1.00	0.54
60	HWLS	11.38	1.43	9.85	0.55
	SWKL	6.93	3.40	2.50	1.04
	WSSL	7.23	3.78	2.24	1.21

Carb. Acid: Carboxylic Acid.

material with higher mechanical properties than PUs synthesized with SWKL or WSSL. However, according to DMA and hardness testing results, HWLS-based PU has the lowest mechanical properties at all lignin loadings. This apparent discrepancy can be explained by the aggregation of the lignin observed by AFM and SEM, which inhibits the accessibility of these hydroxyl groups to react with isocyanate. The limited number of hydroxyl groups able to react with isocyanate results in a PU with fewer cross-links leading to the inferior storage modulus and shore hardness.

Even though SEM images of SWKL PUs showed aggregation within the sample, the AFM images exhibited improved mixing at the nanoscale level compared to HWLS samples. This improved dispersion of SWKL relative to HWLS increases the accessibility of hydroxyl groups of SWKL to react with the isocyanate moieties. This emphasizes that greater hydroxyl group accessibility is more important than the amount of hydroxyl groups present in the formation of cross-links and improvement of the storage modulus of the synthesized PUs. Although there is better dispersion at the nanoscale, SEM images show aggregation throughout SWKL samples, which limits the modulus of the material. The balance of these two factors, therefore, controls the modulus of the SWKL samples, which are higher than that of the HWLS-PU samples, but lower than the WSSL samples.

The large continuous phases observed in the AFM of WSSL PUs and the adhesion between domains in the SEM images indicate a higher level of mixing in WSSL samples. Thus, although WSSL, like SWKL, contains fewer hydroxyl groups than HWLS, even more hydroxyl groups are accessible to react with isocyanate due to the improved mixing. This improved reactivity leads to higher amounts of cross-linking resulting improved adhesion between domains as observed in the SEM images. The greater amount of cross-linking enhances the mechanical properties of the material leading to a higher modulus for WSSL-based PUs compared to the SWKL and HWLS samples.

Therefore, while the amount of hydroxyl groups that exist in each lignin, which is controlled by its plant source, impacts the reaction of the lignin with the isocyanate, the accessibility of hydroxyl groups

is more important in controlling the extent of the reaction. The domain adhesion and mixing found in WSSL, brought on by more rigid urethane linkage formation, produces a more rigid framework increasing the mechanical properties of WSSL-based PU beyond those of HWLS and SWKL-based PU. Aggregation of particles and poor domain adhesion in the HWLS and SWKL PUs leaves voids and decreases the continuity of the lignin/PPG framework lowering the mechanical properties of the material. SWKL-based PU show better overall mechanical properties than HWLS samples due to SWKL's higher level of mixing on the nanoscale, yet are less rigid than the WSSL samples due to the aggregation that is also found throughout the framework albeit to a lesser extent than HWLS.

CONCLUSION

The lignin plant source clearly affects the mechanical properties of lignin-based PU materials. The storage moduli of lignin-based PUs synthesized with PPG cross-linker increased with lignin loading for all three lignin sources due to lignin acting as the rigid component. PUs synthesized with WSSL lignin exhibited the highest storage modulus at all lignin loadings, while HWLS provided the lowest. The shore hardness of lignin-based PUs agreed with storage moduli (DMA results) showing that the hardness of PU increased with lignin loading and that WSSL samples exhibited the highest hardness at all lignin loadings while HWLS provided the lowest.

Thermal study showed multiple T_gs indicating the presence of multi-phase morphology for all lignin-based PUs. Different levels of mixing for all lignin sources were observed in AFM and SEM images. PUs synthesized with HWLS showed the poorest level of mixing with PPG, drastically lowering the mechanical properties. While distinct domains of a continuous phase formed in their AFM images indicated better mixing of SWKL with PPG leading to enhanced mechanical properties. The smaller particle size of WSSL lignin led to better mixing with PPG and the highest storage modulus at all lignin loadings in WSSL-based PUs. These differing levels of mixing correlated well with the observed thermal behavior of PUs where the T_g corresponding to the PPG-rich phase increased, not only with lignin loading but also with the level of mixing indicating a drop in rubbery behavior of PPG chains and ultimately enhancing the storage modulus.

^{31}P-NMR study revealed that HWLS contained the highest total hydroxyl group content while hydroxyl content of SWKL and WSSL were nearly the same. However, higher storage modulus in PU incorporated with SWKL despite having lower hydroxyl concentration than HWLS showed that not all hydroxyl groups were accessible to isocyanate moieties hindering the number of cross-links that could form. Due to the better dispersion amongst lignins, even more cross-links form in WSSL samples allowing WSSL samples to provide the highest storage modulus and shore hardness.

AUTHOR CONTRIBUTIONS

MD conceived the experiments, led the interpretation of the results, and helped write the manuscript. US completed some of the experiments, and contributed to both the data interpretation and manuscript writing. JL completed the majority of the experiments and contributed to both the data interpretation and manuscript writing.

FUNDING

REFERENCES

Akindoyo, J. O., Beg, M. D. H., Ghazali, S., Islam, M. R., Jeyaratnam, N., and Yuvaraj, A. R. (2016). Polyurethane types, synthesis and applications: a review. *RSC Adv.* 6, 114453–114482. doi:10.1039/C6RA14525F

Alexy, P., Kosikova, B., and Podstranska, G. (2000). The effect of blending lignin with polyethylene and polypropylene on physical properties. *Polymer* 41, 4901–4908. doi:10.1016/S0032-3861(99)00714-4

Baker, D. A., and Rials, T. G. (2013). Recent advances in low-cost carbon fiber manufacture from lignin. *J. Appl. Polym. Sci.* 130, 713–728. doi:10.1002/app.39273

Basfar, A. A., Ali, K. M. I., and Mofti, S. M. (2003). UV stability and radiation-crosslinking of linear low density polyethylene and low density polyethylene for greenhouse applications. *Polym. Degrad. Stab.* 82, 229–234. doi:10.1016/S0141-3910(03)00216-7

Bharadwaj, V., Somani, K., and Kansara, S. (2002). The effect of chain length of polyethylene glycol on properties of castor oil based polyurethane elastomers. *J. Macromol. Sci. Pure Appl. Chem.* 39, 115–127. doi:10.1081/MA-120006522

Chakar, F. S., and Ragauskas, A. J. (2004). Review of current and future softwood Kraft lignin process chemistry. *Ind. Crops Prod.* 20, 131–141. doi:10.1016/j.indcrop.2004.04.016

Chan-Chan, L. H., Solis-Correa, R., Vargas-Coronado, R. F., Cervantes-Uc, J. M., Cauich-Rodríguez, J. V., Quintana, P., et al. (2010). Degradation studies on segmented polyurethanes prepared with HMDI, PCL and different chain extenders. *Acta Biomater.* 6, 2035–2044. doi:10.1016/j.actbio.2009.12.010

Chatterjee, S., and Saito, T. (2015). Lignin-derived advanced carbon materials. *ChemSusChem* 8, 3941–3958. doi:10.1002/cssc.201500692

Chen, Y. L., and Rånby, B. (1989). Photocrosslinking of polyethylene. II. Properties of photocrosslinked polyethylene. *J. Poly. Sci. A* 27, 4077–4086. doi:10.1002/pola.1989.080271215

Chung, H., and Washburn, N. R. (2012). Improved lignin polyurethane properties with lewis acid treatment. *ACS Appl. Mater. Interfaces* 4, 2840–2846. doi:10.1021/am300425x

Chung, Y. L., Olsson, J. V., Li, R. J., Frank, C. W., Waymouth, R. M., Billington, S. L., et al. (2013). A renewable lignin-lactide copolymer and application in biobased composites. *ACS Sustain. Chem. Eng.* 1, 1231–1238. doi:10.1021/sc4000835

da Silva, E. A. B., Zabkova, M., Araujo, J. D., Cateto, C. A., Barreiro, M. F., Belgacem, M. N., et al. (2009). An integrated process to produce vanillin and lignin-based polyurethanes from Kraft lignin. *Chem. Eng. Res. Des.* 87, 1276–1292. doi:10.1016/j.cherd.2009.05.008

Dehne, L., Babarro, C. V., Saake, B., and Schwarz, K. U. (2016). Influence of lignin source and esterification on properties of lignin-polyethylene blends. *Ind. Crops Prod.* 86, 320–328. doi:10.1016/j.indcrop.2016.04.005

Doherty, W. O. S., Mousavioun, P., and Fellows, C. M. (2011). Value-adding to cellulosic ethanol: lignin polymers. *Ind. Crops Prod.* 33, 259–276. doi:10.1016/j.indcrop.2010.10.022

Dong, W., Ren, J., Lin, L., Shi, D., Ni, Z., and Chen, M. (2012). Novel photocross-linkable and biodegradable polyester from bio-renewable resource. *Polym. Degrad. Stab.* 97, 578–583. doi:10.1016/j.polymdegradstab.2012.01.008

Duval, A., and Lawoko, M. (2014). A review on lignin-based polymeric, micro- and nano-structured materials. *React. Funct. Polym.* 85, 78–96. doi:10.1016/j.reactfunctpolym.2014.09.017

Fan, J., and Zhan, H. (2008). Optimization of synthesis of spherical lignosulphonate resin and its structure characterization. *Chin. J. Chem. Eng.* 16, 407–410. doi:10.1016/S1004-9541(08)60097-X

Fatechi, P., and Chen, J. (2016). Extraction of technical lignins from pulping spent liquors, challenges and opportunities. *Product. Biofuels Chem. Lignin Springer Nat.* 6, 35–54. doi:10.1007/978-981-10-1965-4_2

Gang, H., Lee, D., Choi, K. Y., Kim, H. N., Ryu, H., Lee, D. S., et al. (2017). Development of high performance polyurethane elastomers using vanillin-based green polyol chain extender originating from lignocellulosic biomass. *ACS Sustain. Chem. Eng.* 5, 4582–4588. doi:10.1021/acssuschemeng.6b02960

Gosselink, R. J. A., de Jong, E., Guran, B., and Abacherli, A. (2004). Co-ordination network for lignin-standardisation, production and applications adapted to market requirements (EUROLIGNIN). *Ind. Crops Prod.* 20, 121–129. doi:10.1016/j.indcrop.2004.04.015

Grand View Research. (2017). *Polyurethane (PU) Market Analysis by Product (Rigid Foam, Flexible Foam, Coatings, Adhesives & Sealants, Elastomers), by End-Use (Furniture & Interiors, Construction, Electronics & Appliances, Automotive, Footwear, Packaging), & Segment Forecasts, 2014-2025*. Available at: http://www.grandviewresearch.com/industry-analysis/polyurethane-pu-market

Grassie, N., and Zulfiqar, M. (1978). Thermal degradation of the polyurethane from 1,4-butanediol and methylene bis(4-phenyl isocyanate). *J. Polym. Sci.* 16, 1563–1574.

Gregorová, A., Košíková, B., and Moravčík, R. (2006). Stabilization effect of lignin in natural rubber. *Polym. Degrad. Stab.* 91, 229–233. doi:10.1016/j.polymdegradstab.2005.05.009

Hon, D. N. S. (1996). *Chemical Modification of Lignocellulosic Materials*. New York: Marcel Dekker.

Horcas, I., Fernandez, R., Gomez-Rodriguez, J. M., Colchero, J., Gomez-Herrero, J., and Baro, A. M. (2007). WSXM: a software for scanning probe microscopy and a tool for nanotechnology. *Rev. Sci. Instrum.* 78, 013701–013708. doi:10.1063/1.2432410

Iype, E., Esteves, A. C. C., and de With, G. (2016). Mesoscopic simulations of hydrophilic cross-linked polycarbonate polyurethane networks: structure and morphology. *Soft Matter* 12, 5029–5040. doi:10.1039/c6sm00621c

Kadla, J. F., and Kubo, S. (2004). Lignin-based polymer blends: analysis of intermolecular interactions in lignin-synthetic polymer blends. *Compos. Part A. Appl. Sci. Manuf.* 35, 395–400. doi:10.1016/j.compositesa.2003.09.019

Laurichesse, S., and Avérous, L. (2013). Synthesis, thermal properties, rheological and mechanical behaviors of lignins-grafted-poly(epsilon-caprolactone). *Polymer* 54, 3882–3890. doi:10.1016/j.polymer.2013.05.054

Laurichesse, S., and Avérous, L. (2014). Chemical modification of lignins: towards biobased polymers. *Prog. Polym. Sci.* 39, 1266–1290. doi:10.1016/j.progpolymsci.2013.11.004

Li, Y., and Ragauskas, A. J. (2012). Kraft lignin-based rigid polyurethane foam. *J. Wood Chem. Technol.* 32, 210–224. doi:10.1080/02773813.2011.652795

Llovera, L., Benjelloun-Mlayah, B., and Delmas, M. (2016). Organic acid lignin-based polyurethane films: synthesis parameter optimization. *BioResources* 11, 6320–6334. doi:10.15376/biores.11.3.6320-6334

Madad, N., Chebil, L., Charbonnel, C., Ioannou, I., and Ghoul, M. (2013). Enzymatic polymerization of sodium lignosulfonates: effect of catalysts, initial molecular weight, and mediators. *Can. J. Chem.* 91, 220–225. doi:10.1139/cjc-2012-0036

Noreen, A., Zia, K. M., Zuber, M., Tabasum, S., and Zahoor, A. F. (2016). Bio-based polyurethane: an efficient and environment friendly coating systems: a review. *Prog. Org. Coat.* 91, 25–32. doi:10.1016/j.porgcoat.2015.11.018

Nozaki, S., Masuda, S., Kamitani, K., Kojio, K., Takahara, A., Kuwarnura, G., et al. (2017). Superior properties of polyurethane elastomers synthesized with aliphatic diisocyanate bearing a symmetric structure. *Macromolecules* 50, 1008–1015. doi:10.1021/acs.macromol.6b02044

Olarte, M. V., Burton, S. D., Swita, M., Padmaperuma, A. B., Ferrell, J., and Ben, H. (2016). *Determination of Hydroxyl Groups in Pyrolysis Bio-Oils Using 31P NMR: Laboratory Analytical Procedure (LAP)*. Washington, DC; Golden, CO (United States): National Renewable Energy Lab (NREL).

Oprea, S. (2010). Dependence of fungal biodegradation of PEG/castor oil-based polyurethane elastomers on the hard-segment structure. *Polym. Degrad. Stab.* 95, 2396–2404. doi:10.1016/j.polymdegradstab.2010.08.013

Prisacariu, C. (2011). *Polyurethane Elastomers: From Morphology to Mechanical Aspects*. Wien, New York: Springer Verlag.

Qui, X., Kong, Q., Zhou, M., and Yang, D. (2010). Aggregation behavior of sodium lignosulfonate in water solution. *J. Phys. Chem. B* 114, 15857–15861. doi:10.1021/jp107036m

Saito, T., Perkins, J. H., Jackson, D. C., Trammel, N. E., Hunt, M. A., and Naskar, A. K. (2013). Development of lignin-based polyurethane thermoplastics. *RSC Adv.* 3, 21832–21840. doi:10.1039/c3ra44794d

SUPPLEMENTARY MATERIAL

The Supplementary Material for this article can be found online at http://www.frontiersin.org/articles/10.3389/fenrg.2018.00004/full#supplementary-material.

Saraf, V. P., and Glasser, W. G. (1984). Engineering plastics from lignin. III. Structure property relationship in solution cast polyurethane films. *J. Appl. Polym. Sci.* 29, 1831–1841. doi:10.1002/app.1984.070290534

Sarkar, S., and Adhikari, B. (2001). Thermal stability of lignin–hydroxy-terminated polybutadiene copolyurethanes. *Polym. Degrad. Stab.* 73, 169–175. doi:10.1016/S0141-3910(01)00084-2

Sen, S., Patil, S., and Argyropoulos, D. S. (2015). Thermal properties of lignin in copolymers, blends, and composites: a review. *Green Chem.* 17, 4862–4887. doi:10.1039/C5GC01066G

Seymour, R. B., and Kauffman, G. B. (1992). Polyurethanes: a class of modern versatile materials. *J. Chem. Educ.* 69, 909–910. doi:10.1021/ed069p909

Silva, A. L., and Bordado, J. C. (2004). Recent developments in polyurethane catalysis: catalytic mechanisms review. *Cat. Revi. Sci. Eng.* 46, 31–51. doi:10.1081/CR-120027049

Smook, G. A. (1992). *Handbook for Pulp & Paper Technologists*. Vancouver: Angus Wilde Publications.

Soto, M., Sebastián, R. M., and Marquet, J. (2014). Photochemical activation of extremely weak nucleophiles: highly fluorinated urethanes and polyurethanes from polyfluoro alcohols. *J. Org. Chem.* 79, 5019–5027. doi:10.1021/jo5005789

Stevens, M. P. (1999). *Polymer Chemistry: An Introduction*. New York: Oxford University Press.

Suhas, P. J. M., and Ribeiro, M. M. L. (2007). Lignin – from natural adsorbent to activated carbon: a review. *Bioresour. Technol.* 98, 2301–2312. doi:10.1016/j.biortech.2006.08.008

Szycher, M. (1999). *Handbook of Polyurethanes*. Boca Raton, FL: CRC Press.

Tejado, A., Peña, C., Labidi, J., Echeverria, J. M., and Mondragon, I. (2007). Physico-chemical characterization of lignins from different sources for use in phenol-formaldehyde resin synthesis. *Bioresour. Technol.* 98, 1655–1663. doi:10.1016/j.biortech.2006.05.042

Teo, L. S., Chen, C. Y., and Kuo, J. F. (1997). Fourier transform infrared spectroscopy study on effects of temperature on hydrogen bonding in amine-containing polyurethanes and poly(urethane-urea)s. *Macromolecules* 30, 1793–1799. doi:10.1021/ma961035f

Tian, D., Chandra, R. P., Lee, J. S., Lu, C., and Saddler, J. N. (2017). A comparison of various lignin-extraction methods to enhance the accessibility and ease of enzymatic hydrolysis of the cellulosic component of steam-pretreated poplar. *Biotechnol. Biofuels* 10, 1–10. doi:10.1186/s13068-017-0846-5

Varanasi, P., Singh, P., Auer, M., Adams, P. D., Simmons, B. A., and Singh, S. (2013). Survey of renewable chemicals produced from lignocellulosic biomass during ionic liquid pretreatment. *Biotechnol. Biofuels* 6, 1–9. doi:10.1186/1754-6834-6-14

Wang, C., Kelley, S. S., and Venditti, R. A. (2016). Lignin-based thermoplastic materials. *ChemSusChem* 9, 770–783. doi:10.1002/cssc.201501531

Wang, Z., Yang, X., Zhou, Y., and Liu, C. (2013). Mechanical and thermal properties of polyurethane films from peroxy-acid wheat straw lignin. *Bioresources* 8, 3833–3843. doi:10.15376/biores.8.3.3833-3843

Wen, T. C., Fang, J. C., Lin, H. J., and Yang, C. H. (2001). Characteristics of PPG-based thermoplastic polyurethane doped with lithium perchlorate. *J. Appl. Polym. Sci.* 82, 389–399. doi:10.1002/app.1863

Xu, F., Sun, J.-X., Sun, R., Fowler, P., and Baird, M. S. (2006). Comparative study of organosolv lignins from wheat straw. *Ind. Crops Prod.* 23, 180–193. doi:10.1016/j.indcrop.2005.05.008

Yamaguchi, A., Mimura, N., Shirai, M., and Sato, O. (2017). Bond cleavage of lignin model compounds into aromatic monomers using supported metal catalysts in supercritical water. *Sci. Rep.* 7, 1–7. doi:10.1038/srep46172

Yoshida, H., Mörck, R., Kringstad, K. P., and Hatakeyama, H. (1990). Kraft lignin in polyurethanes. II. Effects of the molecular-weight of Kraft lignin on the properties of polyurethanes from a kraft lignin polyether triol polymeric MDI system. *J. Appl. Polym. Sci.* 40, 1819–1832. doi:10.1002/app.1990.070401102

Zhang, C., Wu, H., and Kessler, M. R. (2015). High bio-content polyurethane composites with urethane modified lignin as filler. *Polymer* 69, 52–57. doi:10.1016/j.polymer.2015.05.046

Zhao, S., and Abu-Omar, M. M. (2015). Biobased epoxy nanocomposites derived from lignin-based monomers. *Biomacromolecules* 16, 2025–2031. doi:10.1021/acs.biomac.5b00670

Pleiotropic and Epistatic Network-Based Discovery: Integrated Networks for Target Gene Discovery

Deborah Weighill [1,2], Piet Jones [1,2], Manesh Shah [2], Priya Ranjan [2,3], Wellington Muchero [2], Jeremy Schmutz [4,5], Avinash Sreedasyam [5], David Macaya-Sanz [6], Robert Sykes [7], Nan Zhao [3], Madhavi Z. Martin [2], Stephen DiFazio [6], Timothy J. Tschaplinski [2], Gerald Tuskan [2] and Daniel Jacobson [1,2]*

[1] The Bredesen Center for Interdisciplinary Research and Graduate Education, University of Tennessee, Knoxville, TN, United States, [2] Biosciences Division, Oak Ridge National Laboratory, Oak Ridge, TN, United States, [3] Department of Plant Sciences, The University of Tennessee Institute of Agriculture, University of Tennessee, Knoxville, TN, United States, [4] Department of Energy, Joint Genome Institute, Walnut Creek, CA, United States, [5] HudsonAlpha Institute for Biotechnology, Huntsville, AL, United States, [6] Department of Biology, West Virginia University, Morgantown, WV, United States, [7] National Renewable Energy Laboratory, Golden, CO, United States

Biological organisms are complex systems that are composed of functional networks of interacting molecules and macro-molecules. Complex phenotypes are the result of orchestrated, hierarchical, heterogeneous collections of expressed genomic variants. However, the effects of these variants are the result of historic selective pressure and current environmental and epigenetic signals, and, as such, their co-occurrence can be seen as genome-wide correlations in a number of different manners. Biomass recalcitrance (i.e., the resistance of plants to degradation or deconstruction, which ultimately enables access to a plant's sugars) is a complex polygenic phenotype of high importance to biofuels initiatives. This study makes use of data derived from the re-sequenced genomes from over 800 different *Populus trichocarpa* genotypes in combination with metabolomic and pyMBMS data across this population, as well as co-expression and co-methylation networks in order to better understand the molecular interactions involved in recalcitrance, and identify target genes involved in lignin biosynthesis/degradation. A Lines Of Evidence (LOE) scoring system is developed to integrate the information in the different layers and quantify the number of lines of evidence linking genes to target functions. This new scoring system was applied to quantify the lines of evidence linking genes to lignin-related genes and phenotypes across the network layers, and allowed for the generation of new hypotheses surrounding potential new candidate genes involved in lignin biosynthesis in *P. trichocarpa*, including various AGAMOUS-LIKE genes. The resulting Genome Wide Association Study networks, integrated with Single Nucleotide Polymorphism (SNP) correlation, co-methylation, and co-expression networks through the LOE scores are proving to be a powerful approach to determine the pleiotropic and epistatic relationships underlying cellular functions and, as such, the molecular basis for complex phenotypes, such as recalcitrance.

Keywords: multi-omic data layering, LOE scores, lines of evidence, GWAS, SNP correlation, association networks

1. INTRODUCTION

Populus species are promising sources of cellulosic biomass for biofuels because of their fast growth rate, high cellulose content and moderate lignin content (Sannigrahi et al., 2010). Ragauskas et al. (2006) outline areas of research needed "to increase the impact, efficiency, and sustainability of bio-refinery facilities" (Ragauskas et al., 2006), such as research into modifying plants to enhance favorable traits, including altered cell wall structure leading to increased sugar release, as well as resilience to biotic and abiotic stress. One particular research target in *Populus* species is the decrease/alteration of the lignin content of cell walls.

A large collection of different data types has been generated for *Populus trichocarpa*. The genome has been sequenced and annotated (Tuskan et al., 2006), and the assembly is currently in its third version of revision. A collection of 1,100 accessions of *P. trichocarpa* that have been clonally propagated in four different common gardens (Tuskan et al., 2011; Slavov et al., 2012; Evans et al., 2014) have been resequenced, which has provided a large set of ∼ 28,000,000 Single Nucleotide Polymorphisms (SNPs) that has recently been publicly released (http://bioenergycenter.org/besc/gwas/). Many molecular phenotypes, such as untargetted metabolomics and pyMBMS phenotypes, that have been measured in this population provide an unparalleled resource for Genome Wide Association Studies (for example, see McKown et al., 2014). DNA methylation data in the form of MeDIP (Methyl-DNA immunoprecipitation)-seq has been performed on 10 different *P. trichocarpa* tissues (Vining et al., 2012), and gene expression has been measured across various tissues and conditions.

This study involved the development of a method to integrate these various data types in order to identify new possible candidate genes involved in target functions of interest. The importance of *P. trichocarpa* as a bioenergy crop, the availability of the high density SNP data in a GWAS population, as well as the increasing amount of genomic/phenotypic data being generated for *P. trichocarpa* made it an excellent species in which to demonstrate the method. Integrating Genome Wide Association Study (GWAS) data with other data types has previously been done to help provide context and identify relevant subnetworks/modules (Bunyavanich et al., 2014; Calabrese et al., 2017). Ritchie et al. (2015) reviewed techniques for integrating various data types for the aim of investigating gene-phenotype associations. Integrating multiple lines of evidence is a useful strategy as the more lines of evidence that connect a gene to a phenotype lowers the chance of false positives. Ritchie et al. (2015) categorized data integration approaches into two main classes, namely multi-staged analysis and meta-dimensional analysis. Multi-staged analysis aims to enrich a biological signal through various steps of analysis. Meta-dimensional analysis involves the concurrent analysis of various data types,

and is divided into three subcategories (Ritchie et al., 2015): Concatenation-based integration concatenates the data matrices of different data types into a single matrix on which a model is constructed (for example, see Fridley et al., 2012). Model-based integration involves constructing a separate model for each dataset and then constructing a final model from the results of the separate models (for example, see Kim et al., 2013). Transformation-based integration involves transforming each data type into a common form (e.g., a network) before combining them (see for example, Kim et al., 2012).

This study presents a new transformation-based integration technique: the calculation of Lines Of Evidence (LOE) scores across SNP correlation, GWAS, co-methylation, and co-expression networks for *P. trichocarpa*. Association networks for the various different data types were constructed, including a pyMBMS GWAS network, a metabolomics GWAS network, as well as co-expression, co-methylation, and SNP correlation networks, and subsequently the information in the different networks was integrated through the calculation of the newly developed Lines Of Evidence (LOE) scores. These scores quantify the number of lines of evidence connecting each gene to target functions of interest. In this work, we apply this data integration technique to the wealth of *P. trichocarpa* data in order to identify new potential genes involved in lignin biosynthesis/degradation/regulation in *P. trichocarpa*. The LOE scores represent the number of lines of evidence that exist connecting genes to lignin-related genes and phenotypes across the network layers. This is a novel multi-omic data integration approach which provides easily interpretable scores, and allows for the identification of new possible candidate genes involved in lignin biosynthesis/regulation through multiple lines of evidence. This is also the first time all of these *P. trichocarpa* datasets have been integrated on a genome-scale in a network-based manner, allowing for the easy identification of new target genes through their respective connections across network layers.

2. METHODS

2.1. Overview

This approach involved combining various data types in order to identify new possible target genes involved in lignin biosynthesis/degradation/regulation. **Figure 1** summarizes the overall approach. First, association networks were constructed including metabolomics and pyMBMS GWAS networks, co-expression, co-methylation and SNP correlation networks. Known lignin-related genes and phenotypes were then identified, and used as seeds to select lignin-related subnetworks from these various networks. The Lines Of Evidence (LOE) scoring technique was developed, and each gene was then scored based on its Lines Of Evidence linking it to lignin-related genes and phenotypes.

2.2. Metabolomics Phenotype Data

The *P. trichocarpa* leaf samples for 851 unique clones were collected over 3 consecutive sunny days in July 2012. For 200 of those clones, a second biological replicate was also sampled. Typically, leaves (leaf plastocron index 9 plus or minus 1) on a

---

FIGURE 1 | Overview of pipeline for data layering and score calculation. First, the different network layers are constructed. Networks are layered, and lignin-related genes and phenotypes (orange) are identified. LOE scores are calculated for each gene. An example of the LOE score calculation for the red-boxed gene is shown. Thresholding the LOE scores results in a set of new potential target genes involved in lignin biosynthesis/degradation/regulation.
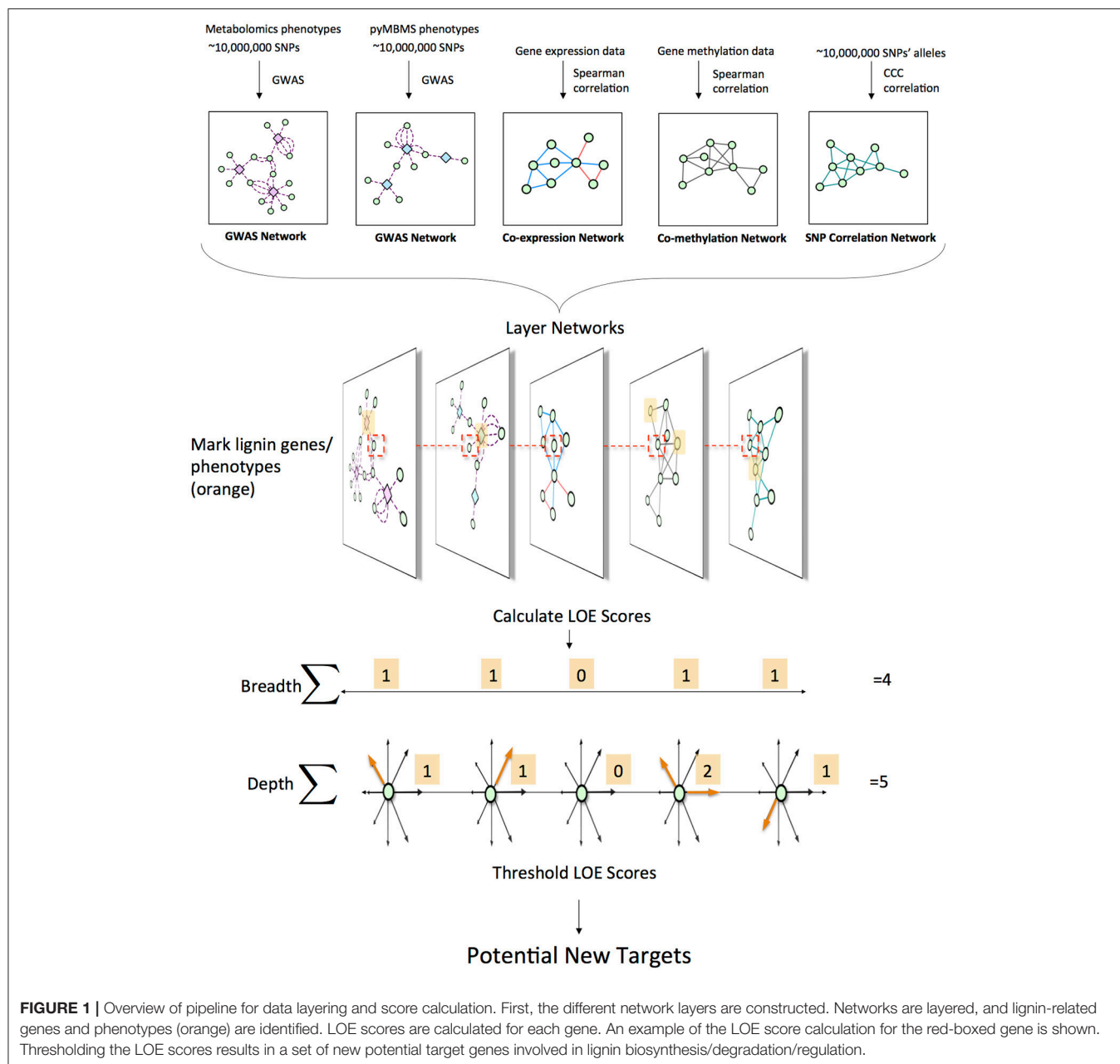
south facing branch from the upper canopy of each tree were quickly collected, wiped with a wet tissue to clean both surfaces and the leaf then fast frozen under dry ice. Leaves were kept on dry ice and shipped back to the lab and stored at $-80°C$ until processed for analyses. Metabolites from leaf samples were lyophilized and then ground in a micro-Wiley mill (1 mm mesh size). Approximately 25 mg of each sample was twice extracted in 2.5 mL 80% ethanol (aqueous) for 24 h with the extracts combined, and 0.5 mL dried in a helium stream. "Sorbitol [(75 µl of a 1 mg/mL aqueous solution)] was added ... before extraction as an internal standard to correct for differences in extraction efficiency, subsequent differences in derivatization efficiency and changes in sample volume during heating" (Zhao et al.,

2015). Metabolites in the dried sample extracts were converted to their trimethylsilyl (TMS) derivatives, and analyzed by gas chromatography-mass spectrometry, as described previously (Li et al., 2012; Tschaplinski et al., 2012), and also described here: Timm et al. (2016): Briefly, dried extracts of metabolites "were dissolved in acetonitrile followed by the addition of N-methyl-N-trimethylsilyltrifluoroacetamide (MSTFA) with 1% trimethylchlorosilane (TMCS), and samples then heated for 1 h at 70°C to generate trimethylsilyl (TMS) derivatives (Li et al., 2012; Tschaplinski et al., 2012). After 2 days, aliquots were injected into an Agilent 5975C inert XL gas chromatograph-mass spectrometer (GC-MS). The standard quadrupole GC-MS is operated in the electron impact (70 eV) ionization mode,

targeting 2.5 full-spectrum (50–650 Da) scans per second, as described previously (Tschaplinski et al., 2012). Metabolite peaks were extracted using a key selected ion, characteristic m/z fragment, rather than the total ion chromatogram, to minimize integrating co-eluting metabolites" (quotation from Timm et al., 2016). As described in Zhao et al. (2015): "...[The peak areas were] normalized to the quantity of the internal standard (sorbitol) [injected, and the] amount of sample extracted... A large user-created database (>2,400 spectra) of mass spectral electron impact ionization (EI) fragmentation patterns of TMS-derivatized metabolites, as well as the Wiley Registry [10th] Edition combined with NIST [2014] mass spectral database, were used to identify the metabolites of interest to be quantified" (Zhao et al., 2015) (Brackets indicate deviations from quoted text).

2.3. pyMBMS Phenotype Data

The pyMBMS phenotype data was generated using the method as described in Biswal et al. (2015): "A commercially

available molecular beam mass spectrometer (MBMS) designed specifically for biomass analysis was used for pyrolysis vapor analysis (Evans and Milne, 1987; Tuskan et al., 1999; Sykes et al., 2009). Approximately 4 mg of air dried 20 mesh biomass was introduced into the quartz pyrolysis reactor via 80 μL deactivated stainless steel Eco-Cups provided with the autosampler. Mass spectral data from m/z 30–450 were acquired on a Merlin Automation data system version 3.0 using 17 eV electron impact ionization."

The pyMBMS mz peaks were annotated as described in Sykes et al. (2009), as done previously in Muchero et al. (2015).

2.4. Single Nucleotide Polymorphism Data

A dataset consisting of 28,342,758 SNPs called across 882 *P. trichocarpa* (Tuskan et al., 2006) genotypes was obtained from http://bioenergycenter.org/besc/gwas/. This dataset is derived from whole genome sequencing of undomesticated *P. trichocarpa* genotypes collected from the U.S. and Canada, and clonally replicated in common gardens (Tuskan et al.,
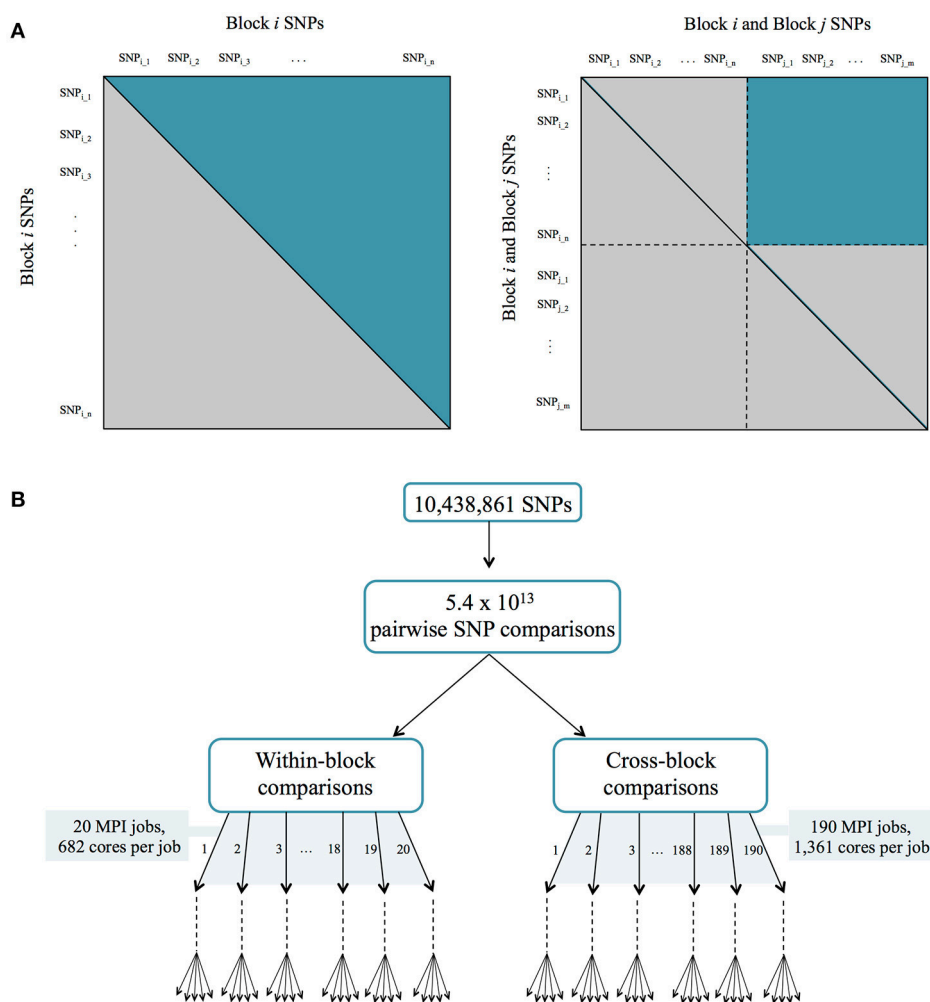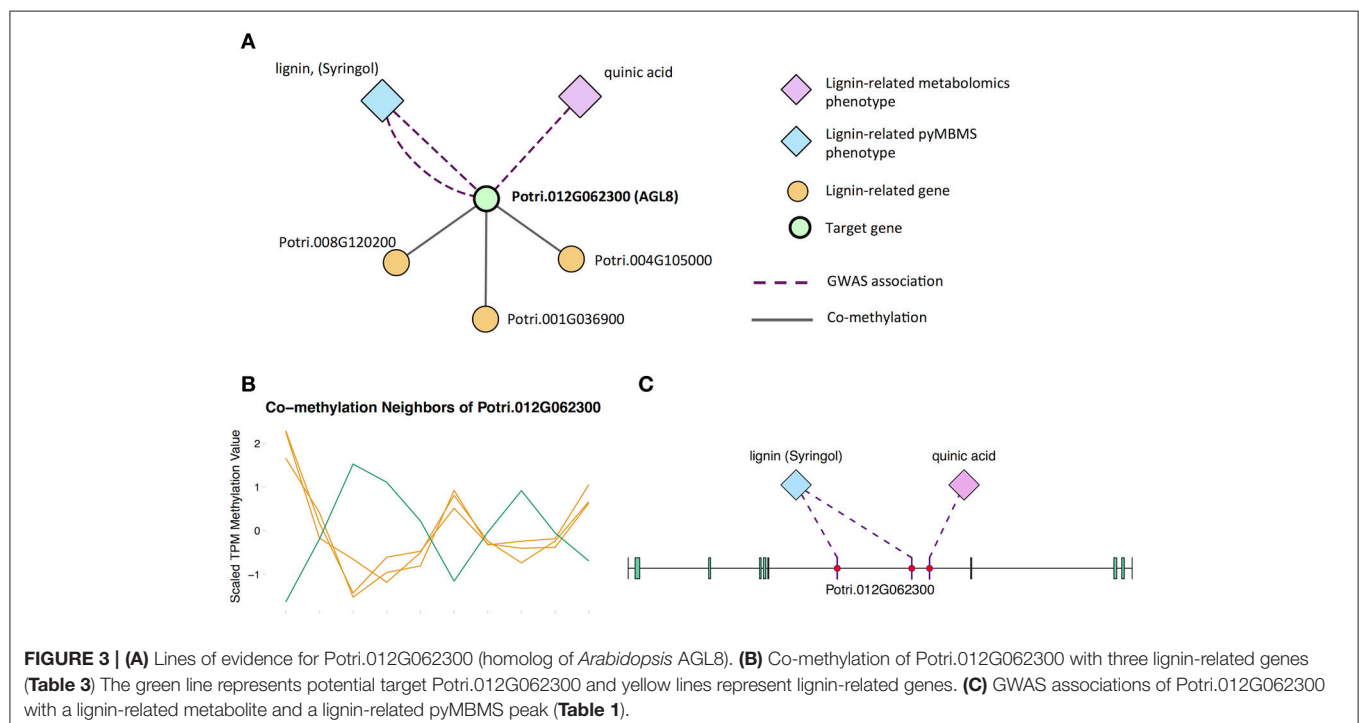

FIGURE 2 | (A) Parallelization strategy for ccc calculation between all pairs of SNPs. (B) MPI jobs for within and cross-block comparisons.

2011). Genotypes from this population have previously been used for population genomics (Evans et al., 2014) and GWAS studies in *P. trichocarpa* (McKown et al., 2014) as well as for investigating linkage disequilibrium in the population (Slavov et al., 2012).

Whole genome resequencing was carried out on a sample 882 *P. trichocarpa* natural individuals to an expected median coverage of 15x using Illumina Genome Analyzer, HiSeq 2000, and HiSeq 2500 sequencing platforms at the DOE Joint Genome Institute. Alignments to the *P. trichocarpa* Nisqually-1 v.3.0 reference genome were performed using BWA v0.5.9-r16 with default parameters, followed by post-processing with the picard FixMateInformation and MarkDuplicates tools. Genetic variants were called by means of the Genome Analysis Toolkit v. 3.5.0 (GATK; Broad Institute, Cambridge, MA, USA) (McKenna et al., 2010; van der Auwera et al., 2013). Briefly, variants were called independently for each individual using the concatenation of RealignerTargetCreator, IndelRealigner, and HaplotypeCaller tools, and the whole population was combined using GenotypeGVCFs, obtaining a dataset with all the variants detected across the sample population. Biallelic SNPs were extracted using the SelectVariants tool and quality-filtered using the GATK's machine-learning implementation Variant Quality Score Recalibration (VQSR). To this end, the tool VariantRecalibrator was used to create the recalibration file and the sensitivity tranches file. As a "truth" dataset, we used SNP calls from a population of seven female and seven male *P. trichocarpa* that had been crossed in a half diallel design. "True" SNPs were identified by the virtual absence of segregation distortion and Mendelian violations in the progeny of these 49 crosses (ca. 500

offspring in total). As a "non-true" dataset, we used the SNP calls of seven open-pollinated crosses from these 7 females ($n = 90$), filtered using hard-filtering methods recommended in the GATK documentation (tool: VariantFiltration; quality thresholds: QD < 1.5, FS > 75.0, MQ < 35.0, missing alleles < 0.5 and MAF > 0.05). The prior likelihoods for the true and non-true datasets were $Q = 15$ and $Q = 10$, respectively, and the variant quality annotations to define the variant recalibration space were DP, QD, MQ, MQRankSum, ReadPosRankSum, FS, SOR, and InbreedingCoeff. Finally, we used the ApplyRecalibration tool on the full GWAS dataset to assign SNPs to tranches representing different levels of confidence. We selected SNPs in the tranche with true sensitivity <90, which minimizes false positives, but at an expected cost of 10% false negatives. The final filtered dataset had a transition/transversion ratio of 2.07, compared to 1.88 for the unfiltered SNPs. To further validate the quality of these SNP calls, we compared them to an Illumina Infinium BeadArray that had been generated from a subset of this population dataset (Geraldes et al., 2013). The average match rate was 96% ($\pm$2% SD) for 641 individuals across 20,723 loci.

SNPs in this dataset were divided into different Tranches, indicating the percentage of "true" SNPs recovered. For further analysis in this study, we made use of the PASS SNPs, corresponding to the most stringent Tranche, recovering 90% of the true SNPs (see http://gatkforums.broadinstitute.org/gatk/discussion/39/variant-quality-score-recalibration-vqsr). VCFtools (Danecek et al., 2011) was used to extract the desired Tranche of SNPs from the VCF file and reformat it into .tfam and .tped files.

FIGURE 3 | (A) Lines of evidence for Potri.012G062300 (homolog of *Arabidopsis* AGL8). **(B)** Co-methylation of Potri.012G062300 with three lignin-related genes (**Table 3**) The green line represents potential target Potri.012G062300 and yellow lines represent lignin-related genes. **(C)** GWAS associations of Potri.012G062300 with a lignin-related metabolite and a lignin-related pyMBMS peak (**Table 1**).

2.5. GWAS Network Construction

The metabolomics and pyMBMS data was used as phenotypes in a genome wide association analysis. The respective phenotype measured over all the genotypes were analyzed to account for potential outliers. A median absolute deviation (MAD) from the median (Leys et al., 2013) cutoff was applied to determine if a particular measurement of a given phenotype was an outlier with respect to all measurements of that phenotype across the population. To account for asymmetry, the deviation values were estimated separately for values below and above the median, respectively. The distribution of the measured values together with the distribution of their estimated deviation was analyzed and a cutoff of 5 was determined to identify putative outlier values. Phenotypes that had non-outlier measurements in at least 20 percent of the population were retained for further analysis, this was to ensure sufficient signal for the genome wide association model. This resulted in 1,262

pyMBMS derived phenotypes and 818 metabolomics derived phenotypes.

To estimate the statistical significant associations between the respective phenotypes and the SNPs called across the population, we applied a linear mixed model using EMMAX (Kang et al., 2010). Taking into account population structure estimated from a kinship matrix, we tested each of the respective 2,080 phenotypes against the high-confidence SNPs and corrected for multiple hypotheses bias using the Benjamini–Hochberg control for false-discovery rate of 0.1 (Benjamini and Hochberg, 1995). This was done in parallel with a Python wrapper that utilized the schwimmbad Python package (Price-Whelan and Foreman-Mackey, 2017).

SNP-Phenotype GWAS networks were then pruned to only include SNPs that resided within genes, and SNPs were mapped to their respective genes, resulting in a gene-phenotype network. SNPs were determined to be

TABLE 1 | GWAS associations for select new potential target genes, indicating the SNP(s) within the potential new target gene which are associated with the lignin-related phenotype(s).

Source SNP	Source gene	Target phenotype
GWAS Associations for Potri.012G062300 (AGL8, AT5G60910)		
12:6952245	Potri.012G062300	Quinic acid
12:6948543	Potri.012G062300	Lignin (Syringol)
12:6951532	Potri.012G062300	Lignin (Syringol)
GWAS Associations for Potri.013G102600 (AGL12, AT1G71692)		
13:11604094	Potri.013G102600	3-O-caffeoyl-quinate
13:11606331	Potri.013G102600	Coumaroyl-tremuloidin
13:11600422	Potri.013G102600	Coumaroyl-tremuloidin
13:11601236	Potri.013G102600	Hydroxyphenyl lignan glycoside
GWAS Associations for Potri.007G115100 (AGL22, AT2G22540/AGL24, AT4G24540)		
07:13650194	Potri.007G115100	Caffeoyl conjugate
07:13651354	Potri.007G115100	Caffeoyl conjugate
07:13642539	Potri.007G115100	Caffeoyl conjugate
07:13639923	Potri.007G115100	Lignin, syringyl (Syringaldehyde)
GWAS Associations for Potri.009G053900 (MYB46, AT5G12870)		
09:5768381	Potri.009G053900	Hydroxyphenyl lignan glycoside
GWAS Associations for Potri.010G141000 (MYB111, AT5G49330)		
10:15273000	Potri.010G141000	Benzoyl-salicylate caffeic acid conjugate
GWAS Associations for Potri.006G170800 (MYB36, AT5G57620)		
06:17847162	Potri.006G170800	mz 297, RT 17.14
GWAS Associations for Potri.016G078600 (CPSRP54, AT5G03940)		
16:5995136	Potri.016G078600	Caffeoyl conjugate
16:5995136	Potri.016G078600	Feruloyl conjugate
16:5996083	Potri.016G078600	Salicyl-coumaroyl-glucoside
16:5999408	Potri.016G078600	Salicyl-coumaroyl-glucoside
16:5999474	Potri.016G078600	Salicyl-coumaroyl-glucoside
16:6000236	Potri.016G078600	Salicyl-coumaroyl-glucoside

Additional RT and mz information for partially identified metabolites can be seen in Table S3.

within genes using the gene boundaries defined in the `Ptrichocarpa_210_v3.0.gene.gff3` from the *P. trichocarpa* version 3.0 genome assembly on Phytozome (Goodstein et al., 2012).
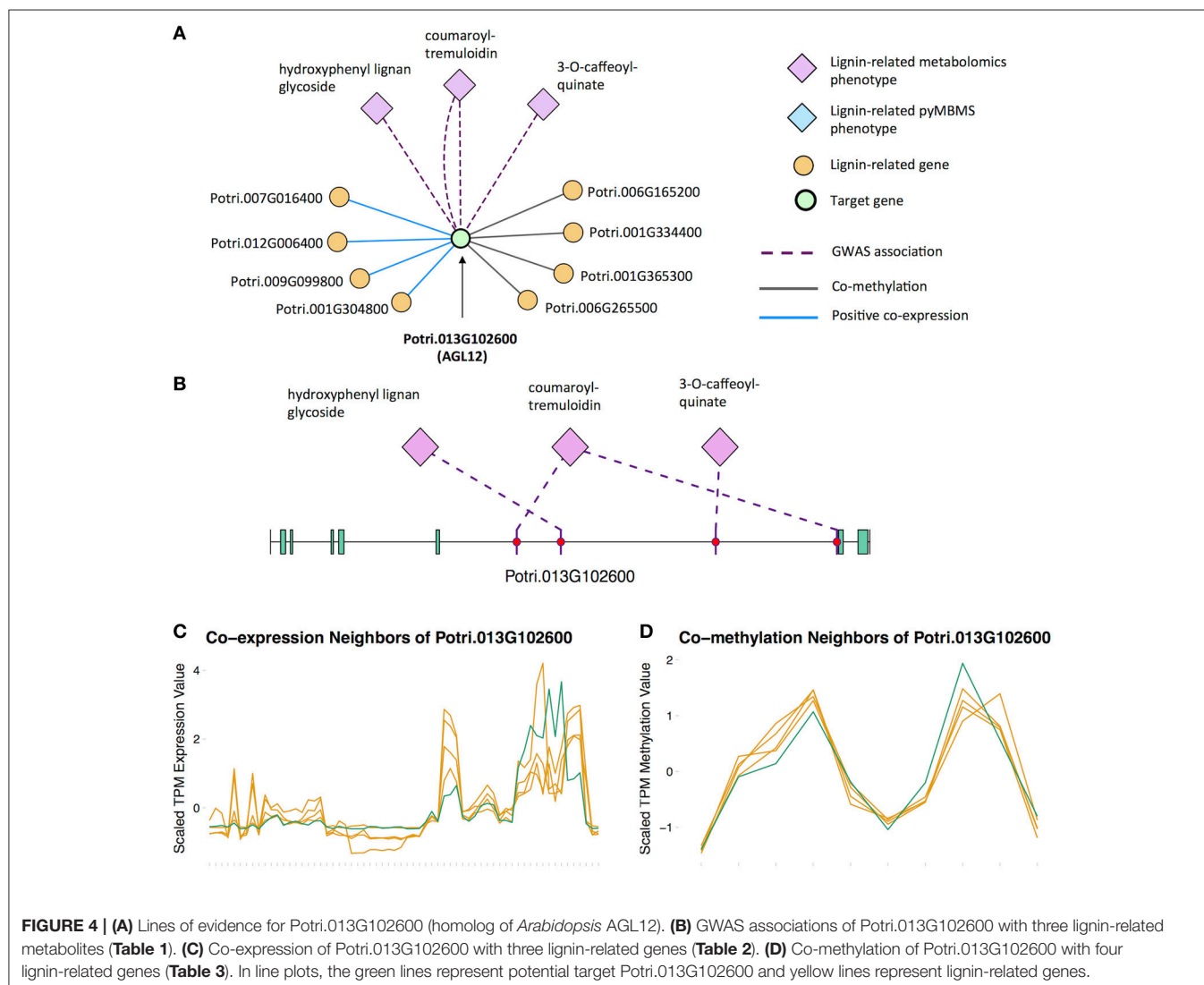
2.6. Gene Expression Data

P. trichocarpa (Nisqually-1) RNA-seq dataset from JGI Plant Gene Atlas project (Sreedasyam et al., unpublished) was obtained from Phytozome. This dataset consists of samples for standard tissues (leaf, stem, root, and bud tissue) and libraries generated from nitrogen source study. List of sample descriptions was accessed from: https://phytozome.jgi.doe.gov/phytomine/aspect. do?name=Expression.

P. trichocarpa (Nisqually-1) cuttings were potted in 4″ X 4″ X 5″ containers containing 1:1 mix of peat and perlite. Plants were grown under 16-h-light/8-h-dark conditions, maintained at 20–23 °C and an average of 235 μmol m^{-2}s^{-1} to generate tissue for (1) standard tissues and (2) nitrogen source study. Plants for standard tissue experiment were watered with McCown's

woody plant nutrient solution and plants for nitrogen experiment were supplemented with either 10 mM KNO3 (NO3⁻ plants) or 10mM NH4Cl (NH4+ plants) or 10 mM urea (urea plants). Once plants reached leaf plastochron index 15 (LPI-15), leaf, stem, root, and bud tissues were harvested and immediately flash frozen in liquid nitrogen and stored at −80°C until further processing was done. Every harvest involved at least three independent biological replicates for each condition and a biological replicate consisted of tissue pooled from 3 plants.

RNA extraction and sequencing was performed as previously described in McCormick et al. (2018). Tissue was ground under liquid nitrogen and high quality RNA was extracted using standard Trizol-reagent based extraction (Li and Trick, 2005). The integrity and concentration of the RNA preparations were checked initially using Nano-Drop ND-1000 (Nano-Drop Technologies) and then by BioAnalyzer (Agilent Technologies). "Plate-based RNA sample prep was performed on the PerkinElmer Sciclone NGS robotic liquid handling system

FIGURE 4 | (A) Lines of evidence for Potri.013G102600 (homolog of *Arabidopsis* AGL12). **(B)** GWAS associations of Potri.013G102600 with three lignin-related metabolites (**Table 1**). **(C)** Co-expression of Potri.013G102600 with three lignin-related genes (**Table 2**). **(D)** Co-methylation of Potri.013G102600 with four lignin-related genes (**Table 3**). In line plots, the green lines represent potential target Potri.013G102600 and yellow lines represent lignin-related genes.

using Illumina's TruSeq Stranded mRNA HT sample prep kit utilizing poly-A selection of mRNA following the protocol outlined by Illumina in their user guide: http://support.illumina. com/sequencing/sequencing_kits/truseq_stranded_mrna_ht_ sample_prep_kit.html, v. The quantified libraries were then prepared for sequencing on the Illumina HiSeq sequencing platform utilizing a TruSeq paired-end cluster kit, v4, and Illumina's cBot instrument to generate a clustered flowcell for sequencing. Sequencing of the flowcell was performed on the Illumina HiSeq2500 sequencer using HiSeq TruSeq SBS sequencing kits, v4, following a 2 × 150 indexed run recipe" (McCormick et al., 2018).

2.7. Co-expression Network Construction

Gene expression atlas data for *P. trichocarpa* consisting of 63 different samples were used to construct a co-expression network. Reads were trimmed using Skewer (Jiang et al., 2014). Star (Dobin et al., 2013) was then used to align the reads to the *P. trichocarpa* reference genome (Tuskan et al., 2006) obtained from Phytozome (Goodstein et al., 2012). TPM (Transcripts Per Million) expression values (Wagner et al., 2012) were then calculated for each gene. This resulted in a gene expression matrix *E* in which rows represented genes, columns represented samples and each entry *ij* represented the expression (TPM) of gene *i* in sample *j*. The Spearman correlation coefficient was then calculated between the expression profiles of all pairs of genes (i.e. all pairs of rows of the matrix *E*) using the mcxarray and mcxdump programs from the MCL-edge package (van Dongen, 2000, 2008) available from http://micans.org/mcl/. This was performed in parallel using Perl wrappers making use of the

Parallel::MPI::Simple Perl module, (Alex Gough, http://search. cpan.org/~ajgough/Parallel-MPI-Simple-0.03/Simple.pm) using compute resources at the Oak Ridge Leadership Computing Facility (OLCF).

Figure S1A shows the distribution of Spearman correlation values for the co-expression network. An absolute threshold of 0.85 was applied.

2.8. Co-methylation Network Construction

Methylation data for *P. trichocarpa* (Vining et al., 2012) re-aligned to the version 3.0 assembly of *P. trichocarpa* was obtained from Phytozome (Goodstein et al., 2012). This data consisted of MeDIP-seq (Methyl-DNA immunoprecipitation-seq) reads from 10 different *P. trichocarpa* tissues, including bud, callus, female catkin, internode explant, leaf, male catkin, phloem, regenerated internode, root, and xylem tissue.

BamTools stats (Barnett et al., 2011) was used to determine basic properties of the reads in each .bam file. Samtools (Li et al., 2009) was then used to extract only mapped reads. The number of reads which mapped to each gene feature was determined using htseq-count (Anders et al., 2014). These read counts were then converted to TPM values (Wagner et al., 2012), providing a methylation score for each gene in each tissue. The TPM value for a gene *g* in a given sample was defined as:

$$TPM_g = \frac{\frac{c_g}{l_g} \times 10^6}{\sum_g \frac{c_g}{l_g}} \qquad (1)$$

where c_g is the number of reads mapped to gene *g* and l_g is the length of gene *g* in kb, calculated by subtracting

---

TABLE 2 | Co-expression associations for select new potential target genes. Annotations are derived from best *Arabidopsis* hit descriptions, GO terms and in some cases MapMan annotations.

Source gene	Target gene	Target *Arabidopsis* best hit	Annotation
Co-expression Associations for Potri.013G102600 (AGL12, AT1G71692)			
Potri.013G102600	Potri.001G304800	AT4G34050	Caffeoyl Coenzyme A O-Methyltransferase 1
Potri.013G102600	Potri.009G099800	AT4G34050	Caffeoyl Coenzyme A O-Methyltransferase 1
Potri.013G102600	Potri.012G006400	AT5G54160	Caffeate O-Methyltransferase 1
Potri.013G102600	Potri.007G016400	AT4G36220	Ferulic acid 5-hydroxylase 1
Co-expression Associations for Potri.009G053900 (MYB46, AT5G12870)			
Potri.009G053900	Potri.003G100200	AT1G32100	Pinoresinol reductase 1
Potri.009G053900	Potri.012G006400	AT5G54160	Caffeate O-Methyltransferase 1
Co-expression Associations for Potri.010G141000 (MYB111, AT5G49330)			
Potri.010G141000	Potri.007G030300	AT3G50740	UDP-glucosyl transferase 72E1
Co-expression Associations for Potri.006G170800 (MYB36, AT5G57620)			
Potri.006G170800	Potri.001G362800	AT3G26300	Cytochrome P450, family 71, subfamily B, polypeptide 34/F5H
Potri.006G170800	Potri.016G106100	AT3G09220	laccase 7
Potri.006G170800	Potri.013G120900	AT4G35160	N-acetylserotonin O-methyltransferase
Co-expression Associations for Potri.016G078600 (CPSRP54, AT5G03940)			
Potri.016G078600	Potri.003G096600	AT2G35500	Shikimate kinase like 2
Potri.016G078600	Potri.017G062800	AT3G26900	Shikimate kinase like 1

the gene start position from the gene end position, and dividing the resulting difference by 1,000. A methylation matrix M was then formed, in which rows represented genes, columns represented tissues and each entry ij represented the methylation score (TPM) of gene i in tissue j. A co-methylation network (see Davies et al., 2012; Akulenko and Helms, 2013; Busch et al., 2016) was then constructed by calculating the Spearman correlation coefficient between the methylation profiles of all pairs of genes using mcxarray and mcxdump programs from the MCL-edge package (van Dongen, 2000, 2008) http://micans.org/mcl/. Figure S1B shows the distribution of Spearman Correlation values. An absolute threshold of 0.95 was applied.

Read counting using htseq-count, as well as Spearman correlation calculations were performed in parallel using Perl wrappers making use of the Parallel::MPI::Simple Perl module, developed by Alex Gough and available on The Comprehensive Perl Archive Network (CPAN) at www.cpan.org and used compute resources at the Oak Ridge Leadership Computing Facility (OLCF).

2.9. SNP Correlation Network Construction

The Custom Correlation Coefficient (CCC) (Climer et al., 2014a,b) was used to calculate the correlation between the occurrence of pairs of SNPs across the 882 genotypes. The CCC between allele x at position i and allele y and position j is defined as:

$$CCC_{i_x j_y} = \frac{9}{2} R_{i_x j_y} \left(1 - \frac{1}{f_{i_x}} \right) \left(1 - \frac{1}{f_{j_y}} \right) \qquad (2)$$

where $R_{i_x j_y}$ is the relative co-occurrence of allele x at position i and allele y at position j, f_{i_x} is the frequency of allele x at position i and f_{j_y} is the frequency of allele y at position j.

This was performed in a parallel fashion using similar computational approaches as described for the co-expression network above. The set of ~10 million SNPs was divided into 20 different blocks, and the CCC was calculated for each within-block and cross-block SNPs in separate jobs, to a total of 210 MPI jobs (**Figure 2**). A threshold of 0.7 was then applied. The resulting SNP correlation network was pruned to only include SNPs that resided within genes and SNPs were mapped to the

TABLE 3 | Co-methylation associations for select new potential target genes. Annotations are derived from best *Arabidopsis* hit descriptions and GO terms and in some cases MapMan annotations.

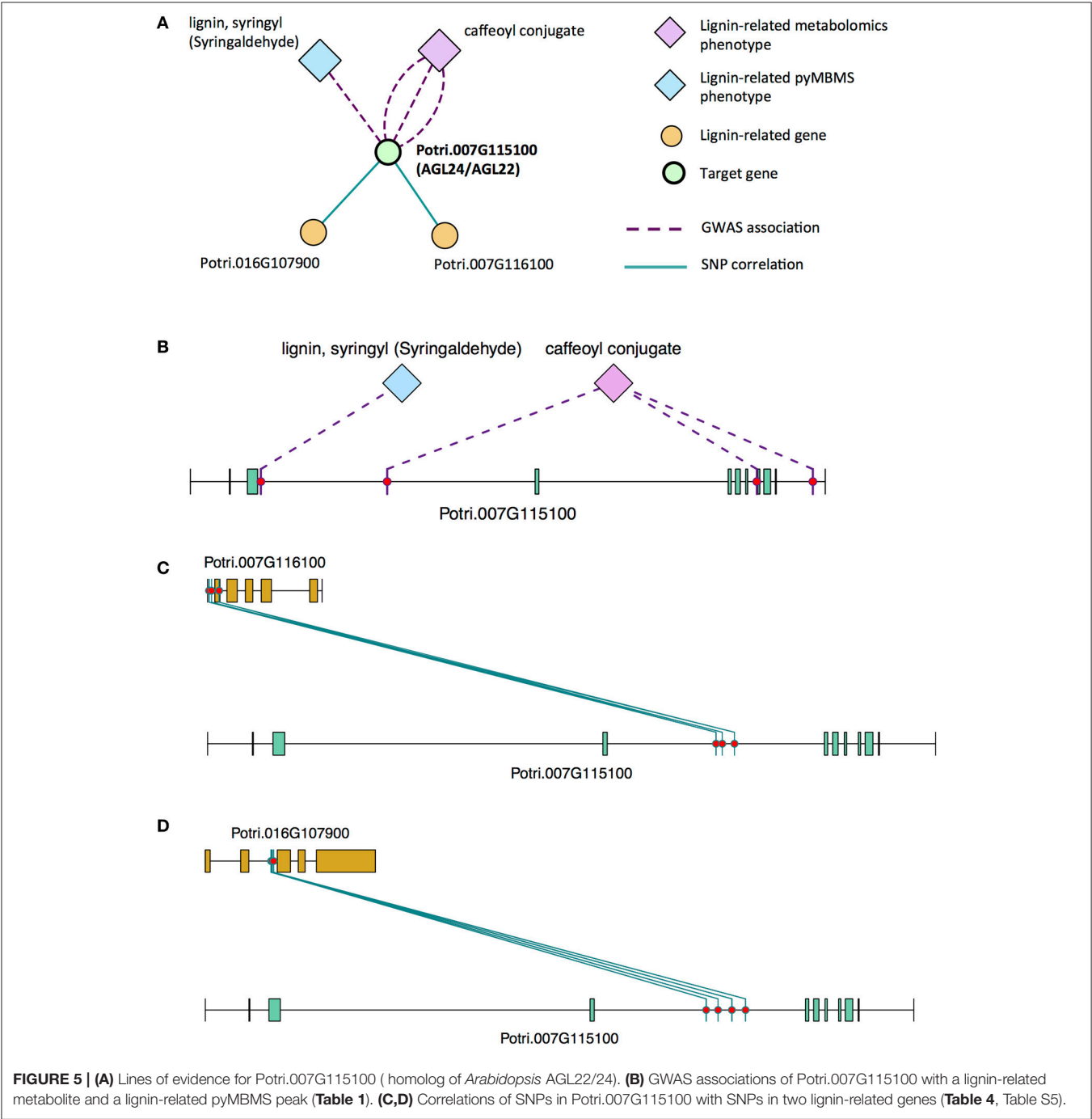| Source gene	Target gene	Target *Arabidopsis* best hit	Annotation
Co-methylation Associations for Potri.012G062300 (AGL8, AT5G60910)			
Potri.012G062300	Potri.001G036900	AT3G21240	4-coumarate:CoA ligase 2
Potri.012G062300	Potri.008G120200	AT1G68540	Cinnamoyl CoA reductase-like 6
Potri.012G062300	Potri.004G105000	AT5G14700	(NAD(P)-binding Rossmann-fold Superfamily protein, cinnamoyl-CoA reductase activity/CCR1
Co-methylation Associations for Potri.013G102600 (AGL12, AT1G71692)			
Potri.013G102600	Potri.001G334400	AT5G63380	4-coumarate-CoA ligase activity /4CL
Potri.013G102600	Potri.001G365300	AT3G26300	cytochrome P450, family 71, subfamily B, polypeptide 34/F5H
Potri.013G102600	Potri.006G265500	AT5G10820	Major facilitator superfamily protein/Phenylpropanoid pathway
Potri.013G102600	Potri.006G165200	AT2G19070	Spermidine hydroxycinnamoyl transferase
Co-methylation Associations for Potri.009G053900 (MYB46, AT5G12870)			
Potri.009G053900	Potri.008G196100	AT3G06350	Bi-functional dehydroquinate-shikimate dehydrogenase enzyme
Potri.009G053900	Potri.002G018300	AT4G39330	Cinnamyl alcohol dehydrogenase 9
Potri.009G053900	Potri.004G102000	AT4G05160	4-coumarate-CoA ligase activity/4CL)
Potri.009G053900	Potri.008G136600	AT1G67980	Caffeoyl-CoA 3-O-methyltransferase
Co-methylation Associations for Potri.010G141000 (MYB111, AT5G49330)			
Potri.010G141000	Potri.008G196100	AT3G06350	Bi-functional dehydroquinate-shikimate dehydrogenase enzyme
Potri.010G141000	Potri.004G102000	AT4G05160	4-coumarate-CoA ligase activity/4CL
Potri.010G141000	Potri.008G074500	AT5G34930	Arogenate dehydrogenase
Potri.010G141000	Potri.005G028000	AT5G48930	Hydroxycinnamoyl-CoA shikimate/quinate hydroxycinnamoyl transferase
Potri.010G141000	Potri.018G100500	AT2G23910	NAD(P)-binding Rossmann-fold superfamily protein, cinnamoyl-CoA reductase activity/CCR1
Potri.010G141000	Potri.010G230200	AT1G20510	OPC-8:0 CoA ligase1, 4-coumarate-CoA ligase activity/4CL
Co-methylation Associations for Potri.006G170800 (MYB36, AT5G57620)			
Potri.006G170800	Potri.016G093700	AT4G05160	AMP-dependent synthetase and ligase family, 4-coumarate-CoA ligase activity/4CL
Co-methylation Associations for Potri.016G078600 (CPSRP54, AT5G03940)			
Potri.016G078600	Potri.014G135500	AT3G06350	Bi-functional dehydroquinate-shikimate dehydrogenase enzyme

genes in which they reside. Gene boundaries used were defined in the `Ptrichocarpa_210_v3.0.gene.gff3` file from the *P. trichocarpa* version 3.0 genome assembly on Phytozome (Goodstein et al., 2012). A local LD filter was then set, retaining correlations between SNPs greater than 10kb apart. The distribution of CCC values can be seen in Figure S1C (Supplementary Note 1).

2.10. Target Lignin Genes/Phenotypes

A scoring system was developed in order to quantify the Lines Of Evidence (LOE) linking each gene to lignin-related genes/phenotypes. The LOE scores quantify the number of lines linking each gene to lignin-related genes and phenotypes across the different network data layers. Thus, the method requires as input a list of known lignin-related genes/phenotypes.

P. trichocarpa gene annotations in the `Ptrichocarpa_210_v3.0.annotation_info.txt` file from the version 3.0 genome assembly were used, available on Phytozome (Goodstein et al., 2012). This included *Arabidopsis* best hits and corresponding gene descriptions, as well as GO terms (Ashburner et al.,

FIGURE 5 | (A) Lines of evidence for Potri.007G115100 (homolog of *Arabidopsis* AGL22/24). (B) GWAS associations of Potri.007G115100 with a lignin-related metabolite and a lignin-related pyMBMS peak (**Table 1**). (C,D) Correlations of SNPs in Potri.007G115100 with SNPs in two lignin-related genes (**Table 4**, Table S5).

2000; Gene Ontology Consortium, 2017) and Pfam domains (Finn et al., 2016). Genes were also assigned MapMan annotations using the Mercator tool (Lohse et al., 2014).

Lignin building blocks (monolignols) are derived from phenylalanine in the phenylpropanoid and monolignol pathways, and phenylalanine itself is produced from the shikimate pathway (Vanholme et al., 2010). To compile a list of *P. trichocarpa* genes which are related to the biosynthesis of lignin, *P. trichocarpa* genes were assigned MapMan annotations using the Mercator tool (Lohse et al., 2014). Genes in the Shikimate (MapMan bins 13.1.6.1, 13.1.6.3, and 13.1.6.4), Phenylpropanoid (MapMan bin 16.2) and Lignin/Lignan (MapMan bin 16.2.1) pathways were then selected. A list of these lignin-related genes and their MapMan annotations can be seen in Table S1.

Lignin-related pyMBMS peaks, as described in Sykes et al. (2009), Davis et al. (2006), and Muchero et al. (2015) were identified among the pyMBMS GWAS hits, and are shown in Table S2. Lignin-related metabolites and metabolites in the lignin pathway were also identified among the metabolomics GWAS hits, a list of which can be seen in Table S3. For partially identified metabolites, additional RT and mz information can be seen in Table S3.

2.11. Extraction of Lignin-Related Subnetworks

Let L_G, L_M, and L_P represent our sets of lignin-related genes, metabolites and pyMBMS peaks, respectively (Tables S1–S3). A network can be defined as $N = (V, E)$ where V is the set of nodes and E is the set of edges connecting nodes in V. In particular, let the co-expression network be represented by $N_{coex} = (V_{coex}, E_{coex})$, the co-methylation network by $N_{cometh} = (V_{cometh}, E_{cometh})$ and the SNP correlation network by $N_{snp} = (V_{snp}, E_{snp})$. The GWAS networks can be represented as bipartite networks $N = (U, V, E)$ where U is the set of phenotype nodes, V is the set of gene nodes, and E is the set of edges, with each edge e_{ij} connecting node $i \in U$ with node $j \in V$. Let the metabolomics GWAS network be represented by $N_{metab} = (U_{metab}, V_{metab}, E_{metab})$ and the pyMBMS GWAS network by $N_{pymbms} = (U_{pymbms}, V_{pymbms}, E_{pymbms})$. We construct the *guilt by association* subnetworks of genes connected to lignin-related genes/phenotypes as follows:

N_{coex}^L is the subnetwork of N_{coex} including the lignin related genes $l \in L_G$ and their direct neighbors:

$$N_{coex}^L = (V_{coex}^L, E_{coex}^L) \text{ where} \tag{3}$$
$$V_{coex}^L = \{g | g \in (L_G \cap V_{coex})\} \cup \{g | (g \in V_{coex}) \wedge (\exists l \in L_G | \{l, g\} \in E_{coex})\} \tag{4}$$
$$E_{coex}^L = \{e = \{i, j\} \in E_{coex} | i \in V_{coex}^L \wedge j \in V_{coex}^L\} \tag{5}$$

N_{cometh}^L is the subnetwork of N_{cometh} including the lignin related genes $l \in L_G$ and their direct neighbors:

$$N_{cometh}^L = (V_{cometh}^L, E_{cometh}^L) \text{ where} \tag{6}$$
$$V_{cometh}^L = \{g | g \in (L_G \cap V_{cometh})\} \cup \{g | (g \in V_{cometh}) \wedge (\exists l \in L_G | \{l, g\} \in E_{cometh})\} \tag{7}$$
$$E_{cometh}^L = \{e = \{i, j\} \in E_{cometh} | i \in V_{cometh}^L \wedge j \in V_{cometh}^L\} \tag{8}$$

N_{snp}^L is the subnetwork of N_{snp} including the lignin related genes $l \in L_G$ and their direct neighbors:

$$N_{snp}^L = (V_{snp}^L, E_{snp}^L) \text{ where} \tag{9}$$
$$V_{snp}^L = \{g | g \in (L_G \cap V_{snp})\} \cup \{g | (g \in V_{snp}) \wedge (\exists l \in L_G | \{l, g\} \in E_{snp})\} \tag{10}$$
$$E_{snp}^L = \{e = \{i, j\} \in E_{snp} | i \in V_{snp}^L \wedge j \in V_{snp}^L\} \tag{11}$$

N_{metab}^L is the subnetwork of N_{metab} including the lignin related metabolites $m \in L_M$ and their direct neighboring genes:

$$N_{metab}^L = (U_{metab}^L, V_{metab}^L, E_{metab}^L) \text{ where} \tag{12}$$
$$U_{metab}^L = \{m | m \in (L_M \cap U_{metab})\} \tag{13}$$
$$V_{metab}^L = \{g | (g \in V_{metab}) \wedge (\exists m \in L_M | (m, g) \in E_{metab})\} \tag{14}$$
$$E_{metab}^L = \{e = (i, j) \in E_{metab} | i \in U_{metab}^L \wedge j \in V_{metab}^L\} \tag{15}$$

TABLE 4 | SNP correlation associations for select new potential target genes. Annotations are derived from best *Arabidopsis* hit descriptions, GO terms and in some cases MapMan annotations.

Source gene	Target gene	Target *Arabidopsis* best hit	Annotation
SNP Correlations for Potri.007G115100 (AGL22, AT2G22540/AGL24, AT4G24540)			
Potri.007G115100	Potri.007G116100	AT2G22570	Nicotinamidase 1
Potri.007G115100	Potri.016G107900	AT3G09220	Laccase 7
SNP Correlations for Potri.016G078600 (CPSRP54, AT5G03940)			
Potri.016G078600	Potri.016G078300	AT4G37970	Cinnamyl alcohol dehydrogenase 6

N_{pymbms}^L is the subnetwork of N_{pymbms} including the lignin related pyMBMS peaks $p \in L_P$ and their direct neighboring genes:

$$N_{pymbms}^L = (U_{pymbms}^L, V_{pymbms}^L, E_{pymbms}^L) \text{ where} \quad (16)$$

$$U_{pymbms}^L = \{p|p \in (L_P \cap U_{pymbms})\} \quad (17)$$

$$V_{pymbms}^L = \{g| (g \in V_{pymbms}) \wedge (\exists p \in L_P|(p,g) \in E_{pymbms})\} \quad (18)$$

$$E_{pymbms}^L = \{e = (i,j) \in E_{pymbms}|i \in U_{pymbms}^L \wedge j \in V_{pymbms}^L\} \quad (19)$$

2.12. Calculating LOE Scores

For a given gene g, the *degree* of that gene $D(g)$ indicates the number of connections that the gene has in a given network. Let $D_{coex}(g)$, $D_{cometh}(g)$, $D_{snp}(g)$, $D_{metab}(g)$, $D_{pymbms}(g)$ represent the degrees of gene g in the lignin subnetworks N_{coex}^L, N_{cometh}^L, N_{snp}^L, N_{metab}^L, and N_{pymbms}^L, respectively. The LOE *breadth* score $LOE_{breadth}(g)$ is then defined as

$$\begin{aligned} LOE_{breadth}(g) = & \text{ bin}\left(D_{coex}(g)\right) + \text{bin}\left(D_{cometh}(g)\right) + \\ & \text{bin}\left(D_{snp}(g)\right) + \text{bin}\left(D_{metab}(g)\right) + \\ & \text{bin}\left(D_{pymbms}(g)\right) \end{aligned} \quad (20)$$

where

$$\text{bin}(x) = \begin{cases} 1 \text{ if } x \geq 1 \\ 0 \text{ otherwise} \end{cases} \quad (21)$$

The $LOE_{breadth}(g)$ score indicates the number of different types of lines of evidence that exist linking gene g to lignin-related genes/phenotypes.

The LOE *depth* score $LOE_{depth}(g)$ represents the total number of lines of evidence exist linking gene g to lignin-related genes/phenotypes, and is defined as

$$LOE_{depth}(g) = D_{coex}(g) + D_{cometh}(g) + D_{snp}(g) + D_{metab}(g) + D_{pymbms}(g) \quad (22)$$

The GWAS LOE score $LOE_{gwas}(g)$ indicates the number of lignin-related phenotypes (metabolomic or pyMBMS) that a gene is connected to, and is defined as:

$$LOE_{gwas}(g) = D_{metab}(g) + D_{pymbms}(g) \quad (23)$$

Distributions of the LOE scores can be seen in Figure S2. Cytoscape version 3.4.0 (Shannon et al., 2003) was used for network visualization. Expression, methylation, SNP correlation, and GWAS diagrams were created using R (R Core Team, 2017) and various R libraries (Wickham, 2007, 2009; de Vries and Ripley, 2016; Arnold, 2017; Auguie, 2017). Data parsing, wrappers and LOE score calculation was performed using Perl. Diagrams were edited to overlay certain text using Microsoft PowerPoint.

3. RESULTS AND DISCUSSION

3.1. Layered Networks, LOE Scores, and New Potential Targets

This study involved the construction of a set of networks providing different layers of information about the relationships between genes, and between genes and phenotypes, and the development of a Lines Of Evidence scoring system (LOE scores) which integrate the information in the different network layers and quantify the number of lines of evidence connecting genes to lignin-related genes/phenotypes. The GWAS network layers provide information as to which genes are potentially involved in certain functions because they contain genomic variants significantly associated with measured phenotypes. The co-methylation and co-expression networks provide information on different layers of regulatory mechanisms within the cell. The SNP correlation network provides information about possible co-evolution relationships between genes, through correlated variants across a population.

Marking known genes and phenotypes involved in lignin biosynthesis in these networks allowed for the calculation of a set of LOE (Lines Of Evidence) scores for each gene, indicating the strength of the evidence linking each gene to lignin-related functions. The breadth LOE score indicates the number of types of lines of evidence (number of layers) which connect the gene to lignin-related genes/phenotypes, whereas the depth LOE score indicates the total number of lignin-related genes/phenotypes the gene is associated with. Individual layer LOE scores (e.g., co-expression LOE score or GWAS LOE score) indicate the number of lignin-related associations the gene has within that layer.

This data layering approach differs from previous data integration methods. Mizrachi et al. (2017) integrate gene expression data with eQTN data and gene relationships from KEGG though matrix multiplication, before correlating genes' Network Based Data Integration (NBDI)-transformed values with measured traits, allowing the ranking of genes. The Mergeomics method (Shu et al., 2016) performs Marker Set Enrichment Analysis, ranking predefined sets of molecular markers based on their enrichment in a disease phenotype. Knetminer (Hassani-Pak et al., 2016; Hassani-Pak, 2017) is a web server which allows the user to search for keywords, producing lists of genes and the associations they have to annotations, genes, phenotypes, publications etc. which match the keywords and that are available in public databases. Knetminer can also produce a network view of the results. While Knetminer is also an approach which utilizes multiple lines of evidence, the main approach and the scoring systems differ. LOE requires input lists of genes and phenotypes of interest to the user, Knetminer uses gene lists and keyword searching. In terms of lines of evidence, Knetminer counts the number of "concepts" (nodes, including publications, phenotypes, annotations etc.) a gene has linking it to a keyword (Hassani-Pak et al., 2016; Hassani-Pak, 2017). However, LOE scores (particularly, breadth LOE scores) count the number of types of relationships (e.g., GWAS association, co-expression, co-methylation, variant correlation *edges*) connecting a gene to specific input genes and phenotypes related to the user's function of interest. This is thus a valuable approach to

identify new target genes based on the *relationships* of a gene to target genes/phenotypes of interest in custom-made association network layers where publically available data is not available.

To select the top set of potential new candidate genes involved in lignin biosynthesis, genes which showed a number of different lines of evidence connecting them to lignin-related functions were identified by selecting genes with a LOE breadth score ≥3. Since the GWAS networks provide the highest resolution, most direct connections to lignin-related functions, it was also required that our potential new targets had a GWAS score ≥1. This provides a set of 375 new candidate genes potentially involved in lignin biosynthesis, identified through multiple lines of evidence (Table S4). This set of Potential New Target genes will be referred to as set of PNTs. A selection of these potential new candidates below and their annotations, derived from their *Arabidopsis* best hits, will be discussed below.

3.2. Agamous-Like Genes

Genes in the AGAMOUS-LIKE gene family are MADS-box transcription factors, many of which which have been found to play important roles in floral development (Lee et al., 2000;

Yu et al., 2002, 2004, 2017; Yoo et al., 2006; Fernandez et al., 2014). Three potential AGAMOUS-LIKE (AGL) genes are found in the set of PNTs, in particular, a homolog of *Arabidopsis* AGL8 (AT5G60910, also known as FRUITFUL), a homolog of *Arabidopsis* AGL12 (AT1G71692), and a homolog of *Arabidopsis* AGL24 (AT4G24540) and AGL22 (AT2G22540).

The first potential AGL gene in our set of PNTs is Potri.012G062300, with a breadth score of 3 and a GWAS score of 2 (**Figure 3A**), whose best *Arabidopsis thaliana* hit is AGL8 (AT5G60910). It has GWAS associations with a lignin-related metabolite (quinic acid) and a lignin pyMBMS peak (syringol) (**Figure 3C**, **Table 1**) and is co-methylated with three lignin-related genes (**Figure 3B**, **Table 3**). There is thus strong evidence for the involvement of *P. trichocarpa* AGL8 in the regulation of lignin-related functions. There is literature evidence that supports the hypothesis of AGL8's involvement in the regulation of lignin biosynthesis. A patent exists for the use of AGL8 expression in reducing the lignin content of plants (Yanofsky et al., 2004). The role of AGL8 (FUL) was described in Ferrándiz et al. (2000), in which they investigated the differences in lignin deposition in transgenic plants in which AGL8 is
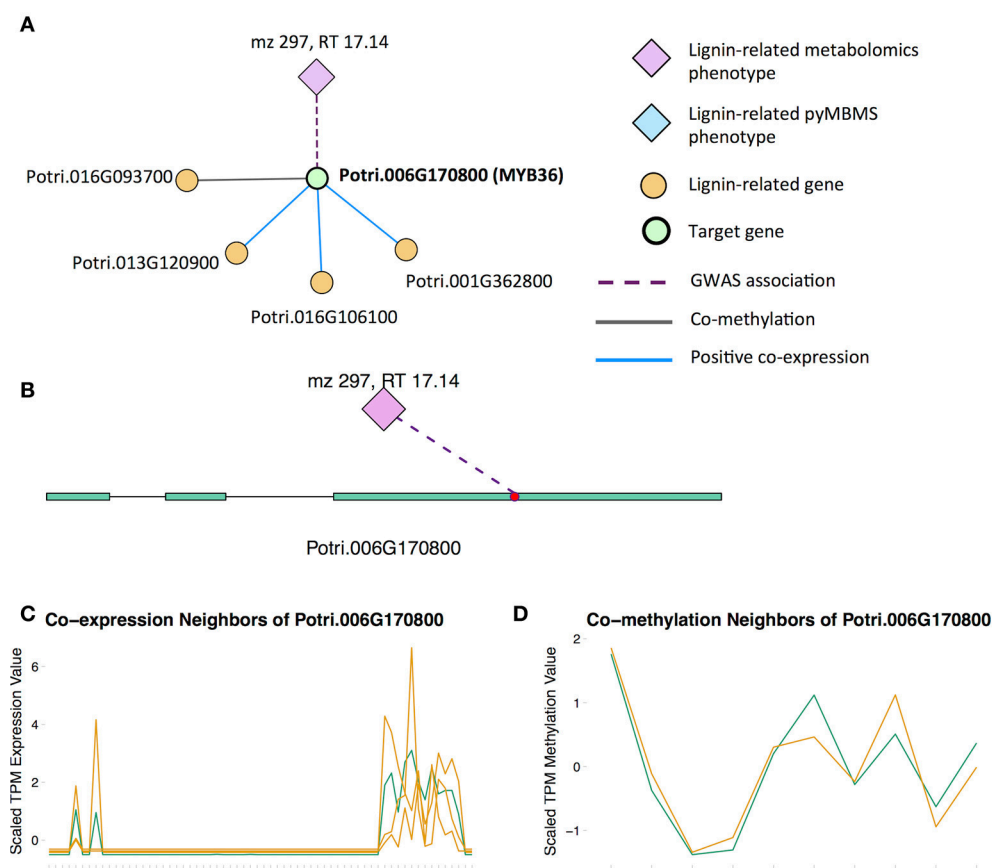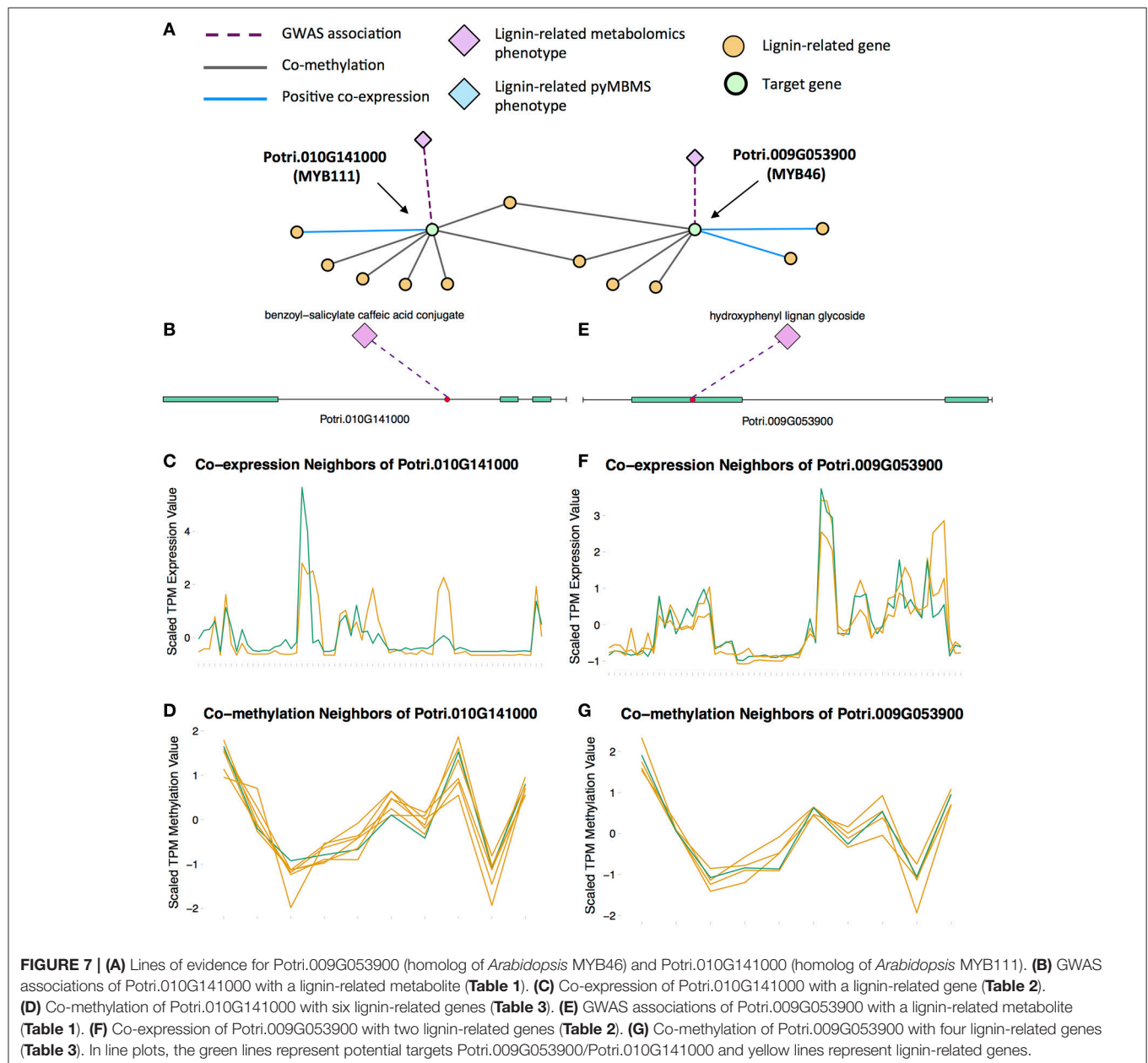

FIGURE 6 | (A) Lines of evidence for Potri.006G170800 (homolog of *Arabidopsis* MYB36). **(B)** GWAS associations of Potri.006G170800 with a lignin-related metabolite (**Table 1**). **(C)** Co-expression of Potri.006G170800 with three lignin-related genes (**Table 2**). **(D)** Co-methylation of Potri.006G170800 with a lignin-related gene (**Table 3**). In line plots, the green lines represent potential target Potri.006G170800 and yellow lines represent lignin-related genes.

constitutively expressed, loss-of-function AGL8 mutants and wild-type *Arabidopsis* plants (Ferrándiz et al., 2000). In wild-type plants, a single layer of valve cells were lignified. In loss-of-function AGL8 mutants, all valve mesophyl cell layers were lignified, while in the transgenic plants, constitutive expression of AGL8 resulted in loss of lignified cells (Ferrándiz et al., 2000). This study thus showed the involvement of AGL8 in fruit lignification during fruit development.

There is evidence of other AGAMOUS-LIKE genes affecting lignin content. A study by Giménez et al. (2010) investigated TALG1, an AGAMOUS-LIKE gene in tomato, and found that TAGL1 RNAi-silenced fruits showed increased lignin content, and increased expression levels of lignin biosynthesis genes (Giménez et al., 2010). A recent study by Cosio et al. (2017)

showed that AGL15 in *Arabidopsis* is also involved in regulating lignin-related functions, in that AGL15 binds to the promotor of peroxidase PRX17, and regulates its expression (Cosio et al., 2017). In addition, PRX17 loss of function mutants had reduced lignin content (Cosio et al., 2017).

There is thus compelling evidence that various AGAMOUS-LIKE genes are involved in regulating lignin biosynthesis/deposition in plants. Two other AGAMOUS-like genes are seen in the set of PNTs, namely a homolog of *Arabidopsis* AGL12 (Potri.013G102600) and a homolog of *Arabidopsis* AGL22/AGL24 (Potri.007G115100). Potri.013G102600 (AGL12) has GWAS associations with three lignin-related metabolites, namely hydroxyphenyl lignan glycoside, coumaroyl-tremuloidin, and 3-O-caffeoyl-quinate

FIGURE 7 | (A) Lines of evidence for Potri.009G053900 (homolog of *Arabidopsis* MYB46) and Potri.010G141000 (homolog of *Arabidopsis* MYB111). **(B)** GWAS associations of Potri.010G141000 with a lignin-related metabolite (**Table 1**). **(C)** Co-expression of Potri.010G141000 with a lignin-related gene (**Table 2**). **(D)** Co-methylation of Potri.010G141000 with six lignin-related genes (**Table 3**). **(E)** GWAS associations of Potri.009G053900 with a lignin-related metabolite (**Table 1**). **(F)** Co-expression of Potri.009G053900 with two lignin-related genes (**Table 2**). **(G)** Co-methylation of Potri.009G053900 with four lignin-related genes (**Table 3**). In line plots, the green lines represent potential targets Potri.009G053900/Potri.010G141000 and yellow lines represent lignin-related genes.

(**Figures 4A,B**, **Table 1**). It is co-expressed with four lignin-related genes including two caffeoyl coenzyme A O-methyltransferases, a caffeate O-methyltransferase and a ferulic acid 5-hydroxylase (**Figures 4A,C**, **Table 2**) and it is co-methylated with four other lignin-related genes (**Figures 4A,D**, **Table 3**). Potri.007G115100 (AGL22/AGL24) has GWAS associations with the syringaldehyde pyMBMS phenotype and a caffeoyl conjugate metabolite (**Figures 5A,B**, **Table 1**). It also has SNP correlations with a laccase and a

nicotinamidase (**Figures 5A,C,D**, **Table 4**, Table S5). The combination of the multiple lines of multi-omic evidence thus suggest the involvement of *P. trichocarpa* homologs of *A. thaliana* AGL22/AGL24 and AGL12 in regulating lignin biosynthesis.

3.3. MYB Transcription Factors

MYB proteins contain the conserved MYB DNA-binding domain, and usually function as transcription factors.
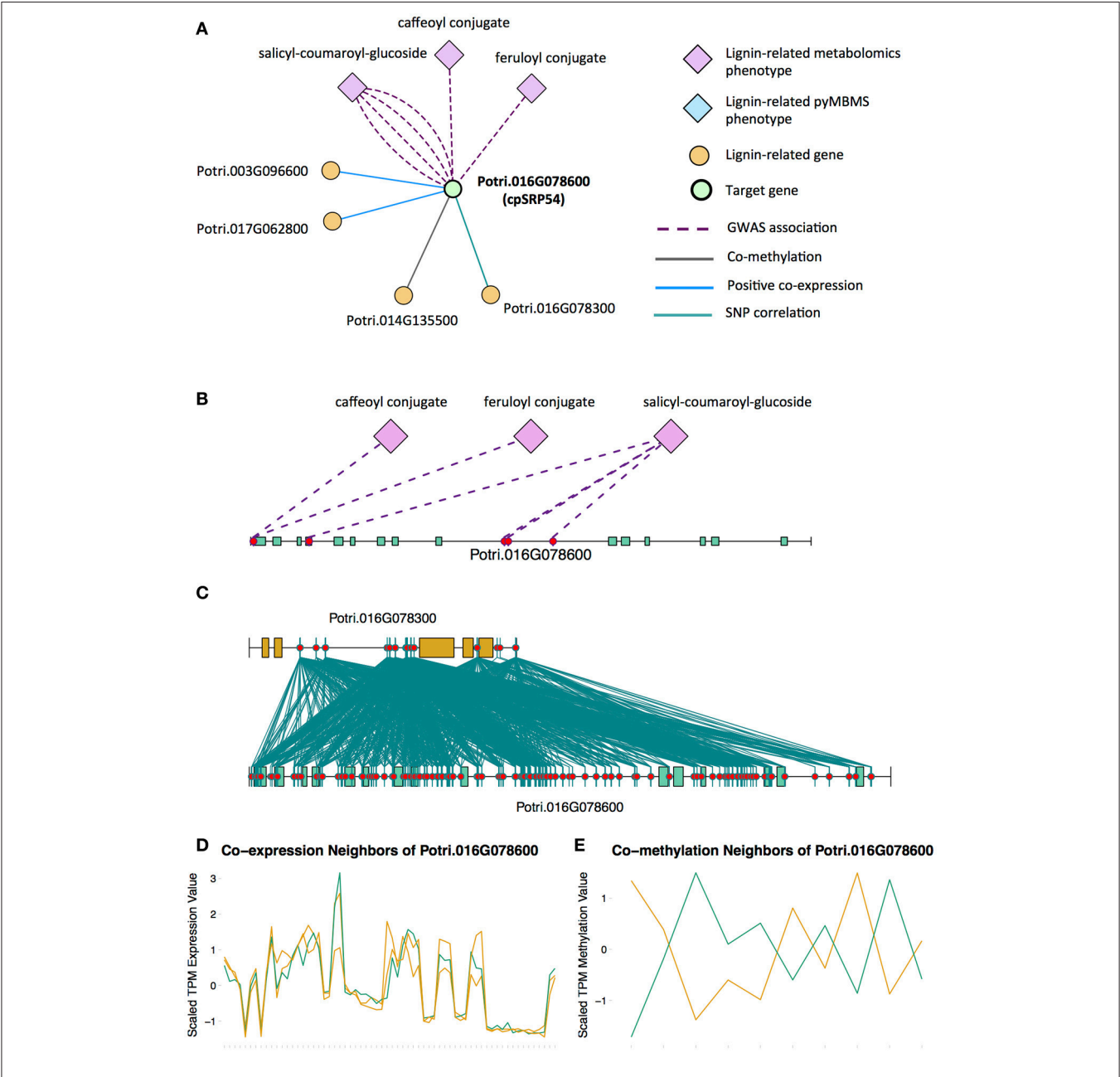
FIGURE 8 | (A) Lines of evidence for Potri.016G078600 (homolog of *Arabidopsis* cpSRP54). **(B)** GWAS associations of Potri.016G078600 with three lignin-related metabolite (**Table 1**). **(C)** Correlations of SNPs within Potri.016G078600 with SNPs in a lignin-related gene (**Table 4**). **(D)** Co-expression of Potri.016G078600 with two lignin-related genes (**Table 2**). **(E)** Co-methylation of Potri.016G078600 with a lignin-related gene (**Table 4**). In line plots, the green lines represent potential target Potri.016G078600 and yellow lines represent lignin-related genes.

R2R3-MYBs have been found to regulate various functions, including flavonol biosynthesis, anthocyanin biosynthesis, lignin biosynthesis, cell fate, and developmental functions (Dubos et al., 2010). The set of PNTs contains several genes which are homologs of *Arabidopsis* MYB transcription factors, including homologs of *Arabidopsis* MYB66/MYB3, MYB46, MYB36, and MYB111.

There is already existing literature evidence for how some of these MYBs affect lignin biosynthesis. Liu et al. (2015) reviews the involvement of MYB transcription factors in the regulation of phenylpropanoid metabolism. MYB3 in *Arabidopsis* is known to repress phenylpropanoid biosynthesis (Zhou M. et al., 2017), and a *P. trichocarpa* homolog of MYB3 is found in our set of potential new targets. Another potential new target is the *P. trichocarpa* homolog of *Arabidopsis* MYB36 (Potri.006G170800) which is connected to lignin-related functions through multiple lines of evidence (**Figure 6**). In *Arabidopsis*, MYB36 has been found to regulate the local deposition of lignin during casparian strip formation, and *myb36* mutants exhibit incorrectly localized lignin deposition (Kamiya et al., 2015).

MYB46 is known to be a regulator of secondary cell wall formation (Zhong et al., 2007). Overexpression of MYB46 in *Arabidopsis* activates lignin, cellulose and xylan biosynthesis pathways (Zhong et al., 2007). The MYB46 homolog in *P. trichocarpa*, Potri.009G053900, is connected to lignin-related functions through multiple lines of evidence (**Figure 7A**), including a GWAS association with a hydroxyphenyl lignan glycoside (**Figure 7E**, **Table 1**), co-expression with pinoresinol reductase 1 and caffeate O-methyltransferase 1 (**Figure 7F**, **Table 2**) and co-methylation with dehydroquinate-shikimate dehydrogenase enzyme, cinnamyl alcohol dehydrogenase 9, 4-coumarate-CoA ligase activity/4CL), and caffeoyl-CoA 3-O-methyltransferase (**Figure 7G**, **Table 3**).

A MYB transcription factor in the set of PNTs which has, to our knowledge, not yet been directly associated with lignin biosynthesis is MYB111 (**Figures 7A–D**). However, with existing literature evidence, one can hypothesize that MYB111 can alter lignin content by redirecting carbon flux from flavonoids to monolignols. There is evidence that MYB111 is involved in crosstalk between lignin and flavonoid pathways. Monolignols and flavonoids are both derived from phenylalanine through the phenylpropanoid pathway (Liu et al., 2015). There is crosstalk between the signaling pathways of ultraviolet-B (UV-B) stress and biotic stress pathways (Schenke et al., 2011). In the study by Schenke et al. (2011), it was shown that under UV-B light stress, *Arabidopsis* plants produce flavonols as a UV protectant. Also, simultaniously applying the bacterial elicitor flg22, which simulates biotic stress, repressed flavonol biosynthesis genes and induced production of defense compounds including camalexin and scopoletin, as well as lignin, which provides a physical barrier preventing pathogens' entry (Schenke et al., 2011). This crosstalk involved regulation by MYB12 and MYB4 (Schenke et al., 2011). This study by Schenke et al. (2011) was performed using cell cultures. A second study (Zhou Z. et al., 2017) used *Arabidopsis* seedlings, and found that MYB111 may be involved in the crosstalk in planta (Zhou Z. et al., 2017). The multiple lines of evidence connecting the *P. trichocarpa* homolog of *Arabidopsis*

MYB111 (Potri.010G141000) to lignin related functions, in combination with the above literature evidence suggests the involvement this gene in the regulation of lignin biosynthesis by redirecting carbon flux from flavonol biosynthesis to monolignol biosynthesis, as part of the crosstalk between UV-B protection and biotic stress signaling pathways.

3.4. Chloroplast Signal Recognition Particle

Potri.016G078600, a homolog of the *Arabidopsis* chloropast signal recognition particle cpSRP54 occurs in the set of PNTs (**Figure 8**). It has a GWAS LOE score of 3, through GWAS associations with salicyl-coumaroyl-glucoside, a caffeoyl conjugate and a feruloyl conjugate (**Figure 8B**, **Table 1**, Table S4). It also has a breadth score of 4, indicating that it is linked to lignin-related genes/phenotypes though 4 different types of associations (**Figure 8**). CpSRP54 gene has been found to regulate carotenoid accumulation in *Arabidopsis* (Yu et al., 2012). CpSRP54 and cpSRP43 form a "transit complex" along with a light-harvesting chlorophyll a/b-binding protein (LHCP) family member to transport it to the thylakoid membrane (Groves et al., 2001; Schünemann, 2004). A study in *Arabidopsis* found that cpSRP43 mutants had reduced lignin content (Klenell et al., 2005). Since CpSRP54 regulates carotenoid accumulation, and cpSRP43 appears to affect lignin content, it is possible that chloroplast signal recognition particles affect lignin and carotenoid content through flux through the phenylpropanoid pathway, the common origin of both of these compounds. In fact, a gene mutation *cue1* which causes LHCP underexpression also results in reduced aromatic amino acid biosynthesis (Streatfield et al., 1999). These multiple lines of evidence, combined with the above cited literature suggests that chloroplast signal recognition particles in *P. trichocarpa* could potentially influence lignin content.

3.5. Practical Implications

The LOE method of data integration provides a useful way for biologists to identify new target genes. Any genes and phenotypes of interest that are present in the networks can be used as input to the method, and thus, the results can be tailored to the particular function of interest of the biologist. The collection of LOE scores will allow the user to rank genes in the genome based on the particular lines of evidence most appropriate to function under investigation, and in so doing, provides a shortlist of genes as targets for genetic modification (knockout/knockdown/overexpression) in order to alter the phenotype of interest. For example, AGL genes, MYB transcription factors and CpSRP genes discussed above could be seen as potential new targets for knockout/knockdown/overexpression in order to alter the lignin content of *P. trichocarpa*.

The LOE scoring method can be applied to any species for which there is multiple data types that can be represented as association networks which the scientist wishes to integrate in order to identify new candidate genes involved in a particular function. This method will be particularly useful for the analysis of new, unpublished datasets where publically available datasets/web servers would not necessarily be able to be used.

4. CONCLUDING REMARKS

This study made use of high-resolution GWAS data, combined with co-expression, co-methylation and SNP correlation networks in a multi-omic, data layering approach which has allowed the identification of new potential target genes involved in lignin biosynthesis/regulation. Various literature evidence supports the involvement of many of these new target genes in lignin biosynthesis/regulation, and these are suggested for future validation for involvement in the regulation of lignin biosynthesis. The data layering technique and LOE scoring system developed can be applied to other omic data types to assist in the generation of new hypotheses surrounding various functions of interest.

AUTHOR CONTRIBUTIONS

DW calculated methylation TPM values, constructed the networks, developed the scoring technique, performed the data layering and scoring analysis, and interpreted the results; PJ performed the outlier analysis and GWAS; MS mapped gene expression atlas reads and calculated gene expression TPM values; SD, GT, and WM lead the effort on constructing the GWAS population; TT led the leaf sample collection for GCMS-based metabolomic analyses, identified the peaks, and summarized the metabolomics data; PR did automated extraction of metabolite intensity from GCMS; MM collected the leaf samples and manually extracted the metabolite data; NZ conducted leaf sample preparation, extracted and derivatized, and analyzed the metabolites by GCMS; JS and AS generated the gene expression atlas data; SD and DM-S generated the SNP calls; RS generated the pyMBMS data; DJ conceived of and supervised the project, generated MapMan annotations, and edited the manuscript; DW, PJ, SD, DM-S, RS, TT, JS, and AS wrote the manuscript.

SUPPLEMENTARY MATERIAL

The Supplementary Material for this article can be found online at: https://www.frontiersin.org/articles/10.3389/fenrg.2018.00030/full#supplementary-material

REFERENCES

Akulenko, R., and Helms, V. (2013). DNA co-methylation analysis suggests novel functional associations between gene pairs in breast cancer samples. *Hum. Mol. Genet.* 22, 3016–3022. doi: 10.1093/hmg/ddt158

Anders, S., Pyl, P. T., and Huber, W. (2014). HTSeq–a Python framework to work with high-throughput sequencing data. *Bioinformatics* 31, 166–169. doi: 10.1093/bioinformatics/btu638

Arnold, J. B. (2017). *ggthemes: Extra Themes, Scales and Geoms for 'ggplot2'*. R package version 3.4.0.

Ashburner, M., Ball, C. A., Blake, J. A., Botstein, D., Butler, H., Cherry, J. M., et al. (2000). Gene Ontology: tool for the unification of biology. *Nat. Genet.* 25, 25–29. doi: 10.1038/75556

Auguie, B. (2017). *gridExtra: Miscellaneous Functions for "Grid" Graphics.* R package version 2.3.

Barnett, D. W., Garrison, E. K., Quinlan, A. R., Strömberg, M. P., and Marth, G. T. (2011). BamTools: a C++ API and toolkit for analyzing and managing BAM files. *Bioinformatics* 27, 1691–1692. doi: 10.1093/bioinformatics/btr174

Benjamini, Y., and Hochberg, Y. (1995). Controlling the false discovery rate: a practical and powerful approach to multiple testing. *J. R. Stat. Soc. Ser. B Methodol.* 57, 289–300.

Biswal, A. K., Hao, Z., Pattathil, S., Yang, X., Winkeler, K., Collins, C., et al. (2015). Downregulation of gaut12 in populus deltoides by rna silencing results in reduced recalcitrance, increased growth and reduced xylan and pectin in a woody biofuel feedstock. *Biotechnol. Biofuels* 8:41. doi: 10.1186/s13068-015-0218-y

Bunyavanich, S., Schadt, E. E., Himes, B. E., Lasky-Su, J., Qiu, W., Lazarus, R., et al. (2014). Integrated genome-wide association, coexpression network, and expression single nucleotide polymorphism analysis identifies novel pathway in allergic rhinitis. *BMC Med. Genomics* 7:48. doi: 10.1186/1755-8794-7-48

Busch, R., Qiu, W., Lasky-Su, J., Morrow, J., Criner, G., and DeMeo, D. (2016). Differential DNA methylation marks and gene comethylation of COPD in African-Americans with COPD exacerbations. *Respir. Res.* 17:143. doi: 10.1186/s12931-016-0459-8

Calabrese, G. M., Mesner, L. D., Stains, J. P., Tommasini, S. M., Horowitz, M. C., Rosen, C. J., et al. (2017). Integrating GWAS and co-expression network data identifies bone mineral density genes SPTBN1 and MARK3 and an osteoblast functional module. *Cell Syst.* 4, 46–59.e4. doi: 10.1016/j.cels.2016.10.014

Climer, S., Templeton, A. R., and Zhang, W. (2014a). Allele-specific network reveals combinatorial interaction that transcends small effects in psoriasis GWAS. *PLoS Comput. Biol.* 10:e1003766. doi: 10.1371/journal.pcbi.1003766

Climer, S., Yang, W., Fuentes, L., Dávila-Román, V. G., and Gu, C. C. (2014b). A custom correlation coefficient (CCC) approach for fast identification of multi-SNP association patterns in genome-wide SNPs data. *Genet. Epidemiol.* 38, 610–621. doi: 10.1002/gepi.21833

Cosio, C., Ranocha, P., Francoz, E., Burlat, V., Zheng, Y., Perry, S. E., et al. (2017). The class III peroxidase PRX17 is a direct target of the MADS-box transcription factor AGAMOUS-LIKE15 (AGL15) and participates in lignified tissue formation. *New Phytol.* 213, 250–263. doi: 10.1111/nph.14127

Danecek, P., Auton, A., Abecasis, G., Albers, C. A., Banks, E., DePristo, M. A., et al. (2011). The variant call format and VCFtools. *Bioinformatics* 27, 2156–2158. doi: 10.1093/bioinformatics/btr330

Davies, M. N., Volta, M., Pidsley, R., Lunnon, K., Dixit, A., Lovestone, S., et al. (2012). Functional annotation of the human brain methylome identifies tissue-specific epigenetic variation across brain and blood. *Genome Biol.* 13:R43. doi: 10.1186/gb-2012-13-6-r43

Davis, M. F., Tuskan, G. A., Payne, P., Tschaplinski, T. J., and Meilan, R. (2006). Assessment of *Populus* wood chemistry following the introduction of a Bt toxin gene. *Tree Physiol.* 26, 557–564. doi: 10.1093/treephys/26.5.557

de Vries, A., and Ripley, B. D. (2016). *ggdendro: Create Dendrograms and Tree Diagrams Using 'ggplot2'.* R package version 0.1-20.

Dobin, A., Davis, C. A., Schlesinger, F., Drenkow, J., Zaleski, C., Jha, S., et al. (2013). STAR: ultrafast universal RNA-seq aligner. *Bioinformatics* 29, 15–21. doi: 10.1093/bioinformatics/bts635

Dubos, C., Stracke, R., Grotewold, E., Weisshaar, B., Martin, C., and Lepiniec, L. (2010). MYB transcription factors in *Arabidopsis. Trends Plant Sci.* 15, 573–581. doi: 10.1016/j.tplants.2010.06.005

Evans, L. M., Slavov, G. T., Rodgers-Melnick, E., Martin, J., Ranjan, P., Muchero, W., et al. (2014). Population genomics of *Populus trichocarpa* identifies signatures of selection and adaptive trait associations. *Nat. Genet.* 46, 1089–1096. doi: 10.1038/ng.3075

Evans, R. J., and Milne, T. A. (1987). Molecular characterization of the pyrolysis of biomass. *Energy Fuels* 1, 123–137.

Fernandez, D. E., Wang, C.-T., Zheng, Y., Adamczyk, B. J., Singhal, R., Hall, P. K., et al. (2014). The MADS-domain factors AGAMOUS-LIKE15 and AGAMOUS-LIKE18, along with SHORT VEGETATIVE PHASE and AGAMOUS-LIKE24, are necessary to block floral gene expression during the vegetative phase. *Plant Physiol.* 165, 1591–1603. doi: 10.1104/pp.114.242990

Ferrándiz, C., Liljegren, S. J., and Yanofsky, M. F. (2000). Negative regulation of the *SHATTERPROOF* genes by FRUITFULL during *Arabidopsis* fruit development. *Science* 289, 436–438. doi: 10.1126/science.289.5478.436

Finn, R. D., Coggill, P., Eberhardt, R. Y., Eddy, S. R., Mistry, J., Mitchell, A. L., et al. (2016). The Pfam protein families database: towards a more sustainable future. *Nucleic Acids Res.* 44, D279–D285. doi: 10.1093/nar/gkv1344

Fridley, B. L., Lund, S., Jenkins, G. D., and Wang, L. (2012). A Bayesian integrative genomic model for pathway analysis of complex traits. *Genet. Epidemiol.* 36, 352–359. doi: 10.1002/gepi.21628

Gene Ontology Consortium (2017). Expansion of the Gene Ontology knowledgebase and resources. *Nucleic Acids Res.* 45, D331–D338. doi: 10.1093/nar/gkw1108

Geraldes, A., Difazio, S. P., Slavov, G. T., Ranjan, P., Muchero, W., Hannemann, J., et al. (2013). A 34K SNP genotyping array for *Populus trichocarpa*: Design, application to the study of natural populations and transferability to other *Populus* species. *Mol. Ecol. Res.* 13, 306–323. doi: 10.1111/1755-0998.12056

Giménez, E., Pineda, B., Capel, J., Antón, M. T., Atarés, A., Pérez-Martín, F., et al. (2010). Functional analysis of the *Arlequin* mutant corroborates the essential role of the *Arlequin/TAGL1* gene during reproductive development of tomato. *PLoS ONE* 5:e14427. doi: 10.1371/journal.pone.0014427

Goodstein, D. M., Shu, S., Howson, R., Neupane, R., Hayes, R. D., Fazo, J., et al. (2012). Phytozome: a comparative platform for green plant genomics. *Nucleic Acids Res.* 40, D1178–D1186. doi: 10.1093/nar/gkr944

Groves, M. R., Mant, A., Kuhn, A., Koch, J., Dübel, S., Robinson, C., and Sinning, I. (2001). Functional characterization of recombinant chloroplast signal recognition particle. *J. Biol. Chem.* 276, 27778–27786. doi: 10.1074/jbc.M103470200

Hassani-Pak, K. (2017). *KnetMiner - An Integrated Data Platform for Gene Mining and Biological Knowledge Discovery.* Ph.D. thesis, Universität Bielefeld.

Hassani-Pak, K., Castellote, M., Esch, M., Hindle, M., Lysenko, A., Taubert, J., et al. (2016). Developing integrated crop knowledge networks to advance candidate gene discovery. *Appl. Trans. Genomics* 11, 18–26. doi: 10.1016/j.atg.2016.10.003

Jiang, H., Lei, R., Ding, S.-W., and Zhu, S. (2014). Skewer: a fast and accurate adapter trimmer for next-generation sequencing paired-end reads. *BMC Bioinformatics* 15:182. doi: 10.1186/1471-2105-15-182

Kamiya, T., Borghi, M., Wang, P., Danku, J. M., Kalmbach, L., Hosmani, P. S., et al. (2015). The MYB36 transcription factor orchestrates Casparian strip formation. *Proc. Natl. Acad. Sci. U.S.A.* 112, 10533–10538. doi: 10.1073/pnas.1507691112

Kang, H. M., Sul, J. H., Zaitlen, N. A., Kong, S.-Y., Freimer, N. B., Sabatti, C., et al. (2010). Variance component model to account for sample structure in genome-wide association studies. *Nat. Genet.* 42, 348–354. doi: 10.1038/ng.548

Kim, D., Li, R., Dudek, S. M., and Ritchie, M. D. (2013). ATHENA: identifying interactions between different levels of genomic data associated with cancer clinical outcomes using grammatical evolution neural network. *Biodata Mining* 6:23. doi: 10.1186/1756-0381-6-23

Kim, D., Shin, H., Song, Y. S., and Kim, J. H. (2012). Synergistic effect of different levels of genomic data for cancer clinical outcome prediction. *J. Biomed. Informatics* 45, 1191–1198. doi: 10.1016/j.jbi.2012.07.008

Klenell, M., Morita, S., Tiemblo-Olmo, M., Mühlenbock, P., Karpinski, S., and Karpinska, B. (2005). Involvement of the chloroplast signal recognition particle cpSRP43 in acclimation to conditions promoting photooxidative stress in *Arabidopsis. Plant Cell Physiol.* 46, 118–129. doi: 10.1093/pcp/pci010

Lee, H., Suh, S.-S., Park, E., Cho, E., Ahn, J. H., Kim, S.-G., et al. (2000). The AGAMOUS-LIKE 20 MADS domain protein integrates floral inductive pathways in *Arabidopsis. Genes Dev.* 14, 2366–2376. doi: 10.1101/gad.813600

Leys, C., Ley, C., Klein, O., Bernard, P., and Licata, L. (2013). Detecting outliers: do not use standard deviation around the mean, use absolute deviation around the median. *J. Exp. Soc. Psychol.* 49, 764–766. doi: 10.1016/j.jesp.2013.03.013

Li, H., Handsaker, B., Wysoker, A., Fennell, T., Ruan, J., Homer, N., et al. (2009). The sequence alignment/map format and SAMtools. *Bioinformatics* 25, 2078–2079. doi: 10.1093/bioinformatics/btp352

Li, Y., Tschaplinski, T. J., Engle, N. L., Hamilton, C. Y., Rodriguez, M., Liao, J. C., et al. (2012). Combined inactivation of the *Clostridium cellulolyticum* lactate and malate dehydrogenase genes substantially increases ethanol yield from cellulose and switchgrass fermentations. *Biotechnol. Biofuels* 5:2. doi: 10.1186/1754-6834-5-2

Li, Z., and Trick, H. N. (2005). Rapid method for high-quality RNA isolation from seed endosperm containing high levels of starch. *Biotechniques* 38:872.

Liu, J., Osbourn, A., and Ma, P. (2015). MYB transcription factors as regulators of phenylpropanoid metabolism in plants. *Mol. Plant* 8, 689–708. doi: 10.1016/j.molp.2015.03.012

Lohse, M., Nagel, A., Herter, T., May, P., Schroda, M., Zrenner, R., et al. (2014). Mercator: a fast and simple web server for genome scale functional annotation of plant sequence data. *Plant Cell Environ.* 37, 1250–1258. doi: 10.1111/pce.12231

McCormick, R. F., Truong, S. K., Sreedasyam, A., Jenkins, J., Shu, S., Sims, D., et al. (2018). The sorghum bicolor reference genome: improved assembly, gene annotations, a transcriptome atlas, and signatures of genome organization. *Plant J.* 93, 338–354. doi: 10.1111/tpj.13781

McKenna, A., Hanna, M., Banks, E., Sivachenko, A., Cibulskis, K., Kernytsky, A., et al. (2010). The Genome Analysis Toolkit: a MapReduce framework for analyzing next-generation DNA sequencing data. *Genome Res.* 20, 1297–1303. doi: 10.1101/gr.107524.110

McKown, A. D., Klápště, J., Guy, R. D., Geraldes, A., Porth, I., Hannemann, J., et al. (2014). Genome-wide association implicates numerous genes underlying ecological trait variation in natural populations of *Populus trichocarpa*. *New Phytol.* 203, 535–553. doi: 10.1111/nph.12815

Mizrachi, E., Verbeke, L., Christie, N., Fierro, A. C., Mansfield, S. D., Davis, M. F., et al. (2017). Network-based integration of systems genetics data reveals pathways associated with lignocellulosic biomass accumulation and processing. *Proc. Natl. Acad. Sci. U.S.A.* 114, 1195–1200. doi: 10.1073/pnas.1620119114

Muchero, W., Guo, J., DiFazio, S. P., Chen, J.-G., Ranjan, P., Slavov, G. T., et al. (2015). High-resolution genetic mapping of allelic variants associated with cell wall chemistry in *Populus*. *BMC Genomics* 16:24. doi: 10.1186/s12864-015-1215-z

Price-Whelan, A. M., and Foreman-Mackey, D. (2017). schwimmbad: a uniform interface to parallel processing pools in Python. *J. Open Source Softw.* 2:357. doi: 10.21105/joss.00357

R Core Team (2017). *R: A Language and Environment for Statistical Computing*. Vienna: R Foundation for Statistical Computing.

Ragauskas, A. J., Williams, C. K., Davison, B. H., Britovsek, G., Cairney, J., Eckert, C. A., et al. (2006). The path forward for biofuels and biomaterials. *Science*, 311, 484–489. doi: 10.1126/science.1114736

Ritchie, M. D., Holzinger, E. R., Li, R., Pendergrass, S. A., and Kim, D. (2015). Methods of integrating data to uncover genotype-phenotype interactions. *Nat. Rev. Genet.* 16, 85–97. doi: 10.1038/nrg3868

Sannigrahi, P., Ragauskas, A. J., and Tuskan, G. A. (2010). Poplar as a feedstock for biofuels: a review of compositional characteristics. *Biofuels Bioprod. Biorefin.* 4, 209–226. doi: 10.1002/bbb.206

Schenke, D., Böettcher, C., and Scheel, D. (2011). Crosstalk between abiotic ultraviolet-B stress and biotic (flg22) stress signalling in *Arabidopsis* prevents flavonol accumulation in favor of pathogen defence compound production. *Plant Cell Environ.* 34, 1849–1864. doi: 10.1111/j.1365-3040.2011.02381.x

Schünemann, D. (2004). Structure and function of the chloroplast signal recognition particle. *Curr. Genet.* 44, 295–304. doi: 10.1007/s00294-003-0450-z

Shannon, P., Markiel, A., Ozier, O., Baliga, N. S., Wang, J. T., Ramage, D., et al. (2003). Cytoscape: a software environment for integrated models of biomolecular interaction networks. *Genome Res.* 13, 2498–2504. doi: 10.1101/gr.1239303

Shu, L., Zhao, Y., Kurt, Z., Byars, S. G., Tukiainen, T., Kettunen, J., et al. (2016). Mergeomics: multidimensional data integration to identify pathogenic perturbations to biological systems. *BMC Genomics* 17:874. doi: 10.1186/s12864-016-3198-9

Slavov, G. T., DiFazio, S. P., Martin, J., Schackwitz, W., Muchero, W., Rodgers-Melnick, E., et al. (2012). Genome resequencing reveals multiscale geographic structure and extensive linkage disequilibrium in the forest tree *Populus trichocarpa*. *New Phytol.* 196, 713–725. doi: 10.1111/j.1469-8137.2012.04258.x

Streatfield, S. J., Weber, A., Kinsman, E. A., Häusler, R. E., Li, J., Post-Beittenmiller, D., et al. (1999). The phosphoenolpyruvate/phosphate translocator is required for phenolic metabolism, palisade cell development, and plastid-dependent nuclear gene expression. *Plant Cell* 11, 1609–1621.

Sykes, R., Yung, M., Novaes, E., Kirst, M., Peter, G., and Davis, M. (2009). High-throughput screening of plant cell-wall composition using pyrolysis molecular beam mass spectroscopy. *Biofuels Methods Protoc.* 581, 169–183. doi: 10.1007/978-1-60761-214-8_12

Timm, C. M., Pelletier, D. A., Jawdy, S. S., Gunter, L. E., Henning, J. A., Engle, N., et al. (2016). Two poplar-associated bacterial isolates induce additive favorable responses in a constructed plant-microbiome system. *Front. Plant Sci.* 7:497. doi: 10.3389/fpls.2016.00497

Tschaplinski, T. J., Standaert, R. F., Engle, N. L., Martin, M. Z., Sangha, A. K., Parks, J. M., et al. (2012). Down-regulation of the caffeic acid *O*-methyltransferase gene in switchgrass reveals a novel monolignol analog. *Biotechnol. Biofuels* 5:71. doi: 10.1186/1754-6834-5-71

Tuskan, G., Slavov, G., DiFazio, S., Muchero, W., Pryia, R., Schackwitz, W., et al. (2011). *Populus* resequencing: towards genome-wide association studies. *BMC Proc.* 5:I21. doi: 10.1186/1753-6561-5-S7-I21

Tuskan, G., West, D., Bradshaw, H. D., Neale, D., Sewell, M., Wheeler, N., et al. (1999). Two high-throughput techniques for determining wood properties as part of a molecular genetics analysis of hybrid poplar and loblolly pine. *Appl. Biochem. Biotechnol.* 77, 55–65. doi: 10.1385/ABAB:77:1-3:55

Tuskan, G. A., Difazio, S., Jansson, S., Bohlmann, J., Grigoriev, I., Hellsten, U., et al. (2006). The genome of Black Cottonwood, *Populus trichocarpa* (Torr. & Gray). *Science* 313, 1596–1604. doi: 10.1126/science.1128691

van der Auwera, G. A., Carneiro, M. O., Hartl, C., Poplin, R., del Angel, G., Levy-Moonshine, A., et al. (2013). From fastQ data to high-confidence variant Calls: the genome analysis toolkit best practices pipeline. *Curr. Protoc. Bioinformatics* 43, 11.10.1-33. doi: 10.1002/0471250953.bi1110s43

van Dongen, S. (2008). Graph clustering via a discrete uncoupling process. *SIAM J. Matrix Anal. Appl.* 30, 121–141. doi: 10.1137/040608635

van Dongen, S. (2000). *Graph Clustering by Flow Simulation*. Ph.D. thesis, University of Utrecht, May 2000.

Vanholme, R., Demedts, B., Morreel, K., Ralph, J., and Boerjan, W. (2010). Lignin biosynthesis and structure. *Plant Physiol.* 153, 895–905. doi: 10.1104/pp.110.155119

Vining, K. J., Pomraning, K. R., Wilhelm, L. J., Priest, H. D., Pellegrini, M., Mockler, T. C., et al. (2012). Dynamic DNA cytosine methylation in the *Populus trichocarpa* genome: tissue-level variation and relationship to gene expression. *BMC Genomics* 13:27. doi: 10.1186/1471-2164-13-27

Wagner, G. P., Kin, K., and Lynch, V. J. (2012). Measurement of mRNA abundance using RNA-seq data: RPKM measure is inconsistent among samples. *Theory Biosci.* 131, 281–285. doi: 10.1007/s12064-012-0162-3

Wickham, H. (2007). Reshaping data with the reshape package. *J. Stat. Softw.* 21, 1–20. doi: 10.18637/jss.v021.i12

Wickham, H. (2009). *ggplot2: Elegant Graphics for Data Analysis*. New York, NY: Springer-Verlag.

Yanofsky, M. F., Liljegren, S., and Ferrandiz, C. (2004). *Selective control of lignin biosynthesis in transgenic plants*. US Patent 6,768,042. Available online at: https://patents.google.com/patent/US6768042B2/en

Yoo, S. K., Lee, J. S., and Ahn, J. H. (2006). Overexpression of *AGAMOUS-LIKE 28* (*AGL28*) promotes flowering by upregulating expression of floral promoters within the autonomous pathway. *Biochem. Biophys. Res. Commun.* 348, 929–936. doi: 10.1016/j.bbrc.2006.07.121

Yu, B., Gruber, M. Y., Khachatourians, G. G., Zhou, R., Epp, D. J., Hegedus, D. D., et al. (2012). Arabidopsis cpSRP54 regulates carotenoid accumulation in *Arabidopsis* and *Brassica napus*. *J. Exp. Bot.* 63, 5189–5202. doi: 10.1093/jxb/ers179

Yu, H., Ito, T., Wellmer, F., and Meyerowitz, E. M. (2004). Repression of AGAMOUS-LIKE 24 is a crucial step in promoting flower development. *Nat. Genet.* 36, 157–161. doi: 10.1038/ng1286

Yu, H., Xu, Y., Tan, E. L., and Kumar, P. P. (2002). AGAMOUS-LIKE 24, a dosage-dependent mediator of the flowering signals. *Proc. Natl. Acad. Sci. U.S.A.* 99, 16336–16341. doi: 10.1073/pnas.212624599

Yu, X., Chen, G., Guo, X., Lu, Y., Zhang, J., Hu, J., et al. (2017). Silencing *SlAGL6*, a tomato *AGAMOUS-LIKE6* lineage gene, generates fused sepal and green petal. *Plant Cell Rep.* 36, 959–969. doi: 10.1007/s00299-017-2129-9

Zhao, Q., Zeng, Y., Yin, Y., Pu, Y., Jackson, L. A., Engle, N. L., et al. (2015). Pinoresinol reductase 1 impacts lignin distribution during secondary

cell wall biosynthesis in Arabidopsis. *Phytochemistry* 112, 170–178. doi: 10.1016/j.phytochem.2014.07.008

Zhong, R., Richardson, E. A., and Ye, Z.-H. (2007). The MYB46 transcription factor is a direct target of SND1 and regulates secondary wall biosynthesis in *Arabidopsis*. *Plant Cell* 19, 2776–2792. doi: 10.1105/tpc.107.0 53678

Zhou, M., Zhang, K., Sun, Z., Yan, M., Chen, C., Zhang, X., et al. (2017). LNK1 and LNK2 corepressors interact with the MYB3 transcription factor in phenylpropanoid biosynthesis. *Plant Physiol.* 174, 1348–1358.

Zhou, Z., Schenke, D., Miao, Y., and Cai, D. (2017). Investigation of the crosstalk between the flg22 and the UV-B-induced flavonol pathway in *Arabidopsis thaliana* seedlings. *Plant Cell Environ.* 40, 453–458. doi: 10.1111/pce.12869

Nanometrology of Biomass for Bioenergy: The Role of Atomic Force Microscopy and Spectroscopy in Plant Cell Characterization

Anne M. Charrier[1], Aude L. Lereu[2], Rubye H. Farahi[3], Brian H. Davison[4] and Ali Passian[3,4,5,6]*

[1] Aix Marseille Univ, CNRS, CINaM, Marseille, France, [2] Aix Marseille Univ, CNRS, Centrale Marseille, Institut Fresnel, Marseille, France, [3] Quantum Information Science, Computational Sciences and Engineering Division, Oak Ridge National Laboratory, Oak Ridge, TN, United States, [4] BioEnergy Science Center (BESC), Biosciences Division, Oak Ridge National Laboratory, Oak Ridge, TN, United States, [5] Department of Chemical and Biomolecular Engineering, University of Tennessee, Knoxville, TN, United States, [6] Department of Physics, University of Tennessee, Knoxville, TN, United States

Ethanol production using extracted cellulose from plant cell walls (PCW) is a very promising approach to biofuel production. However, efficient throughput has been hindered by the phenomenon of recalcitrance, leading to high costs for the lignocellulosic conversion. To overcome recalcitrance, it is necessary to understand the chemical and structural properties of the plant biological materials, which have evolved to generate the strong and cohesive features observed in plants. Therefore, tools and methods that allow the investigation of how the different molecular components of PCW are organized and distributed and how this impacts the mechanical properties of the plants are needed but challenging due to the molecular and morphological complexity of PCW. Atomic force microscopy (AFM), capitalizing on the interfacial nanomechanical forces, encompasses a suite of measurement modalities for nondestructive material characterization. Here, we present a review focused on the utilization of AFM for imaging and determination of physical properties of plant-based specimens. The presented review encompasses the AFM derived techniques for topography imaging (AM-AFM), mechanical properties (QFM), and surface/subsurface (MSAFM, HPFM) chemical composition imaging. In particular, the motivation and utility of force microscopy of plant cell walls from the early fundamental investigations to achieve a better understanding of the cell wall architecture, to the recent studies for the sake of advancing the biofuel research are discussed. An example of delignification protocol is described and the changes in morphology, chemical composition and mechanical properties and their correlation at the nanometer scale along the process are illustrated.

Keywords: AFM, QFM, MSAFM, HPFM, plant cell walls, lignin, biofuel, bioenergy

1. INTRODUCTION

An important scientific focus and challenge of the 21st century is to achieve non-food biofuel mass production and thus replace fossil fuels (Lynd et al., 2008; Sannigrahi et al., 2010; Mohapatra et al., 2017). Significant research is being dedicated to ethanol production using extracted cellulose from the plant cell walls (PCW). Due to the complex structure of the PCW, which contain a variety of organic components (cellulose, hemicellulose, lignin, pectin, etc.), and the phenomenon

of recalcitrance, cellulose extraction is challenging. Overcoming the chemical and structural properties that have evolved in biomass to form strong and cohesive structures hence requires a deep understanding of how the molecular composition and organization in PCW impacts the mechanical properties of the plants. Indeed, the correlation between the molecular traits of the cell walls and its morphological and mechanical characteristics is ultimately expressed in the plant response. Due to their hierarchical structure, the macroscopic appearance and performance of plants have been shown to be inevitably linked to their structure at the micro- and nanometer scales (Gibson, 2012). However, the nanoscale behavior of many physical quantities, such as elasticity and plasticity, intimately connected with such a correlation, is largely unknown or poorly understood. Fundamentally, this inevitably leads to questioning the relationship between chemistry, structural organization and mechanical properties and how such molecular scale variations in the physical quantities of the cell walls translate into the bulk level and on to the whole organism level. From a practical point of view, this leads to questioning how cell wall chemical composition can be altered to intrinsically modify wood properties (Gindl and Gupta, 2002; Pilate et al., 2002), for example, to better suit various applications. Such complexity and heterogeneity of the plant systems therefore question the relevance of macroscopic and microscopic measurements. Often, these can only give an average description of the properties of the considered object. In recent years, many mechanical studies, primarily addressing the cell and cell wall level of plant body, have enlightened important structure–property and structure–function relationships (Fratzl and Weinkamer, 2007). Such advances in biomechanics have been possible due to the development of new technologies allowing mechanical and chemical analysis of surfaces with submicronic or nanometric lateral resolution (Gindl and Schoberl, 2004; Beecher et al., 2009; Tetard et al., 2011; Burgert and Keplinger, 2013). Such methodologies used to map the various properties of plants at the submicron scale are reported in **Table 1**.

TABLE 1 | Available methodologies for mapping the structure, the chemical composition, and the mechanical properties of plants at the submicron scale.

Plant property	Mapping technique	Lateral resolution	Reference
Structure	Scanning electron microscopy	10 nm	Auxenfans et al. (2017)
	Atomic force microscopy	1 nm	Salvadori et al. (2014)
Chemical composition	ToF-SIMS	1 μm	Tolbert and Ragauskas (2017)
	Confocal Raman microscopy	300 nm	Tetard et al. (2015)
	Mode synthesized AFM	1 nm	Tetard et al. (2011)
	Hybrid photonic force microscopy	5 nm	Farahi et al. (2017)
Mechanical properties	Nanoindentation[a]	<1 μm	Wimmer and Lucas (1997)
	Quantitative force–volume mapping	10 nm	Farahi et al. (2017)

[a]Nanoindentation usually provides discrete measurements.

As an example, the method of nanoindentation has proven to be very useful in providing important mechanical information (Gindl and Gupta, 2002; Zickler et al., 2006). This technique pushes a microscopic indenter with a known shape into a material surface while continuously measuring the response of the tip-sample system: the loading and unloading forces, the penetration depth, and the surface restoration to the indentation. Since forces ranging from tens of nanonewtons to millinewtons with submicrometer lateral resolutions can be precisely applied, the nanoindentation testing cycle can be highly sensitive to the mechanical properties of the material. The extent of the material restoration following the penetration into the surface is a measure of the material's elasticity, which is generally quantified by the elastic modulus or Young's modulus (E). Likewise, if any permanent indentation occurs, the material displays plasticity, which is quantified by the plasticity index (PI). The pull-off force when the tip is retreated from the surface is related to the adhesion energy, which are due to attractive van der Waals and electrostatic forces and other attractive forces acting between the tip and sample. In one of the first nanoindentation experiments, Wimmer and Lucas (1997) explored the relationship between hardness and Young's moduli for the secondary cell wall and cell corner middle lamella in spruce wood. They reported that the mechanical properties of secondary walls along their longitudinal direction is correlated with the presence of organized unidirectional cellulosic fibrils (Wimmer et al., 1997) while the reduced elastic modulus in the lignin-rich middle lamella was associated with the absence of cellulose in the region (Wimmer and Lucas, 1997). It was also demonstrated that the elastic modulus in the secondary walls decreased with microfibril angle therefore showing the importance of molecular organization (Gindl et al., 2004). These studies were the first to demonstrate the relationship between chemical composition, molecular organization and mechanical properties. However, in addition to requiring sample processing (polishing) and embedding into a polymeric material to avoid distortion of the measurements due to surface roughness (Konnerth et al., 2008; Burgert and Keplinger, 2013; Wagner et al., 2014; Youssefian et al., 2017), nanoindentation is ultimately limited by the resolution of the apparatus. Furthermore, the measurements are discrete, and do not allow mapping of mechanical properties.

More recently, atomic force microscopy (AFM) and its derivative techniques have emerged as the method of choice to resolve cell wood properties at the nanometer scale. The first force measurements with AFM also invoked a nanoindenter, but with an improved lateral resolution down to a few nanometers (Kirby, 2011; Fernandes et al., 2012). More recently, quantitative force–volume mapping (QFM) was adapted to plant cell wall measurements utilizing continuous force curve recording and therefore solving the problem of heterogeneity observation by imaging the topography with the associated E and PI mappings. Studies on Arabidopsis thaliana reported different characteristic modes of deformation and a spatial distribution of the elastic moduli across the surface (Yakubov et al., 2016), while Radotic et al. (2012) showed the changes in stiffness of the cell walls at different phases of growth. In addition, new innovative AFM techniques such as mode synthesized AFM (MSAFM) (Tetard et al., 2010, 2011) and hybrid photonic force microscopy (HPFM) (Tetard et al., 2015) have been

developed. The MSAFM was utilized to obtain the subsurface nanomorphological properties of wood cell walls with structural changes along the delignification process of poplar (Tetard et al., 2010, 2011), while the HPFM correlated the structural changes with chemical composition (Tetard et al., 2015).

This manuscript aims at demonstrating the input of nanometrology using AFM in understanding how the molecular distribution and organization impacts the mechanical strength and cohesion of PCW to better develop cellulose extraction protocols through delignification. Therein, the different applications of AFM modes for plant cell characterization are reviewed within the context of biofuel research. In Section 2, an example of chemical protocol leading to delignification starting from a cryotomed young poplar is described. In Section 3, the operating principle of AM-AFM, QFM, MSAFM/HPFM modes are described and their use to extract structural, mechanical, and chemical information through the process of delignification is illustrated through examples.
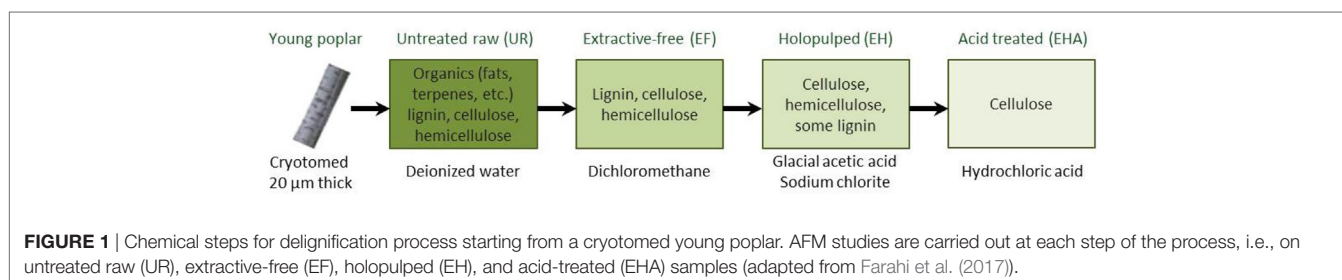
2. DELIGNIFICATION PROCESSES

The extraction of cellulose, while abundant in the secondary plant cell walls, is particularly hindered by the presence of lignin. Lignin is a complex organic polymer widely recognized for playing a role in the structural integrity of plants. As a compound, it is mostly inert and nonreactive, and thus makes a good material candidate for manufacturing and industrial applications (e.g., see lignin-based carbon fibers and nanofibers; Fang et al., 2017). Lignin removal has been a central key issue where a whole variety of complex processes, also referred to as delignification processes, have been developed (Singh et al., 2014). Controlling this process requires the understanding of the relationship between the chemical composition, the structural aspect, the biological infrastructure, and the mechanical properties of the PCW. The many delignification strategies have been based on various approaches (Singh et al., 2014) such as (1) physical treatments including mechanical (Cadoche and Lopez, 1989), pyrolysis (Chen et al., 2016), and steam processes (Tian et al., 2017), (2) chemical using organosolv (Erdocia et al., 2014), acid and alkaline hydrolysis (Singh et al., 2015; Carlos Martinez-Patino et al., 2017), or saccharification and fermentation (Healey et al., 2015), and (3) biological (Asina et al., 2016) and enzymatic (Al-Zuhair et al., 2015; Tian et al., 2017) treatments. To illustrate the complexity of delignification, an example based on a multistep chemical protocol, is given in **Figure 1**, resulting in a set of samples to be investigated using AFM techniques (Farahi et al., 2017).

The chemical processing of the biomass, here in the form of cross-sections (left image of **Figure 1**), was intended to remove lignin and other compounds to facilitate a more efficient extraction of the cellulose. The samples were received, frozen, and sectioned into 20 µm thick sections with a cryotome using a disposable blade that allowed minimal structural damage. For the untreated samples, the cross-section were washed with deionized (DI) water and dried between glass slides, referred as the untreated raw biomass or fresh Populus (UR). Next the extractive-free (EF) Populus were prepared by removing extractives (inorganics: K, Ca, Mg, P, F, Na, Si, S, Mn, etc. and organics: terpenes, fats, waxes, flavanoids, tannins, stilbenes, etc.) by refluxing with dichloromethane and then dried between glass slides to preserve the morphology of the sample and avoid contaminations. The removal of extractives allowed for the cellulose and lignin to be detected with less contamination on the surface when using ToF-SIMS, Raman, AFM, and other characterization methods (Farahi et al., 2017). The EF sample is then subject to glacial acetic acid combined with sodium chlorite resulting in the extractive free holopulped (EH) sample with most of the lignin removed. Finally, hydrochloric acid treatment is imposed on the EH sample to keep only the cellulose by removing hemicellulose and residuals of lignin (EHA sample). See details of the protocols in Farahi et al. (2017). The presented delignification process results in sets of four samples to be investigated.

3. DELIGNIFICATION INVESTIGATION BY ATOMIC FORCE MICROSCOPY

3.1. Amplitude Modulation AFM (AM-AFM): Structural Properties

AFM is based on measuring the interaction between a sharp tip (radius of curvature of a few nanometers), mounted on a cantilever spring (0.01 N/m < k < 150 N/m), and a surface; when the tip is raster-scanned across the surface, a high spatial resolution topographical image may be obtained (Binnig et al., 1986). As the tip comes near the surface, interaction forces induce a bending of the cantilever, which for small amplitudes follows Hooke's law. Depending on the environment, the tip/sample distance and the mode of utilization, the forces associated with AFM include van der Waals, electrostatic, magnetic, capillary, contact mechanical forces, chemical bonding, etc. Forces as small as few tens of piconewton have been measured. AFM offers the possibility of imaging the surface of any material (hard, soft, insulators, heterogeneous) in a variety of environments (solution, air, vacuum, or gas). Among

FIGURE 1 | Chemical steps for delignification process starting from a cryotomed young poplar. AFM studies are carried out at each step of the process, i.e., on untreated raw (UR), extractive-free (EF), holopulped (EH), and acid-treated (EHA) samples (adapted from Farahi et al. (2017)).

the basic modalities of AFM, amplitude-modulation atomic force microscopy (AM-AFM) (Martin et al., 1987; Zhong et al., 1993; Garcia and Perez, 2002; Garcia et al., 2007), also called tapping mode, has provided large improvements to soft materials imaging in general due to its non-invasive and non-destructive operation, and molecular resolution. Lateral resolution is mostly determined by the tip radius of curvature while subnanometric vertical resolution is provided by the piezoelectric modulus and feedback regulation used to control vertical displacements. In AM-AFM, the cantilever is mechanically excited near or at its intrinsic resonant frequency (typically in the range from a few tens to a few hundreds of kHz) with a given amplitude. When the tip is brought to within a few nanometers above the surface, the tip-sample interaction changes the resonance frequency of the cantilever and leads to a decrease of its oscillation amplitude whether the forces involved are attractive or repulsive. To measure the force intensity and its nature (attractive or repulsive), a laser beam (in most systems) is generally positioned at the apex of the cantilever and reflected to a position-sensing photodiode. The bending of the cantilever induces a deflection of the laser resulting in a displacement of the reflected beam on the photodiode. The new position is then used to apply a retroactive feedback to maintain the amplitude of oscillations (referred as a setpoint) of the cantilever.

AM-AFM has been successful in characterizing biomass (Kirby et al., 1996; Salvadori et al., 2014; Farahi et al., 2017) and in particular the architecture of plant cell walls at the molecular level which in turn is essential in improving lignocellulosic feedstock properties (Zhang et al., 2013b, 2017; Keplinger et al., 2014; Torode et al., 2018). AM-AFM mapping of cellulose topography revealed the right-handed twisted nature of microfibrils and the periodic distribution of glucose and fiber unit along the microfibrils (Hanley et al., 1997). Near-atomic resolution of the cellulose structure was reached, revealing the triclinic structure of Iα crystal phase (Baker et al., 2000). AM-AFM has also been useful in measuring surface morphology and roughness changes after treatment (Medeiros et al., 2007; Zhang et al., 2013a; Nanda et al., 2015).

In **Figures 2A–D**, the structural changes (morphology and wall thickness) undergone by the PCW were revealed at each chemical step of the delignification process detailed above. The sharper and well-contrasted PCW appearance after exposure to dichloromethane (EF image of **Figure 2B**) could be explained by the removal of organics, leaving the sample surface cleaned (Farahi et al., 2017). The UR and EF samples appeared very similar with well-defined PCW preserving the cell structure and having an average thickness of 3 μm. However, the structures of EH and EHA samples underwent considerable changes with an average PCW thickness around 2 μm. With the lignin content removed in EHA, the PCW started to collapse and the overall cell sizes became smaller and compressed. The decrease in the average thickness of PCW (**Figure 2E**, gray) along the process was in agreement with the lignin removal.

3.2. Quantitative Force–Volume Mapping (QFM): Mechanical Properties

Force measurements using AFM (Zdunek and Kurenda, 2013) and derivative technologies such as quantitative force–volume mapping (QFM) (Radmacher et al., 1996) and peak-force (Adamcik et al., 2011) allow nanomechanical mapping with nanometer scale lateral resolution, and measurements of forces down to few piconewtons. These techniques are currently used for mechanical characterization in cell biology (living cells) and structural biology, including testing of cartilage (Heu et al., 2012), bones (Spitzner et al., 2015), soft tissues (Burgert and Keplinger, 2013), and wood (Farahi et al., 2017). Similar to nanoindentation, the main principle of force measurements is to calculate hardness and elastic modulus from a load–displacement curve recorded during a local indentation (**Figures 3B,D–F**).

In a single force curve, a local force measurement is realized at a given position, corresponding to one pixel of the image, by only recording the corresponding loading and unloading curves. In quantitative force–volume mapping (Radmacher, 1997), single force curves are measured at points on a 2D grid. Tip-sample force is controlled by discrete force triggering at each point. Peak-force is an advanced version of QFM in which the force curves are acquired simultaneously with the topography mapping (Adamcik et al., 2011; Durkovic et al., 2014).

During an indentation measurement, laser deflection versus vertical (z) displacement is recorded continuously. In order to extract useful quantities, the data are converted into force versus tip/sample distance curves. The cantilever is approximated as a linear elastic spring and its bending, $D(z)$, is related to the applied loading force of the indentation, P, and k the spring constant of the cantilever according to Hooke's law, $P = -kD(z)$.

Nanomechanical information extracted from analysis of force curve measurements include elastic and dissipative components. Young's modulus, E, can be calculated from the slope of the unloading curve (Pharr et al., 1992) (**Figure 3E**) using a suitable model, which depends on the tip shape and dimensions (Bulichev and Alekhin, 1987), sample dimensions (flat, spherical) and whether or not dissipative components such as plastic deformation, adhesion, or viscosity are present (Johnson et al., 1971; Derjaguin et al., 1975; Butt et al., 2005). Dissipative components such as plastic deformation and adhesion hysteresis are included in the force measured in quasistatic equilibrium and can be extracted from a force–distance curve. Determination of non-conservative or velocity-dependent components requires dynamic force measurements (Herruzo et al., 2014).

In addition to the Young's modulus, a plasticity index (PI), including plasticity and viscosity components, can be extracted. From each indentation curve, the area comprised between the loading and the unloading curves above the zero force line, A_1, is a measure of the energy needed for the deformation and dissipated into the sample, whereas the sum $A_1 + A_2$ is the maximal energy that could be stored in the sample during the indentation (Butt et al., 2005), with A_2 being the area below the unloading curve (see **Figure 3F**). The plasticity index can then be defined as $PI = A_1/(A_1 + A_2)$ and can be used to discriminate components with different viscoplasticity. If $PI = 1$, the material is fully viscoplastic. If $PI = 0$, it indicates a perfectly elastic behavior. Finally, adhesion energy can also be extracted for the unloading curve as illustrated in **Figure 3E**, where the A0 area shows the presence of adhesion between the surface and the AFM probe.
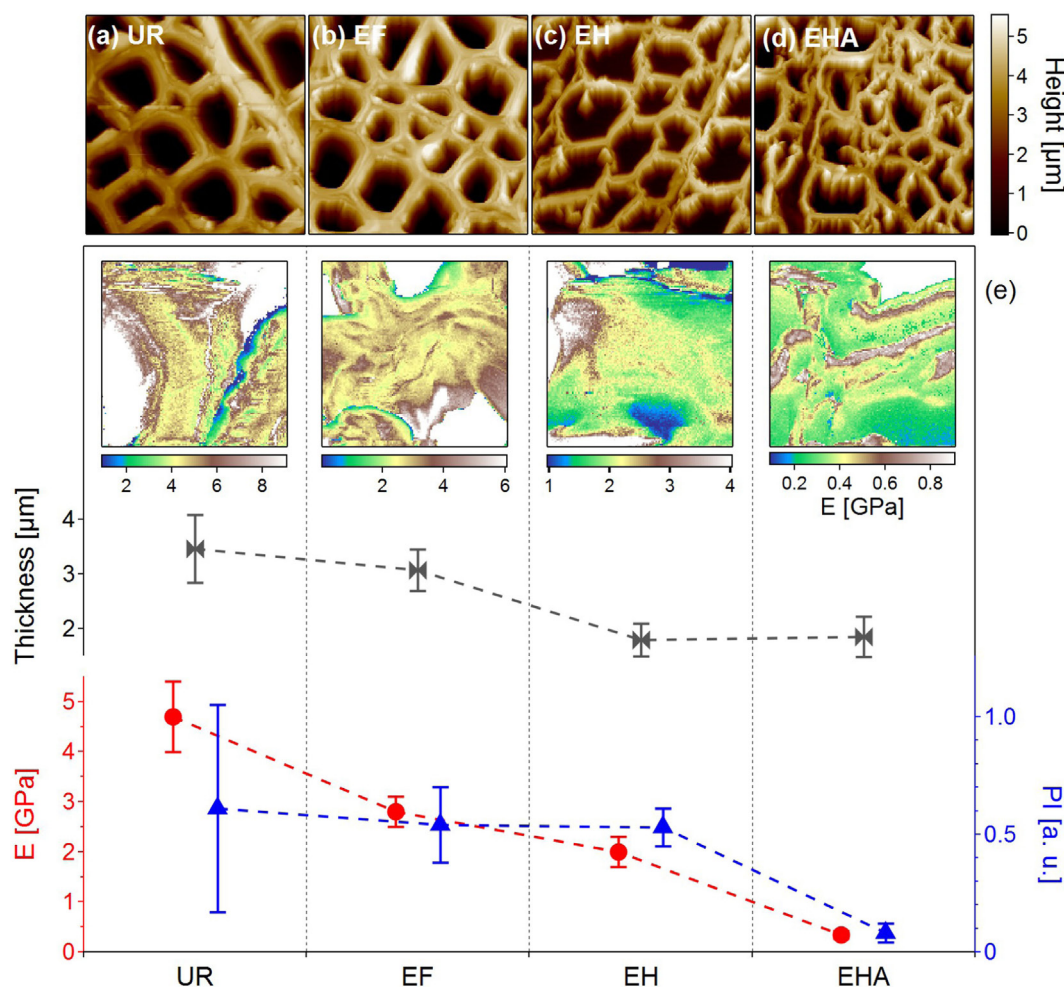
FIGURE 2 | Examination of poplar samples through the delignification process steps. **(A–D)** AM-AFM topographic images of untreated raw (UR), extractive-free (EF), holopulped (EH) and acid-treated (EHA) samples showing the structural changes along the delignification process (image size 50 × 50 μm²). The average PCW thicknesses extracted from the topographic images are plotted in **(E)** (gray curve). (e) Images: Young's modulus (GPa) mappings for each type of samples extracted from quantitative force–volume mappings. Image size is 5 μm × 5 μm. The corresponding average Young's moduli values (E) are reported in red. Blue triangles: Average values of the plasticity index (PI) extracted from the quantitative force–volume mapping. Data from Farahi et al. (2017), revisited.

Examples of E (**Figure 3B**) and PI (**Figure 3C**) mappings extracted from an untreated raw poplar sample were correlated with the topography image in **Figure 3A** (Farahi et al., 2017). The E mapping showed strong Young's modulus heterogeneity. Force curves shown in **Figures 3D–F** are discrete curves measured at the marked points in **Figure 3A**. They were chosen at three regions of the sample to illustrate different mechanical behaviors. In **Figure 2D**, the loading and unloading curves were superimposed showing a perfectly elastic behavior. In **Figures 3E,F**, the unloading curve is below the loading curve, translating into viscoplastic properties. In addition, adhesion between the tip and the surface during unloading (orange region) was observed in **Figure 3E**. The PI values in the mapping of **Figure 3C** varied between 0 and 1, therefore indicating regions with strong elastic or viscoplastic behaviors.

Quantitative force–volume mapping has been used to study the nanomechanical properties of plant cell walls at every step of the delignification process (Peaucelle, 2014; Farahi et al., 2017).

As illustrated in **Figure 2**, the Young's moduli varied toward lower values as the lignin was removed with a decrease from 4.7 ± 0.7 GPa for UR to 0.34 ± 0.07 GPa for EHA therefore suggesting total removal of the hemicellulose and lignin from the sample. Interestingly, the average values of PI (blue curve in **Figure 2E**) evolving around 0.5 for the UR, EF, and EH samples, revealed an important difference after acid treatment (EHA) showing a nearly perfect elastic behavior which did not seem to be directly related to delignification but mainly to the removal of hemicellulose.

3.3. Mode Synthesizing Atomic Force Microscopy (MSAFM) and Hybrid Photonic Force Microscopy (HPFM): Chemical Composition

Chemical composition is another sought-after parameter when investigating plant cell walls or biological samples. Simultaneous mechanical and chemical mapping have been obtained using
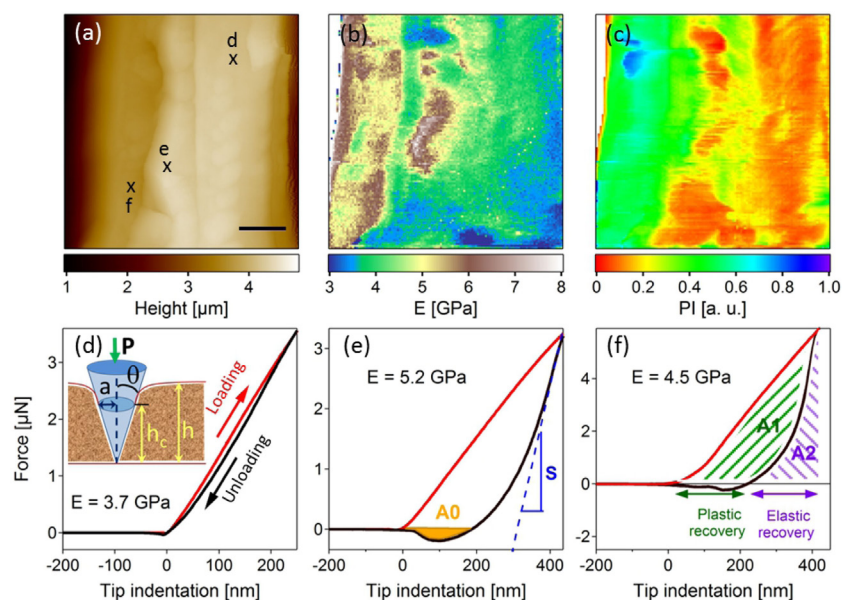
FIGURE 3 | Topographic **(A)** and associated mechanical imaging **(B,C)** (Young's modulus (E) and plastic index (PI) mappings) (scale bar 1 μm) obtained on an untreated raw poplar cell wall. **(D–F)** Discrete force curves extracted at the marked localizations on the topographic image **(A)**. Red and black curves correspond to the loading and unloading during tip indentation [inset **(D)**], respectively. **(D)** gives an illustration of elastic behavior and **(E)** of plasticity with adhesion (A0). S, the slope obtained by fitting the beginning of the unloading curve, is used to calculate the Young's modulus. A1 and A2 in **(F)** are two parameters used to access the plasticity index. Data from Farahi et al. (2017), revisited.

mode synthesizing atomic force microscopy (MSAFM) (Tetard et al., 2008, 2010, 2011) and the additional spectroscopic capabilities of hybrid photonic nanomechanical force microscopy (HPFM) (Tetard et al., 2015; Farahi et al., 2017). Capitalizing on the nonlinear probe-sample forces, microscopy with MSAFM offers a way to image soft samples and probe nanostructures that are below their surfaces (subsurface imaging). Briefly, in MSAFM multiple mechanical excitations (e.g., with megahertz frequencies) introduce small mechanical actuations within the sample and the probe, resulting in a coupled probe-sample dynamics. This intended coupled dynamics assumes that the system possesses suitable mechanical dispersion and supports a propagation mode in the megahertz spectrum. In a typical example such as considered here, two forcings, that is, driving forces with frequencies ω_1 and ω_2, respectively, are delivered to the probe *via* piezoelectric elements driven by waveform generators (Farahi et al., 2017). In both MSAFM and HPFM, the specific type of driving of the sample and the probe is selected based upon the specific application and the need for accessing subsurface, topographical, or chemical information. In general, both the probe and sample can be driven (Tetard et al., 2008) *via* any number and combination of waveform. In either case, the probe-sample interaction *via* the van der Waals force allows for synthesis of new oscillation modes in the system. For the case considered, two modes in the first order coupling are generated: a sum frequency of $\omega_+ = \omega_1 + \omega_2$ and a difference frequency of $\omega_- = |\omega_1 - \omega_2|$. The response signal at ω_- is of greater interest since it can be set in the kHz range and be readily monitored with phase-locked loop techniques. In general, from the effect of various interactions (elastic, dissipative, etc.), a measurement of the amplitude and phase properties

of the probe at the difference frequency, ω_- (or other selected frequencies), high-resolution subsurface images formed by the contrast due to the variations in elasticity, mechanical losses, etc., of the surface and subsurface material domains are constructed. Thus, the contrast measured from the dynamics of the probe can be used to obtain morphological and chemical distinctions in the examined materials. To achieve specific compositional information, HPFM introduces amplitude modulated infrared light with a wavelength λ to the sample at the difference frequency, creating yet another mechanical actuation based on the photothermal absorption of the sample. Mid-IR quantum cascade lasers (QCL) are useful excitation sources since they can be modulated and set at a wavelength to maximize composition-dependent absorption. The induced photothermal effect is exploited, where the absorption of light decays into heat, which in turn is conducted away as it dissipates. The resulting thermal expansion and relaxation is the source of a third mechanical actuation by photonic excitation at $\omega_{QCL} \to \omega_-$, which is associated with the absorption properties of the sample.

HPFM and MSAFM were used in conjunction with confocal Raman microscopy to characterize the distribution of chemical species at the nanoscale on poplar cross-sections (Tetard et al., 2015). Confocal Raman microscopy was first performed over the cell wall to spatially identify the cellulose-rich and lignin-rich regions (**Figure 4A**). Simultaneous AFM (**Figure 4B**), MSAFM (**Figure 4C**), and HPFM (**Figure 4D**) were then carried out over the same region. With the MSAFM image, new detail was found in the lignin-rich region compared to the AFM image, such as the structures within the dashed circled regions. The MSAFM signal was also able to detect substructures in the cellulose-rich region.
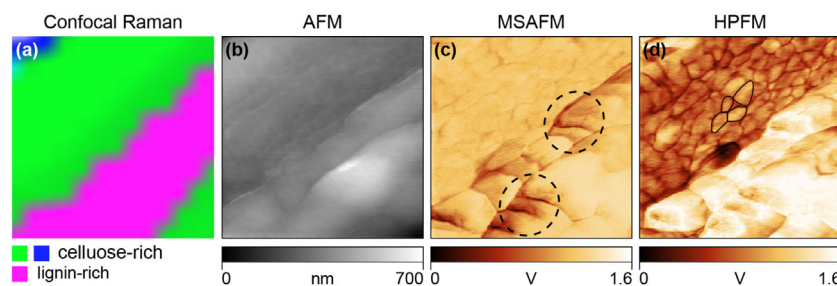
FIGURE 4 | Demonstration of HPFM compared to confocal Raman, AFM, and MSAFM on EF (extractive-free) poplar cell wall. **(A)** Confocal Raman image showing lignin-rich (pink) and cellulose-rich (blue, green) regions. **(B)** Simultaneous AFM image showing only topography. **(C)** MSAFM image at difference frequency, $\omega_- = 26$ kHz, brings additional clarity to the lignin structures indicated by the dashed circled regions. **(D)** HPFM image at photonic actuation, $\omega_{QCL} \rightarrow \omega_- = 26$ kHz, reveals additional detail of the near-surface cellulosic globules shown outlined. Adapted from Tetard et al. (2015).

The cellular ultrastructure was further revealed with HPFM with the addition of modulated infrared light at $\lambda = 10,200$ nm at $\omega_{QCL} \rightarrow \omega_- = 26$ kHz. Cellulose and lignin both absorb light at $\lambda = 10,200$ nm, but at different absorption intensities, resulting in contrasted signal (**Figure 4D**). The surface and subsurface structures disclosed remarkable detail, especially in the cellulose-rich region and the small grain-like structures outlined in black were interpreted to be cellulosic microfibril aggregates (globules), which are known to be located in the secondary cell wall (Salmén, 2004). MSAFM was also used to study the effect of holopulping treatment on holocellulose poplar sections. It was reported that the holopulping process, intended to oxidatively remove the lignin network in the cell, appeared to affect mostly the middle lamella as well as the cell corner regions (Tetard et al., 2011).

4. CONCLUSION

From the review of the reported case studies, we conclude that the AFM based measurement science and technology for exploring, manipulating, understanding, and relating the different properties of plant cell walls constitutes an emerging area of research within the plant biological material characterization. Given the current state of the understanding of the plant cells, there is a tremendous need for innovative approaches to microscopy and spectroscopy that can aid, for example, the development of efficient protocols for polysaccharides extraction in plants and further bioethanol production. From the considered studies to date, it is not difficult to form the opinion that understanding how the different molecular components of the plant cell walls are intermingled and distributed and how these impacts the mechanical properties of the plants will help in developing optimized process for overcoming recalcitrance. Indeed, the AFM techniques, being nondestructive and amenable to operation under ambient conditions with specimens in their native states,

provide a unique opportunity to relate the chemistry (HPFM) to the structure (AFM and MSAFM) and the mechanical properties (QFM and Peak-force) of the same regions at the nanometric scale. Understanding how cell wall chemical composition can be altered to intrinsically modify wood properties is also a highly promising issue; for example to increase the proportion of cellulose in plant cell walls, to reduce the lignin content, or to make delignification an easier process by reducing the elastic modulus of the plant cell walls. With the results reported thus far on plant cell imaging with a resolution of ~5 nm, and on cell wall Young's modulus and plastic index with typical values in the ranges 0.3–5 GPa and 0–0.5, respectively, quantitative biomass characterization is only at its debut. Considering the potential of the emerging AFM-based configurations of MSAFM and HPFM for high-resolution physical and chemical studies of the subsurface domains of the plant cells, we envision that novel and targeted studies based on innovative AFM modalities will continue to play an important role in establishing the basic characteristics of the plant cells as well as contribute to streamlining of biofuel production.

AUTHOR CONTRIBUTIONS

All authors contributed to the manuscript.

ACKNOWLEDGMENTS

REFERENCES

Adamcik, J., Berquand, A., and Mezzenga, R. (2011). Single-step direct measurement of amyloid fibrils stiffness by peak force quantitative nanomechanical atomic force microscopy. *Appl. Phys. Lett.* 98, 193701. doi:10.1063/1.3589369

Al-Zuhair, S., Abualreesh, M., Ahmed, K., and Razak, A. A. (2015). Enzymatic delignification of biomass for enhanced fermentable sugars production. *Energy Technol.* 3, 121–127. doi:10.1002/ente.201402138

Asina, F., Brzonova, I., Voeller, K., Kozliak, E., Kubatova, A., Yao, B., et al. (2016). Biodegradation of lignin by fungi, bacteria and laccases. *Bioresour. Technol.* 220, 414–424. doi:10.1016/j.biortech.2016.08.016

Auxenfans, T., Cronier, D., Chabbert, B., and Paes, G. (2017). Understanding the structural and chemical changes of plant biomass following steam explosion pretreatment. *Biotechnol. Biofuels* 10, 36. doi:10.1186/s13068-017-0718-z

Baker, A., Helbert, W., Sugiyama, J., and Miles, M. (2000). New insight into cellulose structure by atomic force microscopy shows the i-alpha crystal phase at near-atomic resolution. *Biophys. J.* 79, 1139–1145. doi:10.1016/S0006-3495(00)76367-3

Beecher, J. F., Hunt, C. G., and Zhu, J. Y. (2009). "Tools for the Characterization of Biomass at the Nanometer Scale," in *The Nanoscience and Technology of Renewable Biomaterials*, eds L. A. Lucia, and O. J. Rojas (Wiley-Blackwell), 61–90.

Binnig, G., Quate, C. F., and Gerber, C. (1986). Atomic force microscope. *Phys. Rev. Lett.* 56, 930–933. doi:10.1103/PhysRevLett.56.930

Bulichev, S., and Alekhin, V. (1987). Method of kinetic hardness and micro-hardness in testing impression by an indentor. *Ind. Lab.* 53, 1091–1096.

Burgert, I., and Keplinger, T. (2013). Plant micro- and nanomechanics: experimental techniques for plant cell-wall analysis. *J. Exp. Bot.* 64, 4635–4649. doi:10.1093/jxb/ert255

Butt, H., Cappella, B., and Kappl, M. (2005). Force measurements with the atomic force microscope: technique, interpretation and applications. *Surf. Sci. Rep.* 59, 1–152. doi:10.1016/j.surfrep.2005.08.003

Cadoche, L., and Lopez, G. (1989). Assessment of size-reduction as a preliminary step in the production of ethanol from lignocellulosic wastes. *Biol. Wastes* 30, 153–157. doi:10.1016/0269-7483(89)90069-4

Carlos Martinez-Patino, J., Ruiz, E., Romero, I., Cara, C., Carlos Lopez-Linares, J., and Castro, E. (2017). Combined acid/alkaline-peroxide pretreatment of olive tree biomass for bioethanol production. *Bioresour. Technol.* 239, 326–335. doi:10.1016/j.biortech.2017.04.102

Chen, X., Li, H., Sun, S., Cao, X., and Sun, R. (2016). Effect of hydrothermal pretreatment on the structural changes of alkaline ethanol lignin from wheat straw. *Sci. Rep.* 6, 39354. doi:10.1038/srep39354

Derjaguin, B., Muller, V., and Toporov, Y. (1975). Effect of contact deformations on adhesion of particles. *J. Colloid Interface Sci.* 53, 314–326. doi:10.1016/0021-9797(75)90018-1

Durkovic, J., Kardosova, M., and Lagana, R. (2014). Imaging and measurement of nanomechanical properties within primary xylem cell walls of broadleaves. *Bio-protocol* 4, 1360. doi:10.21769/BioProtoc.1360

Erdocia, X., Prado, R., Angeles Corcuera, M., and Labidi, J. (2014). Effect of different organosolv treatments on the structure and properties of olive tree pruning lignin. *J. Ind. Eng. Chem.* 20, 1103–1108. doi:10.1016/j.jiec.2013.06.048

Fang, W., Yang, S., Wang, X.-L., Yuan, T.-Q., and Sun, R.-C. (2017). Manufacture and application of lignin-based carbon fibers (LCFs) and lignin-based carbon nanofibers (LCNFs). *Green Chem.* 19, 1794–1827. doi:10.1039/C6GC03206K

Farahi, R., Charrier, A., Tolbert, A., Lereu, A., Ragauskas, A., Davison, B., et al. (2017). Plasticity, elasticity, and adhesion energy of plant cell walls: nanometrology of lignin loss using atomic force microscopy. *Sci. Rep.* 7, 152. doi:10.1038/s41598-017-00234-4

Fernandes, A. N., Chen, X., Scotchford, C. A., Walker, J., Wells, D. M., Roberts, C. J., et al. (2012). Mechanical properties of epidermal cells of whole living roots of *Arabidopsis thaliana*: an atomic force microscopy study. *Phys. Rev. E Stat. Nonlin. Soft. Matter. Phys.* 85, 1. doi:10.1103/PhysRevE.85.021916

Fratzl, P., and Weinkamer, R. (2007). Nature's hierarchical materials. *Prog. Mater. Sci.* 52, 1263–1334. doi:10.1016/j.pmatsci.2007.06.001

Garcia, R., Magerle, R., and Perez, R. (2007). Nanoscale compositional mapping with gentle forces. *Nat. Mater.* 6, 405–411. doi:10.1038/nmat1925

Garcia, R., and Perez, R. (2002). Dynamic atomic force microscopy methods. *Surf. Sci. Rep.* 47, 197–301. doi:10.1016/S0167-5729(02)00077-8

Gibson, L. J. (2012). The hierarchical structure and mechanics of plant materials. *J. R. Soc. Interface* 9, 2749–2766. doi:10.1098/rsif.2012.0341

Gindl, W., and Gupta, H. (2002). Cell-wall hardness and young's modulus of melamine-modified spruce wood by nano-indentation. *Compos. Part A Appl. Sci. Manuf.* 33, 1141–1145. doi:10.1016/S1359-835X(02)00080-5

Gindl, W., Gupta, H., Schoberl, T., Lichtenegger, H., and Fratzl, P. (2004). Mechanical properties of spruce wood cell walls by nanoindentation. *Appl. Phys. A Mater. Sci. Process.* 79, 2069–2073. doi:10.1007/s00339-004-2864-y

Gindl, W., and Schoberl, T. (2004). The significance of the elastic modulus of wood cell walls obtained from nanoindentation measurements. *Compos. Part A Appl. Sci. Manuf.* 35, 1345–1349. doi:10.1016/j.compositesa.2004.04.002

Hanley, S., Revol, J., Godbout, L., and Gray, D. (1997). Atomic force microscopy and transmission electron microscopy of cellulose from *Micrasterias denticulata*; evidence for a chiral helical microfibril twist. *Cellulose* 4, 209–220. doi:10.1023/A:1018483722417

Healey, A. L., Lee, D. J., Furtado, A., Simmons, B. A., and Henry, R. J. (2015). Efficient eucalypt cell wall deconstruction and conversion for sustainable lignocellulosic biofuels. *Front. Bioeng. Biotechnol.* 3:190. doi:10.3389/fbioe.2015.00190

Herruzo, E. T., Perrino, A. P., and Garcia, R. (2014). Fast nanomechanical spectroscopy of soft matter. *Nat. Commun.* 5, 3126. doi:10.1038/ncomms4126

Heu, C., Berquand, A., Elie-Caille, C., and Nicod, L. (2012). Glyphosate-induced stiffening of hacat keratinocytes, a peak force tapping study on living cells. *J. Struct. Biol.* 178, 1–7. doi:10.1016/j.jsb.2012.02.007

Johnson, K., Kendall, K., and Roberts, A. (1971). Surface energy and contact of elastic solids. *Proc. R. Soc. Lond. Ser. A Math. Phys. Sci.* 324, 301. doi:10.1098/rspa.1971.0141

Keplinger, T., Konnerth, J., Aguie-Beghin, V., Rueggeberg, M., Gierlinger, N., and Burgert, I. (2014). A zoom into the nanoscale texture of secondary cell walls. *Plant Methods* 10, 1. doi:10.1186/1746-4811-10-1

Kirby, A. R. (2011). Atomic force microscopy of plant cell walls. *Methods Mol Biol* 715, 169–178. doi:10.1007/978-1-61779-008-9_12

Kirby, A., Gunning, A., Waldron, K., Morris, V., and Ng, A. (1996). Visualization of plant cell walls by atomic force microscopy. *Biophys J* 70, 1138–1143. doi:10.1016/S0006-3495(96)79708-4

Konnerth, J., Harper, D., Lee, S.-H., Rials, T. G., and Gindl, W. (2008). Adhesive penetration of wood cell walls investigated by scanning thermal microscopy (SThM). *Holzforschung* 62, 91–98. doi:10.1515/HF.2008.014

Lynd, L. R., Laser, M. S., Bransby, D., Dale, B. E., Davison, B., Hamilton, R., et al. (2008). How biotech can transform biofuels. *Nat. Biotechnol.* 26, 169–172. doi:10.1038/nbt0208-169

Martin, Y., Williams, C., and Wickramasinghe, H. (1987). Atomic force microscope force mapping and profiling on a sub 100-a scale. *J. Appl. Phys.* 61, 4723–4729. doi:10.1063/1.338807

Medeiros, R. G., Silva, L. P., Azevedo, R. B., Silva, F. G. Jr., Ximenes, F., and Filho, E. (2007). The use of atomic force microscopy as a tool to study the effect of a xylanase from *Humicola grisea* var. thermoidea in kraft pulp bleaching. *Enzyme Microb. Technol.* 40, 723–731. doi:10.1016/j.enzmictec.2006.06.004

Mohapatra, S., Mishra, C., Behera, S. S., and Thatoi, H. (2017). Application of pretreatment, fermentation and molecular techniques for enhancing bioethanol production from grass biomass – a review. *Renew. Sustain. Energ. Rev.* 78, 1007–1032. doi:10.1016/j.rser.2017.05.026

Nanda, S., Maley, J., Kozinski, J. A., and Dalai, A. K. (2015). Physico-chemical evolution in lignocellulosic feedstocks during hydrothermal pretreatment and delignification. *J. Biobased Mater. bioenergy* 9, 295–308. doi:10.1166/jbmb.2015.1529

Peaucelle, A. (2014). Afm-based mapping of the elastic properties of cell walls: at tissue, cellular, and subcellular resolutions. *J Vis Exp* 24, e51317. doi:10.3791/51317

Pharr, G., Oliver, W., and Brotzen, F. (1992). On the generality of the relationship among contact stiffness, contact area, and elastic-modulus during indentation. *J. Mater. Res.* 7, 613–617. doi:10.1557/JMR.1992.0613

Pilate, G., Guiney, E., Holt, K., Petit-Conil, M., Lapierre, C., Leple, J., et al. (2002). Field and pulping performances of transgenic trees with altered lignification. *Nat. Biotechnol.* 20, 607–612. doi:10.1038/nbt0602-607

Radmacher, M. (1997). Measuring the elastic properties of biological samples with the afm. *IEEE Eng. Med. Biol. Mag.* 16, 47–57. doi:10.1109/51.582176

Radmacher, M., Fritz, M., Kacher, C., Cleveland, J., and Hansma, P. (1996). Measuring the viscoelastic properties of human platelets with the atomic force microscope. *Biophys. J.* 70, 556–567. doi:10.1016/S0006-3495(96)79602-9

Radotic, K., Roduit, C., Simonovic, J., Hornitschek, P., Fankhauser, C., Mutavdzic, D., et al. (2012). Atomic force microscopy stiffness tomography on living *Arabidopsis thaliana* cells reveals the mechanical properties of surface and deep cell-wall layers during growth. *Biophys. J.* 103, 386–394. doi:10.1016/j.bpj.2012.06.046

Salmén, L. (2004). Micromechanical understanding of the cell-wall structure. *C. R. Biol.* 327, 873–880. doi:10.1016/j.crvi.2004.03.010

Salvadori, M. R., Oller Nascimento, C. A., and Correa, B. (2014). Nickel oxide nanoparticles film produced by dead biomass of filamentous fungus. *Sci. Rep.* 4, 6404. doi:10.1038/srep06404

Sannigrahi, P., Ragauskas, A. J., and Tuskan, G. A. (2010). Poplar as a feedstock for biofuels: a review of compositional characteristics. *Biofuels Bioprod. Biorefin.* 4, 209–226. doi:10.1002/bbb.206

Singh, R., Shukla, A., Tiwari, S., and Srivastava, M. (2014). A review on delignification of lignocellulosic biomass for enhancement of ethanol production potential. *Renewable Sustain. Energy Rev.* 32, 713–728. doi:10.1016/j.rser.2014.01.051

Singh, S., Cheng, G., Sathitsuksanoh, N., Wu, D., Varanasi, P., George, A., et al. (2015). Comparison of different biomass pretreatment techniques and their impact on chemistry and structure. *Front. Energy Res.* 2:62. doi:10.3389/fenrg.2014.00062

Spitzner, E.-C., Roeper, S., Zerson, M., Bernstein, A., and Magerle, R. (2015). Nanoscale swelling heterogeneities in type I collagen fibrils. *ACS Nano* 9, 5683–5694. doi:10.1021/nn503637q

Tetard, L., Passian, A., Farahi, R. H., Davison, B. H., Jung, S., Ragauskas, A. J., et al. (2011). Nanometrology of delignified populus using mode synthesizing atomic force microscopy. *Nanotechnology* 22, 465702. doi:10.1088/0957-4484/22/46/465702

Tetard, L., Passian, A., Farahi, R. H., Thundat, T., and Davison, B. H. (2015). Opto-nanomechanical spectroscopic material characterization. *Nat. Nanotechnol.* 10, 870–877. doi:10.1038/nnano.2015.168

Tetard, L., Passian, A., and Thundat, T. (2010). New modes for subsurface atomic force microscopy through nanomechanical coupling. *Nat. Nanotechnol.* 5, 105–109. doi:10.1038/nnano.2009.454

Tetard, L., Passian, A., Venmar, K. T., Lynch, R. M., Voy, B. H., Shekhawat, G., et al. (2008). Imaging nanoparticles in cells by nanomechanical holography. *Nat. Nanotechnol.* 3, 501–505. doi:10.1038/nnano.2008.162

Tian, D., Chandra, R. P., Lee, J.-S., Lu, C., and Saddler, J. N. (2017). A comparison of various lignin-extraction methods to enhance the accessibility and ease of enzymatic hydrolysis of the cellulosic component of steam-pretreated poplar. *Biotechnol. Biofuels* 10, 157. doi:10.1186/s13068-017-0846-5

Tolbert, A., and Ragauskas, A. J. (2017). Advances in understanding the surface chemistry of lignocellulosic biomass via time-of-flight secondary ion mass spectrometry. *Energy Sci. Eng.* 5, 5–20. doi:10.1002/ese3.144

Torode, T. A., O'Neill, R., Marcus, S. E., Cornuault, V., Pose, S., Lauder, R. P., et al. (2018). Branched pectic galactan in phloem-sieve-element cell walls: Implications for cell mechanics. *Plant Physiol* 176, 1547–1558. doi:10.1104/pp.17.01568

Wagner, L., Bader, T. K., and de Borst, K. (2014). Nanoindentation of wood cell walls: effects of sample preparation and indentation protocol. *J. Sci. Mater.* 49, 94–102. doi:10.1007/s10853-013-7680-3

Wimmer, R., and Lucas, B. (1997). Comparing mechanical properties of secondary wall and cell corner middle lamella in spruce wood. *IAWA J.* 18, 77–88. doi:10.1163/22941932-90001463

Wimmer, R., Lucas, B., Tsui, T., and Oliver, W. (1997). Longitudinal hardness and young's modulus of spruce tracheid secondary walls using nanoindentation technique. *Wood Sci. Technol.* 31, 131–141. doi:10.1007/BF00705928

Yakubov, G. E., Bonilla, M. R., Chen, H., Doblin, M. S., Bacic, A., Gidley, M. J., et al. (2016). Mapping nano-scale mechanical heterogeneity of primary plant cell walls. *J. Exp. Bot.* 67, 2799–2816. doi:10.1093/jxb/erw117

Youssefian, S., Jakes, J. E., and Rahbar, N. (2017). Variation of nanostructures, molecular interactions, and anisotropic elastic moduli of lignocellulosic cell walls with moisture. *Sci. Rep.* 7, 2054. doi:10.1038/s41598-017-02288-w

Zdunek, A., and Kurenda, A. (2013). Determination of the elastic properties of tomato fruit cells with an atomic force microscope. *Sensors (Basel)* 13, 12175–12191. doi:10.3390/s130912175

Zhang, M., Chen, G., Kumar, R., and Xu, B. (2013a). Mapping out the structural changes of natural and pretreated plant cell wall surfaces by atomic force microscopy single molecular recognition imaging. *Biotechnol. Biofuels* 6, 147. doi:10.1186/1754-6834-6-147

Zhang, M., Wang, B., and Xu, B. (2013b). Measurements of single molecular affinity interactions between carbohydrate-binding modules and crystalline cellulose fibrils. *Phys. Chem. Chem. Phys.* 15, 6508–6515. doi:10.1039/c3cp51072g

Zhang, T., Vavylonis, D., Durachko, D. M., and Cosgrove, D. J. (2017). Nanoscale movements of cellulose microfibrils in primary cell walls. *Nat. Plants* 3, 17056. doi:10.1038/nplants.2017.56

Zhong, Q., Inniss, D., Kjoller, K., and Elings, V. (1993). Fractured polymer silica fiber surface studied by tapping mode atomic-force microscopy. *Surf. Sci.* 290, L688–L692. doi:10.1016/0039-6028(93)90582-5

Zickler, G., Schoberl, T., and Paris, O. (2006). Mechanical properties of pyrolysed wood: a nanoindentation study. *Philos. Mag.* 86, 1373–1386. doi:10.1080/14786430500431390

Characterization of Whole Biomasses in Pyridine Based Ionic Liquid at Low Temperature by ^{31}P NMR: An Approach to Quantitatively Measure Hydroxyl Groups in Biomass As Their Original Structures

Haoxi Ben[1,2*†], Xiaole Chen[1,2†], Guangting Han[3,4], Yingjuan Shao[1,2], Wei Jiang[3,4], Yunqiao Pu[5] and Arthur Jonas Ragauskas[5,6,7]

[1] Key Laboratory of Energy Thermal Conversion and Control of Ministry of Education, Nanjing, China, [2] School of Energy and Environment, Southeast University, Nanjing, China, [3] Laboratory of New Fiber Materials and Modern Textile (The Growing Base for State Key Laboratory), Qingdao, China, [4] College of Textiles, Qingdao University, Qingdao, China, [5] Biosciences Division, Oak Ridge National Laboratory, Oak Ridge, TN, United States, [6] Department of Chemical and Biomolecular Engineering, University of Tennessee, Knoxville, TN, United States, [7] Department of Forestry, Wildlife, and Fisheries, University of Tennessee, Knoxville, TN, United States

In this study, the dissolution of biomass components—cellulose, hemicellulose, and lignin, and two whole biomasses—switchgrass and poplar in a pyridine based ionic liquid at a low temperature—50°C has been examined, which will provide an opportunity to explore the original structures of biomass components. The following phosphitylation, and ^{31}P NMR measurement could provide quantitative results for various hydroxyl groups, including aliphatic, condensed phenolic, guaiacyl phenolic, p-hydroxyl phenyl and carboxylic hydroxyl groups in the biomass components, and whole biomass. By employing various biomass model compounds (glucose, cellotriose, and cellohexose), artificial mixtures of biomass components (cellulose, hemicellulose, and lignin), and computational simulation for the assignments by using density functional theory calculation in Gaussian, reliability and accuracy of this method have been examined as well, which indicated that this method is a reliable and accurate way to quantitatively characterize five different types of hydroxyl groups in biomass and its components.

Keywords: ionic liquid, biomass, lignin, cellulose, hemicellulose, ^{31}P NMR

INTRODUCTION

Biomass is a renewable resource for the sustainable production of fuels and chemicals that, to date, have been made primarily from fossil resources. Because of its carbon neutrality, relative abundance and non-food competition (David and Ragauskas, 2010), the use of biofuels and biochemicals could increase economic growth and provide environmental benefits. Lignocellulosic biomass contains three major constituents: cellulose, hemicelluloses, and lignin. Several reviews have summarized the distribution of these three major biopolymers in several hardwoods, softwoods, and agricultural residue species (Ragauskas et al., 2006; Huang et al., 2011).

Although lignocellulosic resources are readily becoming available for bioethanol production, their processing requires an aggressive pretreatment step to overcome their natural recalcitrance toward biological deconstruction to simple sugars. Clearly, the characterization of plant cell wall structure

and its three major components has become a crucial research topic (Foston and Ragauskas, 2012). The traditional methods for the characterization of lignin, cellulose, and hemicellulose in the whole biomass always involve the isolation of the individual components by separation procedures followed by spectroscopic techniques (Hallac et al., 2009; Hu et al., 2010; Huang et al., 2011; Ben and Ragauskas, 2012). Furthermore, the traditional methods may change the original chemical structures of biomass components due to the relatively high-temperature treatment, oxidation, and hydrolysis. All of these limitations for the traditional methods are calling for new ways to quantitatively characterize the biomass without separation procedures, such as NMR characterization especially performed in a whole biomass solution (Ben and Ferrell Iii, 2016; Hao et al., 2016; Yoo et al., 2016; Li et al., 2018). A solvent system, which has the ability to dissolve whole biomass and could keep all the original chemical structures intact, appears to be very pragmatic. A DMSO-based system reported in the literature is a promising approach (Lu and Ralph, 2003). Most recently, some researchers used ionic liquid as a tool for dissolution and pretreatment of whole biomass (da Costa Lopes et al., 2013a,b) and employed various analytical methods including FT-IR and NMR to characterize the biomass. Argyropoulos' group (Kilpeläinen et al., 2007; Xie et al., 2007; King et al., 2008, 2009, 2010; Sadeghifar et al., 2014) has developed various imidazole-based ionic liquid to dissolve and characterize whole biomass and biomass components. Characterization of biomass in ionic liquid solutions have been reported including the use of ^{1}H, ^{31}P NMR, and FT-IR. Kishimoto's group (Qu et al., 2012, 2013) has investigated imidazole based ionic liquid to dissolve several hardwood, softwood, and bamboo samples, and HSQC NMR was also employed to characterize biomass solutions. Similarly, Muhammad (Muhammad et al., 2011) and Sun's groups (Wen et al., 2012; Yang et al., 2013) also used the imidazole family ionic liquid to dissolve various biomasses and biomass components, including lignin, cellulose, hemicellulose, and holocellulose. FT-IR, ^{13}C, and HSQC NMR have been used to characterize these ionic liquid solutions. All the imidazole type ionic liquids reported (Kilpeläinen et al., 2007; Xie et al., 2007; King et al., 2008, 2009, 2010; Muhammad et al., 2011; Qu et al., 2012, 2013; Wen

et al., 2012; Yang et al., 2013) in the literature need a relatively high temperature (~100°C) to dissolve biomass. However, on the basis of reported TGA results (Yang et al., 2007), some biomass components, such as cellulose and hemicellulose, could be slightly decomposed even at ~80°C (Figure S3 in Supplementary Material). Ragauskas' group (Jiang et al., 2009, 2010; Samuel et al., 2011; Foston et al., 2012) has developed various pyridine ionic liquids and employed various NMR analytical methods, including ^{1}H, ^{13}C, and HSQC NMR, to characterize the chemical structures of biomass. Based on the screening of various pyridine-based ionic liquids (with different side chains), 1-allyl-3-butylpyridinium chloride is the most potential one, which could dissolve the whole biomass and biomass components at a relatively low temperature (50°C). To preserve as much as original chemical structures of biomass, this study will report a dissolution of biomass and its components at 50°C. Normally, ^{1}H and HSQC NMR characterizations of ionic liquid solutions require deuterated ionic liquids, which are relatively expensive. Nevertheless, the phosphitylation of hydroxyl groups using 2-chloro-4,4,5,5-tetramethyl-1,3,2-dioxaphospholane (TMDP) has been developed to quantitatively determine hydroxyl functional groups in various substrates including coal pyrolysis condensates (Wroblewski et al., 1988), coal extracts (Wroblewski et al., 1991), lignin, and pyrolysis oils (Ben and Ragauskas, 2011; Kosa et al., 2011). These hydroxyl functional groups which include aliphatic, condensed phenolic, guaiacyl phenolic, p-hydroxyl phenyl, and carboxylic OH groups are very important to understand the chemical structures of biomass and will also affect the following conversion process. In this study, ^{31}P NMR will be employed to analyze biomass solutions, which could provide quantitative structure information for various hydroxyl groups and will not require deuterated ionic liquids.

EXPERIMENTAL

Synthesis of 1-Allyl-3-Butylpyridinium Chloride

Allyl chloride (4.23 g, 55 mmol), 3-butylpyridine (6.75 g, 50 mmol), and anhydrous toluene (4.0 g) was added to a 25-ml
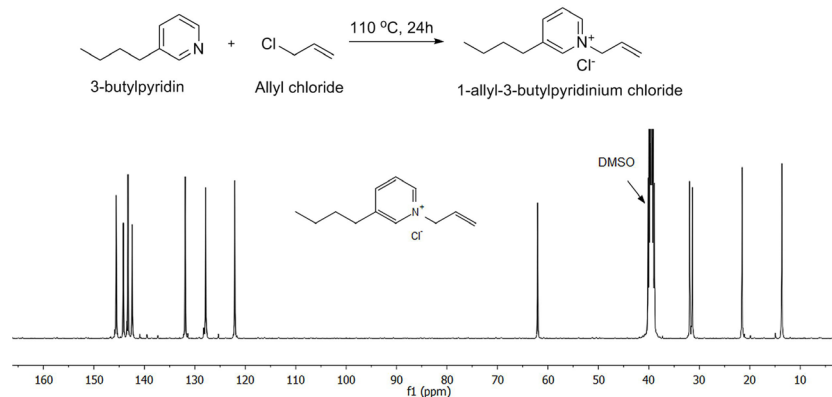

FIGURE 1 | Synthesis pathway and 13 C NMR result for the 1-allyl-3-butylpyridinium chloride ionic liquid.

vial. The mixture was heated at 110°C for 24 h under nitrogen. After decanting the toluene, the mixture was placed under direct vacuum at 80°C for 48 h. **Figure 1** shows the synthesis pathway and ^{13}C NMR spectrum (see Figure S1 in Supplementary Material for the detailed assignments. Based on ^{31}P NMR analysis, the water content for the ionic liquid is <0.1 wt%).

Biomass Components and Biomasses Preparation

Holocellulose was isolated from extractives-free Poplar by treatment with NaClO$_2$ and acetic acid at 70°C for 2 h (see Supplementary Material for detail). The process was repeated twice to ensure maximum lignin removal.

Ball-milled lignin was isolated by ball-mill extractive-free Poplar in a porcelain jar with ceramic balls using a rotatory ball-mill running at 96 rpm for 14 days under N$_2$. The ball-milled cell wall powder was then extracted with *p*-dioxane/water (96:4, v/v) and concentrated by evaporation and freeze–dried (Huang et al., 2011).

Two different types of hemicellulose are used in this study, one was commercially purchased (Sigma Aldrich) hemicellulose (xylan) produced from oak wood (hemicellulose #1) and the other was isolated by KOH extraction from Poplar holocellulose (hemicellulose #2). The differences from the natural and isolation process can lead to some different chemical structures for hemicellulose #1 and #2. Glucose, cellotriose, cellohexose, and cellulose were commercially purchased.

Baseline *populous* (*Populous trichocarpa × deltodies*) and lowland cultivar Alamo switchgrass (*Panicum virgatum*) samples

were first Wiley-milled to pass 0.13-cm screen and then ball-milled with a Retsch MM 200 Mixer Mill equipped with a 10-ml stainless steel jar and two 7-mm stainless steel grinding balls, and milled for 20 min × 6 times at 25 s^{-1} frequency. The detailed information about the component analyses of feedstock has been reported in the literature (Foston and Ragauskas, 2010).

Dissolution and ^{31}P NMR Analysis of Biomass and Biomass Components in Ionic Liquid

Biomass and biomass components (5 mg, which is the maximum loading amount for the whole biomasses. For biomass components, the maximum dissolved amount could be even higher than 20 mg, for lignin it can be ~100 mg, however, to be consistent with the whole biomass samples, all the reported solution in this study have the similar concentrations) were dissolved in 1-allyl-3-butylpyridinium chloride ionic liquid (300 mg) at 50°C under nitrogen for 48 h. With 100–200 μl anhydrous pyridine added into the biomass solution, 80 μl 2-chloro-4, 4, 5, 5-tetramethyl-1,3,2-dioxaphospholane was carefully added to the solution. For whole biomass and cellulose samples, anhydrous 1-methyl-2-pyrrolidinone (NMP) and anhydrous *N,N*-dimethylformamide (DMF, 200 μl, each) were added to improve the dissolution of phosphitylation products. After fully dissolution and phosphitylation, an internal standard (50 μl, 20 mg/ml, cyclohexanol/CDCl$_3$) and relaxation reagent [50 μl, 20 mg/ml Cr(acac)$_3$/CDCl$_3$] were added into the final solution. (Note: The normally used internal standard—endo-*N*-hydroxy-5-norbornene-2,3-dicarboximide will be decomposed in this type of ionic liquid.)
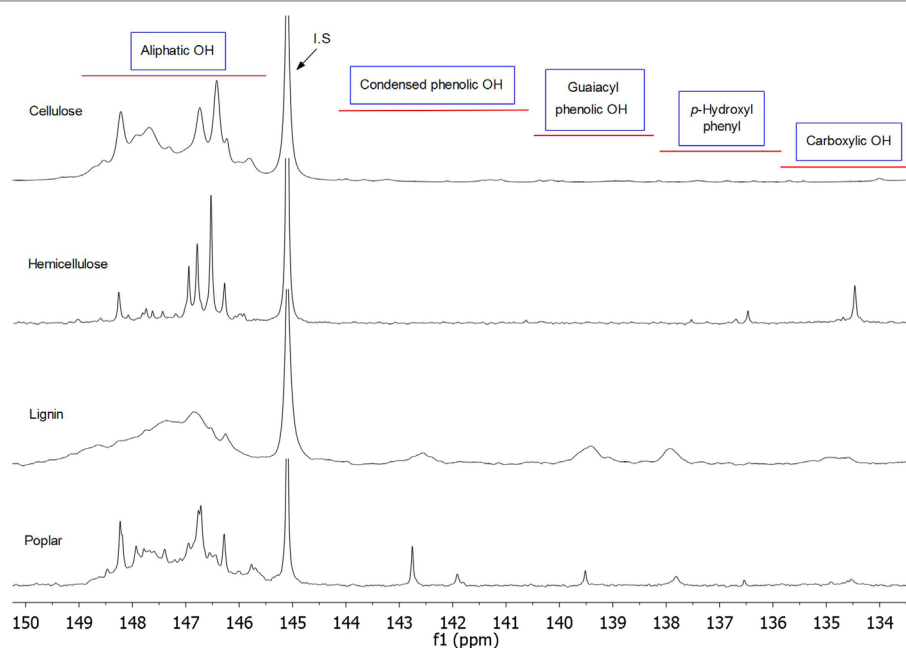

FIGURE 2 | Possible dissolution and phosphitylation of biomass components and whole biomass in the ionic liquid.
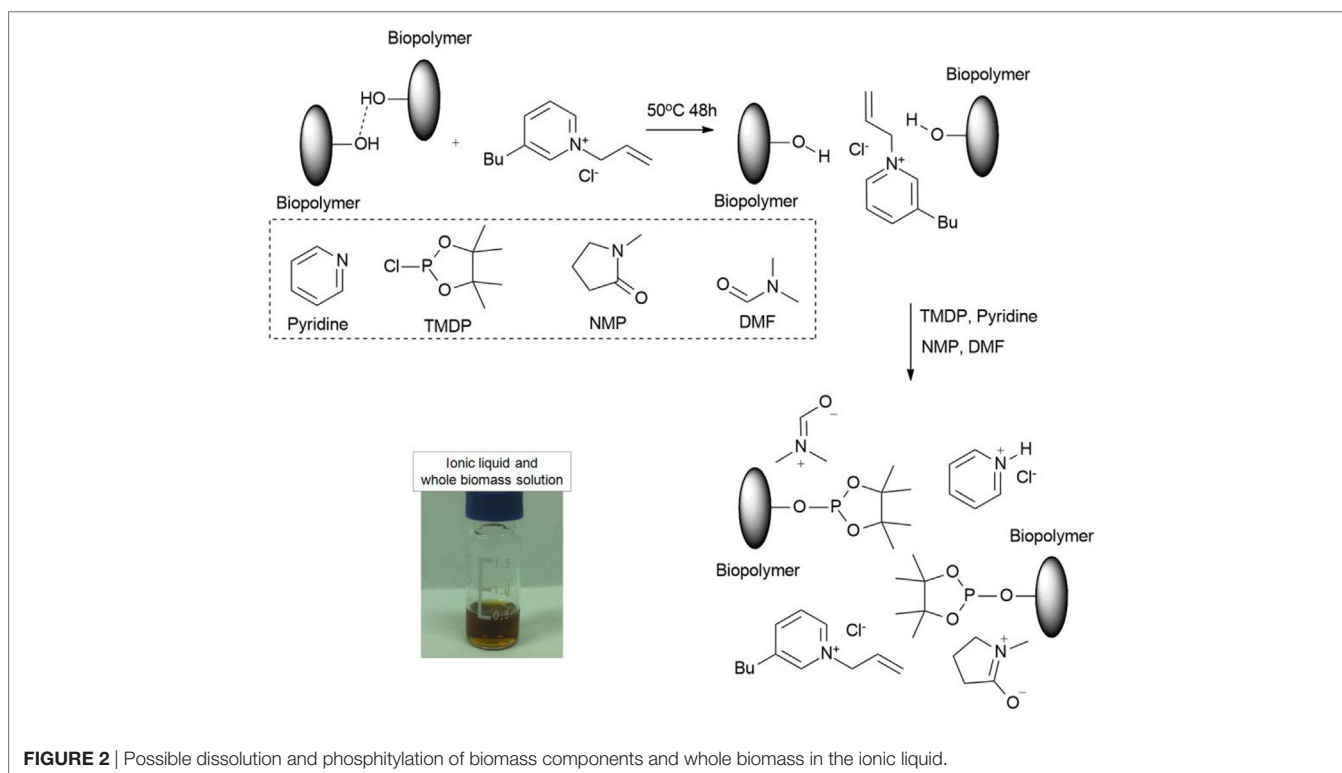
FIGURE 3 | ³¹P NMR spectra for cellulose, hemicellulose, lignin, and poplar whole biomass after dissolution and phosphitylation with TMDP in ionic liquid.

³¹P NMR was recorded at room temperature with a 5-mm BBO probe in the Bruker Avance/DMX 400 MHz NMR spectrometer and used an inverse gated decoupling pulse sequence, 90° pulse angle, 25 s pulse delay [optimized based on literature report (Zawadzki and Ragauskas, 2001; Ben and Ragauskas, 2011; Pu et al., 2011)], and 512 scans with a LB of 4.0 Hz. Spectral width is 200 ppm, and the acquisition time is 0.98 s. The cyclohexanol peak signal at 145.1 ppm was used as reference.

RESULTS AND DISCUSSION

It has been reported (Pinkert et al., 2009) that the mechanism for dissolution of biomass and its components in ionic liquid involves the disrupture of hydrogen bonds between biopolymers and replacing these hydrogen bonds between ionic liquid and biopolymer. By employing the new developed pyridine-based ionic liquids, the biomass and its components can be dissolved at a low temperature (50°C) very well, which indicate the original hydrogen bond in the biomass has been destroyed and formed a new equilibrium with the ionic liquid. However, after phosphitylation (see Figure S2 in Supplementary Material for reactions) of biomass solutions, some precipitate particles may appear, which may be due to the TMDP reacted with all the OH groups in the biomass and broke the equilibrium between ionic liquid and biomass. It is also evident that TMDP can react with all the OH groups in the biomass ionic liquid solution, which will also change the polarity for the biomass and lead to precipitate. It has been reported (Rinaldi, 2011) that NMP could improve the dissolution of cellulose, and DMF (Pu et al., 2011) was used to dissolve lignin samples. Therefore, to regain the balance and equilibrium, two extra solvents such as NMP and DMF were added into the solution to improve the dissolution. The result
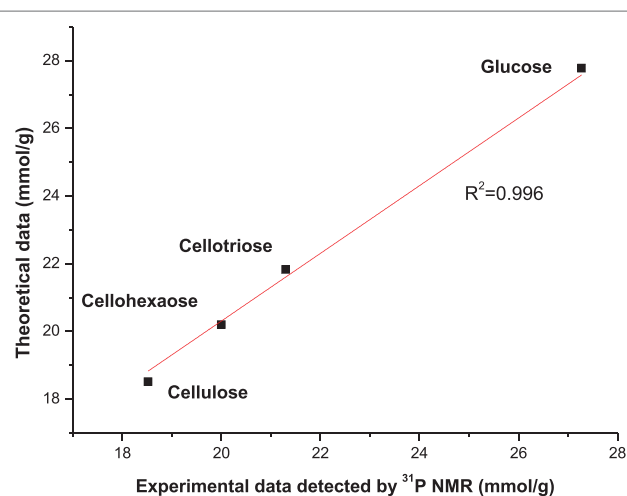

FIGURE 4 | The correlation between experimental and theoretical data of hydroxyl group contents of cellulose and cellulose model compounds.

indicated that NMP will work perfectly for cellulose sample but not for whole biomass samples. DMF is a necessary step for the total dissolution of whole biomass, but DMF will not work as a single enhancer even for cellulose sample. The final solution is transparent with an amber color. **Figure 2** shows the possible dissolution and phosphitylation pathways of biomass in ionic liquid. It has been found the commonly used internal standard NHND (endo-*N*-hydroxy-5-norbornene-2,3-dicarboximide) is not stable in this type of ionic liquid, with the peak for this internal standard disappeared after 24 h. The similar phenomena have been reported in the literature as well (Ben and Ferrell Iii, 2016); however, the peak for NHND still remained 80%

OH content (mmol/g)[a]	Cellulose	Hemicellulose #1	Hemicellulose #2	Lignin	Holocellulose
Aliphatic OH	18.52	3.72	5.81	3.83	13.88
Condensed phenolic OH	0.00	0.00	0.00	0.51	0.00
Guaiacyl phenolic OH	0.00	0.00	0.00	0.49	0.02
p-Hydroxyl phenyl	0.00	0.00	0.00	0.24	0.07
Carboxylic OH	0.00	0.59	1.40	0.22	0.46

Detected by ³¹P NMR after dissolution and phosphitylation with TMDP in ionic liquid.
[a]Duplicated tests have been done for all the samples, and the SD is lower than 2%.

TABLE 2 | Hydroxyl group contents of two mixtures of cellulose, hemicellulose, and lignin.

OH content (mmol)	Mixture #1	Theoretical OH content	Mixture #2	Theoretical OH content
Aliphatic OH	64.51	60.92	90.06	94.01
Condensed phenolic OH	0.67	0.61	1.05	0.92
Guaiacyl phenolic OH	0.57	0.58	0.83	0.88
p-Hydroxyl phenyl	0.35	0.29	0.29	0.32
Carboxylic OH	1.93	2.2	7.01	7.12

Detected by ³¹P NMR after dissolution and phosphitylation with TMDP in ionic liquid.
*Mixture #1 made by lignin (~20 wt%), hemicellulose #1 (~45 wt%), and cellulose (~35 wt%).*
Mixture #2 made by lignin (~20 wt%), hemicellulose #2 (~45 wt%), and cellulose (~35 wt%).

intensity after 14 days, which means this type of ionic liquid can accelerate the decomposition process for NHND. Therefore, for a precise and accurate data, in this study, cyclohexanol has been used as internal standard. By employing the same ionic liquid system, the obtained ³¹P NMR spectrums for cellulose, hemicellulose, lignin, and poplar whole biomass are shown in **Figure 3**. Aliphatic OH, condensed phenolic OH (combined C5 substituted/condensed phenolic hydroxyl groups including β-5, syringyl, 4-O-5, and 5-5 structures. Table S1 for detailed assignment ranges and structures), guaiacyl phenolic OH, p-hydroxyl phenol, and carboxylic acid OH can be quantitatively characterized by this method.

To further evaluate the accuracy of this method, various oligomers of glucose and cellulose have been examined. Figure S2 in Supplementary Material demonstrates the dissolution and phosphitylation of aliphatic hydroxyl bonds with TMDP in ionic liquid, and **Figure 4** shows the correlation between experimental and theoretical data of hydroxyl groups in cellulose and oligomers of glucose, which is the evidence that this method is a reliable way to provide quantitative data for the contents of hydroxyl group for cellulose.

To explore more about this proposed ionic liquid system, two hemicellulose samples, lignin and holocellulose, were studied and the results are shown in **Table 1**. It was found that hemicellulose and lignin readily dissolved in this type of ionic liquid and will not precipitate after adding TMDP. Two cosolvents such as DMP and DMF were added for experimental consistency. As anticipated, the results show that there are no phenolic hydroxyl signal in cellulose and hemicellulose. The holocellulose sample contained a very small peak which can be assigned to guaiacyl and p-hydroxyl phenyl OH, which may be due to the residues of lignin. For lignin sample, the results of hydroxyl group contents
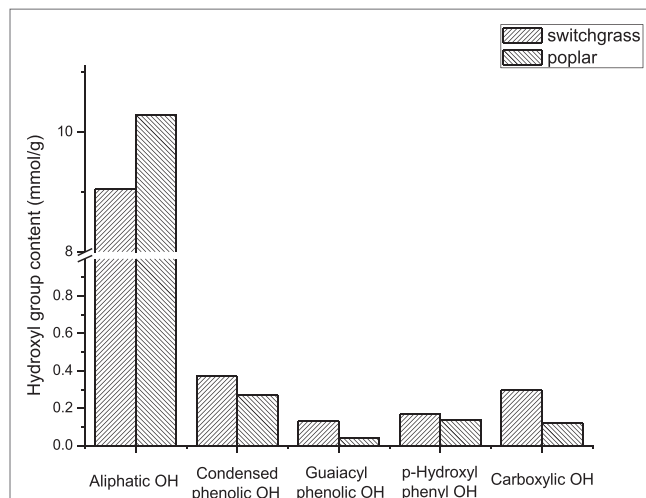
FIGURE 5 | Hydroxyl group contents of switchgrass and poplar. Detected by ³¹P NMR after dissolution and phosphitylation with TMDP in ionic liquid. (Due to the possible overlap and shift, the content of syringy type OH is only a preliminary number. There were ~65% of C5 substituted/condensed phenolic OH in poplar belong to syringyl OH, and there were ~40% of C5 substituted/condensed phenolic OH in switchgrass belong to syringyl OH.).

between employing ionic liquid and routine ³¹P NMR solvent are virtually identical. Therefore, this method can also provide detailed information of hydroxyl groups for all the three major biomass components—cellulose, hemicellulose, and lignin. To further evaluate this methodology, a set of biomass mixtures were prepared and examined as summarized in **Table 2**. The artificial mixtures of lignin, hemicellulose, and cellulose have the similar contents for each biomass components in the whole biomass tested in this study to represent the real biomass. The only difference for these two mixtures is the difference for the types of hemicellulose. Since the OH groups contents for all of these three biomass components have been fully characterized (**Table 1**), the artificial mixtures have the theoretical results for these different OH groups. By using the proposed ionic liquid system, the experimental and theoretical results for these two artificial mixtures are consistent with each other, which indicated that the proposed system can provide quantitative data for complex mixtures, which is the preapproval for this system to perform precise analysis for the real whole biomass.

Having successfully characterized major biomass components and artificial mixtures of these components, this method has also been used to analyze two whole biomasses—switchgrass and poplar. The ³¹P NMR results are shown in **Figure 5**. The

integration results indicated that compared to poplar, switchgrass has relatively less amount of aliphatic OH, but more aromatic and carboxylic OH. The carbohydrate and Klason lignin contents of these two biomasses (poplar: ~lignin 30%, ~cellulose 50%; switchgrass: ~lignin 28, ~cellulose 40%) also provide similar results (Foston and Ragauskas, 2010). Compare to the literature reported (Akim Leonid et al., 2001) lignin OH groups in the poplar, this study presents a relatively lower content. The reason for this difference is still unclear, which may be due to the benefit of low temperature treatment of biomass in this study or can be due to the differences between the biomass samples and characterization methods.

CONCLUSION

The dissolution of biomass components—cellulose, hemicellulose, and lignin, and two whole biomasses—switchgrass and poplar in 1-allyl-3-butylpyridinium chloride—was examined. The phosphitylation and ³¹P NMR measurement provided quantitative results for various hydroxyl groups, including aliphatic OH, condensed phenolic OH, guaiacyl phenolic OH, *p*-hydroxyl phenyl OH, and carboxylic OH in the biomass components and whole biomass. Several evaluations of this process including the use of cellulose and various oligomers of glucose, and artificial mixtures of major biomass components have been examined. All the results show that this method is a reliable and accuracy way to quantitatively characterize hydroxyl groups in biomass and its components. The ³¹P NMR results for the whole biomasses are also consistent with the traditional analysis method. Nevertheless, the established method in this work opens up a new way to dissolve whole biomass and biomass components at a low temperature (50°C), which provide an opportunity to explore the original structures of biomass (Figure S3 in Supplementary Material). The ongoing research in our group involves detailed assignments

for cellulose (Figures S4 and S5 in Supplementary Material) and hemicellulose and evaluation of various pretreatment processes by this method.

SUPPORTING INFORMATION

Experimental details, ³¹P NMR assignments and spectrums, computational simulations are available free of charge *via* the Internet at http://pubs.acs.org.

AUTHOR CONTRIBUTIONS

HB conducted all the major experiments and wrote the manuscript. GH provided the NMR facility in Qingdao University to finish some additional tests from China. YS did the sample preparation and helped with the manuscript preparation. WJ did some NMR tests and helped with the manuscript preparation. YP did the sample preparation, NMR tests in the US, and helped with the manuscript preparation. AR provided very valuable information on the whole idea and manuscript writing.

FUNDING

SUPPLEMENTARY MATERIAL

The Supplementary Material for this article can be found online at https://www.frontiersin.org/articles/10.3389/fenrg.2018.00013/full#supplementary-material.

REFERENCES

Akim Leonid, G., Argyropoulos Dimitris, S., Jouanin, L., Leplé, J.-C., Pilate, G., Pollet, B., et al. (2001). *Quantitative 31P NMR Spectroscopy of Lignins from Transgenic Poplars*. Bordeaux: Holzforschung, 386.

Ben, H., and Ferrell Iii, J. R. (2016). In-depth investigation on quantitative characterization of pyrolysis oil by 31P NMR. *RSC Adv.* 6, 17567. doi:10.1039/C5RA23939G

Ben, H., and Ragauskas, A. J. (2011). NMR characterization of pyrolysis oils from Kraft lignin. *Energy Fuels* 25, 2322. doi:10.1021/ef2001162

Ben, H., and Ragauskas, A. J. (2012). Torrefaction of Loblolly pine. *Green Chem.* 14, 72. doi:10.1039/C1GC15570A

da Costa Lopes, A. M., João, K. G., Morais, A. R. C., Bogel-Łukasik, E., and Bogel-Łukasik, R. (2013a). Ionic liquids as a tool for lignocellulosic biomass fractionation. *Sustain. Chem. Process.* 1, 1. doi:10.1186/2043-7129-1-3

da Costa Lopes, A. M., Joao, K. G., Rubik, D. F., Bogel-Lukasik, E., Duarte, L. C., Andreaus, J., et al. (2013b). Pre-treatment of lignocellulosic biomass using ionic liquids: wheat straw fractionation. *Bioresour. Technol.* 142, 198. doi:10.1016/j.biortech.2013.05.032

David, K., and Ragauskas, A. J. (2010). Switchgrass as an energy crop for biofuel production: a review of its ligno-cellulosic chemical properties. *Energy Environ. Sci.* 3, 1182. doi:10.1039/b926617h

Foston, M., and Ragauskas, A. J. (2010). Changes in lignocellulosic supramolecular and ultrastructure during dilute acid pretreatment of *Populus* and switchgrass. *Biomass Bioenergy* 34, 1885. doi:10.1016/j.biombioe.2010.07.023

Foston, M., and Ragauskas, A. J. (2012). Biomass characterization: recent progress in understanding biomass recalcitrance. *Ind. Biotechnol.* 8, 191. doi:10.1089/ind.2012.0015

Foston, M. B., McGaughey, J., O'Neill, H., Evans, B. R., and Ragauskas, A. (2012). Deuterium incorporation in biomass cell wall components by NMR analysis. *Analyst* 137, 1090. doi:10.1039/c2an16025k

Hallac, B. B., Sannigrahi, P., Pu, Y., Ray, M., Murphy, R. J., and Ragauskas, A. J. (2009). Biomass characterization of *Buddleja davidii* a potential feedstock for biofuel production. *J. Agric. Food Chem.* 57, 1275. doi:10.1021/jf8030277

Hao, N., Ben, H., Yoo, C. G., Adhikari, S., and Ragauskas, A. J. (2016). Review of NMR characterization of pyrolysis oils. *Energy Fuels* 30, 6863. doi:10.1021/acs.energyfuels.6b01002

Hu, Z., Sykes, R., Davis, M. F., Charles Brummer, E., and Ragauskas, A. J. (2010). Chemical profiles of switchgrass. *Bioresour. Technol.* 101, 3253. doi:10.1016/j.biortech.2009.12.033

Huang, F., Singh, P. M., and Ragauskas, A. J. (2011). Characterization of Milled Wood Lignin (MWL) in Loblolly Pine Stem Wood, Residue, and Bark. *J. Agric. Food Chem.* 59, 12910. doi:10.1021/jf202701b

Jiang, N., Pu, Y., and Ragauskas, A. J. (2010). Rapid determination of lignin content via direct dissolution and 1H NMR analysis of plant cell walls. *ChemSusChem* 3, 1285. doi:10.1002/cssc.201000120

Jiang, N., Pu, Y., Samuel, R., and Ragauskas, A. J. (2009). Perdeuterated pyridinium molten salt (ionic liquid) for direct dissolution and NMR analysis of plant cell walls. *Green Chem.* 11, 1762. doi:10.1039/b913609f

Kilpeläinen, I., Xie, H., King, A., Granstrom, M., Heikkinen, S., and Argyropoulos, D. S. (2007). Dissolution of wood in ionic liquids. *J. Agric. Food Chem.* 55, 9142. doi:10.1021/jf071692e

King, A. W., Zoia, L., Filpponen, I., Olszewska, A., Xie, H., Kilpelainen, I., et al. (2009). In situ determination of lignin phenolics and wood solubility in imidazolium chlorides using (31)P NMR. *J. Agric. Food Chem.* 57, 8236. doi:10.1021/jf901095w

King, A. W. T., Jalomaki, J., Granstrom, M., Argyropoulos, D. S., Heikkinen, S., and Kilpelainen, I. (2010). A new method for rapid degree of substitution and purity determination of chloroform-soluble cellulose esters, using 31P NMR. *Anal. Methods* 2, 1499. doi:10.1039/c0ay00336k

King, A. W. T., Kilpeläinen, I., Heikkinen, S., Jä̈rvi, P., and Argyropoulos, D. S. (2008). Hydrophobic interactions determining functionalized lignocellulose solubility in dialkylimidazolium chlorides, as probed by 31P NMR. *Biomacromolecules* 10, 458. doi:10.1021/bm8010159

Kosa, M., Ben, H., Theliander, H., and Ragauskas, A. J. (2011). Pyrolysis oils from CO_2 precipitated Kraft lignin. *Green Chem.* 13, 3196. doi:10.1039/c1gc15818j

Li, M., Yoo, C. G., Pu, Y., and Ragauskas, A. J. (2018). 31P NMR chemical shifts of solvents and products impurities in biomass pretreatments. *ACS Sustain. Chem. Eng.* 6, 1265. doi:10.1021/acssuschemeng.7b03602

Lu, F., and Ralph, J. (2003). Non-degradative dissolution and acetylation of ball-milled plant cell walls: high-resolution solution-state NMR. *Plant J.* 35, 535. doi:10.1046/j.1365-313X.2003.01817.x

Muhammad, N., Man, Z., Bustam, M., Mutalib, M. I. A., Wilfred, C., and Rafiq, S. (2011). Dissolution and delignification of bamboo biomass using amino acid-based ionic liquid. *Appl. Biochem. Biotechnol.* 165, 998. doi:10.1007/s12010-011-9315-y

Pinkert, A., Marsh, K. N., Pang, S., and Staiger, M. P. (2009). Ionic liquids and their interaction with cellulose. *Chem. Rev.* 109, 6712. doi:10.1021/cr9001947

Pu, Y., Cao, S., and Ragauskas, A. J. (2011). Application of quantitative ³¹P NMR in biomass lignin and biofuel precursors characterization. *Energy Environ. Sci.* 4, 3154. doi:10.1039/c1ee01201k

Qu, C., Kishimoto, T., Hamada, M., and Nakajima, N. (2013). Dissolution and acetylation of ball-milled lignocellulosic biomass in ionic liquids at room temperature: application to nuclear magnetic resonance analysis of cell-wall components. *Holzforschung* 67, 25. doi:10.1515/hf-2012-0037

Qu, C., Kishimoto, T., Ogita, S., Hamada, M., and Nakajima, N. (2012). Dissolution and acetylation of ball-milled birch (*Betula platyphylla*) and bamboo (*Phyllostachys nigra*) in the ionic liquid [Bmim]Cl for HSQC NMR analysis. *Holzforschung* 66, 607. doi:10.1515/hf.2011.186

Ragauskas, A. J., Nagy, M., Kim, D. H., Eckert, C. A., Hallett, J. P., and Liotta, C. L. (2006). From wood to fuels: integrating biofuels and pulp production. *Ind. Biotechnol.* 2, 55. doi:10.1089/ind.2006.2.55

Rinaldi, R. (2011). Instantaneous dissolution of cellulose in organic electrolyte solutions. *Chem. Commun.* 47, 511. doi:10.1039/C0CC02421J

Sadeghifar, H., Dickerson, J. P., and Argyropoulos, D. S. (2014). Quantitative 31P NMR analysis of solid wood offers an insight into the acetylation of its components. *Carbohydr. Polym.* 113, 552. doi:10.1016/j.carbpol.2014.07.046

Samuel, R., Foston, M., Jaing, N., Cao, S., Allison, L., Studer, M., et al. (2011). HSQC (heteronuclear single quantum coherence) 13C-1H correlation spectra of whole biomass in perdeuterated pyridinium chloride–DMSO system: an effective tool for evaluating pretreatment. *Fuel* 90, 2836. doi:10.1016/j.fuel.2011.04.021

Wen, J.-L., Sun, S.-L., Xue, B.-L., and Sun, R.-C. (2012). Quantitative structures and thermal properties of birch lignins after ionic liquid pretreatment. *J. Agric. Food Chem.* 61, 635. doi:10.1021/jf3051939

Wroblewski, A. E., Lensink, C., Markuszewski, R., and Verkade, J. G. (1988). Phosphorus-31 NMR spectroscopic analysis of coal pyrolysis condensates and extracts for heteroatom functionalities possessing labile hydrogen. *Energy Fuels* 2, 765. doi:10.1021/ef00012a008

Wroblewski, A. E., Reinartz, K., and Verkade, J. G. (1991). Moisture determination of Argonne Premium coal extracts by phosphorus-³¹NMR spectroscopy. *Energy Fuels* 5, 786. doi:10.1021/ef00030a003

Xie, H., King, A., Kilpelainen, I., Granstrom, M., and Argyropoulos, D. S. (2007). Thorough chemical modification of wood-based lignocellulosic materials in ionic liquids. *Biomacromolecules* 8, 3740. doi:10.1021/bm700679s

Yang, D., Zhong, L.-X., Yuan, T.-Q., Peng, X.-W., and Sun, R.-C. (2013). Studies on the structural characterization of lignin, hemicelluloses and cellulose fractionated by ionic liquid followed by alkaline extraction from bamboo. *Ind. Crops Prod.* 43, 141. doi:10.1016/j.indcrop.2012.07.024

Yang, H., Yan, R., Chen, H., Lee, D., and Zheng, C. (2007). Characteristics of hemicellulose, cellulose and lignin pyrolysis. *Fuel* 86, 1781. doi:10.1016/j.fuel.2006.12.013

Yoo, C. G., Pu, Y., Li, M., and Ragauskas, A. J. (2016). Elucidating structural characteristics of biomass using solution-state 2 D NMR with a mixture of deuterated dimethylsulfoxide and hexamethylphosphoramide. *ChemSusChem* 9, 1090. doi:10.1002/cssc.201600135

Zawadzki, M., and Ragauskas, A. (2001). N-hydroxy compounds as new internal standards for the ³¹P NMR determination of lignin hydroxy functional groups. *Holzforschung* 55, 283. doi:10.1515/HF.2001.047

Advantages of publishing in Frontiers

OPEN ACCESS
Articles are free to read for greatest visibility and readership

FAST PUBLICATION
Around 90 days from submission to decision

HIGH QUALITY PEER-REVIEW
Rigorous, collaborative, and constructive peer-review

TRANSPARENT PEER-REVIEW
Editors and reviewers acknowledged by name on published articles

REPRODUCIBILITY OF RESEARCH
Support open data and methods to enhance research reproducibility

DIGITAL PUBLISHING
Articles designed for optimal readership across devices

FOLLOW US
@frontiersin

IMPACT METRICS
Advanced article metrics track visibility across digital media

EXTENSIVE PROMOTION
Marketing and promotion of impactful research

LOOP RESEARCH NETWORK
Our network increases your article's readership